Flume investigation of the effects of sub-threshold rising flows on the entrainment of gravel beds

Miguel M Piedra©

Civil Engineer, MSc, CEng, CWEM

Thesis submitted in fulfilment of the requirements for the Degree of PhD

School of Engineering

Department of Civil Engineering

University of Glasgow

Glasgow, UK

September 2010

To my Dad,
and the days we spent trout fishing with my brother,
when I learned to love rivers.

Abstract

Recent research on sediment transport in gravel bed rivers shows evidence of the influence of sub-threshold flow history on values of entrainment thresholds (Paphitis and Collins, 2005; Monteith and Pender, 2005; Haynes and Pender, 2007; Haynes and Ockelford, 2008). The research presented here analyses the effect of the characteristics of hydrograph rising limbs (flow magnitude and duration) on entrainment thresholds of gravel beds, with discharges ranging from 0.25-1.6 times the estimated bed threshold flow and durations from 0.5h to 6h. This analysis uses results from flume experimentation. Entrainment thresholds were determined by two well documented methods: a) particle movement counts (visual method, Yalin, 1977); and b) the reference transport method (RTM) (Parker *et al.*, 1982a; Shvidchenko *et al.*, 2001). Results obtained with near-uniform and uniform bed material sizes show a clear influence of flow magnitude and duration on entrainment thresholds, with bed resistance increasing up to c. 25% for longer durations of antecedent flows when using the visual method, similarly to Paphitis and Collins (2005). The results from the unimodal gravel bed suggest an intermediate duration of rising limb (c. 2h) producing the strongest bed, with more mobile beds resulting from both shorter and longer rising limbs. Total bedload transport rates reduce with increased bed resistance, this effect is also noted during the stability test phase. These results are used to develop a new simplified method for estimating critical bed shear stress using only total bedload data. The performance of a new formulation for bedload rates derived in this thesis is tested against a number of traditional bedload transport equations and appropriately discussed. In-depth analyses of bed surface and bedload size composition and surface grain structure show that bed surface undergoes little change of size composition, with a slightly proportionally larger reduction of fine content, suggesting penetration of fines below the surface. The analysis of coarse-grain bed surface structures, mobility and clustering, based on the size class containing D_{90} and using digital images taken under UV light, suggests that the surface distribution of coarse grains has a primary role on bed stability.

Table of contents

Section Page

List of Tables

Appendices

List of Figures

Appendices

Acknowledgements

Many individuals have contributed in one way or another to the completion of this PhD. To all of them I am very grateful.

In the first place, I would like to thank my two supervisors, Dr. Heather Haynes and Prof. Trevor B. Hoey, not only for their guidance, support and patience but, primarily, for giving me the opportunity of doing this PhD. It was a once in a lifetime chance that I enthusiastically embraced three and a half years ago. I have not regretted it a single time.

Secondly, I would like to express my gratitude to the academic, administrative and laboratory staff of the Department of Civil Engineering of the University of Glasgow for their help and contribution to the various activities that undertaking a doctorate requires. I would also like to thank the Department for their funding support and, in particular, for extending my research grant.

Thirdly, I would like to manifest my appreciation for the help and advice I received at various stages of my research from Prof. Alan Ervine (University of Glasgow) Prof. Marwan Hassan (University of British Columbia), Ass. Prof. Joanna Curran (University of Virginia) and Prof. Roger Bettes (HR Wallingford).

Also, I would like to thank the various funders of my PhD and the conferences I have attended during it: The Engineering and Physical Sciences Research Council (EPSRC), the Department of Civil Engineering of the University of Glasgow, Scottish Natural Heritage (SNH), the Royal Academy of Engineering UK (RAEng), the Scottish International Education Trust (SIET), and Universitas 21 (U21).

Finally, my sincere gratitude goes to my friends, who encouraged and supported me before and throughout the entire PhD. Thanks to all, but especially to Linda and Pattie, they know why.

Author's declaration

I state that this thesis is a record of the original work carried out solely by myself in the Department of Civil Engineering of the University of Glasgow, UK, during the period March 2007 to September 2010. The copyright of this thesis therefore belongs to the author under the terms of the United Kingdom Copyright Acts. Due acknowledgement must always be made of the use of any material contained in, or derived from, this thesis. This thesis has not been presented elsewhere in consideration for a higher degree.

Miguel M Piedra
Glasgow, September 2010

Symbols

A	surface area
A_{tot}	total surface area
a_i	average individual surface area of clusters
b	channel width
C	Integration constant of the logarithmic velocity profile equation
D	diameter of grain
D_i	particle diameter corresponding to size *i*
D_x	particle diameter corresponding to x percentile finer
D_{xs}	Surface particle diameter corresponding to x percentile finer
D_{xsub}	Subsurface particle diameter corresponding to x percentile finer
d	displacement of zero-plane
F_i	percentage of size class *i* on bed bulk mix
f_i	percentage of size class *i* on bed surface
f	friction factor
f_b	bed friction factor
f_w	wall friction factor
g	gravity acceleration
H	total flow depth, measured from u = 0 level
h	flow depth, measured from bed surface
k_s	grain roughness
l	Mixing length
$ln(-)$	natural logarithm
N	number of grain movements
N_e	number of elements or clusters on bed surface
pi	percentage of size class I on bedload sample
Q	Fluid discharge
Q_{cr}	Critical flow
Q_{ini}	Initial low flow
Q_t	Target flow
Q_{ref}	Reference flow
q_{bi}^*	dimensionless mass bedload transport rate of size class *i*
q_b	total bedload transport rate
q_{bivol}	volumetric bedload transport rate of size class *i*
q_{biw}	mass bedload transport rate of size class *i*
R^2	Correlation coefficient
Re_*	Grain Reynolds number
R_h	hydraulic radius
S	bed slope
S_0	slope of energy line
t	time
U	depth-averaged streamwise flow velocity
u	streamwise flow velocity
u_b	area-averaged streamwise velocity over the exposed-frontal particle surface
U_∞	free stream velocity
u, v, w	x, y, and z velocity components of flow velocity
u', v', w'	turbulent components of x, y, and z velocities

u_*	Streamwise bed shear velocity
V	cross section averaged flow velocity
W_i^*	dimensionless volumetric bedload transport rate
x	distance along flow direction
y	distance in the cross flow direction
z	vertical distance from bed
z_0	bed hydraulic roughness

β	Exponent of hiding function
δ	Thickness of boundary layer
κ	von Kárman constant
μ	Fluid viscosity
ν	kinematic viscosity
ρ	fluid density
ρ_s	sediment density
σ_g	Geometric sorting coefficient
τ	bed shear stress
τ_{cr}	Critical bed shear stress
τ_{max}	Maximum bed shear stress
θ	Shields parameter
θ_{cri}	Critical Shields parameter of size i
ω	Stream power

Chapter 1
Introduction

"Water is the driving force of all nature"
– Leonardo da Vinci.

Introduction

1.1 *Scientific context*

The scientific, engineering and ecological relevance of river bed stability has been highlighted by many authors (eg. Andrews, 1983; Kuhnle, 1993; Buffington and Montgomery, 1997). Systematic research into the relationship between acting fluid forces and resisting particle forces has been carried out for many decades, but without a unifying theory having been developed (Buffington and Montgomery, 1997). A large proportion of this previous work was based on laboratory experimentation running a range of uniform flows over granular beds and recording the flow at which a certain grain size of interest moved, or relating bedload transport data to flow records (Neill and Yalin, 1969; Wilcock, 1988; Shvidchenko *et al.*, 2001; Paphitis and Collins, 2005). The hydraulic conditions, typically flow or bed shear stress, at which this movement (entrainment) occurred are adopted as the entrainment threshold of the particular grain size. This approach formed the basis of Albert Shields' work in the 1930s, which produced the most widely used set of results in sediment transport science (Shields, 1936). However, this simple conceptual procedure has been challenged by continuously emerging data sets that do not fit the values of entrainment traditionally set by Shields (Grass, 1970; Miller *et al.*, 1977; Shvidchenko and Pender, 2000; Paphitis, 2001; Monteith, 2001), partly

because of the simplifications adopted in his work, eg. uniform grain size beds, and definition of entrainment (Buffington and Montgomery, 1997) . The presence and unpredictability of hysterisis cycles in bedload transport records leads one to question the nature of sediment entrainment and its relationship with discharge (Chapter 2). Also, the widely reported inadequacy of existing bedload transport equations to predict solid transport rates in a wide variety of conditions and environments (Chapter 5) supports the need to further study particle entrainment mechanisms.

The science of sediment transport is highly complex, not so much due to the physical principles and equations required, as to the large number of factors that affect granular bed mobility (Sutherland, 1987; Knighton, 1998). The effect on entrainment of particle size, shape and imbrication, bed size composition, hiding effects and channel slope (Chapter 3) have been previously reported (Parker *et al.*, 1982a; Wilcock and Southard, 1988; Wilcock, 1993; Shvidchenko and Pender, 2000). As research on sediment transport mechanics developed, a new element affecting river bed grain entrainment was identified: The effect of antecedent conditions, defined as the previous recent flow history which a river bed has been subject to, appeared to alter bed stability and entrainment values (Reid *et al.*, 1985; Buffington and Montgomery, 1997; Church *et al.*, 1998). Reid and Frostick (1986) pointed at flood event magnitude and inter-flood periods as causes of the variability of entrainment and bedload transport rates found in Turkey Brook, a small river in the UK. Church *et al.* (1998) directly related the history of recent flows to the structural development of the bed; and Allan and Frostick (1999) discussed the effects of changes in river regime on the character of the river bed matrix and river ecology. Richards (1982) summarises these effects in noting that the impact of floods on river systems can be seen as a queuing problem, with inter-arrival time of events potentially being as significant as peak flow magnitude.

The effect of flow magnitude and duration on bed composition and therefore stability is intuitive when large discharges, capable of disturbing the entire river bed (full mobility, Frey and Church, 2009), are considered. However, it is not so clear that bed stability may depend on flow history when the flows involved are

below the estimated entrainment threshold of the bed. Recent research has demonstrated that sub-threshold flow conditions alter grain stability and with it the entrainment threshold of granular beds (Saadi, 2002; Paphitis and Collins, 2005; Monteith and Pender, 2005; Haynes and Pender, 2007; Haynes and Ockelford, 2008). These studies directly relate the magnitude and duration of sub-threshold flows with variations of entrainment and bedload transport production. However, all but Saadi (2002) used constant flows throughout the entire duration of the antecedent conditions. Constant sub-threshold flows may represent inter-flood periods and therefore relate to the findings by Reid and Frostick (1986); however, river flows are very rarely constant, displaying hourly, daily and seasonal variations. Despite these flow fluctuations, only a small proportion of river flows are large enough to fully mobilise the bed in gravel bed rivers, i.e. flows above threshold (Parker *et al.*, 1982b; Parker and Klingemann, 1982; Church *et al.*, 1998). Consequently, the majority of flow conditions throughout the year belong to the sub-threshold range. River flow fluctuations and small events generate different flow acceleration rates, considered here as the rates of increase of flows with time of the hydrograph rising limbs. Other authors have partly analysed the effect of flood hydrograph shape on bed composition (Powell *et al.*, 2001; Parker, 2004; Hassan *et al.*, 2006); only Saadi (2002) had previously focussed on the influence of rising and falling limbs on entrainment values. However, his test hydrographs appeared to be above threshold and therefore, as methioned above, may not represent the low transport capacity conditions most often found in rivers. In addition, a number of methodological issues (eg. unclear definition of the estimation of bed shear stress, little justification of the flow range used and only one repetition per experiment) granted further exploration of the effect of unsteady antecedent conditions on the stability of gravel beds. All this previous research clearly shows that, despite the growing evidence that river bed entrainment thresholds will change depending on sub-threshold flow history, very little research has been undertaken on the evaluation of entrainment thresholds of granular beds subjected to increasing sub-threshold flows.

River flows are not only naturally variable. Artificial river management and regulation activities such as river impoundment, flood control, river abstraction

and hydropower generation disturb natural river flow regimes, with the consequent change of flow history applied to the river bed material. Further, future modifications of hydrological regimes due to climate change (Chapter 2) may also affect river bed stability and bed particle size composition; which have implications for river habitat and ecology (Parker *et al.*, 1982b). Species such as salmonids, depend on certain characteristics of river bed size composition to spawn, and any changes in the river bed size distribution caused by changes of grain stability may affect their reproduction. In addition, since fluvial geomorphology is intimately related to river bed stability and sediment transport, studying the effect of antecedent conditions on particle mobilisation is implicitly connected to studying morphological changes in river systems. Further, as the drive for implementation of renewable energy sources continues, with a UK target of 15% of energy production from renewable sources by 2020 (HM Government, 2009), hydropower generation is increasingly being considered and implemented, which requires appropriate policy and regulation. For instance, in Scotland, application for licences to construct and operate of hydropower schemes require the consequences of river regulation to be considered, including the potential impacts on sediment movement (SEPA, 2005). As previously mentioned, changes in hydrological regimes may affect bed stability and habitat conditions downstream and therefore, this research is also relevant to regulators and policy makers (Chapter 2). The potential environmental and policy consequences of this research were recognised by Scottish Natural Heritage, who co-funded this work.

The research work presented in this thesis is therefore an advance on recent research on the relationship between sub-threshold antecedent conditions and non-cohesive granular beds, specifically, the effect of increasing duration and flow magnitude (acceleration rates) of hydrograph rising limbs on entrainment threshold of gravel bed rivers. The potential links of this research extend from the purely engineering applications on improved estimation of river bed stability and sediment transport quantities to environmental and policy issues, such as river geomorphology and habitat preservation (Chapter 2). Thus, this is timely and targeted research, relevant to a range of scientific, environmental and policy requirements.

1.2 *Research objectives*

Based on the above research context, the objectives of this research are to:

1. measure and quantify the extent to which entrainment thresholds in gravel bed rivers are affected by unsteady antecedent conditions, specifically, increasing duration and magnitude of sub-threshold flows;
2. increase and advance existing data and knowledge of entrainment mechanisms and of the link between hydrograph shape and granular bed stability;
3. investigate a possible relationship between flow duration and magnitude and change of entrainment flows for granular beds; and,
4. based on the above, suggest a suitable correction due to flow history for existing bedload transport equations.

1.3 *Conceptual procedure*

The research presented here is based on the comparison of bed entrainment thresholds obtained after subjecting granular beds to a range of increasing flows over a range of durations. Detailed analyses of bedload quantities and composition, bed surface composition and bed structure complete the main areas of this work.

Experimental flume investigation was best suited to the aims of this study as the strict discharge control and data acquisition requirements of this research were unattainable in the field. The experimental work presented here was undertaken at the Laboratory of Hydraulics in the Department of Civil Engineering of the University of Glasgow, UK.

The development of the experimental work was based on stages of incremental complexity and available equipment:

- First, a near-uniform gravel bed was tested, whose entrainment thresholds were estimated based only on particle movement counts (section 3.4.6.1), since no bedload trap was available at the time. The

simplicity of the bed composition and methodology were intended as a test of the research hypothesis and previously reported research using uniform material (eg. Paphitis and Collins, 2005), i.e. confirming the existence of a relationship between antecedent conditions and bed entrainment thresholds. In addition, the use of a near single size gravel bed reduced the degree of complexity that multiple-size beds have on results, isolating the effect of antecedent flows from other factors related to bed composition, such as hiding and exposure, fine content and bimodality; and therefore, helped to establish the basis of the research. These experiments are called the *Pilot Runs*.

- More complex bed composition and sampling procedures were adopted for *Stage 1* and *Stage 2* experiments, using a sand-gravel unimodal bed (Chapter 3). They replicated the conceptual experimental procedure of the Pilot Runs, collecting bedload and bed surface composition data in addition to particle movement counts.

- Finally, a *uniform gravel* bed of similar size to the one used during the Pilot Runs was tested to re-analyse and confirm the previous work once bedload data was available.

1.4 *Thesis structure*

This thesis is divided into the following main sections:

1. Literature review and justification of the research work (Chapter 2).
2. Explanation of techniques and methods used for collecting and analysing data (Chapter 3).
3. Presentation and discussion of experimental results (Chapter 4).
4. Study of bedload transport equations and the new methodology for bedload predictions developed by this research work (Chapter 5).
5. Critical assessment of the work carried out and suggestions for improvement and future research (Chapter 6).
6. Summary of the main findings of this research and conclusions (Chapter 7).

Chapter 2
Literature review

"*You cannot step into the same river twice*"
– Heraclitus.

Literature review

2.1 *Introduction*

The study of the movement of solid particles under the action of fluid forces in river channels faces the highly complex and variable nature of its two components: hydraulics and sediment material. Fluid forces are directly related to not only a time-average current discharge or velocity but also to the fluctuations of the velocity components, i.e. fluid turbulence, which is highly variable even for constant flows (Paphitis and Collins, 2005; van Rijn, 2007a). On the other hand, river bed material displays complex size compositions that vary over the breadth and length of the channel. In addition to this size disparity, other particle characteristics such as shape, angularity, geology, and density (equation 2-1) affect individual particle mobility (Knighton, 1998). The interrelations among bed grains result in yet more degrees of freedom of the bed characteristics and complicates the definition of a relationship between acting forces and bed sediment properties. These interrelations are represented by the diagram shown in Fig. 2-1, based on Ashworth and Ferguson (1986).

Therefore, bedload transport equations should include a range of bed and fluid characteristics (equation 2-1):

$$q_b = f(Q \text{ or } \tau, b, D, S, h, D_i/D_{50}, \sigma_g, \text{ etc.}) \qquad \textit{Eq. 2-1}$$

q_b = bedload transport rate, Q = fluid discharge, b = channel width, D = particle diameter, S = channel slope, h = flow depth, D_i/D_{50} = relative size (hiding/exposure), σ_g = sorting of bed material.

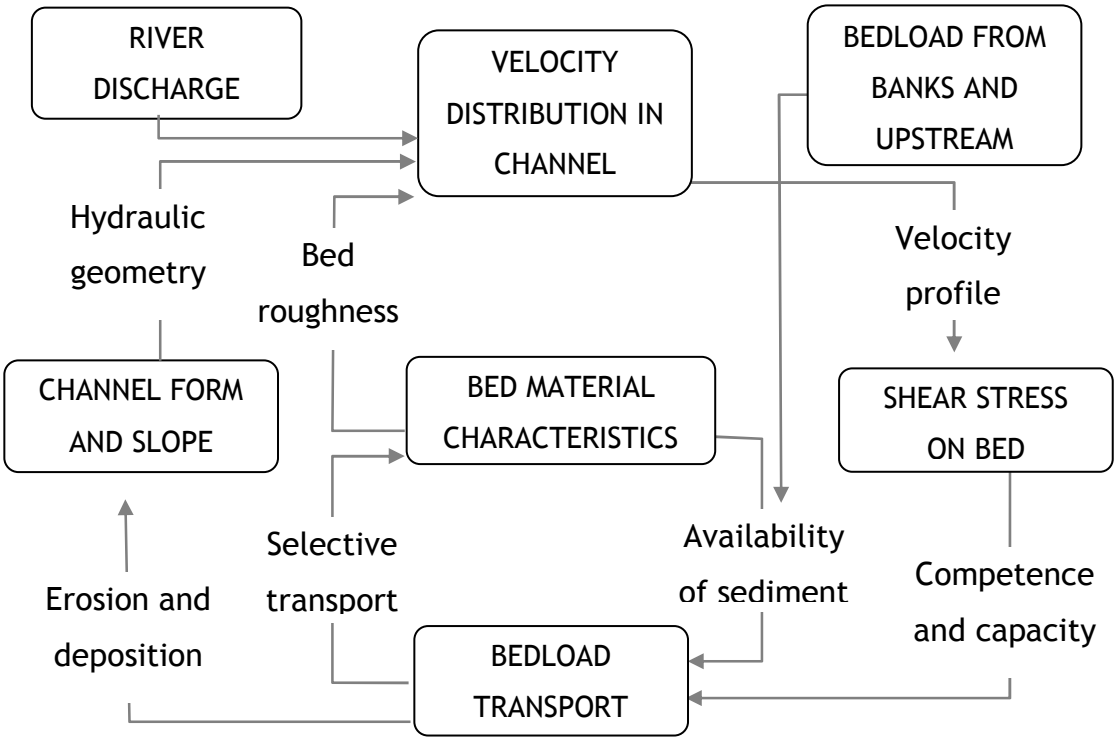

Fig. 2-1. Diagram representing the interrelationships among channel characteristics, flow and bedload transport in gravel bed rivers (modified from Ashworth and Ferguson, 1986).

The complexity of the relationship in equation 2-1 is evident. Generally, bedload transport equations use either flow magnitude or bed shear stress (or variables derived from them such as stream power or dimensionless bed shear stress) to quantify flow intensity. The influence of slope and channel width are included when stream power or specific discharge are used; and bed shear stress for uniform flows can be estimated using equation 2-2, which includes slope and hydraulic radius (channel geometry). Bedload transport equations such as Parker (1990) and Wilcock and Crowe (2003) explicitly incorporate bed composition and relative size effects (Chapter 5).

$$\tau = \rho g S R_h \qquad \text{Eq. 2-2}$$

Due to the large number of factors affecting particle entrainment and transport, developing an equation that produces consistent and accurate quantifications of solid transport is difficult and remains unresolved (Frey and Church, 2009). A

range of commonly used bedload transport equations is presented and discussed in Chapter 5.

It is difficult to summarise the relevant available knowledge on sediment transport in just a few pages without being intentionally brief. The following literature review presents the main aspects directly related to the subject of this thesis: sediment entrainment and flow history. The author is aware that the available knowledge is far greater that the sucint discussion in this chapter. The reader is referred to the cited literature to expand on the issues discussed here.

2.2 *Elements in sediment transport studies*

2.2.1 Need for sediment transport assessments

Predicting river bed stability and sediment bedload quantities and composition remains a major requirement in river engineering and geomorphology (Garde and Ranga Raju, 1977; Andrews, 1983; Ashmore, 1988; Newson and Sear, 1998; Wu *et al.*, 2000; Haynes and Pender, 2007; Bathurst, 2007; Recking *et al.* 2008). Assessments of river channel mobility and evolution, solid material supply to reservoirs, potential hazards such as bridge collapse or culvert blocking, and in-stream and riparian ecology are some of the areas where sediment transport predictions are required (Pender *et al.*, 2001; Peviani and Alterach, 2005; Wallerstein *et al.*, 2006). There is also increasing recognition that the restoration of the physical processes that create river habitats is an essential component of fluvial restoration (Goodwin, 2004). However, despite this widespread need among river practitioners, accurate quantification of sediment transport remains one of the biggest challenges (Wiberg and Smith, 1989; Wu *et al.*, 2000; Frey and Church, 2009). Considerable efforts continue to be put into developing bedload transport equations that sequentially improve those already available (de Linares and Belleudy, 2007), yet none of the available bedload equations appears to be universally applicable (Bathurst, 2007), with large under- or overestimations being reported when the equations are applied to conditions different to those from which the formulations were developed (Reid *et al.*, 1985; Gomez and Church, 1989; Wiberg and Smith, 1989; Powell *et al.*, 2001). Variations in the characteristics of the river bed, such as particle size,

shape and composition, particle interactions, hiding, channel slope, hydraulic regime and channel geometry are some of the factors affecting particle mobility and hence, particle motion (Parker *et al.*, 1982b; Andrews and Parker, 1987; Kuhnle, 1992; Knightonon, 1998; Shvidchenko and Pender, 2000; Bathurst, 2007). This complexity of the mechanics of particle transport makes multi-parameter equations difficult to develop.

An essential element of any approach to sediment transport quantification is the definition and estimation of the flow conditions at entrainment and the associated threshold of motion. These are concepts invariably linked to sediment transport equations as they define their applicability and greatly affect their results. The definition of entrainment conditions are discussed in section 2.3.

Bedload is defined as the solid material transported over the bed surface by rolling, sliding and saltating (Knighton, 1998). The large majority of bedload transport equations employ a deterministic approach based on the functional relationship between bedload discharge q_b and an excess hydraulic force over a threshold, below which little or no transport is considered (Garde and Ranga Raju, 1977; Andrews and Parker, 1987; Knighton, 1998). This definition has two consequences: (1) the determination of a meaningful minimum value of hydraulic force that is characteristic of the bed; and, (2) the repesentativeness and reliability of this value. It is noted here that two extensively used methods for estimating entrainment flows (Visual and Reference transport, see section 3.4.6) are based on the adoption of a sufficiently low minimum number of particle movements or bedload amount respectively (Neill and Yalin, 1969; Yalin, 1977; Paphitis and Collins, 2005; Parker *et al.*, 1982a; Parker, 1990; Wilcock and Crowe, 2003); implying that particle movements can occur below such flows, albeit in small quantities. This is reasonable, since defining entrainment based on a single particle movement (or associated transport rate) will be subject to errors due to the considerable stochastic component of sediment movement (Miller *et al.*, 1977; Dancey *et al.*, 2001; Bottacin-Busolin *et al.*, 2008). However, since these thresholds of movement are defined by the author of the particular technique, it is clear that there is no unique absolute definition of entrainment. The concepts of meaningful and representative

minimum flow conditions will be discussed below. At this stage it suffices to point out that not only the determination of a minimum value for entrainment is difficult, but if this value is taken as the one corresponding to the initiation of motion, bedload equations may underestimate transport amounts, since, as demonstrated by Reid and Frostick (1986) and McEwan *et al*. (2004), bedload transport certainly occurs below the calculated incipient motion "threshold". However, the application of a minimum flow or shear stress associated to initiation of movement is widely accepted (Meyer-Peter and Müller, 1948; Parker, 1990; Wilcock and Crowe, 2003).

There is a considerable number of bedload transport equations, which relate hydraulic forces to sediment transport rates. These hydraulic forces can be represented by flow Q (Hassan and Woodsmith, 2004; Goodwin, 2004; Bathurst, 2007; Barry *et al*., 2008), stream power ω (Bagnold, 1980; Reid and Frostick, 1986; Ashmore, 1988), velocity V (Ackers and White, 1973; Thompson, 1985) bed shear stress τ (Parker, 1990; Wilcock and Crowe, 2003) or Shields' dimensionless shear stress θ (Meyer-Peter & Müller, 1948; Zhang and McConnachie, 1994; Recking, 2009). Although ultimately related to one another and so inter-related, the selection of one variable over the others is rarely justified theoretically, rather, it is more of a personal choice or a generally accepted variable/procedure in the field of expertise of the author (Ashmore, 1988; Gomez and Church, 1989). In addition to the absence of a unique independent variable, there does not appear to be a universal equation that can successfully encompass all the variability encountered in laboratory and natural channels (Wiberg and Smith, 1989; Bathurst, 2007). Some authors even question the possibility of developing a unique relationship between sediment transport rate and hydraulic conditions (Davoren and Mosley, 1986). After their extensive analysis of bedload equation performance, Gomez and Church (1989) suggested that different formulations should be used depending on the purpose and available data. They concluded that none of the equations tested, and possibly no formula, was capable of producing generally adequate predictions of transport rates. Batalla (1997) pointed out that bedload formulae are based on the assumption that specific relationships exist between hydraulic variables, sedimentological conditions and bedload transport rates; yet, bedload variability

is also associated with size-segragated transport and the advance of bedload sheets and bedload pulses (Whiting *et al.*, 1988; Hoey and Sutherland, 1991). Batalla (1997) also indicated that temporal and spatial variability is inherent to solid transport processes. This reported difficulty to produce accurate predictions of solid transport is not only based on the formulation adopted, but most importantly, on the innate difficulty to account for the wide range of factors influencing particle mobility in river flows (Church *et al.*, 1998; Knighton, 1998). Despite these challenges, the importance of assessing bed material stability (Ferguson, 1994) and the constant need for accurate estimations of river bed mobility and sediment transport continues (Bathurst, 2007), there is a demand for further research in the mechanics of granular beds (Frey and Church, 2009).

2.2.2 Uniform-Non-uniform bed material

Grain mobility depends on individual particle size, larger grains will have a greater submerged weight and thus be, in principle, more resistant to movement. However, the relative size of the particles in relation to the surrounding ones alters this size-selective mobility (Wilcock, 1992; Kuhnle, 1992). In essence, finer particles are protected by larger, more exposed grains, reducing the differences of mobility related to grain size. This alteration of the mobility characteristics of fine and coarse material due to relative size is called *hiding* and *exposure* respectively (Parker and Klingeman, 1982; Andrews and Parker, 1987; Wathen *et al.*, 1995; Wilcock and Crowe, 2003; van Rijn, 2007b; Vericat *et al.*, 2008).

Many studies of sediment transport, including some parts of this work, have been conducted using uniform material (eg. Shields, 1936; Ackers and White, 1973; Shvidchenko and Pender, 2000; Paphitis and Collins, 2005). The simplicity provided by narrowly-distributed granular compositions indirectly reinforces the notion of added complications when multi-sized beds are used in sediment transport studies. However, the results obtained using uniform beds may not necessarily be readily applicable to non-uniform mixtures (Carling, 1983; Bathurst, 2007; Recking, 2009), where hiding and other particle interactions

modify grain mechanics and mobility (Graf, 1970; Ashworth and Ferguson, 1989; Wilcock and Crowe, 2003).

2.2.3 Channel geometry

Channel geometry affects the hydraulic terms in many bedload equations. A number of bedload transport equations use unit discharge Q/b or stream power $\omega = \rho g Q S$ as the independent variable (Bagnold, 1980; Reid and Frostick, 1986; Ashmore, 1988; Hassan and Woodsmith, 2004; Barry *et al.*, 2008). Two rivers, or even two different reaches of the same river, may carry the same flow at the same slope; however, cross section geometry may well result in different flow widths and depths, altering the forces acting on the bed, and with them, entrainment and sediment transport capacity. Bagnold (1977, 1980) and Shvidchenko and Pender (2000) reported reductions of channel bedload transport capacity with increasing relative depth h/D; while Carling (1983) reported critical shear stress four times larger in a narrow river than a wider one. Smaller relative depth implies higher penetration of the roughness elements (grains) into the flow depth, increasing hydraulic roughness, altering the distribution of flow velocities and shear stresses (Fig. 2-1), with stronger turbulent eddies being closer to the bed; thus, affecting entrainment capacity and the sediment transporting power of the flow (Bagnold, 1977; Carling 1983; Reid *et al.*, 1985; Buffington and Montgomery, 1999; Shvidchenko and Pender, 2000). The result is yet another source of variability of bedload equations, which may not be applicable to channels with different cross sectional geometries. As hydraulic conditions depend on channel geometry (Fig. 2-1, Ashworth and Ferguson, 1986), a representative variable that can be universally applied is required. Bedload transport equations based on the description of the forces acting over the grains, such as those that used bed shear stress of Shields dimensionless stress (Meyer-Peter and Müller, 1948; Parker, 1990; Wilcock and Crowe, 2003) (Chapter 5), are likely to eliminate the influence of channel geometry, as they quantify forces over the bed, regardless of the cross section geometry.

2.2.4 Hiding

It is intuitive that higher flows are required for entraining and transporting coarser bed grains than for finer particles, as shown by Shields (1936) with the dimensionless shear stress values being constant for large Reynolds stress values. However, when studying selective entrainment of river bed particles with increasing shear stress (or flows) some authors have noted that all grain sizes appear to move at approximately the same shear stress, *equal mobility*, (Parker *et al.*, 1982a; Wilcock and Southard, 1988), whereas others found a degree of size selectivity, i.e. higher shear stresses are required to move the coarser particles (Ashworth and Ferguson, 1989, Kuhnle 1993, Wilcock and MacArdell, 1993, Wathen *et al.*, 1995). These differences are due to the influence of sediment protrusion/exposure and finer fractions being "protected" by larger grains (Parker *et al.*, 1982b; Andrews and Parker, 1987). The effect of grain size on entrainment can be expressed with a relationship between critical shear stress and sediment size (Fig. 2-2), often called a hiding function (eg. equation 2-3).

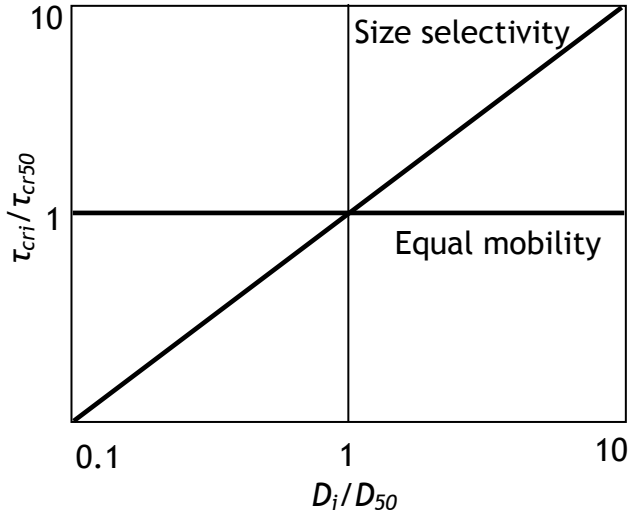

Fig. 2-2. Sketch representing the effect of equal mobility and size selectivity on entrainment thresholds in relation to the bed material median size threshold. τ_{cri} *and* τ_{cr50} *are the entrainment thresholds of size class* D_i *and median size* D_{50} *respectively, (modified from Parker and Klingeman, 1982).*

Thus, the intuitive relationship between particle size and stability, for which larger, heavier particles will move at larger flow rates, is reduced or even inverted by hiding effects, whereas smaller particles are protected from hydraulic forces by the presence of larger ones. On the contrary, coarse grains

are more exposed to flow and hence more likely to be entrained than their size and weight would suggest (Parker, 1990; Knighton, 1998).

In his thorough review of hiding functions Sutherland (1992) highlights the relevance of appropriate hiding functions for the predictions of transport rates and as descriptors of bed behaviour. He analyses the different sensitivity to hiding of fine and coarse size classes, where finer sizes reflect proportionally larger increases of entrainment thresholds relative to the scaling size (eg. D_{50}) than coarser fractions, resulting in the common asymmetry of the hiding functions respect D_i/D_{50} (see Figure 3 in Sutherland, 1992). If hiding functions are derived from entrainment threshold data obtained assuming a certain reference transport rate, the value of that reference transport will affect the function, since departures from equal mobility are observed with increasing values of transport rates used as reference (Sutherland, 1992). Hiding functions are also influenced by (1) bed surface composition and (2) structure, as mobility conditions depend on these two elements (section 2.2.6). Regarding the former, Sutherland (1991) questions the adequacy of D_{50} and σ_g as descriptors of the bed grain size distribution for use in hiding function studies, as the behaviour of the tails of the size distributions affect the hiding functions but are not incorporated in σ_g. In relation to bed structure, this can change without altering bed surface composition (sections 4.2.3 and 4.2.8), with spacing, size and arrangement of larger elements (grains or groups of grains, section 4.2.8) being specifically identified by this author as primary factors affecting hiding.

Hiding has received considerable attention and a number of equations are available for its quantification (White and Day, 1982; Parker *et al.*, 1982a; Ashworth and Ferguson, 1989; Wathen *et al.*, 1995; Wilcock and Crowe, 2003). In general, hiding functions take the form:

$$\frac{\theta_{cri}}{\theta_{cr50}} = \left(\frac{D_i}{D_{50}} \right)^{\beta} \qquad \text{Eq. 2-3}$$

where θ_{cri} and θ_{cr50} are the critical dimensionless shear stress ($\theta = \tau/[(\rho_s-\rho)gD]$) of particle size D_i and D_{50} respectively and β is a parameter, with ρ_s *and* ρ being the solid material and fluid densities. Values of β range from -1 to 0, with

values depending on the degree of bed bimodality (Wilcock, 1993), and are indicative of the degree of transport equality shown by the bed material. If β = 0, then $\tau_{cri} = D_i \tau_{cr50} / D_{50}$ and critical shear stress is proportional to grain size (Fig. 2-2); thus, sediment transport is size-selective. If β = -1, then $\tau_{cri} = \tau_{cr50}$ and critical shear stress is constant for all sizes, i.e. equal entrainment is achieved. Most common values of β range from -0.6 to -1 (Parker *et al.*, 1982; Andrews,1983; Ashworth and Ferguson, 1989; Sutherland, 1992; Kuhnle, 1992), showing a degree of hiding.

For instance, Andrews (1983) obtained an exponent value of -0.872, with D_{50} based on the subsurface material, showing some divergence from equal entrainment. Wathen *et al*. (1995) obtained an exponent of -0.70 based on the gravel fractions , clearly supporting size selectivity. However, when both sand an gravel fractions are included, the exponent becomes -0.90, reflecting that sand is more likely to display equal entrainment than gravel (Wathen et al, 1995). In addition, Wilcock and McArdell (1993) argued that in poorly sorter beds, the sand and gravel fractions appear to behave differently, with selective entrainment of the gravel and more equal mobility of the sand fraction. Thus, the composition of the bed will affect the values of the exponent β. Ashworth and Ferguson (1989) and Parker (1990) conclude that for low flow conditions departure from equal entrainment is more likely, with values of exponents reducing to around -0.65 (Asworth and Ferguson, 1989), while as flows increase and general mobility of the bed occurs, the behaviour of the bed particles moves towards equal entrainment.

2.2.5 Particle shape

The shape of particles has also been identified as affecting grain mobility (Krumbein, 1941; Carling *et al.*, 1992; Knighton, 1998; Monteith, 2001). Krumbein (1941) highlighted the influence of particle shape on selective transport and related grain sphericity (ratio of surface area to volume) to the response of particles to lifting forces, so the behaviour of particles during movement could be different depending on their sphericity (Gomez, 1994). For

instance, Monteith (2001) showed how critical bed shear stress of marine gravel was approximately 30-60% larger than fluvial gravel of the same diameter (2–4 mm), with differences increasing with grain size. Fluvial grains were angular and sub-angular and marine particles were rounded or sub-rounded. Sphericity ranges were 0.66-0.85 and 0.63-0-75 for marine and fluvial particles respectively. Carling *et al.* (1992) and Sutherland (1987) highlighted the dependency of bed packing and probability of entrainment on particle shape, in the sense that grain shape affects the particle contact, pivoting angles and exposure to flow, with plate-like grains being less exposed to flows than more spherical grains of the same intermediate diameter (b-axis). They also indicated that the imbrication potential depends on particle shape and size. Their results showed that critical conditions changed with particle shape and orientation for the same grain size.

2.2.6 Armouring

A bed surface layer that is noticeably coarser than the subsurface material is a common characteristic of gravel bed rivers (Andrews and Parker, 1987; Church *et al.*, 1987), with its depth being approximated by the size of an arbitrary large (or largest) particle size on the surface (Andrews and Parker, 1987; Sutherland, 1987). Since the presence of a range of particle sizes is necessary, non-uniform material is essential for the formation of this coarser layer (Parker *et al.*, 1982b). Two types of coarse surface layers have been defined, depending on their originating processes: (1) *armour* or *static armour* appears when there is a lack of sediment supply and fine material is winnowed away during flows of limited competence, leaving mainly immobile coarse particles on the river bed (Sutherland, 1987; Andrews and Parker, 1987); (2) *pavement* or *mobile armour* is formed under equilibrium transport conditions in which the concentration of larger particles increases (Andrews and Parker, 1987; Church *et al.*, 1987); mobile armour is a mobile bed phenomenon and coexists with the mobilisation of all available sizes (Parker *et al.*, 1982b), unlike the static armour. Mobile armouring may be expected under partial mobility conditions, when only some of the grains within a certain mobile size class actually move (Parker and Klingeman,1982: Wilcock, 1997; Lisle *et al.*, 2000; Hassan and Church, 2000).

Lisle *et al*. (2000) defined partial and fully mobile channels when $0.03 < \theta < 0.06$ and $\theta > 0.06$ respectively, or alternatively, $\tau > 2\tau_{cr}$ (Church *et al*., 1998). In any of the two types of armours, the formation of a coarse surface layer is directly related to incipient motion, size selective entrainment and material availability. Armouring results in relative greater exposure of larger particles to flow forces and relative abundance of coarse particles compared to fine grains; thus, reducing differences in mobility between grain sizes (Parker and Klingeman, 1982). In addition, the size distribution of the bed surface affects bed roughness and hydraulic conditions (Carling *et al*., 1992; Clifford *et al*., 1992; Papanicolaou *et al*., 2001); hence, changes of bed surface composition by armouring may alter the stability of the bed.

In the experiments presented here neither sediment feed or recirculation were included (Chapter 3). Thus, this research falls within static armour conditions. Parker *et al*. (1982b) reported an initial abundance of fines in the bedload samples and coarsening of the bed surface and finer particles penetrating below the bed surface. Although the flows employed were above threshold, contrary to those used as antecedent conditions in the present thesis, some evidence of this is seen in the results reported (Chapter 4). The time scale for the formation of armoured layer under static armour conditions depends on the flow magnitude applied and the characteristics of the bed (Tait *et al*., 1992). For instance, Tait *et al*. (1992) found a decline of the transport rate under constant flow occurred after periods of 100-500 minutes of flow exposure. Sutherland (1987) analysed the work of Proffit (1980) and reported that bedload transport rates remained approximately constant for the first hour. Using flume experimentation Pender *et al*. (2001) showed that the stabilisation of bedload transport rates (representing the appearance of an armoured layer) depended on the shear stress applied, but typically occurred after hundreds of minutes (200-800 approximately). Further, Andrews and Parker (1987) qualify the armouring process as "slow", reporting periods of over 50h before the size distribution of the armour layer stabilised in flume experiments. In the work presented here, periods of constant flow were brief compared to those discussed above (typically around or below 1h, Chapter 3). Thus the time available for armouring was limited. Contrary to the majority of the degradation experiments (static

armouring formation) typically carried out in studies of sediment transport, the discharge magnitudes were constantly increasing in the experiments reported in this thesis. This makes the assessment of the level of armouring expected very difficult as each flow stage can be viewed as a short duration degradation experiment, which is interrupted after a short period by a new increase of flow. Further, all flows employed here as antecedent conditions are sub-threshold, i.e. the mobility of the bed expected is minimal. As Andrews and Parker (1987) express, armouring will occur when a gravel mixture is exposed to a flow just above to transport most of the available particles, in the absence of sediment supply from upstream. This leads to the requirement of a minimum flow value sufficient to move "most of the available sizes", which is not the case in the sub-threshold flows used in this research. Thus, the development of a clear armour layer is not expected in the experiments presented in this thesis.

2.2.7 Bedforms

Bedforms are recognisable bed surface features comprising multiple grains. They can be identified at reach scale (step-pools, riffles-pools, point bars) or local scale (pebble clusters, ripples, dunes, plane beds, bedload sheets, sand ribbons, transverse ribs) (Bluck, 1987). Reach-scale features are more relevant to fluvial geomorphology as they cover large lengths of rives, and in terms of sediment transport, they are more related to sediment supply rather than entrainment (Knighton, 1998). However, small-scale bedforms have a direct impact on the boundary roughness and turbulence at grain scale (Carling *et al.*, 1992; Clifford *et al.*, 1992; Papanicolaou *et al.*, 2001), and therefore studied in this thesis, since bedforms impose a flow resistance (drag) on the flow additional to that associated with the grains themselves (Carson and Griffiths, 1987; Knighton 1998; Buffington and Montgomery, 1999a).

The presence of particle groups or clusters have been widely reported (Bluck, 1987; Reid and Frostick, 1986, Church *et al.* 1987, Hassan and Reid, 1990; Marion *et al.*, 1997, Reid *et al.* 1997, Knighton, 1998; 2003; Church *et al.*, 1998; Marion *et al.*, 2003 Oldmeadow and Church, 2006). Clusters are small-scale accumulations of grains of varying sizes, generally supported by a coarse grain

(key stone) larger than D_{84} (Hassan and Church, 2000) that resist larger fluid forces than as individual grains, increasing general bed stability and reducing bedload transport rates (Church *et al.*, 1987; Sutherland, 1987; Hassan and Reid, 1990; Reid *et al.*, 1997; Knighton, 1998; Oldmeadow and Church, 2006; Frey and Church, 2009). Their formation is related to partial transport and bed structure development (Hassan and Church, 2000). Marion *et al.* (1997, 2003) noted that for flow conditions where bed shear stresses are between once and twice the entrainment threshold, particles at the bed surface rearrange horizontally, forming stabilising groups of particles or pebble clusters. These authors concluded that for shear stresses slightly above critical, horizontal sorting (formation of surface structures) is more likely than vertical sorting (armouring and size segregarion over the bed depth), although the two are in competition (Marion *et al.*, 1997). Since the purpose of the research presented in this thesis is studying the effect of sub-threshold flow exposure on bed entrainment, these bed compositional and structural changes are important.

2.2.8 Slope

The impact of bed slope on entrainment has only been recently analysed systematically (Shvidchenko and Pender, 2000; Shvidchenko *et al.*, 2001; Recking *et al.*, 2008 and Recking, 2010). Channel slope is closely related to relative depth R_h/D or h/D ($R_h \approx h$ for wide channels, Garde and Ranga Raju, 1977, where R_h = hydraulic radius, h = depth and D = particle size); as, for a given channel bed material carrying a certain flow, an increase of slope will lead to a reduction of flow depth and with it a decrease of relative depth. An indirect analysis of the influence of slope or relative depth was carried out by Bagnold (1977) using flume and field data, where a relationship between bedload rate and stream power ω included an inverse relationship with h/D. However, Ashmore (1988) reported lower values of bedload transport rates for the same flow for shallower slopes. Shvidchenko and Pender (2000) and Recking (2009) showed flume and field results in which the minimum flows required for initiation of movement increased for steeper slopes. The former authors justified their results by means of the relationship between flow resistance and relative depth, for which Darcy-Weisbach friction factor $f = 8gR_hS/U^2$ (Knighton,

1998; Shvidchenko and Pender, 2000) increases with decreasing relative depth for transitional and rough turbulent flows. According to Recking (2009), hiding effects increase with increasing slope, and therefore, transport rates decrease for a given θ/θ_{cr}, with θ and θ_{cr} being the dimensionless bed shear stress of the fluid and critical conditions respectively.

This effect can be explained when considering the relationship of friction factor and relative depth for a constant bed slope. For higher flows depths are larger and the effect of bed roughness is limited to a smaller proportion of the flow depth, resulting in smaller friction factors. However, as flow depths decrease with smaller discharges, the penetration of roughness elements reaches closer to the fluid surface, making friction factors higher (Recking, 2008, 2009). In addition, when small relative depths are present, a proportionally larger component of the available fluid forces is dedicated to maintain the flow, resulting in smaller ability to entrain and transport bed particles. Buffington and Montgomery (1999) suggested that as hydraulic roughness of the channel increases, smaller proportion of the total shear stress exerted by the fluid is available for sediment transport. Thus, the reduction of relative depth with steeper beds produces the acceleration of flow velocities, changing the hydraulic conditions. The increase of critical shear stress with slope observed by Shvidchenko and Pender (2000) and Recking (2009) may also result from an enhanced friction between grains as the component of the particle submerged weight parallel to the bed plane *Wp* increases for steeper slopes (Fig. 2-3). This will increase flows required for entraining the particle, in agreement with Shvidchenko and Pender (2000). Pender *et al*. (2001) noted that bedload rates and total material increased with steepness, and Bathurst (2007) showed how unit bedload transport rates (kg/m/s) increased with larger bed slopes for the same sediment size (D_{50} = 22 mm). Whereas as mentioned above, Shvidchenko *et al*. (2001) and Recking (2009) found that entrainment thresholds increase with slopes. This may indicate that steeper slopes delay initiation of movement but once this onset occurs, transport rates produced are higher. Bathurst (2007) derived from Bagnold (1980) that as depth decreases for a given stream power ω sediment transport becomes more efficient and bedload transport increases.

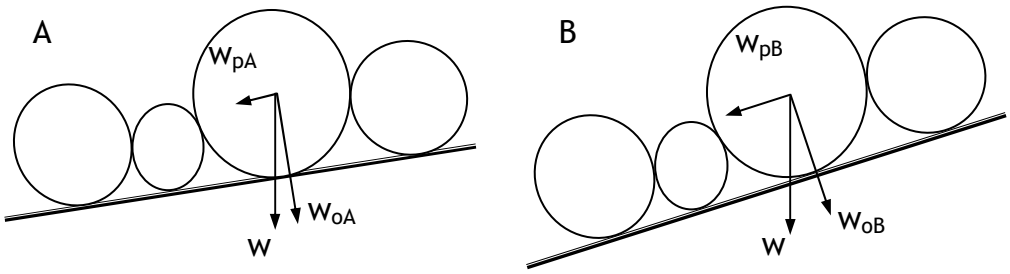

Fig. 2-3. Comparison of submerged weight components parallel and orthogonal Wp and Wo to bed plane for two bed slopes: A) small slope and, B) steep slope. WpA < WpB and therefore, the friction between particles is enhanced for steeper slopes.

Therefore, river bed slope is yet another factor affecting particle mobility. The effect of bed slope is investigated in this research for the data sets where comparison was possible (Chapter 4).

2.3 *Definition of entrainment*

The concept of entrainment of river bed sediment material is complex, with different definitions being used for different purposes. Entrainment is used to describe the physical inclusion of solid particles into the fluid motion, i.e. transport of grains by the fluid. This mobilisation of bed particles occurs when fluid forces reach a minimum value, or threshold, sufficiently large to overcome resisting forces, point in which the particle is *entrained* (van Rijn, 2007a). Experiments using video recording have observed the vibration of particles prior to entrainment (Allan and Frostick, 1999). This threshold of motion is also called the *critical* flow, stress or stream power, depending on the variable used. This critical flow should not be confused with the hydraulic conditions for which the Froude number *Fr* = 1. Whenever appropriate, the use of critical flow will be replaced by entrainment flow to avoid misunderstanding. Van Rijn's rather idealised definition of threshold of motion is more practically defined by Paphitis and Collins (2005) as the *specific point within the sequential process of transport where a small (arbitrary) amount of sediment grains are entrained or set in motion (p. 828)*. This allowance of a small amount of sediment transport before defining the threshold is crucial for determining an appropriate value of entrainment threshold and is the basis of a number of methods for estimating

entrainment (Yalin, 1977; Parker *et al.*, 1982; Shvidchenko and Pender, 2001; Wilcock and Crowe, 2003; Paphitis and Collins, 2005). However, the existence of a small number of grain movements below the accepted threshold has also implicitly associated the stochastic nature of sediment transport (Einstein, 1950; Miller *et al.*, 1977; Andrews and Parker, 1987; Sutherland, 1987). Van Rijn (2007a) defined initiation of motion or entrainment as the moment when "*…instantaneous fluid force on a particle is just larger than the instantaneous resisting force related to the submerged particle weight and the friction coefficient*" (van Rijn, 2007a p.651). He considered that driving forces are strongly related to the local near bed velocities. In turbulent flows these velocities fluctuate in space and time, which, together with the randomness of particle characteristics such as size, shape and position, introduces a stochastic component to the initiation of motion (eg. Grass, 1970). Authors such as McEwan *et al*. (2004) accepted that grain motion can occur at any non-zero time averaged flow by turbulent fluctuations of the instantaneous stress above the thresholds of individual sediment grains. Grass (1970), Andrews and Parker (1987) and Paphitis and Collins (2005) associated probability functions to acting and resisting forces where the overlap of these two functions defines the degree of solid transport (section 2.5.4). If threshold of movement was to be rigidly defined as that flow that produces the first entrainment of a single grain of certain size, the critical condition might be achieved by the combination of a turbulent burst and a particularly unstable grain, equivalent to a very small overlap of the above probability functions.

Despite all the factors affecting bedload movement noted above, the value of the threshold of motion is often assumed to be a characteristic parameter for a given particle size when shape and hiding effects are considered. However, this assumption is questioned by much of the work noted above, with recent research showing two main limitations to this assumption: (1) entrainment thresholds appear to increase with steeper slopes or smaller relative depth (Shvidchenko and Pender, 2000; Shvidchenko *et al.*, 2001; Recking, 2010), and (2) entrainment thresholds change depending on the flow history to which the bed has been exposed (Reid and Frostick, 1986, Paphitis and Collins, 2005;

Monteith and Pender, 2005; Haynes and Pender, 2007; Haynes and Ockelford, 2008).

2.4 *Effects of hydrographs and flow history*

The vast majority of sediment transport experiments undertaken in the last 70 years have used constant flow and equilibrium sediment transport (Shields, 1936; Meyer-Peter and Müller, 1948; Parker *et al.*, 1982a,b; Hassan and Reid, 1990; Tait *et al.*, 1992; Wilcock, 1993, Buffington and Montgomery, 1997; and Paphitis an Collins, 2005). There are multiple reasons for this, some related to the complexity of the transport processes, others to the difficulties of measuring grain movement at times when laboratory apparatus were inadequate for certain measurements (Carollo *et al.*, 2005). Advances in technology have since resulted in the development of acoustic Doppler velocimeters (ADV), laser scanning, accurate control of pumps, photography/video recording, etc. The use of simplified laboratory conditions were sometimes simply due to the need for developing the little available knowledge on sediment transport from simple ideas and processes. Thus, many of the transport equations, entrainment threshold criteria and sediment movement theories have been developed under these steady flow conditions (Shields, 1936; Parker *et al.*, 1982a; Meyer-Peter-Muller, 1948; Yalin, 1972; Buffington and Montgomery, 1997).

There is increasing evidence that antecedent flow history affects the mobility of gravel beds and produce differences of bedload rates and entrainment flows (Reid and Frostick, 1986; Church *et al.*, 1998; Paphitis and Collins, 2005; Hassan *et al.*, 2006, Haynes and Pender, 2007, Haynes and Ockelford, 2008) and also plays a relevant role on the development of surface structures (Church *et al.*, 1998 and Oldmeadow and Church, 2006), which are also linked to bed stability and hydraulic condiditons (Laronne and Carson, 1976; Brayshaw *et al.*, 1983; Hassan and Reid, 1990; Hassan and Church, 2000; Frey and Church, 2009). This leads to question what are the factors affecting these reported changes and what are the consequences of the findings.

There are three main issues related to flow variability when it comes to particle entrainment and transport: (1) different bedload amounts for the same flows located either side of the peak in a flood hydrograph (hysteresis); (2) effect of hydrograph shape on bedload rates and bed composition; and, (3) the influence of antecedent conditions and flow history on bed stability. Although separated here for ease of discussion, these three factors are interrelated.

2.4.1 Hysterisis

Different bedload amounts can be produced by the same flow magnitude, depending on whether the flow occurs on the rising or falling limb of a hydrograph. The consequence is the production of hysterisis loops (Fig. 2-4), with different solid transport rates in the falling and rising limbs (Reid *et al.*, 1985; Church *et al.*, 1991; Knighton, 1998; Saadi, 2002; Hassan *et al.*, 2006). These have been linked to the bed conditions and stability prior to the occurrence of particle mobilising flows (Reid *et al.*, 1985; Reid *et al.*, 1997). According to Reid *et al.* (1997), armouring contributes to the differences in transport rates between the rising and falling limb of a hydrograph. Current conventional bedload transport equations cannot reproduce these hysteretic cycles, as the relationship between acting forces and solid discharge is uniquely defined, i.e. certain flow/stress will result in only one bedload quantity. Reid and Frostick (1986) identified two thresholds, one for initiation of motion and another one for cessation, where cessation threshold was only about 20% that of initiation. These different motion thresholds were present in the rising and falling limb of hydrographs respectively. While the threshold for the cessation of motion is closely linked to particle size and the balance of forces applied on an individual particle, the entrainment threshold depends, as discussed earlier, on additional factors such as particle imbrication, surface structures and relative sizes surrounding the grain, which appear to be affected by the recent previous flows to which the bed material has been exposed (Reid and Frostick, 1986; Church *et al.*, 1998).This highlights the apparent different behaviour of solid transport before and after entrainment, which bedload equations cannot appropriately represent (Reid *et al.*, 1985).

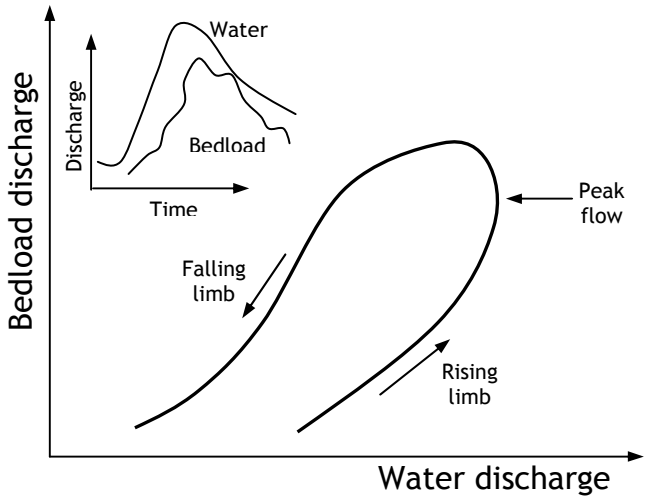

Fig. 2-4. Examples of hysteresis loop (after Reid et al., 1997).

2.4.2 Effect of hydrograph characteristics

Reid *et al*. (1985) highlighted the influence of the separation between flood events on entrainment and sediment transport rates, where longer periods of low flows (approximately 2 months) appeared to produce more resistant beds. Conversely, high flow events that were shortly preceeded by another spate resulted in bed mobilisation for lower flows than isolated events and produced larger bedload rates for the same discharge (see next section). They linked this effect to higher entrainment thresholds when floods are distant apart and to hysterisis cycles, where transport rates either side of the peak flow reflect the initial stability of the bed. In the last few years, the effects of individual hydrograph shape have been specifically analysed (Powell, *et al*. 2001; Parker, 2004; and Hassan *et al*. 2006). These authors studied the link between hydrograph shape, magnitude and duration on bed composition and vertical mixing of the sediment; showing that bed surface and bedload compositions are dependent on the flood event. For instance, Hasan *et al*. (2006) found that the experiments with constant hydrographs produced well armoured structured surfaces, while short asymmetrical hydrographs did not result in substantial vertical sorting. Therefore, the characteristics of recent flow events will produce different bed conditions that will affect the stability of the bed for the next flood. Lisle *et al*. (2000) used constant flows so "*…surface particle sizes were not affected by hydrographs, as it would occur in natural channels*" (p.

3744). The reverse of Lisle *et al.*'s argument clearly suggests that bed composition may be affected by hydrograph characteristics.

2.4.3 Antecedent conditions

Stress history, or flow history, can be defined as the series of discharge magnitudes and durations which beds are subject to prior to entrainment. These are also called antecedent conditions (Haynes and Pender, 2007) and flow magnitudes can be either above or below threshold. Despite the primary importance of the estimation of bed mobility, very little research has been undertaken on the effect of flow history on sediment transport. Previous authors have suggested flow history as a factor on the observed variability of sediment transport in gravel bed rivers (Reid *et al.*, 1985; Reid *et al.*, 1997, and Church *et al.*, 1998).

Reid *et al.* (1985) were some of the first authors to point out flow history and time between floods as responsible for the observed variability of bedload amounts and patterns in the Turkey Brook, although they did not specifically studied it. When floods were preceded by a long period of low flows (longer than 2 months) over 90% of the total bedload was transported during the falling limb of hydrographs. In contrast, when a recent flood had occurred, the next high flow event carried much larger proportions of bedload during the rising limb (Fig. 2-5). Particle interlocking, hiding, cluster formation and differences between static and dynamic friction were identified as responsible for these results. The action of low flows for prolonged periods (several weeks) created a more stable, armoured bed, and the action of sub-threshold flows rearranged bed grains without removing them from the surface, increasing their imbrication.

Pender *et al.* (2001) used flume experimentation to analyse bed surface evolution during long periods of steady flows (up to 100 h). These are important as they represent conditions which occur during the low flow phases between floods. Consequently, the bed surface that results will determine bed stability and volume of sediment transported during subsequent flood events. They noted

both little change of bed surface composition and fine percolation below the bed surface. Yet, they observed that bed topography changed with duration, resulting in increasing irregularity, producing an average increase of Manning's roughness parameter (approximately 18%) and a reduction of bed shear stress (12-14%); therefore, reducing the possibility of entrainment of bed material.

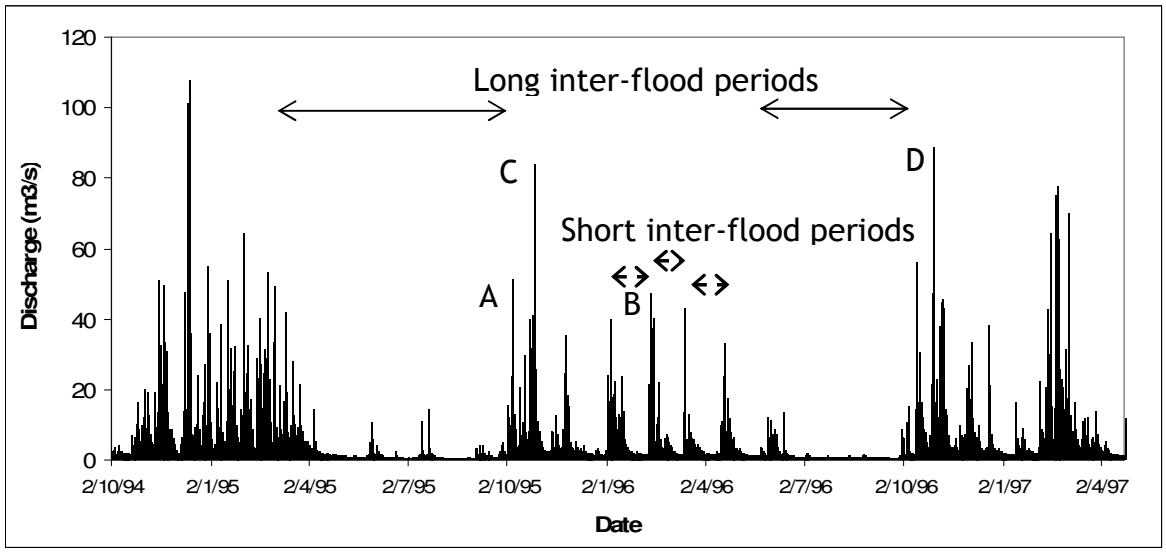

Fig. 2-5. Schematic of interflood periods. Following Reid et al. (1985), bedload transport rates for the similar flow events A - B and C-D will be different due to the time lapsed since the previous spate.

In the last few years other authors have started undertaking dedicated studies to analyse the influence of flow magnitude and duration of antecedent conditions on particle entrainment (Saadi, 2002; Paphitis and Collins, 2005; Monteith and Pender, 2005; Haynes and Pender, 2007; and Ockelford and Haynes, 2008). Saadi (2002) used a bimodal sand-gravel mixture and a series of steady and unsteady flows in laboratory flume to analyse the effect of flow history and hydrograph shape on entrainment values. Although his test hydrographs were not sub-threshold, results for his steady flow experiments showed that beds became stronger with the duration of flow exposure, with averaged critical bed shear stress values accorss all grain sizes in the region of 30%, 45% and 60% higher than the 3h run for the 6h, 9h and 12h experiments respectively. In contrast, when accelerating flows were used as antecedent conditions (range of duration 6-12h), maximum bed stability (+14% higher than the 6h run) was achieved for an intermediate (9h) flow duration. Paphitis and Collins (2005) used uniform sand beds to study the effect of the duration (5-120 min) and magnitude (70-95% of

threshold velocity) of antecedent steady flows on entrainment. Their flume-based results showed that granular bed stability (measured as critical shear velocity) increased up to 27% with flow exposure duration and with magnitude of the sub-threshold flows applied. They suggested that particle rearrangement under sub-threshold conditions (no general movement) resulted in grain re-orientation, increased particle imbrication and bed compactation. They developed a correction factor for critical shear velocity based on their results and using the duration of exposure as main variable. Hassan *et al.* (2006) analysed the effect of flood hydrograph shape on bed composition and armouring using 1D mathematical modelling. Although the flows they used were above threshold, their results are still relevant. Using long steady flows (96 h) and hydrographs of varying duration and shape, they noted that bed resistance increased with flow duration for experiments with similar discharge rates due to increased armouring. They concluded that long steps of constant flows within hydrographs, i.e. slowly rising flows, produce equivalent effects to entire runs of constant flow. Haynes and Pender (2007) used steady flows of varying magnitudes (53-91% of critical bed shear stress for the D_{50}) and durations (30-5760 min) to water work a bimodal sand-gravel bed (D_{50} = 4.8mm, σ_g = 2.1). They showed a general increase of bed stability with flow duration but, contrary to Paphitis and Collins (2005), a decrease of bed strength with the magnitude of sub-threshold flows, with increases of cumulative bedload of 5.6 and 7.5 times for durations of 30 and 1440 min respectively when the percentage of bed shear stress applied increased from 53% to 91%. Haynes and Pender (2007) proposed that this opposing result could potentially be explained by the differences of bed material, where fines were winnowed from the bimodal bed in Haynes and Pender (2007). In contrast, no size selectivity was possible in the uniform sand of Paphitis and Collins (2005) and different bed stability mechanisms related to multi-size mixtures may alter the effect of antecedent conditions. In situ particle rearrangements were also used by Haynes and Pender (2007) to explain the increase of bed stability with flow exposure. Ockelford and Haynes (2008) ran increasingly longer durations of steady flows, set at 50% of bed critical shear stress, over three granular mixtures (uniform, unimodal and bimodal) with common median diameter D_{50} = 4.8 mm. They showed that critical bed shear stress consistently increased with duration of flow exposure, with the uniform

and bimodal gravels being most and least responsive to antecedent conditions respectively. Similarly to Haynes and Pender (2007), they also showed signs of maximum stability reached by antecedent conditions related to the longest duration, 60 minutes. Their results suggest that the bed surface becomes hydraulically smoother as the length of flow exposure increases. It is seen then, that the magnitude and duration of flow exposure changes bed resistance and sediment available for transport.

Current knowledge of the effect of antecedent conditions on entrainment of granular beds can be summarised as follows:

- There is evidence that the magnitude and duration of antecedent conditions modifies bed entrainment thresholds. There are some indications that the characteristics of antecedent flows (constant or increasing flows) produce different results.
- There are differences in the effects of sub-threshold flows depending on bed composition, related to local mechanisms of imbrication and surface structuring.
- There appears to be a maximum increase of bed resistance achievable by flow history; which varies with bed and flow properties.
- Almost all relevant research on the relationship between flow history and bed stability has been carried out using constant flows. If only sub-threshold flows are considered, there appears to be no research on the link between particle entrainment and varying flows.

Whilst the above demonstrates the potential implications of flow history on bed stability and the need for advancement in this area of flow-sediment research, there are few investigations available. Thus, there is a clear absence of research on the influence of sub-threshold rates of flow acceleration (rising limb gradient) on the stability of non-uniform gravel beds.

2.5 *Methods for estimating entrainment*

While it has been shown above that entrainment thresholds do change with particle and bed characteristics, slope and flow history, the key question of how to estimate their value remains, as entrainment thresholds are essential for a range of aspects of river engineering and morphology (section 2.2.1), eg. the estimation of solid transport rates (Chapter 5).

The problem of sediment transport and initiation of particle motion has been studied for many decades (Buffington and Montgomery, 1997). Work by Gilbert (1914) (in Lisle and Church, 2002, and Camenen and Larson, 2005) and Hjulström (1935) (in Miller *et al.*, 1977, Knighton, 1998) started the study of particle motion under fluid forces. Shields (1936) produced a major advancement in sediment transport studies, who determined the bed critical shear stress by extrapolating paired measurements of shear stress and bedload transport rates to a zero level of transport (Carson and Griffiths, 1985, 1987) (Fig. 2-6). Shields' work proved pivotal in the development of entrainment threshold research and his parameter and graph are widely used in sediment transport studies.

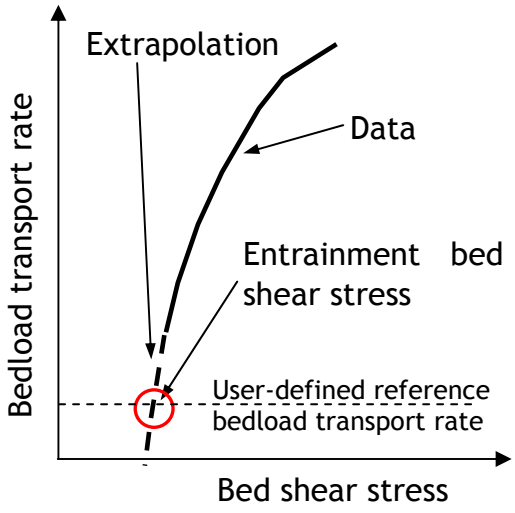

Fig. 2-6. Schematic of estimation of entrainment threshold by extrapolation to a low (or zero) reference bedload transport.

However, despite continued revisions and development of Shields' work, there is still a large degree of uncertainty in accurately quantifying the critical conditions required for particle movement (Buffington and Montgomery 1997; Knighton, 1998; Church *et al.*, 1998). Miller *et al.* (1977) redrew Shields' curve using a *threshold envelope* to denote the upper and lower bounds of threshold

uncertainty, reflecting the partial stochastic nature of entrainment, which some later researchers believe that the concept of a unique entrainment threshold is not only practically impossible but also its definition is meaningless given the highly variable character of flow turbulence (Lavelle and Mofjeld, 1987). Although subsequent studies have included uncertainty envelopes to include large scatter in the results using Shields' methodology, the Shields' curve and his dimensionless parameter, have formed the basis of numerous sediment transport studies (Miller *et al.*, 1977; Wilcock and McArdell, 1993; Buffington and Montgomery, 1997; Shvidchenko and Pender, 2000; Paphitis, 2001).

The available methods for estimating entrainment thresholds can be divided into deterministic and stochastic, depending on the approach adopted. Note that the use of the term *estimation* is very much intended here, given the described uncertainties of its value. Within the deterministic methodologies, the visual method (Neill and Yalin, 1969) and reference transport method (Shields, 1936; Parker *et al.*, 1982a, Wilcock and Southard, 1988; Shvidchenko *et al.*, 2001; Wilcock and Crowe, 2003) are the most widely applied. Other methods include the largest mobile grain. Pertinent to the present thesis is a review of the main available approaches to entrainment estimation. This is provided below.

2.5.1 Competence or largest grain method

The largest mobile grain criterion, also called competence method, is based on assuming that the bed critical shear stress is that required to move the coarsest size within the mixture mobilised during the flood event (Andrews, 1983). It requires the presence in the bed of larger, immobile particles than the size class used as reference; hence, it is only applicable in graded material (Buffington and Montgomery, 1997). The largest grain method is sensitive to size and efficiency of the sediment trap, sample size, sampling strategy and the availability of coarser grains (Buffington and Montgomery, 1997); thus, it is not appropriate for situations in which equal mobility is present. This method is seldomly used, with the visual method and the reference transport methods being much more widely applied.

2.5.2 Visual Method

The visual observation method considers entrainment is achieved when an arbitrary minimum number of grains N is displaced from a certain bed area A within a specified time t of observation. Although easy to understand qualitatively, the visual method contains an intrinsic degree of subjectivity when it comes to defining the *degree of movement* and the minimum number of grain detachments necessary. Some attempts to reduce this subjectivity and make this method more quantitatively sound were made by Neill and Yalin, (1969), who proposed $ND^3/u_* = 10^{-6}$ as a quantitative criterion of movement for uniform material, with D = grain size, u_* = bed shear stress and the constant 10^{-6} defined as the practical limit that can be reasonably be observed in open channel experiments (Neill and Yalin, 1969) . Paphitis and Collins (2005) proposed an expression that explicitly included A and t (section 3.4.6.1). Wilcock (1988) modified Neill and Yalin's (1969) procedure to be applicable to multi-size beds. If the time required to record the minimum number of particles is considerable, the reworking and strengthening of the bed due to stress history may alter the results (Paphitis and Collins, 2005). Thus, the application of this method is conditioned by time and space scale issues. The number of grains required for entrainment will vary with the area of observation, as more grains available for movement are pesent in larger areas. Similarly, the longer the observation period is, the higher the number of grain movements will be necessary to define entrainment. In the case of graded material, the percentage of the size class selected for defining the bed mobility on the bed will also affect number of particles (Wilcock, 1988), as the more abundant the grains are on the bed, the higher the number of movements will be required to achieve the condition of entrainment (section 3.4.6.1). However, neither Wilcock (1998) or Paphitis and Collins (2005) changed or indeed questioned the value of the constant 10^{-6}.

Dancey *et al.* (2002) proposed an alternative entrainment threshold based on the movement of a minimum number of particles over an area and time scale related to the total number of particles available on the surface, given by the *packing density*, defined as the ratio of the total projected area of the sediment to the total bed area. They showed that for low packing density (approximately < 0.25) values of sediment transport load and Shields' stresses are fairly

independent of the packing configuration, as for low packing density grains approach isolation and independence of movement. For larger packing, transport load and Shields' stresses increase with packing, due to particle interaction. This additional entrainment threshold was developed using uniform flows over unisize spherical glass grains, thus very different to real flow and sediment conditions in natural rivers and therefore, is restricted to this special case. However, it highlights the effect of particle interaction on entrainment.

2.5.3 Reference transport rate

The reference transport method is based on the extrapolation of the relationship between bedload rate and bed shear stress to a zero, or small, *reference* transport rate to determine the entrainment threshold (Fig. 2-6). This method has been extensively used by a number of authors (Shields, 1936; Parker *et al.*, 1982a; Shvidchenko *et al.*, 2001; Wilcock and Crowe, 2003). Shields (1936) effectively used this criterion for his analysis of entrainment threshold by extrapolating his results to a zero transport value. He used uniform material where the definition of the relevant size D is unique. However, when graded material is used, the analysis is carried out for each size fraction and individual particle sizes are defined by D_i. The methodology, and especially the value of reference dimensionless volumetric transport rate W_i^*, usually taken as 0.002 (Parker *et al.*, 1982a, Wilcock, 1988, Wilcock and Southard, 1988, Kuhnle, 1993), has been widely followed by those authors applying this technique (Wilcock, 1988; Wilcock and Southard, 1988; Kuhnle, 1993; Paphitis, 2001; and Almedeij *et al.*, 2006). Parker *et al.* (1982a) initially used the size composition of the subsurface layer; however, as Ashworth and Ferguson (1989) had done before, Parker later changed it to the bed surface grading (Parker, 1990).

Shvidchenko *et al.* (2001) presented an alternative reference transport method, which defined critical conditions when the dimensionless mass transport rate q_b^*, based on the Einstein (1950) bedload parameter, reached 10^{-4}. Shvidchenko *et al.* (2001) linked the value of q_b^* to the intensity of sediment motion, which they interpreted as the probability of a particle on the bed surface will be entrained any given second (Shvidchenko and Pender, 2000). Their bedload data

q_b* were fitted by an equation that produces straight lines when ploted against Shields parameter in logarithmic axes (Fig. 2-7, section 3.4.6.2).

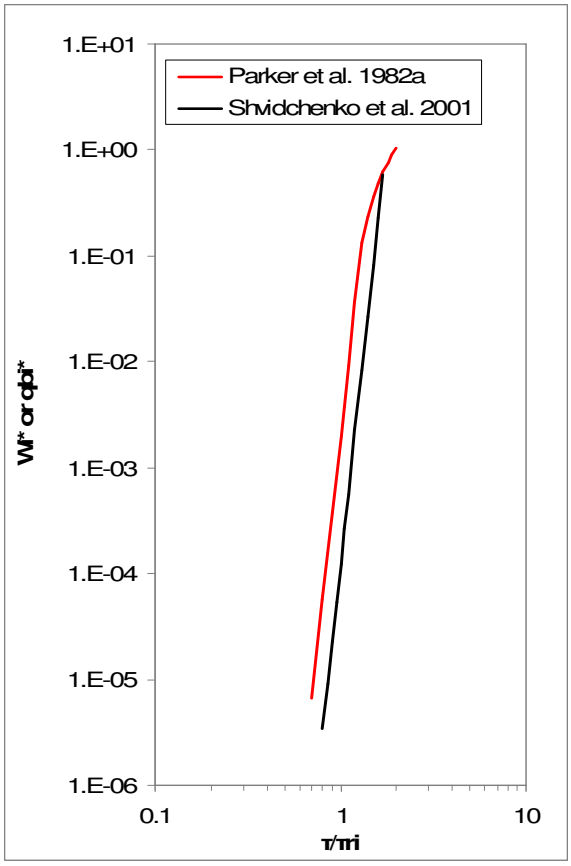

Fig. 2-7. Comparison of fitting lines of Parker et al.'s (1982a) and Shvidchenko et al.'s (2001) reference transport method.

Plots of Parker *et al.*'s (1982a) and Shvidchenko *et al.*'s (2001) procedures are similar: both based on values of bedload transport rates and bed shear stress. However, Parker *et al.*'s (1982a) method uses volumetric transport rates whereas Shvidchenko *et al.*'s (2001) method uses mass rates. This change of units results in different values of W_i* and q_b* for the same shear stress (Fig. 2-7). In addition, as mentioned above, Shvidchenko *et al.*'s (2001) method only considers a single curve, whereas the equation proposed by Wilcock and Crowe (2003), used here during the application of Parker *et al.*'s (1982a) procedure, includes two sections, a straight line similar to Shvidchenko *et al.* (2001) for low-medium transport rates and a convex curve for higher transport rates (Fig. 2-7).These discrepancies result in the two methods producing different values of entrainment thresholds for the same data sets. The relationship between these two criteria was provided by Shvidchenko *et al.* (2001) as θ_{cri} *Parker* = 1.20 [θ_{cri} *Shvidchenko*]$^{1.09}$. Both methodologies are used for the experiments presented, allowing the contrasting of their results, benefits and applicability. These are contained in the appropriate section in Chapters 3, 4 and 6.

2.5.4 Stochastic approach

The stochastic nature of sediment transport has been widely discussed in literature (Papanicolaou *et al.*, 2002; Kleinhans and van Rijn, 2002; Dancey *et*

al., 2002; Sarmiento and Falcon, 2006). In recent years, a number of researchers have explored the quantification of sediment entrainment and transport assuming that the entrainment threshold is a stochastic variable, since turbulence is mainly responsible for the entrainment of grains (Paphitis and Collins, 2005). Stochastic or theoretical models are based on the idealisation of particle size, shape and arrangement. A balance of moving and resisting forces is established in order to obtain the required mobility threshold. These methods usually adopt spherical particles of unisize mixtures of varying packing conditions (McEwan and Heald, 2001; Papanicolaou *et al.,* 2002). The concept of stochastic models is based on the assumption that both the destabilising and resisting forces are statistical variables to which a probability distribution function can be associated (Grass, 1970; Andrews and Parker, 1987; Papanicolaou *et al.*, 2002; Kleinhans and van Rijn, 2002; Sarmiento *et al.,* 2006). If the two curves do not overlap, there is no movement (Fig. 2-8). When the tails of the curves first touch the critical entrainment condition is achieved. As the curves continue to overlap more and more grain sizes are likely to be entrained and the intensity of particle transport increases (Andrews and Parker, 1987).

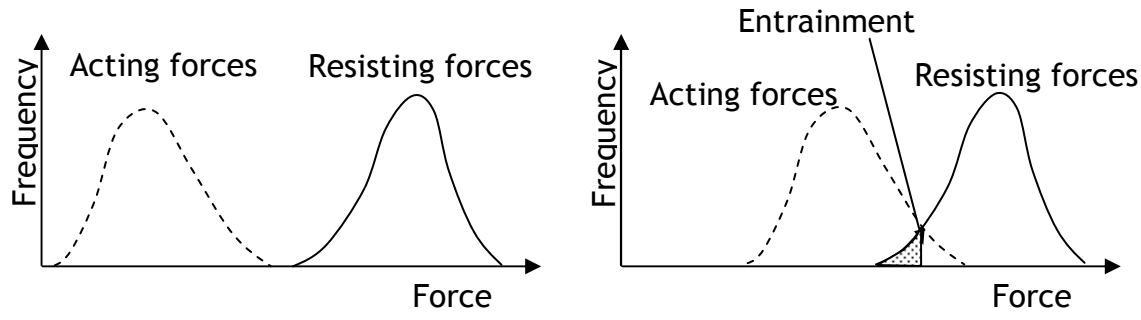

Fig. 2-8. Schematic illustrating the concept of probabilistic entrainment. Overlapping of acting and resisting forces will result in entrainment of particles from the bed.

Stochastic methods are based on the generation of a probability density function for particle movement, based on dynamic equilibrium equations. They generally include simplified representations of the fluid forces (McEwan and Head, 2001; Papnicolaou *et al.*, 2002; Wu and Chou, 2003; Sarmiento and Falcon, 2006). The simplifications of grain geometry, packing and hydraulics adopted by the stochastic approaches, although adequate for the development of theoretical equations, are too onerous for accurately representing natural sediments and, hence, differ too much from the conditions present in this thesis. Ironically, the

stochastic character of sediment transport and entrainment favour the introduction of an entrainment threshold that assumes a minimum (low) amount of transport so some stability of the threshold can be obtained under turbulent conditions (Parker *et al.*, 1982a; Wilcock, 1993; Shvidchenko and Pender, 2000; Paphitis and Collins, 2005); this would thus support using a deterministic method of estimating entrainment threshold, rather than stochastic, for the conditions of natural, graded sediment used in the present thesis.

2.5.5 Discussion of methods

Depending on the choice of criterion, hydraulic conditions for incipient motion will differ (Garde and Ranga Raju, 1977; Carson and Griffiths, 1985, 1987). Buffington and Montgomery (1997) reviewed the results presented by various authors who used any of the above methods, and highlighted some advantages and disadvantages. They found that the dimensionless critical shear stresses for the median size θ_{cr50} obtained by the largest grain method (also called competence-based method) are roughly 15% to 30% smaller than the reference transport method estimates, when obtained from the same study site. For high values of Reynolds number Re_*, critical shear stress determined by the reference transport rate is usually larger than the results from the visual method (Buffington and Montgomery, 1997). This difference is further discussed in this thesis. Sampling techniques and the definition of D_{50} also influence θ_{cr} (Buffington and Montgomery, 1997). The method, equipment and efficiency of the sampler used for collecting bedload data may determine the maximum or minimum grain size recorded and therefore change bedload composition values. Similarly, errors in the estimation of characteristic bed surface grain diameters, eg. D_{50}, which are commonly used in calculations and to represent the bed size, may produce scatter in the results.

Since the visual method is based on the determination of the minimum number of displacements, the estimation of critical stress is directly based on recorded particle movements. However, the reference transport method relies on the extrapolation of transport curves, which is often based on subjective judgement in line fitting (Parker *et al.*, 1982a; Wilcock and Southard, 1988; Wilcock, 1993;

and Wilcock and McArdell, 1993). As a result, the comparison of results provided by different methods may prove very difficult or even impossible. For instance, Wilcock (1988) could not find an independent way of assessing the accuracy of either of the data sets obtained when using the reference transport and largest-grain methods. Practical considerations (time and area scaling depending on particle size used) were suggested by Wilcock (1988) for his preference of the reference transport method over the largest-grain method.

It has been demonstrated that there is a large degree of uncertainty in the estimation of entrainment thresholds due to: (1) the method and criterion applied; (2) the random nature of fluid forces; and, (3) the very high variety of factors associated with bed particle characteristics (packing, grading, particle shape, bed slope, etc.). However, it is considered here that the adoption of a value of threshold of motion is still the most practical approach to define entrainment for their essential role in sediment transport equations (Chapter 5) (Wilcock and Crowe, 2003; van Rijn, 2007a; Recking, 2010). As discussed by McEwan and Heald (2001), probabilistic methods for determining entrainment have not been widely adopted for practical purposes because they are more complex to implement than deterministic ones without providing considerable improvement in the accuracy and reliability of the results. Of the methods presented, the visual method and the reference transport method will be applied in this research because their wide use and possibility to compare results with previous authors.

Finally, the estimation of bed shear stress is an essential component of the application of entrainment methods and the calculations performed in this thesis. A number of methods for calculating bed shear stress are available (Wilcock, 1993; Durst *et al.*, 1996; Graf, 1998), three of the most widely used: bed-slope, Reynolds stresses and velocity profile, are discussed in Chapter 3. Because of the higher complexity of the method based on the use of velocity profiles, a dedicated section to its theoretical background and applicability issues is presented below.

2.6 *Velocity profiles*

2.6.1 Law of the Wall

It is commonly accepted that Prandtl's log-law (Prandtl, 1925) describes the vertical distribution of streamwise velocity *u* in the inner layer of open channel flows, i.e. from the top of the viscous layer to approximately z/h = 0.2, where *z* is the distance from the bed level and *h* is the flow depth (Nezu and Nakagawa 1993; Graf 1998; Pokrajac *et al.*, 2006; Nystrom *et al.*, 2007). This range of validity of the logarithmic profile has been used by many authors when applying the Clauser method (Robert, 1990; Song and Chiew, 2001; Pokrajac *et al.*, 2006; Dey and Raikar, 2007), which involves fitting a straight line to the velocity data points plotted against the natural logarithm of z (Fig. 2-9), to obtain bed shear velocity u_*. Thus, it is commonplace to employ the log-law in hydraulics to analyse flow characteristics and estimate shear stress at the flow-bed boundary.

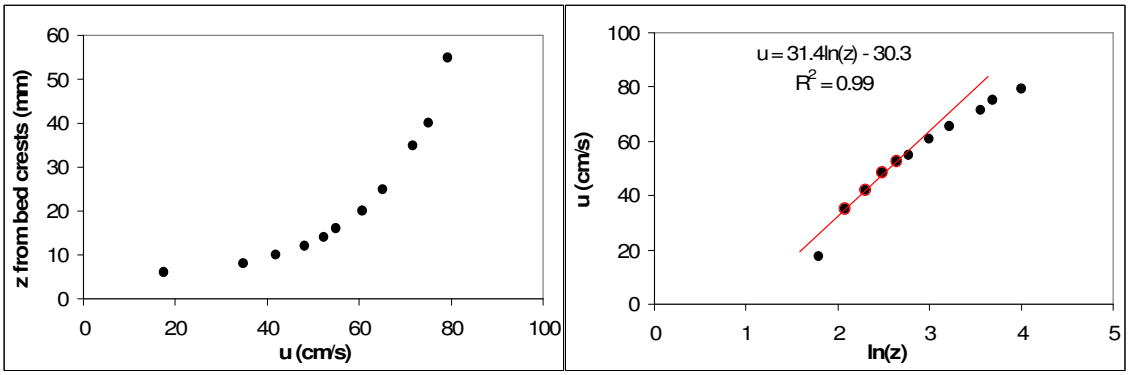

Fig. 2-9. Example of application of the Clauser method. A) Velocity profile data, B) Plot of velocity values against ln(z) and line fit.

The logarithmic velocity profile formulation stems from Prandtl's (1925) universal Law of the Wall and it is generally represented by:

$$\frac{u(z)}{u_*} = \frac{1}{\kappa}\ln(z) + C \qquad \text{Eq. 2-4}$$

where *C* is the constant of integration, and κ = von Karman's constant, usually taken as 0.4.

According to Oertel *et al.* (2004) the total shear stress is made of the mean value of the viscous stress and the apparent shear stress due to turbulence:

$$\tau = \mu\frac{du}{dz} + \rho l^2\left(\frac{du}{dz}\right)^2 \qquad \text{Eq. 2-5}$$

The first term is only important very close to the bed, in the viscous sub-layer (a classical subdivision of the flow depth into layers at various distances from the boundary, including a viscous, logarithmic or inner layer and an outer layer). For large Reynolds numbers, i.e. turbulent flows, the second term is much larger than the first and the shear stress due to viscosity may be neglected; the resulting equation gives the relationship between shear stress and velocity variation with distance from the bed:

$$\sqrt{\frac{\tau}{\rho}} = l\frac{du}{dz} \qquad \textit{Eq. 2-6}$$

The proportionality factor is the mixing length l. The simplest expression relating l and z is $l = \kappa z$ (Chadwick *et al.*, 2004; Oertel, 2004; Dey and Raikar, 2007), where κ= von Kármán constant (0.4 for clear flow). When this expression is inserted in equation 2-6, calling $\sqrt{\tau/\rho} = u_*$ shear velocity, the following equation is obtained:

$$u_* = \kappa z\frac{du}{dz} \qquad \textit{Eq. 2-7}$$

The integration of equation 2-7 results in the well known log-law (equation 2-4), which has two main expressions:

$$\frac{u}{u_*} = \frac{1}{\kappa}\ln\left(\frac{z+d}{k_s}\right) + B \qquad \textit{Eq. 2-8}$$

$$\frac{u}{u_*} = \frac{1}{\kappa}\ln\left(\frac{z+d}{z_0}\right) \qquad \textit{Eq. 2-9}$$

These two equations come from using a grain roughness parameter k_s and a constant of integration B (Graf, 1998; Dey and Raikar, 2007) or imposing the boundary condition u = 0 at the virtual bed level, with z_0 representing the bed roughness height (Wilcock, 1996; Prokrajac *et al.*, 2006). Fig. 2-10 contains a sketch of the main physical parameters discussed in this thesis.

The above equations represent a simplified theoretical framework for much more complex coherent flow structures. Thus, Prandtl´s theory and formulation originated from the assumptions that: (a) shear stress τ is constant throughout the region outside the viscous sub-layer; and (b) the mixing length l is linearly

related to distance from the wall by the von Kármán constant κ. Despite recognising that, in reality, shear stress reduces with distance from the wall. Oertel (2004) states that these assumptions produce useful approximations as the greater part of the velocity change happens near the boundary. Pokrajac *et al.* (2006) also indicate that the log-law can be successfully applied with linearly variable shear stress as long as depths are considerably larger than roughness heights. Thus, the logarithmic expression on equation 2-4 will hold as long as $l = \kappa \cdot z$ applies. Dey and Raikar (2007) used this criterion to determine the range of applicability of the log-law in their experiments.

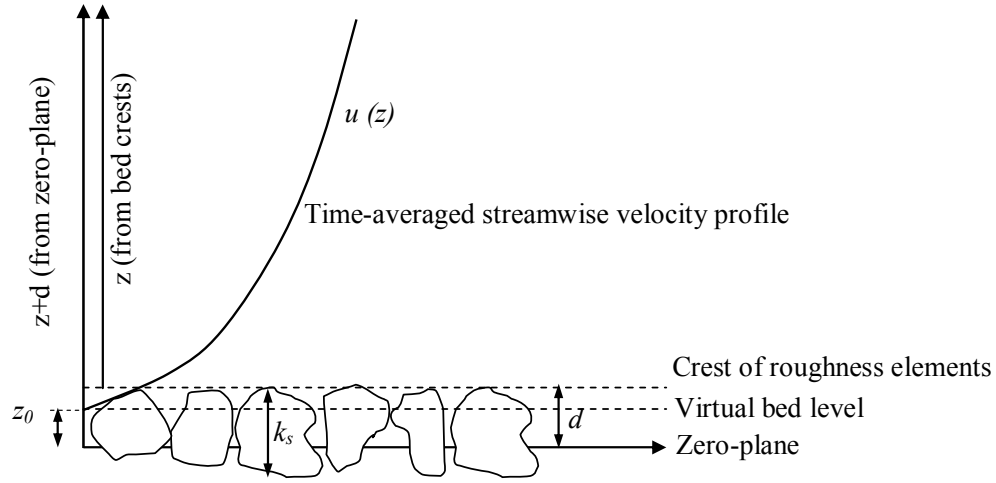

Fig. 2-10. Sketch of the geometrical elements for the log-law equation.

2.6.2 Background for the adoption of z/h = 0.2

The applicability of the log-law is commonly assumed to be within the logarithmic layer, approximately the lower 20% of the depth (Nezu and Nakagawa, 1993; Graf, 1998; Oertel *et al.*, 2004). This range is quoted from author to author with little exploration of its validity. Nikuradse's (1933) work and experimental data are often used to justify the value of z/h=0.2. Nikuradse's measurements of velocity were carried out in pipes lined with sand. Although his experiments represent a great advance in the knowledge of flow velocity and resistance in pipes, its extension to larger open channels may not be directly applicable. Monin and Yaglom (1971) state that the thickness of the logarithmic layer will not be larger than 10-20% of the thickness of the boundary layer δ, defined as the distance from the wall at which u/U_∞ = 0.99, with U_∞ = free stream velocity; or as a vertical length scale that can be either pipe radius,

boundary layer thickness or, crucially, channel half-width; this can be very different to 20% of the boundary layer.

The suitability of z/h =0.2, or the influence of larger values of z/h, is very rarely reported in open channel flow literature. Citing Bathurst *et al*. (1982), Robert (1990) notes that divergence from the logarithmic profile may be expected for $z/h > 0.2$; although does not provide any reasoning. Biron *et al*. (1998) studied the effect of the percentage of flow depth and minimum height above the bed on the estimation of bed shear stress. They reported an increase of shear stress with the percentage of flow considered until a maximum was reached in the area of 20% of flow depth. From there, shear stress values reduce with z/h. However, they recognised the considerable errors associated with their calculations and offer no conclusive explanation on whether the maximum value of shear stress is the appropriate one. Song and Chiew (2001) also considered $z/h = 0.2$ as the upper limit of the applicability of the log-law based on the widespread use of this threshold. Chen and Chiew (2003) state that the log-law is *usually* applied in the inner region, $z/h < 0.2$ and the wake law in the outer region ($z/h > 0.2$). Again, there is no justification for the value of 0.2. Pokrajac *et al*. (2006) say that "*to ensure that the log-layer is sufficiently far away from the outer boundary of the boundary layer, it is assumed to be limited to some small proportion, usually 0.15-0.2 of the boundary layer thickness*" (p. 92). Again, there is little physical reasoning provided in support of the z/h ratios cited.

Despite the repeated use of $z/h \leq 0.2$, it is very rare to find clear explanation of this value. Those who attempt to explain the origin of the depth range refer to experimental data or the work by Nikuradse (1933) (Petit, 1990; Oertel *et al*., 2004). One of the few possible justifications for $z/h \approx 0.2$ is found in Dey and Raikar (2007), where they obtain the value of the von Kármán constant based on the application of mixing length. They reported a ratio of l/δ as approximately constant up to $z/\delta = 0.23$. This is connected to the assumption of the linear relationship between mixing length l and distance from the wall z, which allows the development of the log-law in equation 2-4. Also, Nezu and Nakagawa (1993) include a general expression of the vertical variation of velocity applicable for

the entire channel, which results in the log-law when $l = \kappa \cdot z$ is assumed. The range of application of the log-law appears to rest on the linearity between l and z. However, the more general defect law, applicable in the outer layer (z/h > 0.2) (Nezu and Nakagawa, 1993) also contains equation 2-4, together with a correction term or wake function. Thus, the pertinence of the linearity of the mixing length expression as the condition for z/h = 0.2 is questioned.

Many of the referenced publications use the concept of boundary layer flows to support their adoption of z/h < 0.2. However, Monin and Yaglom (1971) state that flow in the boundary layer is different from that in pipes and channels, where the logarithmic equation may be used up to the pipe axis or the middle of the channel. This is somewhat confusing as many authors refer to boundary layer flows when analysing velocity profiles in flumes and rivers. Furthermore, to complicate matters, Nezu and Nakagawa (1993) state: *"In many instances of open-channel flows, in contrast to boundary layers, the log-law applies over the whole flow depth, from the bed to the free surface"* (p. 49). This suggests that the application of the log-law to open-channel flows should not be restricted to the lower 20% of the flow depth, thus contradicting the large body of research carried out to date.

2.6.3 Emerging argument for greater z/h ratios

In any case, definition of the range of applicability of log-law is based on fitting of the data points to a straight line in the semi-logarithmic plot and is therefore dependent on the specific data set examined. Accepting this case-dependent approach, a number of authors have used larger depth ranges to obtain bed shear stress τ and bed roughness length z_0. Robert *et al.* (1992) used the lower 30% of the flow depth for the estimation of u_* and z_0 in their flume measurements. They justified their selection based on the linearity of the semi-log plot of the velocity profile within this range. However, for their river flow data, they used the full profile "*whenever the profiles appear relatively straight on a semi-logarithmic scale*" (p. 732). In explanation of his methods applied to field data Wilcock (1996) assumes that the upper limit of the log-law is $h/5$; however, he uses the lower 50% of the flow depth for his line fitting in order to

include at least 6 data points. Furthermore, citing Cardoso *et al*. (1989), Smart (1999) reported that the log-law was successfully applied to his field data over the entire channel depth. Smart (1999) also says that where velocity data follow the log-law, plotting u as a function of $ln(z)$ will indicate a straight line with gradient u_* / κ and intercept $-u_*/\kappa ln(z_0)$. Hence, this leaves open the range of applicability of the log-law so long as data fit a straight line. Smart (1999) reported ranges of straight line fitting up to 80%, with typical values ranging from 5-50%. Lamarre and Roy (2005) also used the full depth range for the best fit in the semi-logarithmic plot of their field velocity data. They found that most velocity profiles were approximately linear over the full depth and, therefore, results using 20% were similar to those obtained using the full (100%) depth. They also commented on Biron *et al*.'s (1998) study of the sensitivity to depth range and the underestimation of shear velocity found by these authors when using the full flow depth. However, the field work by Biron *et al*. (1998) only considered three velocity profiles and one of these provided results considerably different to the other two, so their conclusions should be taken with care. Overall, these studies clearly suggest that the size of the logarithmic layer is variable and can extend to well over z/h = 0.2. Furthermore, in a recent study of the use of the log-law to estimate bed shear velocity in flume experiments and a range of beds (uniform medium gravel D_{50} = 4.8 mm, unimodal graded gravel D_{50} = 6.9 mm and near uniform gravel bed D_{50} = 4.8 mm), Piedra *et al*. (2009)[1] observed that a logarithmic equation could describe streamwise velocity values for flow ranges of at least z/h=0.5. Thus, there is sufficient evidence to question the restriction of application of the logarithmic Law of the Wall to the lower 20% of the depth in river and flume flows. The extension of the log-law further than this limit will be tested in this research work.

2.7 *Present and future hydrological context*

Daily, monthly and seasonal flow cycles occur in rivers, whether these correspond to natural or artificial regimes. Continuous fluctuations of river flows due to rainfall events and catchment characteristics determine the rate of flow

[1] A copy of this publication is enclosed in Appendix 9.

rise and with it, hydrograph shape. Short intense rainfall events tend to produce rapidly rising discharges, resulting in very steep hydrographs; whereas longer rains result in lower flow increase rates. These differences in rising limb characteristics can be extended to seasonal variations, where the transition from summer to winter will progressively increase water depths in river channels. The character of the river flow regime will also exercise an influence on the bed composition and mobility (Allan and Frostick, 1999; Powell *et al.*, 2001). In catchments characterised by short intense floods (ephemeral, Mediterranean rivers, Reid and Laronne, 1995) the effect of flow history will be smaller, as there is little time for sub-threshold flows to act over the bed before the sediment material is remobilised. On the contrary, in climates where continuous baseflows are larger and where flood events occur during longer periods, the effects of flow history discussed here may be more prevalent (Hassan *et al.*, 2006). Similar arguments also apply to climates where frequent floods remobilise and remix the bed material regularly, as opposed to catchments where high flow events are only present once or twice a year (snow-melt regimes) with sub-threshold flows acting for the majority of the year.

Artificial hydrological regimes imposed by river regulation will also produce different rates of flow increases; for instance, (1) hydropower generation is characterised by short periods of water release, producing rapid peak flows; (2) reservoir releases aimed at channel management include flushing flows designed to reduce fine content of the bed material (Kondolf and Wilcock, 1996; Wilcock *et al.*, 1996) must be carefully designed and carried out for optimum results. Given the prevalence that renewable energy sources, in particular hydropower, will continue to have in the future (MacLeod *et al.*, 2006), research into the impacts of changes of hydrological conditions on river bed stability/mobility is essential.

Furthermore, the ever present uncertainty of climate change and its effect on regional and local hydrology clearly increases the need for assessment of the potential effect on our rivers (Goudie, 2006) and the innumerable amount of structures within or at the edge of river channels. Recent research on the future UK climate suggests that winter precipitation is likely to exhibit a marked

increase, whereas summer rainfall will decrease, albeit in smaller quantity. Approximate broad ranges of rainfall changes from the 1961-90 baseline for the 2050s are -1 to +30% and -35 to +10% for winter and summer respectively (UKCP09[2]). More specifically, the climate in Scotland is likely to become considerably wetter in winter, with more intense stormy rainfall events; and summers may become longer and drier (Werritty with Chatterton, 2004). These climatic changes will cause more marked seasonality with a significant effect on catchment hydrology and the fluvial system. Flood peak discharges will become higher in magnitude and longer in duration in response to increases in the number of days of heavy rain and the intensity of the rainfall (Barnett, *et al.*, 2006). Baseflows will become more extreme, with wetter winters raising baseflow levels and drier summers lowering them. If these trends actually occur, changes of river regimes and flood event hydrographs are to be expected. The links between hydrograph shape, interflood spacing, sub-threshold flows and grain entrainment suggest consequences for the stability of river channels. Werritty and Hoey (2004) recognised that there is need for further studies of river response to climatic conditions, particularly the changes in river channel geometry, where the identification of trends is restricted by a lack of available data. Current national and international policy (EU, 2000; SEPA, 2007) explicitly includes the maintenance and improvement of the geomorphological status of fluvial systems.

However, not only fluvial geomorphology could be affected by modified river regimes (Richter and Richter, 2000; Gordon and Meentemeyer, 2006; Goudie, 2006). Living species that depend on flow regimes and river bed conditions for their survival may also be affected (Power *et al.*, 1996; Dixon, 2003). Hoey and Thomas (2006) showed that hydrological regimes can affect the development of pearl mussel communities. In their study of the River Kerry, NW Scotland, they suggest that pearl mussel populations thrive in a regulated flow regime, which seems to be in contradiction with general concepts of flow regulation and human impact on living species. Scotland's gravel bed rivers form ideal salmon spawning grounds that are important for economic, recreational and environmental

[2] http://ukclimateprojections.defra.gov.uk, accessed on 07/04/10

reasons. However, this habitat requires a delicate balance between flow and sediment variables that can be disturbed by river regulation or changes in seasonal flows. Salmon spawning requires river bed particle composition that allows adult fish to wash out fine material from the bed, using the interstices left by the coarser matrix to lay their eggs (Parker *et al.*, 1982b). Whilst substrate stability is necessary for adequate egg protection, too low a flow reduces oxygenation and waste removal and suffocates eggs by the deposition of fines (Lisle and Lewis, 1992). If bedload transport and bed grain composition are affected by changes of hydrological conditions, their natural habitats may also change.

Since, only on very few occasions gravel bed rivers experience large enough flows to mobilise the bed (Parker *et al.*, 1982a; Parker and Klingemann, 1982; Church *et al.*, 1998) river flows will remain sub-threshold for long periods of time. As summarised above, these frequent non-mobilising flows can potentially cause changes in bed stability through partial transport, and bed restructuring. The changes in hydrological conditions and variability of rising limbs, together with the evidence of the effect of magnitude and duration of sub-threshold flows, lead to question whether different rates of flow increase will alter bed material stability, and therefore bedload transport and bed composition, during these long periods of sub-threshold flows and particle mobilising events.

2.8 *Concluding comments*

Grain entrainment has been shown to depend on many factors: absolute and relative particle sizes, imbrication, bed slope, hydraulic conditions, etc. Despite the practical and theoretical limitations for the estimation of entrainment discussed here, a value of the fluid forces required for initiation of motion must be defined, as calculations and comparison between data sets are necessary. It has also been discussed that the large majority of existing knowledge on entrainment processes and especially values is based on constant flows. The past work presented provides some evidence for the importance of flow history and hydrograph shape on entrainment and solid transport in gravel bed rivers. However, little specific research has been carried out on the impact of flood

hydrograph shape on bed stability. In particular, the effect of increasing flow rates during the rising limb of hydrological events has not been considered.

This literature review clearly demonstrates the complexity of sediment transport mechanics and the large number of factors influencing particle entrainment. Thus, achieving a generally valid definition and estimation of entrainment thresholds remains difficult. More specifically, the influence of flow history, which includes duration and magnitude of interflood periods as well as hydrograph shape and frequency, is being increasingly studied. The study of sediment transport and validation of the proposed equations are further complicated by the fact that most transporting river flows are too large for safe sampling, which makes available data at high transport rates very limited (Powell *et al.*, 2001; Wilcock and Crowe, 2003; Parker, 2004). The result is a forced reliance on laboratory experimentation, where particle characteristics, channel geometry and flows are easier to control. However, limitations of flume experiments such as particle and geometry scaling, reduced particle size range and flow conditions, may not result in comprehensive reproduction of the processes present in full scale rivers. Thus, results and formulae produced in a laboratory may not be entirely applicable to prototype channels (Ashmore, 1988; Bathurst, 2007; Recking, 2009). However, major advantages of flume investigation are the highly controlled physical conditions set, improved ability to collect multiple data and deploy equipment unattainable in the field and, importantly, do so under safe conditions.

As described, the need for appropriate assessments of sediment transport quantities and river channel stability continues to be required, driven further by climatic and energy factors. Therefore, improving results of bedload transport equations remains a priority in hydraulic engineering. Ackers and White (1973) recommended studying the combination of graded material and unsteady flows thirty-seven years ago, and this recommendation remains relevant today. The research presented here aims to contribute to this goal by providing increased understanding of the mechanics of sediment transport and proposing new methodologies and formulations to estimate entrainment and bedload transport quantities.

The brief summary of factors affecting grain entrainment presented here shows the extreme complexity of the sediment transport mechanisms and the difficulty of accurately representing them. One can appreciate better why most of the research carried out to date has been based on steady flow. However, as research progresses, it is required to extend our understanding of the general processes of sediment entrainment and transport under varying flows, as they are more representative of natural (if more complex) flow conditions and therefore a step towards universal application of the findings. This research is a step in that direction. Here, the work of previous authors such as Saadi (2002), Paphitis and Collins (2005) and Haynes and Pender (2007), is combined and extended to analyse the effect of sub-threshold flow acceleration rates on entrainment and bedload transport of gravel beds.

Chapter 3
Experimental methods and techniques

"This is the foundation of all. We are not to imagine or suppose, but to discover, what nature does or may be made to do." - Francis Bacon.

Experimental methods and techniques

This chapter explains the equipment and techniques used in this research. The explanation focuses on new techniques or the use of standard methods applied here that are not specific to sediment transport. Where conventional techniques widely used in sediment transport studies are applied these are described briefly, with reference to relevant bibliography. The experimental work was divided in essentially three phases, related to the complexity of particle interactions and bed composition: a) The first one used near uniform gravel (Pilot Runs), b) the second used a unimodal sand-gravel mixture (Stages 1 and 2); and, c) a final phase revisited previous experimental conditions from the Pilot Runs using uniform sediment and collecting additional bedload data previously unavailable.

3.1 *Characteristics of the test beds*

3.1.1 Uniform and near-uniform gravel

A near uniform gravel mix, ranging from 2 to 8 mm (D_{50} = 4.8 mm) was used for the preliminary (pilot) runs. This mix had previously been used (Olafsdottir, 2006) for a study of entrainment and antecedent conditions, and data from this study was available for comparison. The size of this bed material was large

enough for the visual identification of individual grains for the application of the visual method, at the same time as being sufficiently mobile under the flow conditions anticipated for the research and flume characteristics; constituting a reasonable bed material for the initial experimental work. Therefore, the same bed composition was used for this research phase. The uniform gravel bed (4-5.6 mm) tested in the final phase of the experimental work, c) in the above paragraph, was used in order to compare the results between this bed and the Pilot Runs. The motivation for this comparison was two-fold: 1) the bed slopes of the Pilot Runs (1/200) and the uniform gravel phase (1/150) were different, so the effect of the slope could be assessed; and, 2) repetition of the experiments will allow confirmation of the trends observed during the Pilot Runs using both the visual and reference transport method, as bedload data was not available for the Pilot Runs.

3.1.2 Size composition of the unimodal sand-gravel bed

The selection of the sand-gravel mixture was based on the following conditions:

- The shape of the size distribution should be representative of natural stream beds. Gravel bed rivers may contain a large variety of size fractions, ranging from very coarse particles (D > 64 mm) to very fine sand (D < 0.09mm) (Church *et al.*, 1987). A scaled and truncated grain-size distribution is thus needed to represent this range in the laboratory since very small particle size may produce bedforms not present in the prototype channels and very large grains may not move under the flows attainable in the flume used.
- The size distribution must include a combination of mobile and non-mobile particles that reflect, at least partially, the grain interactions occurring in natural channels.
- The bed material must be sufficiently mobile in relation to the range of shear stress values achievable in the flume.

Many sediment transport studies have been carried out by scaling down the grain size composition of a prototype gravel bed river to create a model bed (Parker *et al.*, 1982b; Ashmore, 1988; Hassan and Reid, 1990; Church *et al.*, 1998; Hassan and Church, 2000). In the present thesis, generic scaling of the

characteristics of the bed size distribution was based on a local prototype river. The Endrick Water, a river draining into Loch Lomond, Scotland (catchment area = 271 km^2) was selected for bed size sampling. This river holds national importance and had been previously studied, including by the research partner Scottish Natural Heritage (SNH), and therefore, some information on the channel was already available (Bluck, 1971; McEwen and Lewis, 1999; Forth Fisheries Foundation, 2004).

Field data was collected during the summer of 2007 and early 2008, including bed composition, cross section geometry and hydrology of the study site. The methodology used for collecting and analysing bed size composition on site followed similar work described in Kellerhals and Bray (1971), Hey and Thorne (1983), Mosley and Tindale (1985) and Fripp and Diplas (1993). A total of over 300 kg where analysed on site, from which 4 sub-samples (2 surface and 2 subsurface, D < 16 mm) totalling around 18 kg where dried and sieved in the laboratory. The resulting surface and subsurface size distributions correspond to bulk (weight) sampling. Fig. 3-1 and Table 3-1 show the combined results obtained at two adjacent sites on a gravel bar, placed near the centre of an approx. 1 km long straight reach of the river (approx. NGR 250335, 685975).

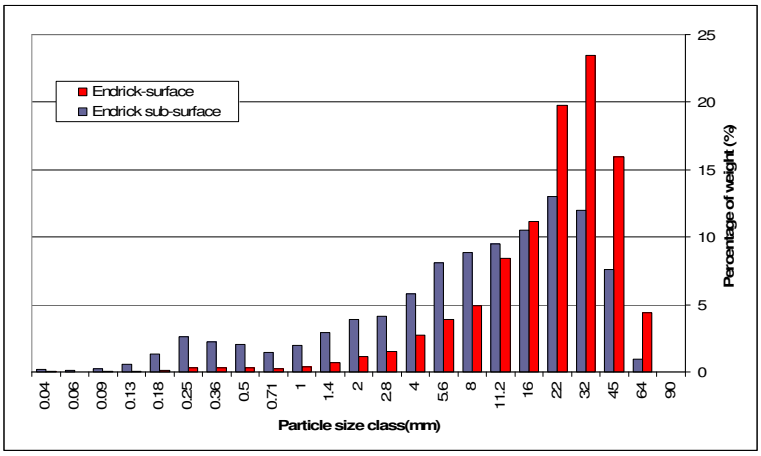

Fig. 3-1. Grain size distribution for the Endrick Water (surface layer- red, sub-surface material- blue). Particle sizes correspond to square sieve sizes in mm.

Percentile	Surface	Subsurface
D_{90}	57.3	43.4
D_{84}	50.2	36.9
D_{50}	28.9	13.0
D_{16}	10.6	2.1
sorting (σ_g)	2.17 (poorly sorted)	4.22 (very poorly sorted)

Table 3-1. Summary of grain size distributions for the Endrick Water. Diameters are in mm.

A large range of sizes are present in both surface and sub-surface samples. Sizes range from 0.063 mm to 90 mm; with higher percentages of fine material (< 1 mm) in the sub-surface (10.8%) than in the surface sample (1.6%). The surface size composition shows a strong unimodality, skewed towards the largest sizes, whereas the sub-surface data indicates a slight bimodality; nonetheless, there is still a clear skew towards large particle sizes. Church *et al*. (1987), Fripp and Diplas (1993) and Petrie and Diplas (2000) indicated that the surface layer is related to frictional characteristics of the river bed. As mobilisation of the surface layer must occur before the material present below is entrained, it is considered that the mechanics of the surface layer, and therefore its size composition, are more relevant to the study of initiation of movement (Buffington and Montgomery, 1997). Thus, a unimodal coarse-skewed size distribution was preferred. Surface bed distribution of the Endrick Water was then used to define the shape of the laboratory bed size composition. Direct geometric scaling was not possible due to the flume dimensions.

A size range containing 8 size classes (1/2 phi intervals) between 1 mm and 16 mm was used. A minimum particle size of 1 mm limited the appearance of bed forms (ripples and dunes) in the flume, not normally present in gravel bed rivers (Young and Warburton, 1996). The maximum size of 16 mm provided particles that were largely stable under flows attainable in the flume; this met the requirement of partial mobility highlighted above. The adopted unimodal, coarse-skewed size distribution met the conditions set for the experimental work (Fig. 3-2 and Table 3-2). The comparison of main size percentiles shows that for the coarser fractions the laboratory mixture has a scaling factor of 5.2-5.4, with this factor reducing for D_{50} and D_{16} to 4.4 and 2.7 respectively, indicating that the finer fraction of the laboratory mix is proportionally larger than the field

prototype. This results in the sorting parameter σ_g for the laboratory bed material being smaller than that of the field data (Table 3-2). This, as discussed earlier, is caused by the necessary truncation of the fine sizes to avoid the appearance of bedforms.

Percentile	Endrick Water (A)	Unimodal mix (B)	Ratio (A/B)
Size range	0.053-90	1-16	-
D_{90}	57.3	10.6	5.4
D_{84}	50.2	9.6	5.2
D_{50}	28.9	6.6	4.4
D_{16}	10.6	4.0	2.7
sorting (σ_g)	2.17, poorly sorted	1.57, moderately sorted	-
Skewness [(1)]	coarse skewed	coarse skewed	-

Skewness description based on Hoey (2004).

Table 3-2. Comparison of surface grain size distribution characteristics of Endrick Water and unimodal mix used in the laboratory . Size units are mm.

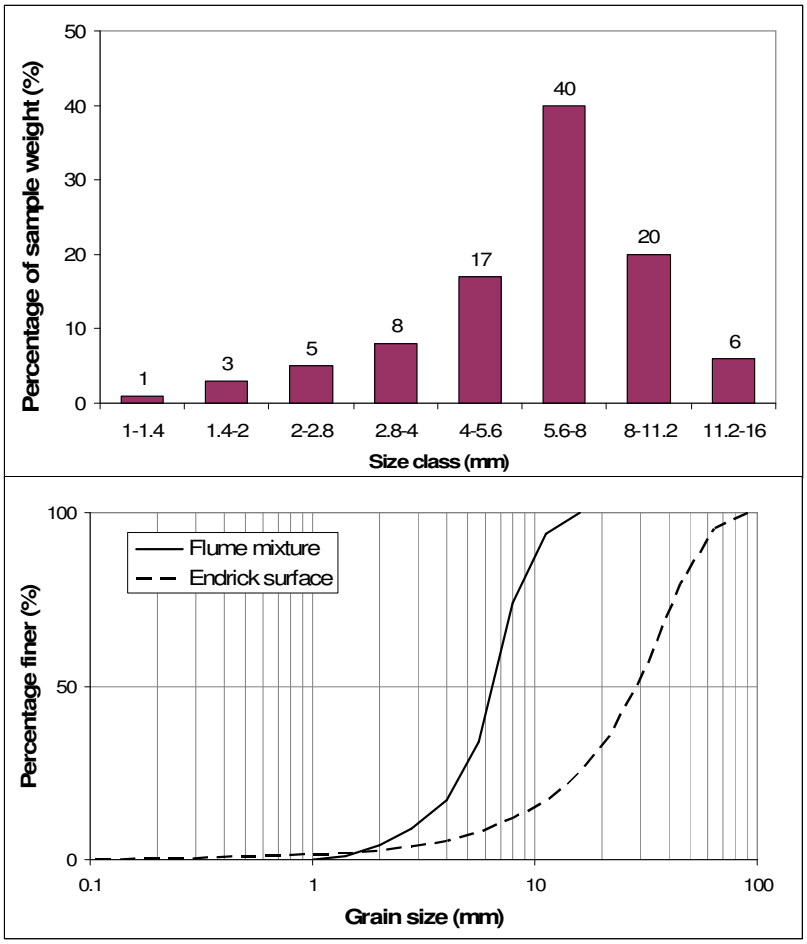

Fig. 3-2. Final bed material size distribution and comparison of cumulative size distribution between the flume mixture and surface samples of the Endrick Water.

3.1.3 Bed material type and characteristics

As discussed in Chapter 2, the properties of the bed material may influence particle stability and behaviour during running flows, eg. higher imbrication of angular grains and smaller exposure to flow of rod- or plate-like particles. The near-uniform and uniform gravel beds were made up of crushed gravel of size ranges 2.8-8 mm and 4-5.6 mm respectively and a density of 2560 kg/m^3; whereas the sand-gravel mix was composed of natural beach sediment, with the density = 2540 kg/m^3 very close to that of the crushed grains. Density values were calculated based on the volumes displaced from a measuring cylinder by 3 approximately 0.7 kg samples of different size classes. Characteristic values of grain size and sorting of the bulk mix of all the sediments are shown in Table 3-1. Particle shape analyses were also carried out following Krumbein (1941), Hayakawaa and Oguchib (2005) and UCDAVIS (2007). Results for the analysis of particle shape for the two beds used are summarised in Table 3-3.

	Near uniform Gravel	Uniform gravel	Unimodal sand-gravel
Size range	2-8	4-5.6	1-16
D_{16}	--	--	4.0
D_{50}	4.8	4.8	6.6
D_{84}	--	--	9.6
D_{90}	5.6	--	10.6
Sorting - σ_g	1.45, very well sorted	Single size	1.57, moderately sorted
Roundness [(1)]	Approx. 0.3	Approx. 0.3	0-5-0.6
Sphericity	Mainly spherical	Mainly spherical	Mainly disc or spherical

[(1)] *Mixed-size gravel data comes from direct measurements of three perpendicular axes of particles of sieve size 8-11.3mm; whereas, given the smaller size of the grains of the near-uniform bed, assessment of particle shape was carried out through visual inspection.*

Table 3-3. Grain size characteristics of test beds. Size units are mm.

It is noted here that grain shape characteristics may affect the mobility of the individual grains (Chapter 2). In particular, the use of crushed gravel for the uniform and near-uniform beds should be viewed as a result of experimental constraints. Natural gravel such as the one used for the unimodal bed are likely to represent the behaviour of gravel bed rivers more closely than the angular material used to make the well sorted beds. In particular, Monteith (2001) showed that the entrainment threshold of angular grains can be over 30% higher than river sediment of the same grain size. In this respect, values of entrainment

thresholds obtained for the well sorted material may differ from those obtained if a more natural sediment had been used. Nonetheless, the general findings of grain mechanics and the effects of antecedent conditions on granular beds (Chapter 4) are likely to be applicable to real river bed compositions.

3.1.4 Particle painting and bed mixing

The use of the reference transport method (RTM) (section 3.4.6.2) required the estimation of the bed surface composition throughout the experimental runs. Since results from the automated grading software were inadequate (section 3.4.2), an alternative semi-automated procedure, similar to that described by Wilcock and McArdell (1993), was adopted (section 3.4.3). This required painting each size class of the unimodal bed in a different colour. As visual colour identification was essential for the success of this technique, good colour contrast was a priority. Colour combination tests were carried out until appropriate colour identification and contrast were achieved. This reduced the possibility of confusion identifying the colours, essential for the estimation of the bed surface composition (section 3.4.3). The paint used was standard exterior masonry paint for all size classes except the classes containing D_{50} and D_{90}, which were painted in ultra violet (UV) paint. Table 3-4 shows the colour scheme adopted together with approximate samples of the colours used.

Sieve size (mm)	Colour	Colour sample
1-1.4	Yellow	
1.4-2	White	
2-2.8	Light blue	
2.8-4	Green	
4-5.6	Lilac	
5.6-8	Red (UV)	
8-11.2	Blue (UV)	
11.2-16	Black	

Table 3-4. Colours used in the unimodal bed

One coat of paint was applied to all but the two smallest size classes, for which two coats were applied, as yellow and white paints had some transparency. Particle sieve size cross over due to painting was minimal with efficiency rates of sieving after the painting process (% of painted particle weight passing the

same sieve) between 95% and 98% for the size classes between 1 and 5.6 mm; which are comparable to those reported by Wilcock and McArdell (1993) (mean efficiency = 95%). The influence of the paint coat on larger sizes was observed to be much smaller, so classes larger than 5.6 mm were not re-sieved.

A total of 425 kg of sediment mix were made and placed into the flume channel. The sediment was thoroughly mixed again in the flume and levelled to a depth of approximately 50 mm. The mixing procedure minimised particle segregation and ensured appropriate mixing of sizes. Preparation of the bed for each experiment run included full remixing of the bed; thus, bulk mix composition remained constant throughout all experiments. The consistency of the grain size distribution of the initial bed during the preliminary tests (section 3.4.3.3) and throughout the experimental work (Table 3-5) confirms this.

	Average	Std. dev.	Average	Std. dev.
	Stage 1		Stage 2	
D_{16}	4.19	0.10	4.19	0.17
D_{50}	6.41	0.13	6.34	0.11
D_{84}	9.05	0.47	8.74	0.34
D_{90}	10.27	0.36	10.03	0.28

Table 3-5. Statistics of main particle sizes of initial beds for Stage 1 and Stage 2. Sizes in mm.

3.2 *Flume components and setup*

3.2.1 Description of the flume

A flow-recirculating Armfield flume with an effective length of 7 m, an internal width of 0.9 m, and glass side-walls 0.45 m high, was used (Fig. 3-3). The channel can tilt in order to adjust the channel slope. Flow depth is controlled by regulating the tailgate at the downstream end of the flume. Flow recirculation was provided by a pump controlled by a signal inverter (section 3.2.2.4). Two instrument carriages that could travel the entire length of the flume channel were used to mount equipment, including ADV, point gauges, light lamps and, video and photographic cameras. A bedload trap was designed and installed under the flume bed near the downstream end of the flume.

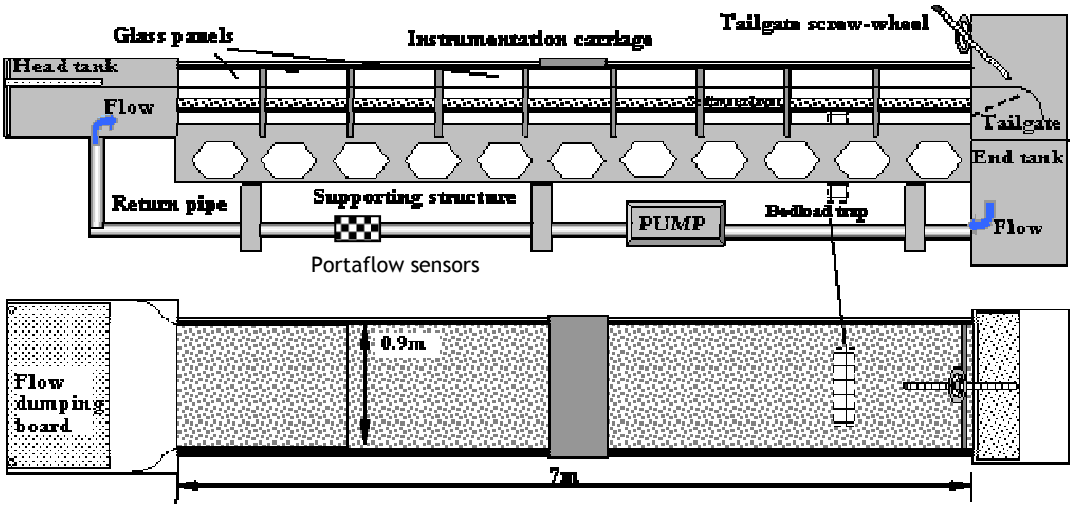

Fig. 3-3. Sketch of flume and main components

3.2.2 Flume equipment and instrumentation

3.2.2.1 Pump

Two pumps were used: the first, a 22.5 Kw propeller pump capable of a maximum discharge of 120 l/s, provided the flow for the Pilot Runs. Due to age this pump failed (slipped propeller) and was replaced in March 2009. This new pump, a close coupled centrifugal pump with an 18.5 Kw motor capable of providing a maximum flow of 100 l/s, was used for the remaining laboratory work.

3.2.2.2 Point gauge

A Mitutoyo SD12" pointer gauge, providing readings at 0.01 mm intervals, was used for calculating flow depths by measuring the difference of readings between bed and water surface. Readings were taken along the centreline of the channel at 0.5 m intervals.

3.2.2.3 Bedload trap

A new bedload trap was installed, based on a rectangular opening on the base of the flume that is connected to a removable collection box by a perforated rotating shaft acting as a valve (Fig. 3-4). The trap opening is located in the centre of the channel approximately 6 m downstream from the flume channel

entrance. Its dimensions are 450 x 50 mm^2, with the longer side perpendicular to the direction of the flow. Attached to the base of the flume and immediately below it is the valve system, composed of a self lubricated nylon compound block (Nylon 66), vertically perforated by 6 equal slots connecting the flume opening with the collection box below. A cylindrical brass shaft, also perforated with 6 matching slots (the dimensions of each opening are 42x50 mm^2 approximately), was embedded within the block in the direction of the trap opening. The rotation of the shaft by 90º opens and closes the valve, allowing sediment to fall from the flume to the collection box below. This box is made of transparent Perspex® and its internal dimensions are (in mm) 300 x 80 x 210 (length x width x height). Two clips attached to the sides of the box, one either side, maintained the box firmly attached to the trap valve block. A neoprene rim over the top of the collection box keeps the system watertight while the box is attached to the flume. Two collection boxes were available for continuous bedload sampling.

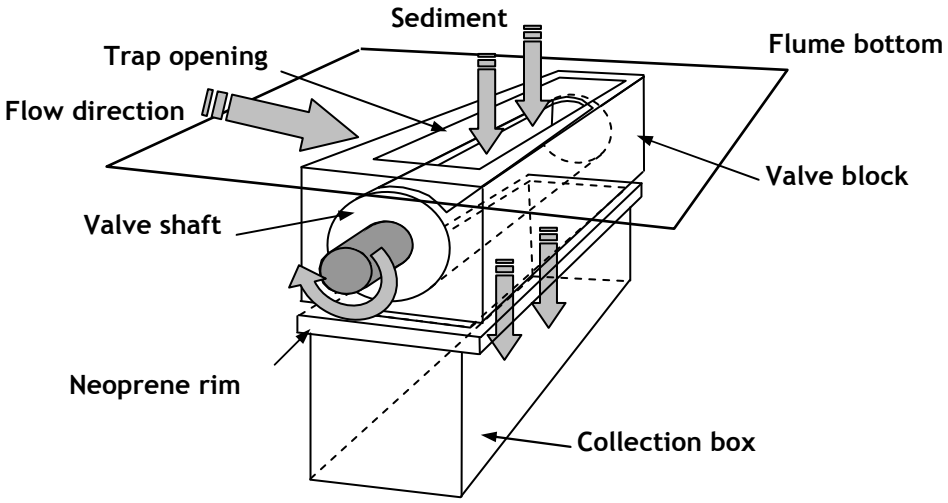

Fig. 3-4. Sketch of the sediment trap.

Individual sampling times covered the entire duration of each flow stage and therefore varied with the duration of the flow steps employed in each acceleration rate run (6, 12, 24, 48, 72 and 120 min. for the hydrographs of duration 0.5, 1, 2, 4, 6 and 10h respectively); however, the sampling period for the stability test (6 min.) was common to all experiments in which bedload samples were available. Thus, the entire period for which the bed was subject to

flow action was accounted form, with the bedload rate being the total dry weight of each sample divide by the duration of the sampling interval.

It is noted that the change of the collection box produced air bubbles, trapped within the valve shaft, which escaped vertically into the channel flow when the valve was reopened. These bubbles destabilised some grains around the leading edge of the trap opening, which fell into the box. Thus, additional particles were collected in the samples. Based on visual observation the maximum additional solid sample was estimated as 20% of volume for the smallest samples, rapidly reducing as the volume of collected material increased for high flows. This may slightly distort amounts and compositions of bedload samples, especially when samples are very small, due to the bias introduced by the analysis-by-weight of the bedload data processing. Thus, at higher discharges larger amounts of mobilised sediment reduce the impact of air bubbles and give a more reliable data set. Furthermore, since the collection box was replaced a number of times within each experiment, falling of unstable grains due to air bubbles was largely reduced as experiments progressed. The impact of this overestimation of the solid samples was minimised by the visual fitting technique used when estimating entrainment thresholds based on the reference transport method, which associated larger weighting to the samples collected during the stability test, for which the oversampling was negligible.

3.2.2.4 Signal inverter

The pump speed was controlled by an IMO VXM1850 torque controller, called here signal inverter. This inverter regulates the pump frequency via a remote keypad to a precision of 0.01 Hz. Details of flow control are below.

3.2.2.5 Flow measuring device: Portaflow

A Microelectronics Ltd. Portaflow™ was used to monitor flow in the return pipe. It is an acoustic device that measures the average fluid velocity in the discharge pipe from the pump, transforming this into flow rates with a precision of 0.01 l/s. The device automatically recalibrates with changes of water temperature, which required slight manual adjustments of the distance between sensors. The

manufacturer recommends a minimum signal strength value of 40%; values obtained during experiments were in excess of 70% for all experiments, which ensured the reliability of the measurements. It is worth noting nonetheless that the Portaflow readings were not contrasted against another method of flow measurement. However, no instability or malfunctioning of the Portaflow was noticed during the experimental work; thus, inaccuracies in the flow readings are not anticipated. In any case, bed shear stress values were estimated based on water depth-slope or velocity data measurements (section 3.4.5), independent of the flow readings.

3.2.3 Flow control

Pump speed was directly controlled by the signal inverter by regulating the electric impulse to the pump motor. During the Pilot Runs, flow was directly regulated by changing the electric signal of the inverter. This meant that signal frequency, not flow, was observed and controlled by the user, with flow then being monitored by the Portaflow. The inverter could be programmed with a series of up to 7 time steps, which could be reprogrammed to create a continuous semi-automated pump control. Since the electrical signal was used to control the pump at this stage, a relationship between the inverter signal and the flow in the flume was obtained for a range of flows spanning those used during the experiments (Table 3-6). This relationship was used in the Pilot Runs to create the test hydrographs. Fig. 3-5 shows the excellent correspondence between signal inverter frequency and flows measured and the very small range of flows observed for each frequency.

Inverter signal (Hz)	16	18	20	22	24	26	28	30
Average flow (l/s)	12.9	19.1	25.2	31.3	37.4	43.5	49.6	55.7

Table 3-6. Summary of the relationship between inverter signal and average flow readings by the Portaflow for the Pilot Runs.

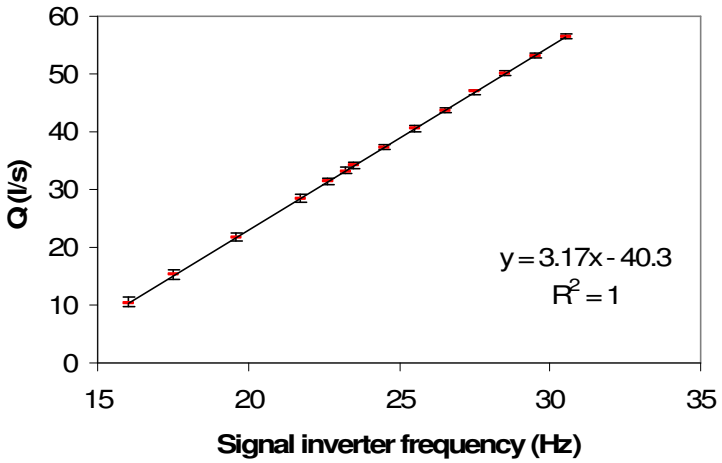

Fig. 3-5. Relationship between signal inverter frequency and discharge measured with Portaflow. Errors bars indicate the range of flows measured for each frequency. Range of bars reduce with increasing flows, which indicates a more stable pump regime for higher flows.

A self-regulating system, between the inverter, the pump and the Portaflow, was later installed. The inverter, now capable of functioning using flow values, was set at a specific flow by the user. The inverter continuously compared the Portaflow readings with the target flow and adjusted the speed of the pump to match the target flow. An analysis of the performance of the system, comparing Portaflow readings under manually and automatically regulated flow conditions was undertaken for the first pump. When manual setting was used data showed that differences between the target flow and the average measured flow, obtained during 3 minute sampling periods with 10 seconds sampling frequency, ranged between 1 % and 4 %, with the actual value being lower than the target flow. In the case of controlled conditions the same differences ranged from 0.2 % to 0.5 %, with actual flows always lower than objective ones. The differences clearly show the improvement achieved by linking the pump, Portaflow and inverter. A second check of the flow control system was performed for the second pump, with differences varying from -0.5% to 0.4 %, demonstrating the stability of the system regardless the pump used. However, using this self-regulating system meant that the inverter could no longer be programmed and all flow changes had to be manually set by the user.

3.2.4 Uniform flow set up

All the experiments were conducted under uniform flow conditions, where the surface of the water was parallel to the bed and therefore, flow depth and velocity were constant along the flume. Uniform flow conditions are important as they permit comparison of measurements of hydraulic and bed characteristics that are often taken at different locations within the flume. In addition, some formulae, including bed shear stress estimation methods (see 3.4.5.3), require uniform flow conditions.

Uniform flow was established for each flow as follows: for a given bed slope and flow, repeat measurements of depth were taken at 10 locations along the flume at 0.5 m interval, adjusting the tailgate to produce approximate uniform flow (defined when slope of the fitted line to water levels was within ± 2 % of the objective slope). Repeating this procedure for the full range of flows produced a relationship between flow, tailgate position and average flow depth. These data were subsequently used to set uniform flow conditions during the experiments and to estimate shear stress for each flow.

3.2.5 Configuration of granular beds

Each experiment series had associated a different configuration of the granular bed and test area in the flume. Fig. 3-6 shows schematic of each of them.

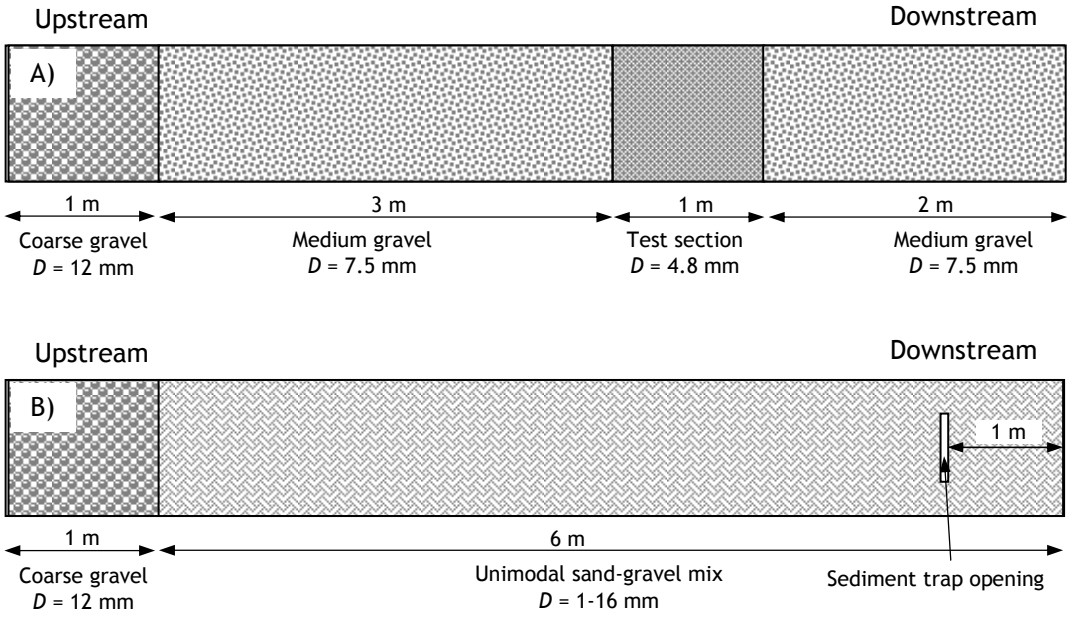

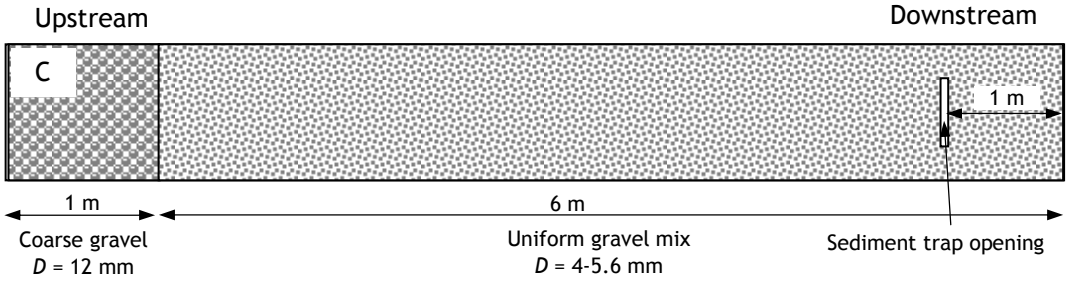

Fig. 3-6. Schematics of sediment bed configuration. A)Pilot Runs; B)Unimodal sand-gravel bed (Stages 1 and 2); C) Unifrom gravel.

3.3 *Measuring equipment*

3.3.1 Acoustic Doppler Velocimeter (ADV)

An Acoustic Doppler Velocimeter (ADV) was used for measuring the velocity components at a single point. A Nortek AS Vectrino 3D side-looking velocimeter with a 40 cm fixed stem was used. ADVs measure flow velocities using the Doppler effect, as sound frequency changes when reflected from particles in the flow. ADVs consist essentially of a sound emitter, two to four sound receivers and a signal conditioning electronic module. The ADV receivers are aligned to intersect with the transmission beam at a common sampling volume (Fig. 3-7), located 50 mm from the tip of the probe (for the ADV used here). The sampling volume is a cylinder of water with a fixed diameter of 6 mm and a user-defined height of 3-15 mm (for the velocimeter described here).

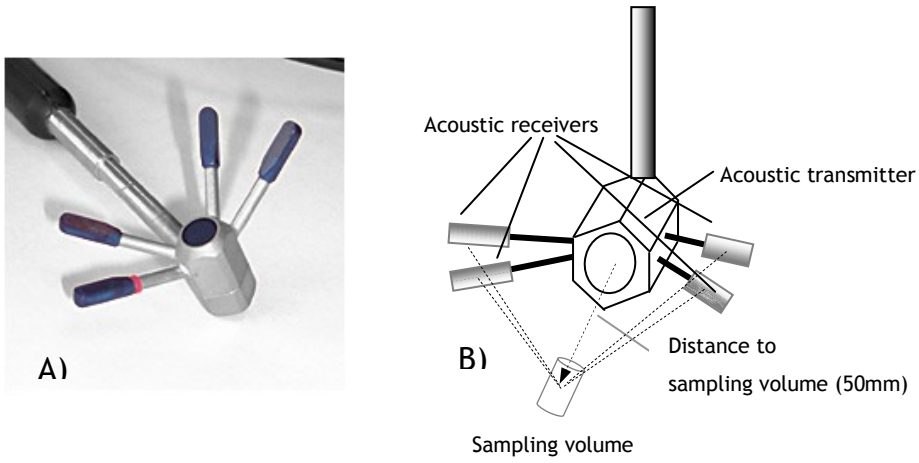

Fig. 3-7. A) Image of ADV head (side-looking) used in the experimental work (nortek-as.com); B) schematisation of location of sampling volume.

The minimum elevation of the flow depth to be sampled was limited to 6 mm above the sediment bed by the size of the ADV head (12 mm) (Fig. 3-8). This

reduced the availability of data very close to the bed, which pose a challenge when estimating shear velocity and stress from velocity data (section 3.4.5).

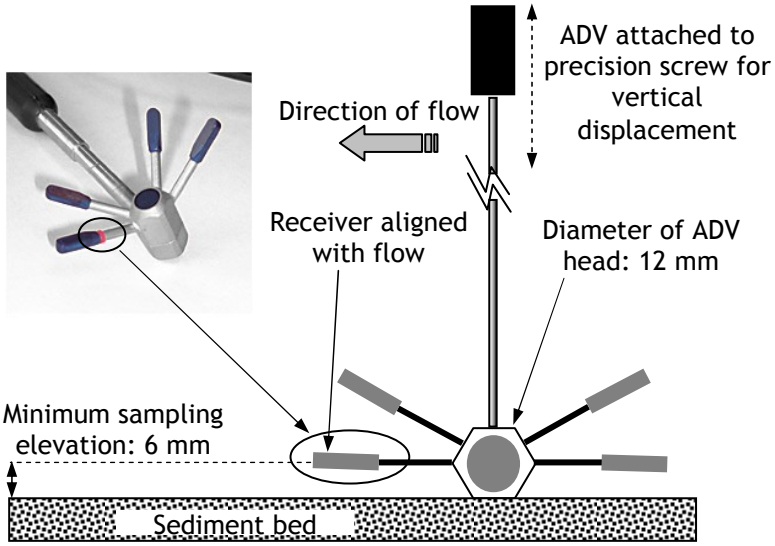

Fig. 3-8. Sketch indicating alignment of ADV and minimum sampling elevation due to ADV head size.

The emitter generates an acoustic signal that is reflected back by sound scattering particles present in the water (normally air bubbles, naturally occurring fine particles or seeding material) assumed to move at the fluid velocity. The scattered signal is detected by the receivers and used to compute the signal Doppler phase shift from which the flow velocity components are estimated (Sontek, 1997; Papanicolaou *et al.*, 2001; Nortek AS, 2004; Garcia *et al.* 2005). The ADV measures the sound scatter from two consecutive pulses. After the signal is processed, the phase difference determines the velocity (Voulgaris and Trowbridge 1998), and the correlation is a measure of the similarity of the two pulses. Thus, the ADV correlations are a measure of data quality related to the velocity calculations, computed for each acoustic receiver. Correlation is expressed as a percentage, with values close to 100 % indicating reliable, low-noise velocity measurements, whereas low correlations indicate low noise reflection (insufficient seeding), the probe is out of the water, the signal-to-noise ratio (SNR) is too low, or ADV malfunctioning. It is commonly accepted that correlation should be above 70 % (Wahl, 2000; Mori *et al.*, 2007; Masaló *et al.*, 2008); thus, ensuring reliable data. This threshold was followed in the calculations presented in this thesis.

ADVs are designed to measure velocity as rapidly as possible. A single estimate of the velocity field is referred to as a ping. The data noise in a single ping is too high for practical use, so the ADV averages the values from a number of pings before producing a velocity reading; here, 10 pings per velocity value. In the thesis data set the sampling volume was typically 155 mm^3 and the sampling frequency was 25 Hz, providing 1500 data values per minute and sampling position. Values of velocity were taken over a vertical profile located at the centre line of the flume channel and at 5 m from the upstream end (Fig. 3-9); and averaged over a 3 minute (Pilot Runs) and 2 min. (unimodal and uniform gravels) sampling period. Between 7 and 12 elevations were sampled, depending on the flow depth. The Vectrino ADV was equipped with temperature correction, self-adjusting for sound propagation speed depending on the water temperature, which was read by a thermometer included within the ADV.

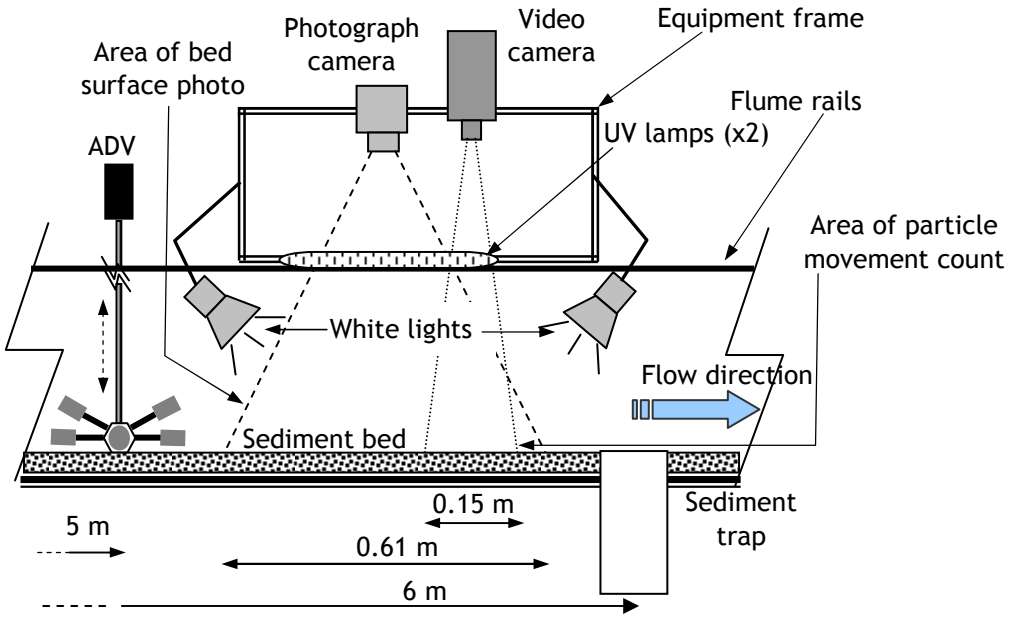

Fig. 3-9. Schematic representing the position of the main equipment used for data collection. (Not to scale, indicative only).

3.3.2 Photography and video

Video and photographic images were extensively used during the experiments. Two video cameras and one digital still camera were used at different stages. A Panasonic NV-DS30 video camera was used for the near-uniform gravel experiments to record particle movements. Images were recorded on standard VHS tapes on a JVC HR-S6700 VCR and projected on a 26" Goodmans GD2880 TV.

For the remaining experimental work a Panasonic NV-GS230 digital video camera and a SONY DSC-3H 8Mp digital still camera were used for video and photographic images respectively. All cameras were mounted on the flume carriages above the channel and set up to cover the specific area of interest (Fig. 3-9). All cameras were focused on the granular bed while dry, and automatic focussing switched off to keep the image in focus under moving water. Images from the video cameras were directly recorded on tape and replayed for particle movement counting (section 3.4.1), whereas the still images were recorded on the camera 1Gb memory card and downloaded onto the computer at the end of the run.

3.3.3 Lighting

Additional lighting was required to increase image quality for the particle movement counts. Initially, for the near-uniform gravel experiments, standard incandescent 100 W bulbs were mounted on desk lamps and placed on the side of the flume pointing towards the bed. For the remaining experimental work two sets of Interfit Tungsten 3200 professional lamps and 500 W white light bulbs were used. These were fixed to two Manfrotto adjustable arms mounted on the same instrument carriage as the video and photographic cameras, so the entire image collection equipment moved together (Fig. 3-9).

Water running through the flume provided a considerable challenge to the photography and video as the water surface reflected vertical light. Thus, conventional lights on the laboratory ceiling directly above the flume were covered, hence the data set was recorded with only lighting provided as described above and with these lights set at an angle to the water surface to minimise reflections.

In addition to white light for the video and still images, two Blacklighting T8 20W ultra violet (UV) lamps were used to distinguish particles painted in UV paint from the rest of the sediment grains (section 3.1.4). The effect of the UV light was to dramatically increase the contrast of the UV painted grains and a large reduction of contrast for the remaining particles. Thus, identification of D_{50} and

D_{90} grains (Table 3-4) was largely improved. Fig. 3-10 shows an example of images of the same bed area taken under white and ultraviolet light.

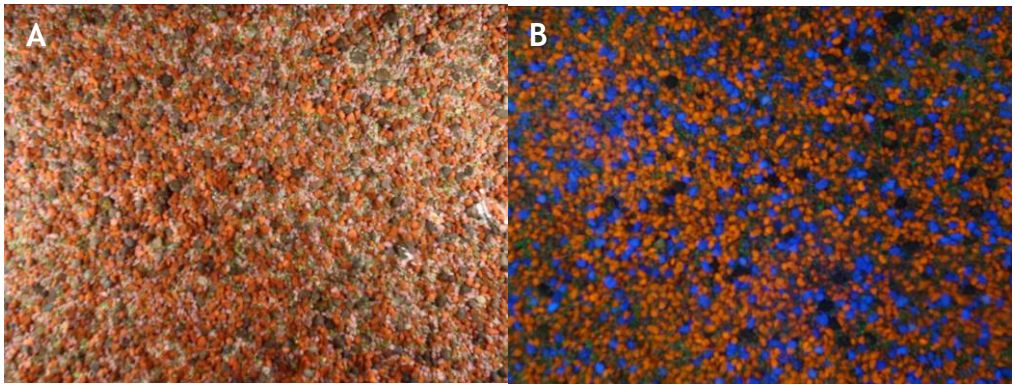

Fig. 3-10. Example of bed surface images under white light (A) and UV light (B). Image area size is 460 x 61 0mm^2.Particle sizes correspond to the colours specified in Table 3-4.

3.4 *Experimental techniques*

3.4.1 Particle movement count

The application of the visual method for the estimation of entrainment (section 3.4.6.1) was based on manual counting of particle movements over an area of 150 x 150 mm^2 symmetrically placed over the flume centre line. This area was located 4.5 m from the upstream end of the flume for the Pilot Runs, where fully uniform flow conditions were observed. For the remaining experiments, the same size of the test area was used, although its location was further downstream, approximately 300 mm from the sediment trap opening, about 5.5 m from the upstream end of the flume. Consistency of measurements was guaranteed by placing an aluminium frame on the bed surface, onto which the camera was zoomed in to optimise image area. The camera was oriented so that the flow direction was from right to left on the image. The test area was magnified to approximately 46 x 46 cm^2 when projected on the TV screen. This magnification aided clear identification of individual particles although it was difficult for the operator to focus on the entire screen and note all movements occurring simultaneously. Therefore, the screen was horizontally divided into two equal rectangular areas with the long side parallel to the direction of movement, optimising particle recognition conditions in comparison with the undivided screen. Once the experiment was concluded, the video recording was

played twice, one per screen division, and particle movements were counted. The aggregated particle counts were used to define a relationship between flow and the number of grain movements recorded for each discharge. Although no systematic test of count repeatability was carried out, the measures taken for optimising the procedure meant that variability of counts is likely to be minimal. This was confirmed by the anecdotal instances in which counts were repeated, where differences between counts were in single figures, reducing with smaller *N*. During Stages 1 and 2 grain visualisation of the modal size class (5.6-8 mm) was improved by recording images under UV light (this size class was painted in red UV-reactive paint, see section 3.1.4), which made particles stand out from the bed, increasing reliability of count.

3.4.2 Automated bed surface composition

A number of techniques and software packages have been developed to provide bed surface composition automatically (eg. Lane *et al.*, 2001; Sime and Ferguson, 2003; Carbonneau *et al.*, 2003, 2004,2005; Rubin, 2004; Graham *et al.* 2005a; Buscombe *et al.*, 2010). One of these packages is Digital Gravelometer (DG), developed by Dr. David Graham and his team at Loughborough University[3]. In the current thesis, a free, fully functional trial version was used. Details of the theoretical basis and technique background can be found in Graham *et al.* (2005a, 2005b).

Tests of the performance of Digital Gravelometer used natural beach gravel separated in three individual size classes: 1.4-2, 4-5.6 and 8-11.3 mm. These size classes provided a good representation of the full range of sizes present in the test beds. In addition, painted grains of the same material (4-5.6 and 8-11.3 mm) were included to determine the possible influence of coloured grains on the results (Appendix 1). The images were taken following the recommendations found in the references to the software and information from the software website.

[3] http://www.sedimetrics.com

Results from DG were inadequate, with very poorly sorted grain size distributions displaying long tails on the finer classes (< 0.18 mm) that were very different from those used to test this software (Fig. 3-11 and Appendix 1). Therefore, the use of Digital Gravelometer for automated grain size distribution was discarded. Appendix 1 contains the results of the tests carried out.

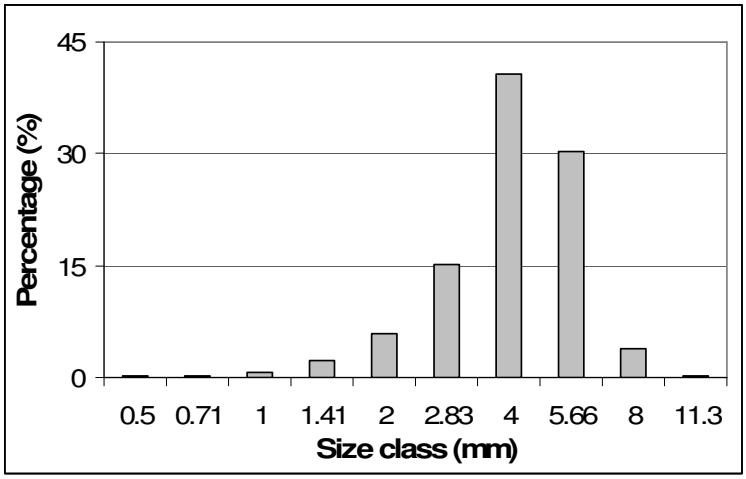

Fig. 3-11. Example of best output from Digital Gravelometer for images containing single size class 4-5.6 mm. Note that the percentage associated to 4 mm should be close to 100%.

3.4.3 Manual bed surface composition using ImageJ

The inadequate results obtained with grading software meant that manual assessment of bed particle size composition was unavoidable. Wilcock and McArdell (1993) painted each size class in a different colour and took photographs of the bed surface, performing particle counts similar to the Wolman (1954) method (grid-by-number), which is equivalent to volume-by-weight data commonly used in bulk sample analyses (Kellerhals and Bray, 1971; and Church *et al.*, 1987; Wilcock and McArdell, 1993). They projected each image onto a square grid and recorded the colour of grains falling on each grid line crossing. As the colours of the grains were uniquely related to their size class, data provided bed surface composition of the area covered by the image.

One major advantage of this method over the automated grading is that sediment beds do not need to be dry as it is the case with DG. Thus, photographs of the bed surface can be taken at any time during runs, ensuring the continuity of the experiments. Other authors (Wiclcock and McArdell, 1993; Hassan *et al.* 2006) have taken images of the bed after reducing the flow in the flume or

draining it completely, before increasing the flow back to its original value. This procedure is not followed here as it adds artificial cycles of high-low flow which are both unnecessary for the procedure and problematic for the purposes of this study where flow antecedency is a primary focus. Therefore, images were taken without reducing discharge. This method is non-invasive, with no disruption to the bed and hence, there is no effect on the flow history.

The assessment of bed surface composition was based on particle counts over four images of the bed taken at successive locations along the flume, each covering an area of approximately 460 x 610 mm^2. This image area is intended to maximise the area of observation of the flume bed in a single image, and it covers the entire width of the sediment trap opening (450 mm) in the short side of the image area. The image length (610 mm) was fixed by the camera image ratio (3/4). Images locations are listed in Table 3-7. The downstream edge of the first image was approximately 150 mm upstream from the sediment trap opening and the image included the entire area of interest for the particle movement count. The total area covered by the images was 1.1 m^2, which represents 22 % of the total test bed upstream of the sediment trap. This was very similar to the 24% bed coverage used by Wilcock and McArdell (1993).

Image 1	Image 2	Image 3	Image 4
At u/s edge of sediment trap opening (approx. 5.88m)	5m	4m	3m

Table 3-7. Position of photographic images (distance from flume u/s end) measured from the position of the downstream edge of the carriage.

The particle count was carried out using a free image processing and analysis software package, called ImageJ, developed by the USA National Institute of Health (NIH)[4]. The version used in this work was ImageJ 1.39u. The standard suite of functions of ImageJ can be enhanced by incorporating tools, called Plug-ins, developed by others. Among these plug-ins are two of particular interest: *Grid*, created by Wayne Rasband at the NIH[5]; allowing the projection of a square grid onto the image and, *Cell Counter*, developed by Kurt De Vos at the

[4] http://rsb.info.nih.gov/ij/

[5] http://rsbweb.nih.gov/ij/plugins/grid.html

University of Sheffield[6], which provides individual cumulative counts of up to 8 feature types. As images can be scaled in ImageJ, dimensions of the grid could be set at scale 1:1. The grid square size was determined by balancing a size that avoided counting the same particle twice and providing an appropriate number of grid crossings. The grid was randomly placed by ImageJ each time it was projected.

Rice and Church (1996) showed how the percentile standard error s_p expressed in absolute units (phi or mm) is inversely proportional to the square root of the sample size *ns*. Therefore, errors of particle counts reduce with larger sample sizes. Other authors such as Wolman (1954) and Mosley and Tindale (1985) suggested sample sizes of around 100 particles. Tait *et al*. (1992) also used 100 particle counts per image for analysing bed surface composition. An initial analysis of the sensitivity of the results to sample size was carried out using a minimum of 100 and 200 particle counts per image for a selection of images. Rice and Church (1996) contains a detailed analysis of the effect of sample size on field size distribution results; they recommended a sample size of 400 particles when 95% confidence limits of approximately ±0.1 phi are acceptable; which is the minimum number of coloured stone counts performed for this research work (100 particles for each of the 4 photographs analysed). It is highlighted that Rice and Church's (1996) recommendation applied to field measurements, in which areas of sampling (tens of square meters) are much larger than the flume bed area sampled in the experiments presented in this thesis (5-6 m^2). Thus, 400 particle counts are well above that minimum recommended.

Sample size variability resulted from the random positioning of the projected grid, which causes variations in the number of line crossings included within the area of interest. Repeatability of the procedure was tested by replicating particle counts (named A and B) randomly repositioning the grid over the image, thus providing two independent bed surface compositions. The sides of the grid squares were set at approximately 50 mm and 35 mm for the 100 and 200 counts

[6] http://rsbweb.nih.gov/ij/plugins/cell-counter.html

respectively; much larger than the largest grain (16 mm) so ensuring that no particle was counted more than once in the same count.

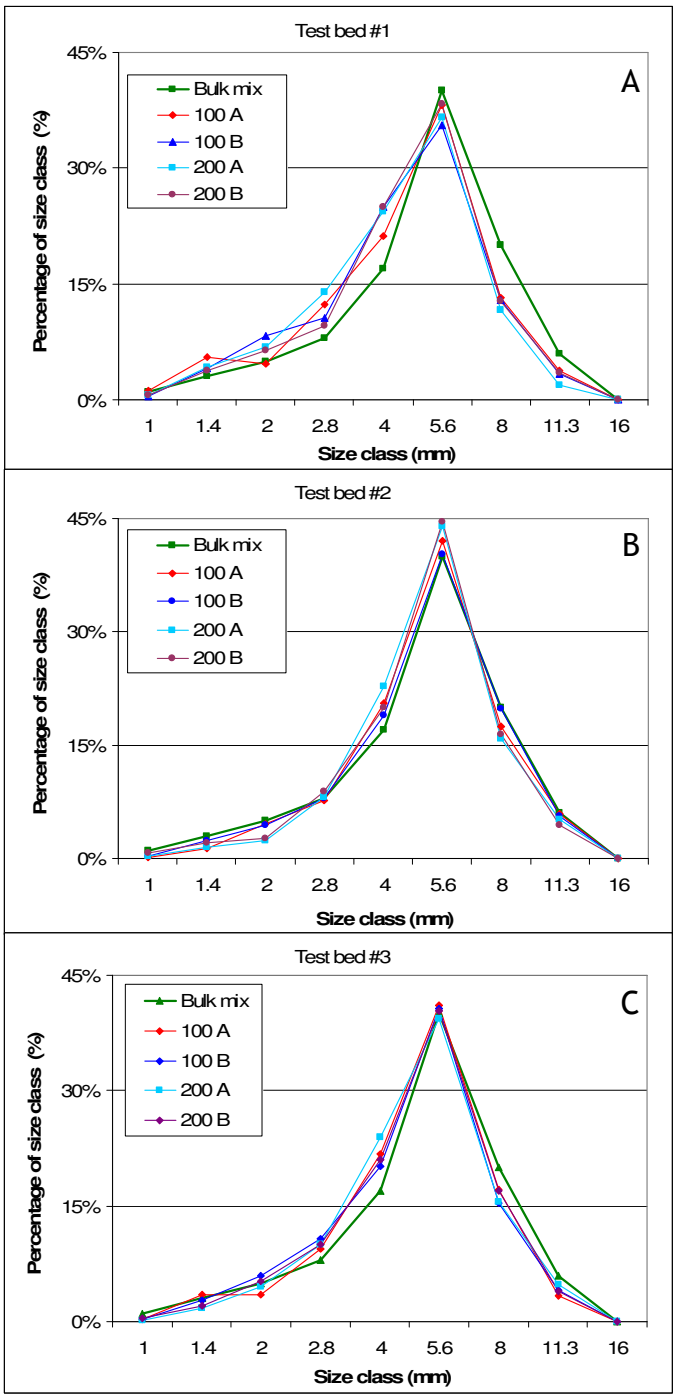

Fig. 3-12. Results of test of bed surface particle count. Numbers 100 and 200 represent the minimum number of particles counted per image; A and Bafter the number of particle counts, eg. 100A, refer to each count replicate.

The bed surface compositions presented here are summations of the particle counts for the four images of the bed surface taken each time (Image 1-4). Hence, bed surface composition was defined by a minimum of over 400 and 800 particle counts, for the 100 and 200 point per image counts, respectively. These

particle counts were then transformed into individual percentages for each size class. A table summarising the results is in Appendix 1; Fig. 3-12 shows the comparison with bulk mix.

3.4.3.1 Differences between 100 and 200 particle counts

Comparison of results obtained using 100 and 200 particle counts per image (Appendix 1, Fig. 3-12) show no clear difference. Both 100 and 200 counts provide similar results: general over-counting of the 2.8-4 mm and 4-5.6 mm size classes, and under-counting of 8 -11.2 mm and 11.2 -16 mm size classes. These differences between particle counts and bulk mix are displayed by all three test beds, so it is likely that the shift of particle count is due to an actual absence of larger particles on the surface. To quantify the accuracy of each count, Root Mean Square Errors (RMSE) relative to bulk mix were obtained for all cases for the individual and cumulative percentages. It is noted that the calculations were carried out using bed composition percentages and so the results are shown as percentage units (Table 3-8); not to be confused with a relative percentage of change.

	100-A	100-B	200-A	200-B
		Test bed #1		
RMSE (individual %)	1.2%	1.6%	1.7%	1.4%
RMSE (cum. %)	2.0%	2.4%	2.8%	2.0%
		Test bed #2		
RMSE (individual %)	0.6%	0.3%	1.1%	0.9%
RMSE (cum. %)	0.7%	0.4%	1.1%	0.9%
		Test bed #3		
RMSE (individual %)	0.8%	0.8%	1.1%	0.7%
RMSE (cum. %)	1.0%	1.2%	1.2%	1.0%

Table 3-8. Comparison of 100 counts and 200 counts. RMSE corresponds to the differences between individual percentage weight of a size class on the sample results and bulk size composition.

Results show very similar values in all cases. In general, RMSE values of both the individual and cumulative percentages of the surface bed composition show smaller divergence of the bed surface composition from the bulk mix for the 100 count. Since counting 200 particles per image did not provide any measurable improvement to the results, counting 100 particles per image was adopted. This

means a minimum aggregated sample size of 400 particles, in line with Rice and Church (1996).

3.4.3.2 Repeatability

The consistency and repeatability of the particle count was assessed in two ways, similar to Wilcock and McArdell (1993), by calculating absolute values of differences between surface composition f_i (in % units) provided by replicate counts (named A and B); and the change between replicates relative to the average value of f_i of each replicate pair (average of f_i(A) and f_i(B)), (Fig. 3-13).

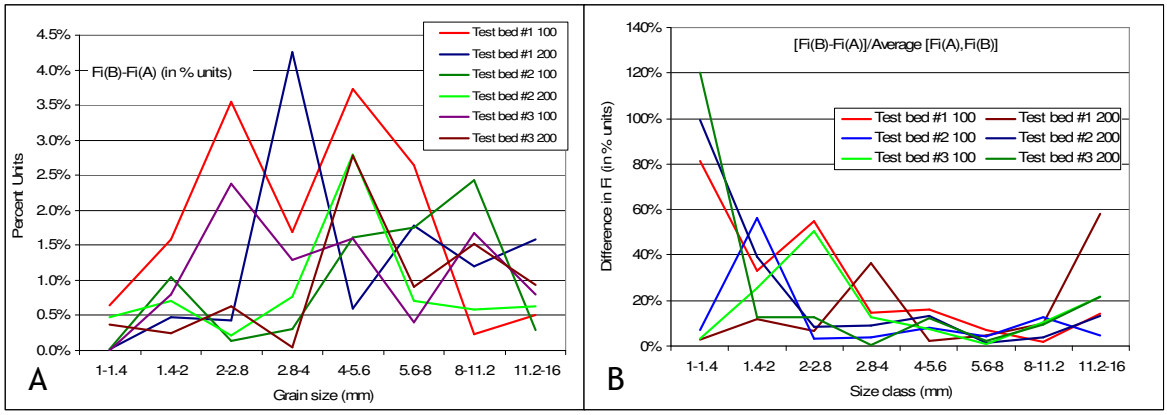

Fig. 3-13. Repeatability of particle count results. A) absolute values of $|f_i(B)-f_i(A)|$; B) relative percentage of change of $|f_i(B)-f_i(A)|$ over the average of $f_i(A)$ and $f_i(B)$.

Differences in f_i remain below 4.5%. This is the same as the maximum values reported by Wilcock and McArdell (1993). When these differences are scaled by the relative composition of the size class in the mixture, many of these values remain under 20% (Fig. 3-13B), comparable to the 25 % cited by Wilcock and McArdell (1993). Yet, variatios of size composition between replicates increase up to 120% for the smallest size class (1-1.4 mm). Since this size class has the lowest value of *fi* (1% in bulk mix) a small variation of the recorded value of *fi* relative to this 1% in the bulk mix results in large relative fluctuations. However, the absolute variation is up to 0.6% units (Fig. 3-13A). The impact of the value of *fi* of class 1-1.4 mm on the bed surface composition data is minimal since the contribution of this class is very small, typically < 1%.

Contrary to the pattern found by Wilcock and McArdell (1993), there is no obvious relationship of the between-replicate differences of f_i with grain size.

There is however, a clear correspondence of the relative differences of f_i between replicates with f_i values in the bulk mix, as differences rapidly decrease as the size class f_i increases, reaching values below 10% for the mix mode. This can be explained considering that variations of 1-2 grains on the colour count have a larger impact on f_i for classes with small f_i than those with larger ones.

An additional assessment of the repeatability of the method was carried out during Stage 1. Three images were selected, covering a range of bed and flow conditions, for which 100 particle counts per image were performed ten times. The variability of the results was analysed, as above, by comparing results to the average of all ten bed surface composition data sets for each image (Fig. 3-14). The average of ten absolute between-replicate differences reaches a maximum of 4% units, with values having a positive correlation with the percentage of each size on the bed surface f_i; a similar result to that found by Wilcock and McArdell (1993).

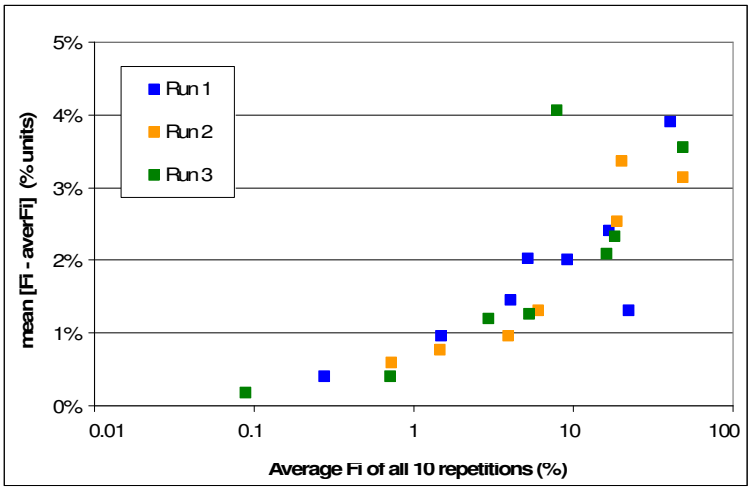

Fig. 3-14. Variability of 10 repetitions of particle count with surface bed composition. Runs 1, 2 and 3 correspond to data collected during 3 different Stage 1 experiments (Q_{ref}, AccRate1 and AccRate2) and flow stages (initial bed, 31.5 l/s and 50 l/s) respectively.

Confirmation of the repeatability of the method came from the complementary analysis carried out by Dr. Luca Mao at the University of Hull of another set of three images (Image 1-3) sent by the author of this thesis. Dr. Mao performed the same particle count procedure detailed here counting 280 particles per image, selected by a randomly placed square grid, replicated three times for Image 1. In addition, Dr. Mao obtained bed surface composition data by digitising the b-axis of the same 280 particles previously selected. The number of particle

counts (280) was adopted by Dr. Mao for consistency with his previously established b-axis digitation method, which uses 280 particle diameter measurements. The results are plotted in Fig. 3-15 and Fig. 3-16.

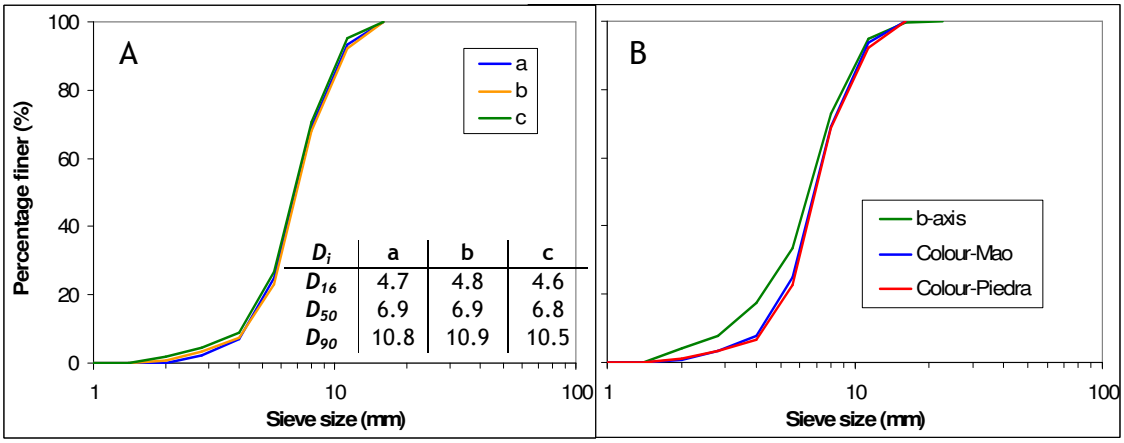

Fig. 3-15. Results from coloured particle count and b-axis digitisation for Image 1. A) Comparison between replicates of coloured particle count, 280 grains per count, performed by Dr. Mao. Insert table shows a summary of mixture diameters (mm) for the three repetitions , b and c. B) Comparison between b-axis digitisation and particle count of 100 and 280 grains per count.

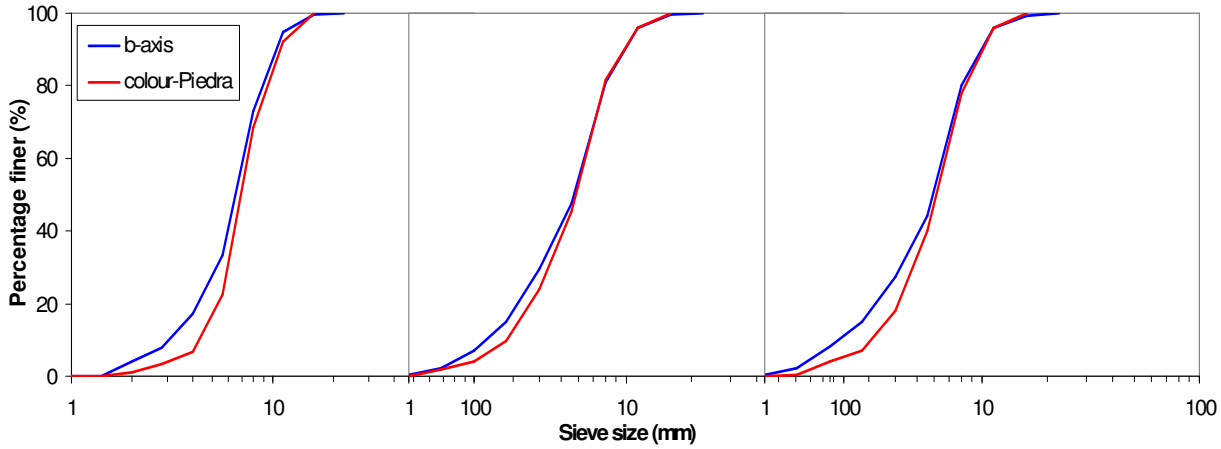

Fig. 3-16. Comparison of bed surface composition results from b-axis digitisations and coloured particle count (100 grains per image) for each image analysed.

Cumulative grain size distributions for the three colour counting replicates performed for Image1 show near identical values (Fig. 3-15A), with D_{50} for the three repetitions being 6.9, 6.9 and 6.8 mm respectively, confirming the repeatability of the method. These values are also in agreement with the cumulative size distribution using 100 particles per count (Fig. 3-15B). Thus, these results confirm that the proposed method is consistent and variations due to grid position or operator cause minimal effect on bed compositions, but also

clearly show that there is no increased benefit by using a large number of particle counts (280) over the adopted 100.

The comparison between digitising particle b-axes (280 grains) and counting painted particles (100 and 280 grains) shows that digitised diameters were consistently finer for sizes below D_{50} (ratio of D_{16} 0.76-0.85) and very similar for D greater than D_{50} (ratio of D_{90} 0.96-1.00) (Table 3-9). This may be explained by the errors associated with digitising visible diameters, which might not be sufficiently exposed and are likely to be smaller than the actual ones (Church *et al.*, 1987). This underestimation of diameter has a smaller effect on larger particles, where a potential 1 mm error is a small proportion of the particle size and hence is unlikely to change its size class. Conversely, for smaller classes, the same error of 1 mm is more likely to alter the size class under which the particle is classified, as it is a larger percentage of the grain size. Thus, bed surface composition based on axis digitisation is more sensitive in the smaller particle range.

Percentile	b-axis digitation			Particle count		
16	3.8	2.9	2.9	4.9	3.4	3.9
50	6.6	5.8	6.0	7.0	5.9	6.2
90	10.6	10.0	10.1	11.0	10.0	10.2

Table 3-9. Comparison of main particle diameters (mm) from b-axis digitation and particle count.

Bed surface composition results from particle count were also compared to those obtained by areal sampling (Church *et al.* 1987). Surface samples were taken using soft plasticine over a rectangular area of 300 x 225 mm^2. This area corresponds to approximately 1/4 of the standard image area used for the coloured particle counting. The size of the sampling area was limited by the ability to retrieve the bed grains reliably. Soft plasticine was used for its adherence properties, similarly to clay, without the drawbacks of having to wash the sample (Fripp and Diplas, 1993) and of penetration below surface layer present in wax sampling (Marion and Fraccarollo, 1997), ensuring surface-only samples. Grains extracted by the plasticine were sieved and weighed to obtain the size distribution. These area-by-weight results are not directly comparable to particle counts; hence, the method proposed by Marion and Fraccarollo (1997) was applied to convert the area-by-weight data of the areal sample into volume-

by-weight, i.e. conventional bulk sieve analysis, which is equivalent to the particle count procedure used here (Kellerhals and Bray, 1971; and Church *et al.*, 1987; Wilcock and McArdell, 1993; Rice and Church, 1996).

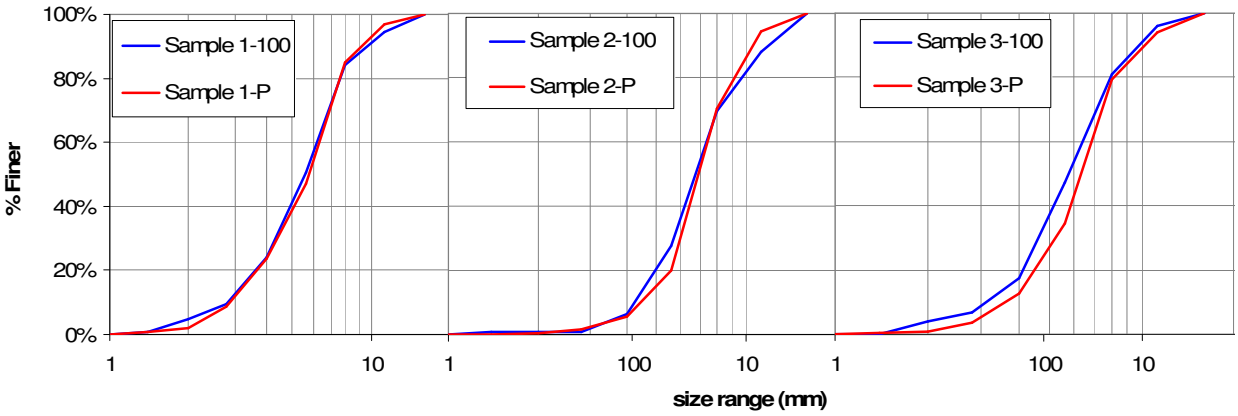

Fig. 3-17. Comparison of bed surface compositions data from particle count and areal sampling (plasticine). Sample i-100: particle count of 100 particles. Sample i-P: areal sample using soft plasticine. Deviation between particle count and areal sample for Sample 3 is likely due to fine material not having been fully picked by the plasticine.

Counts of 25 particles of the same surface sampling area were replicated four times to produce total counts of 100. These samples produce size distribution curves that are similar to those from the areal sampling (Fig. 3-17 and Table 3-10), with ratios of main particle diameters for particle count over areal sampling in the range of 0.91-1.09. Of particular similarity are samples 1 and 2 (Table 3-10), with bed surface composition from particle count obtained for sample 3 being finer than the results from the areal sample. This may be linked to lower efficiency of the plasticine picking finer grains from the bed in this sample. This comparison of the results from the particle counts and other sampling methods confirmed that the methodology proposed was valid to represent bed size distribution of the sediment bed surface, as shown by the similarity and consistency of results shown in Fig. 3-17.

	Sample 1		Sample 2		Sample 3	
	Particle count	Areal sample	Particle count	Areal sample	Particle count	Areal sample
D_{16}	3.33	3.39	4.72	5.17	4.14	4.24
D_{50}	5.57	5.79	6.88	7.03	6.08	6.42
D_{90}	9.89	9.39	11.66	10.69	9.89	10.36

Table 3-10. Comparison of main mixture diameters from coloured particle count (100) and areal sampling.

3.4.3.3 Bed preparation and comparison with bulk mix

Preparation of the bed followed conventional procedure similar to that described in Wilcock and McArdell (1993). Bed material was thoroughly mixed manually and then levelled following the flume slope to create a planar surface. The resulting bed was called *screeded bed*. These initial beds are compared with the bulk mix, to assess the effect of the preparation procedure. Ten beds are used for this: the three beds initially tested above, plus seven of the beds prepared during Stage 1. The aims of this analysis were: (1) testing the consistency of the mixing and, (2) whether any bias on the bed surface composition was introduced by the bed preparation procedure. Fig. 3-18 shows a summary of the results.

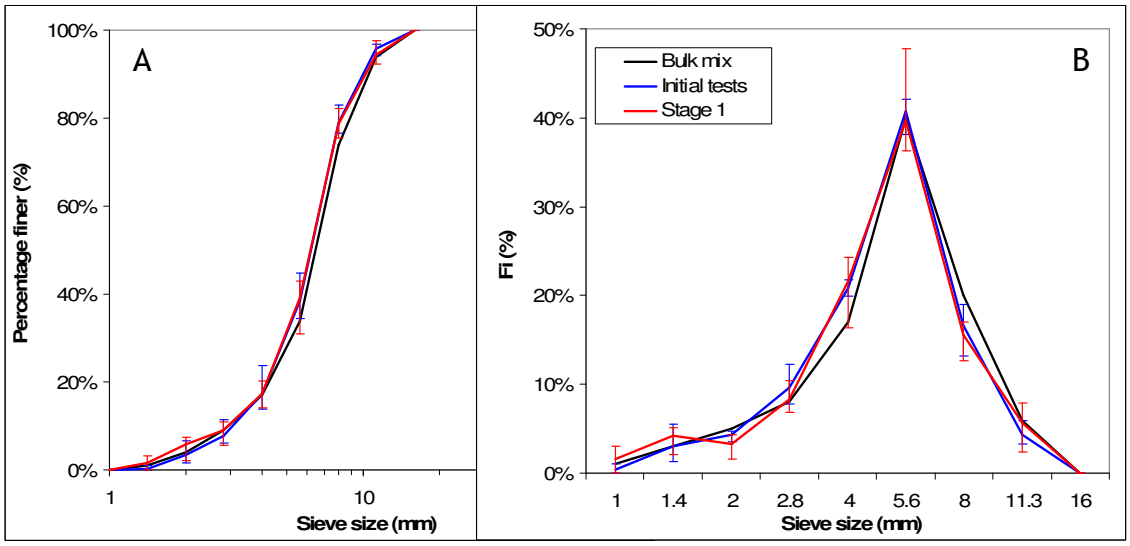

Fig. 3-18. Comparison of screeded bed and bulk mix. A) Cumulative grain size distribution, B) Individual percentage weight of each size class. Vertical error bars indicate the range of data obtained.

Results from both the initial tests and Stage 1 are consistent with those of the bulk mix for individual values of f_i and for the cumulative grain size distribution. The bed preparation procedure appears to increase the presence of the 4-5.6 mm size class by approximately 4-5 % units, combined with approximately 3.5% units reduction in the presence of the 8-11.3 mm and 11.3-16 mm classes. The overall result was that the bed surface composition was slightly finer than the bulk mix (D_{50} = 6.4 and 6.6 mm respectively). Differences for all other size classes are below 2%. Average values closely follow the size distribution of the bulk mix demonstrating that the bed preparation procedure did not introduce

major bias or grain size segregation on the experimental beds and could be assumed to be similar to the designed bulk bed composition.

These findings contrast those of Wilcock and McArdell (1993), where colour bias is suggested. They report a general overcounting of brighter colours and undercounting of darker colours. However, surface bed composition of their test beds clearly shows values of $f_i/F_i > 1$ for D < 8 mm and $f_i/F_i < 1$ for D > 8 mm regardless the colour. They also projected a grid over the photographs to define the grain count; therefore, selecting grains automatically, eliminating user bias. Wilcock and McArdell (1993) did not report colour confusion among orange, yellow and pink as one might expect, but overall excess of particle count for these three colours. Data in Wilcock & McArdell (1993) suggest finer bed surface composition of the prepared beds than that of their bulk mix. This is confirmed by the surface bed size distribution graphs (Fig. 5 of Wilcock & McArdell, 1993), where the start-up beds are noticeably finer than the bulk bed. Thus, their values of f_i/F_i are not a consequence of grain colour but a real change in size distribution of their start-up beds. Thus, values of $f_i/F_i > 1$ and $f_i/F_i < 1$ should be referred to as over-presence and under-presence respectively. It is reiterated that there cannot be over or under counting of particles of a specific colour range unless (1) grains are individually selected by the operator, which is not the case as an automatically generated grid was projected simultaneously over the entire image area, or (2) colours are not clearly distinguishable, so user subjectivity affects the colour choice. This last issue was avoided in this research by ensuring that no two consecutive size classes had similar colours.

3.4.4 Clustering analysis using UV light

The use of UV painted grains and UV lights meant that these specific particle size classes could be visually isolated from the others. This was used to analyse potential clustering of grains. The study of particle clustering was based on the assumption that bed particles were initially randomly distributed over the bed surface prior to exposure to flow. As increasing flows are applied to the bed for a range of durations (section 1.3), particles, specifically the larger sizes, are expected to move and become arranged into groups of grains or clusters (Reid *et al.*, 1997; Church *et al.*, 1998; McEwan *et al.*,2004; Oldmeadow and Church,

2006). Thus, if the initial number and average surface area of clusters of a given particle size can be estimated, subsequent variations of these values (such as reduction of the number of groups and increase of their average size) would indicate such clustering, provided that the total area occupied by the grains remains approximately constant. Visual inspection of the images can be used to support any identification of clustering in this way.

Statistical methods for clustering analysis are available, such as the nearest-neighbour analysis (Unwin, 1981). These are based on the spatial position, *x* and *y* coordinates, of each element. However, such methods require a degree of accuracy and consistency of the image positioning that was not achievable in this work, as the frame supporting the camera was cyclically repositioned along the flume for each image series. Thus, an alternative technique was required for the experimental conditions in the present thesis.

The conceptual scheme applied in this research relies on the identification of individual particles or groups of them and the estimation of their surface area. This was done using an additional plug-in for ImageJ, called *Threshold Colour*, created by Prof. Gabriel Landini, School of Dentistry, University of Birmingham[7]), and available under General Public Licence. Among other capabilities, this application can threshold a specific colour from an image by selecting a range of values within the HSB (Hue, Saturation, Brightness) range. Two grain size classes, 5.6-8 mm (D_{50}) and 8-11.3 mm (D_{90}), were painted in red and blue UV paint respectively. Fig. 3-19 shows an example of image of the bed surface under UV light and corresponding HSB histograms provided by Threshold Colour. Hue values clearly show the detection of the red and blue colours on the image, represented by the peaks of the histogram. The red colour falls approximately in the range 0-40 whereas the blue colour falls within the range 70-190. The brightness histogram also displays a peak around a value of 70, approximately differentiating areas of shadow and those illuminated. As two size classes were painted, clustering analysis was initially attempted for both particle sizes. However, as the red colour corresponds to the bed grain size

[7] http://www.dentistry.bham.ac.uk/landinig/software/software.html

distribution mode, with values of f_i > 40%, a large percentage of the image area was covered by this colour and the result was large interconnected areas across the image (Fig. 3-20), making the analysis of particle clustering meaningless. However, results from thresholding the blue colour, corresponding to the 8-11.3 mm size class, with f_i ≈ 15%, showed better individual particle/group identification (Fig. 3-21). Therefore, only the 8-11.3 mm size class was used for clustering analysis. After thresholding for blue in ImageJ, using the parameters of hue and brightness defined above, images were transformed into binary, after which individual particle/group surface areas were automatically calculated by ImageJ. This data set formed the basis of the numerical analysis.

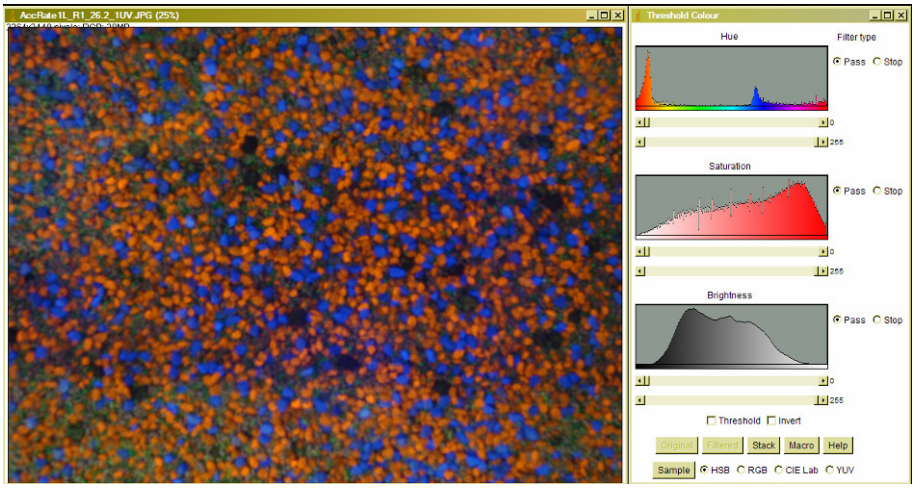

Fig. 3-19. Example of UV image and Threshold Colour histograms

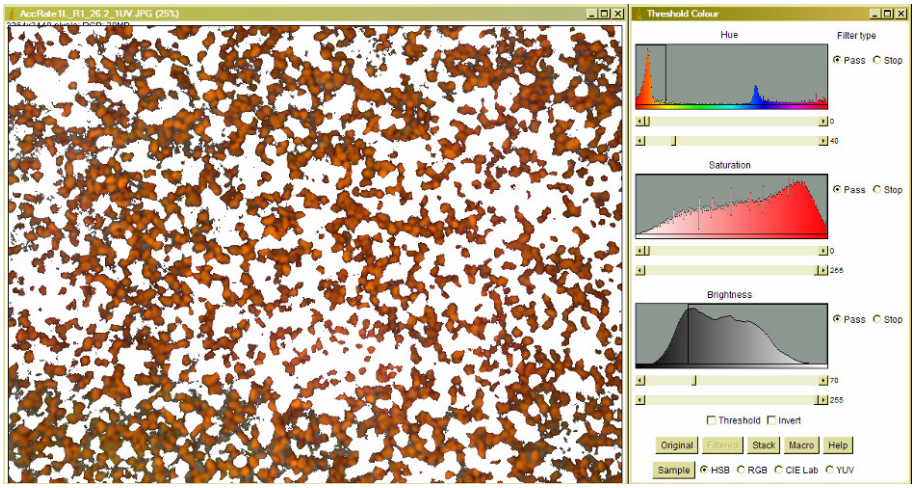

Fig. 3-20. Example of resulting image after applying the thresholding ranges to red colour

Very small areas were typically produced by this procedure (circled areas in Fig. 3-21). These were eliminated from the final calculations by setting a minimum

area size for the raw data provided by ImageJ. This filter, set at 0.2 cm^2 after testing a range of values, dramatically reduced the number of particles/groups with minimal effect on the total area. This minimum surface area is over 30 times smaller than that of an 11.3-16 mm grain (using *b-axis* = 11.3 mm and *b-axis*/*a-axis* = 0.6). Values of total area A_{tot}, total number of particle groups or *elements* N_e and average element size a_i were calculated for the filtered data set.

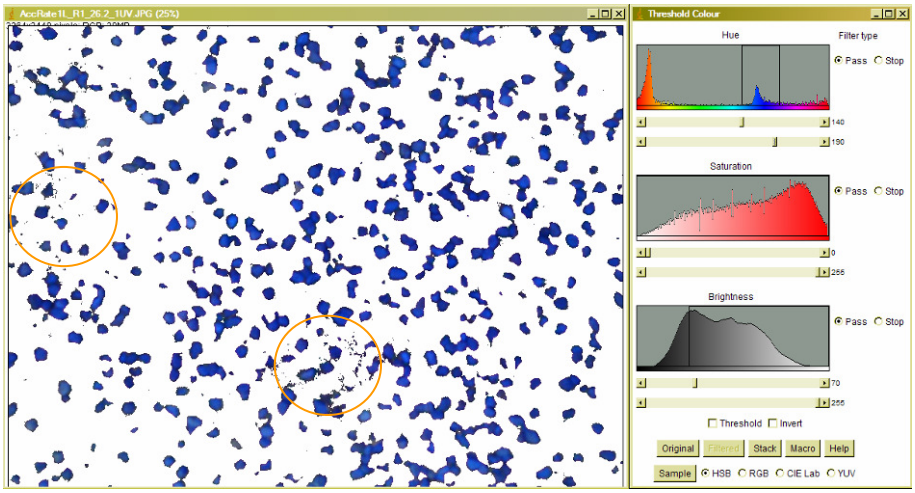

Fig. 3-21. Example of resulting image after applying the thresholding ranges to blue colour. Circles show very small thresholded areas removed during the filtering process.

The clustering data allowed calculation of the evolution of the abundance and position of the 8-11.3 mm size class with flows and thus, cluster formation. This data is only available for Stage 2. The results of the clustering analysis are detailed in section 4.2.8.

3.4.5 Methods for estimating bed shear stress and velocity

Estimation of bed shear stress is a fundamental aspect of this research, as the analysis of entrainment thresholds and thus, bed stability, will be based on shear stress values and their variability with antecedent conditions. Three available methods are discussed here, two of them based on velocity data at individual locations (using velocity profiles and Reynolds stresses) and a third one based on cross sectional averaged bed shear stress (depth-slope).

3.4.5.1 Velocity profiles and the Law of the wall

Velocity profiles were obtained at a single location on the centre line of the flume using ADV (section 3.3.1). Manipulation of equation 2-8 and equation 2-9 results in the equation of a straight line with independent variable *ln(z+d)*, slope u_* / κ and intercept $C = u_* B - u_* / \kappa \ln(k_s)$ for eq. 2-8 or $C = -u_* / \kappa \ln(z_0)$ for eq. 2-9. Therefore, a straight line fitted to the data plot of *ln(z+d)* against *u(z)*, provides values for u_* , z_0 and *B*. This procedure for estimating u_* by fitting a straight line to the velocity profile data is called the Clauser method (Graf, 1998). Shear stress is then determined using $\tau = \rho \cdot u_*^2$. Further details of the procedure and range of depth to which the line is fitted to are described in Wilcock (1996), Graf (1998), Dey and Raikar (2007) and Piedra *et al*. (2009).

3.4.5.2 Reynolds shear stress

Velocity time series can be manipulated to derive the turbulent components of streamwise and vertical components of velocity, *u'* and *w'*, respectively. In this way, the values of the Reynolds shear stress $\tau = -\rho\overline{u'w'}$ can be estimated for the entire flow depth. Under uniform flow conditions, the plot of τ against the dimensionless depth *z/H* (*z* = distance from the bed and *H* = total depth) produces a profile to which a straight line with a negative slope can be fitted (Song and Chiew, 2001; Franca and Czernuszenko, 2006). The intersection of this straight line with bed elevation provides an estimate of the bed shear stress over the bed surface. Using the equation $\tau = \rho \cdot u_*^2$ the shear velocity can be obtained.

3.4.5.3 Depth-slope

Under uniform flow conditions, as present here, bed shear stress can be calculated using equation 3-1 (Shvidchenko *et al*., 2001)

$$\tau = \rho g R_h S_0 \qquad \text{Eq. 3-1}$$

with τ = shear stress (kg/m/s^2 or Pa), ρ = water density (kg/m^3), g = gravity acceleration (9.81 m/s^2), R_h = hydraulic radius (m), and S_0 = energy slope (m/m) (parallel to the water surface and bed for uniform flow).

Equation 3-1 provides a cross-section averaged shear stress, so including all elements of boundary roughness (bed grain roughness, bedforms, flume walls, and turbulent energy dissipation). The values obtained with this method are likely to differ from those obtained with the velocity profile and Reynolds stresses, which are based on data taken at a single profile at one location (Dey and Raikar, 2007, Piedra *et al*. 2009). In laboratory experimentation, where the width of the channel is relatively small compared to the flow depth, the influence of the walls has to be eliminated if accurate estimates of the bed shear stress are required. Two equations commonly used for wall-effect correction are:

$$\tau = \rho g h S \left(1 - \frac{0.114}{b} \left(\frac{V^7 \nu}{S^4 g^4} \right)^{0.2} \right) \qquad \textit{Eq. 3-2}$$

(Einstein, 1942), where h = flow depth (m); S = energy line gradient; V = cross-sectional average velocity (m/s); ν= kinematic viscosity of the fluid (m2/s); b = channel width (m), and

$$\frac{\tau}{\rho g h S} = \frac{b}{b + 2h} \frac{fb}{f} \qquad \textit{Eq. 3-3}$$

(Vanoni and Brooks, 1957) where $f = 8gRhS/V^2$ channel friction factor; $fb = f + 2h(f - fw)/b$ bed friction factor; and $fw = \left[20(R/f)^{0.1} - 39\right]^{-1}$ wall friction factor, where $R = 4VR/\nu$.

The adoption of one correction method over the other does not appear to be based on any particular factor. Kleinhans and van Rijn (2002) used Vanoni and Brooks' (1957) equation; whereas Olmeadow and Church (2006) and Shvidchenko and Pender (2000) used the Einstein method. In the calculations presented herein, corrected values of bed shear stress provided by the Einstein (1942) and Vanoni and Brooks (1957) methods were identical (< 0.2 %) in all cases. The wall correction reduced bed shear stress values between 2-5% for the flow range 15-50 l/s, with percentages increasing with flow magnitude. Table 3-11 shows a summary of the values used for Stages 1 and 2 of this study.

Slope (m/m):		0.0067	Width of flume (m):		0.90
Average Temp (°C):		23	Kinematic viscosity (m^2/s):		9.4e-07
Density of material (kg/m^3):		2,540	Density of water (kg/m^3):		997.62
Q (l/s)	**h (mm)**	**A (cm^2)**	**V (cm/s)**	**u_* (cm/s)**	**τ_b (Pa)**
12	33.8	304.0	39.5	4.66	2.16
15	37.8	339.9	44.1	4.91	2.41
20	44.2	397.4	50.3	5.30	2.80
25	50.2	451.9	55.3	5.64	3.18
30	55.9	503.5	59.6	5.95	3.53
35	61.3	552.1	63.4	6.22	3.85
40	66.4	597.7	66.9	6.46	4.16
45	71.1	640.3	70.3	6.67	4.44
50	75.6	680.0	73.5	6.87	4.71

Table 3-11. Summary of values of discharge Q, average depth h , wetted area A, average cross section flow velocity V, bed shear velocity u, and bed shear stress τ_b estimated using Vanoni and Brooks (1957). Note that results from Einstein (1942) method are the same.*

3.4.6 Estimation of entrainment thresholds

Two of the methods for the estimation of bed entrainment threshold discussed in Chapter 2 were applied here: Visual and Reference Transport methods.

3.4.6.1 Visual method (Yalin)

The visual, or Yalin's, method is based on the definition of a minimum number of particle movements, *N*, over a defined bed surface area *A* (m^2), for a limited time period, *t* (s). In this thesis, grain dislodgement, i.e. horizontal displacement of at least 1 particle diameter, is used as criterion for the particle movement count. The visual method was proposed by Neill and Yalin (1969) and modified by Yalin (1977), who suggested the following equation to calculate the minimum number of particles movements to define the threshold.

$$N = K \cdot \left[\left(\rho_s / \rho - 1 \right) g D \right]^{0.5} \cdot D^{-3} \qquad \text{Eq. 3-4}$$

with *K* = constant.

A modification to this approach is to calculate *N* explicitly from the bed properties and the parameters *A* and *t* (Paphitis and Collins, 2005).

$$N = \varepsilon \cdot A \cdot t \cdot \left[\frac{\rho D^5}{(\rho_s - \rho) g} \right]^{-0.5} \qquad \text{Eq. 3-5}$$

where ε = 10^{-6} (lower limit suggested by Yalin, 1977). The value of *N* refers to the number of grain entrainments (movements) per unit area and time of observation; however, *N* in equation 3-5 does not have units once the values of *A* and *t* are introduced, although its value remains intrinsically associated to the combination of *A* and *t*.

Equations 3-4 and 3-5 only provide a value of *N* for a sediment bed composed of a single particle size. Wilcock (1988) modified equation 3-4 to include graded material, using D_{65} as the representative diameter of the bed mix. The minimum number of particle movements N_i of class *i* was defined as $N_i = m_i \cdot A$, with $m_i = X f_i / D_i^2$, f_i = proportion of class *i* on the bed surface, D_i = diameter of size class *i*, and $X = m_{D_{65}} \cdot D_{65}^2 / f_{65}$, $m_{D_{65}} = N_{D_{65}} \cdot t$; with $N_{D_{65}}$ obtained by applying equation 3-5 using D_{65}.

In the present thesis, the application of equation 3-5 to the uniform and near-uniform gravels (*D* = 4.8 mm) and Wilcock's (1988) method to the sand-gravel mix (D_{50} = 6.6 mm, D_{65} = 7.5 mm and f_{D65} = 0.4) over an area *A* = 150 x 150 mm^2 and recording time *t* = 180 s resulted in threshold numbers of grain movements of *N* = 10 and *N* = 4 respectively.

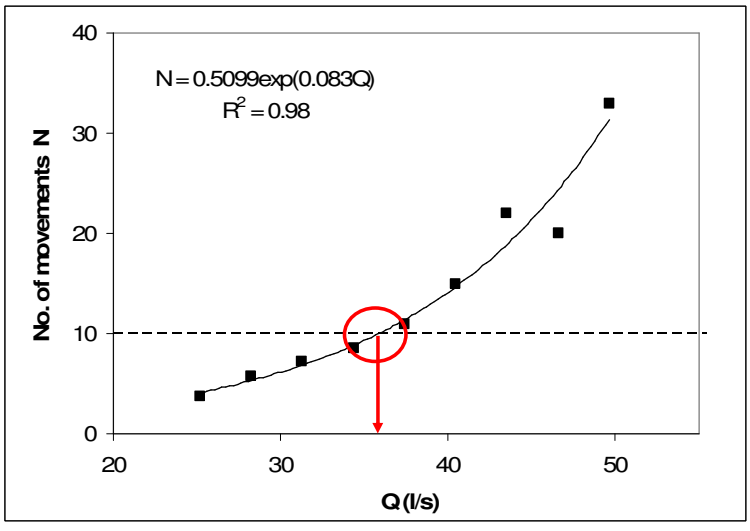

Fig. 3-22. Example of estimation of critical flow using exponential line fitting.

The relationship between flow and *N* could typically be represented by an exponential equation. The intersection of the fitted line with the threshold

criterion provided an estimate of critical flow (*Fig. 3-22*). When several replicates of the same experiments were available the exponential trend line was fitted to the average number of particle movements of the corresponding replicates.

3.4.6.2 Reference transport method (RTM)

The estimation of the dimensionless bedload transport rate W_i^*, or q^*_{bi}, was based on three main elements: bedload transport rate q_{bi} , shear stress τ and bed surface composition of class i, f_i. The equations used to estimate W_i^* and q^*_{bi} are as follows:

$$W_i^* = \frac{(\rho_s/\rho - 1)g \cdot q_{bi\ vol}}{f_i \cdot u_*^3} \qquad \textit{Eq. 3-6}$$

$$q_{bi}^{\ *} = \frac{q_{biw}}{f_i \rho_s \sqrt{(\rho_s/\rho - 1)g D_i^{\ 3}}} \qquad \textit{Eq. 3-7}$$

where, ρ_s is the sediment and fluid densities respectively, q_{bivol} = volumetric bedload transport rate, q_{biw} = mass bedload transport rate, f_i = proportion of size class i on the bed surface, u_* = bed shear velocity and D_i = particle diameter of size class i.

The bedload transport rate (kg/m/s) was calculated from the dry weight of each sample collected in the sediment trap divided by the sampling period (duration of flow step). Volumetric rates were calculated by dividing by the material density (2.54 x10^3 kg/m^3). Bed shear stress was estimated using the relationship between flow and average flow depth in the flume obtained for the uniform flow settings (section 3.2.4). The depth-slope method (section 3.4.5.3) was used to calculate values of shear stress for each flow. The proportion of each size class on the bed surface was calculated from the image particle count results (section 3.4.2).

The calculated W_i^* (or q^*_{bi}) values were plotted against Shields parameter θ using logarithmic scales (Fig. 3-22). A complete data set for each experiment provided a series of approximately parallel lines of data that could be fitted by equations similar to those proposed by Shvidchenko *et al.* (2001) and Wilcock and Crowe

(2003) (with modified parameters as discussed in Chapters 4 and 5) (Fig. 3-23). The intersection of each fitted line with the corresponding reference transport rate ($W_i^* = 0.002$ – Parker *et al.*, 1982a; $q^*_{bi} = 10^{-4}$ – Shvidchenko *et al.*, 2001) provided a value of the entrainment threshold for each size class. The bed entrainment thresholds used for the assessment of the influence of antecedent conditions were those corresponding to the bed modal size class, which contained D_{50}.

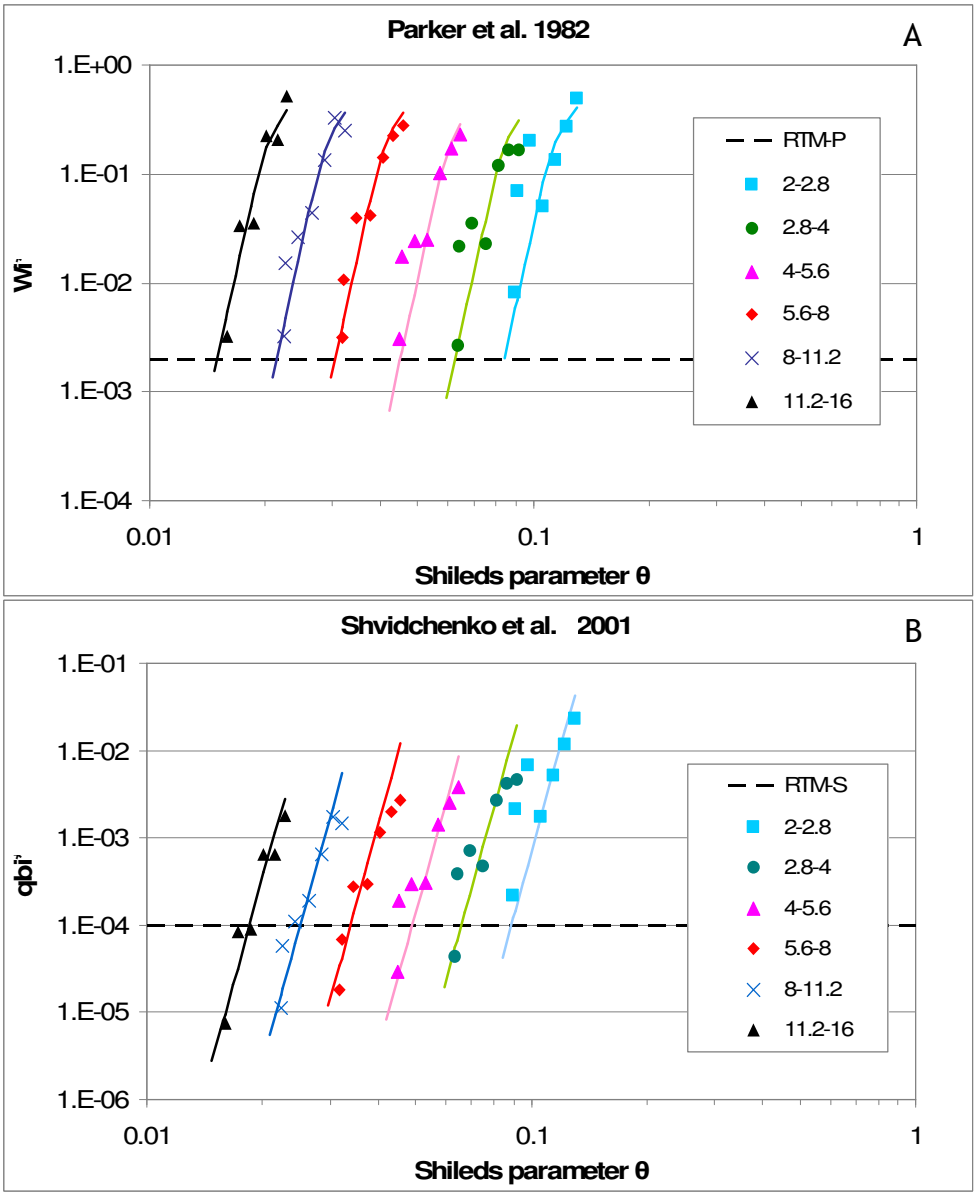

Fig. 3-23. Example of data plots for reference transport methods. A) Parker et al. (1982a) and, B) Shvidchenko et al. (2001). Note how the fitting lines for the RTM-P curve inwards following the data point trends for larger transport rates.

Bedload samples were typically collected for the last two flow steps of the antecedent conditions phase and for each of the flow stages of the stability test

in order to maximise the number of data points both sides of the reference transport rate line (Fig. 3-23). Visual fitting was used to position the fitting lines by iterative adoption of an entrainment threshold, with increased weighting to the data range corresponding to the stability test. All values of τ_{cr} resulting from the reference transport method (in its two alternatives, i.e. RTM-P and RTM-S) presented here were obtained following this procedure. There is an argument for not including the data corresponding to the latter stages of the antecedent conditions based on the fact that conditions are not comparable among acceleration rates since the bed is evolving under different duration of flows. A sensitivity test of the results of τ_{cr} was undertaken for the full data set of Stage 1 for all the bed size classes. This consisted of the re-estimation of the entrainment threshold stresses, by re-fitting the lines, considering only those flows equal or larger than Q_{ref} (31.5 l/s); thus, including only homogeneous flow steps and durations. Of the 89 shear stress values considered, only 2 of them changed, with differences between original and updated values within ±3% with respect of the original ones (these results relate to RTM-P). Therefore, the effect of the data points on the values of τ_{cr} is negligible. These results confirm the suitability of the methodology adopted and the appropriateness of the weighting applied to the stability test data. The values presented throughout this thesis correspond to the initially estimated ones.

In order to obtain the parameters of the equations proposed by Shvidchenko and Pender (2000), Shvidchenko *et al*. (2001) and Wilcock and Crowe (2003), all data sets were collapsed by plotting W_i^* and q^*_{bi} against τ/τ_{cr} producing an approximate collapse onto a single line (*Fig. 3-24*). Values of the parameters were obtained after reiteratively visually optimising the fit. Visual fitting of this type of curves has been previously used by others, including the technique's authors (eg. Shvidchenko *et al.*, 2001; Saadi, 2002; Wilcock and Crowe, 2003), as the method requires a degree of judgement due to the wide range of transport rates and the bias towards reducing errors of the large transport rates introduced by least-square error fitting. Thus, it is noted that the results and parametisation have a degree of subjectivity. Chapter 5 shows the final parameters used.

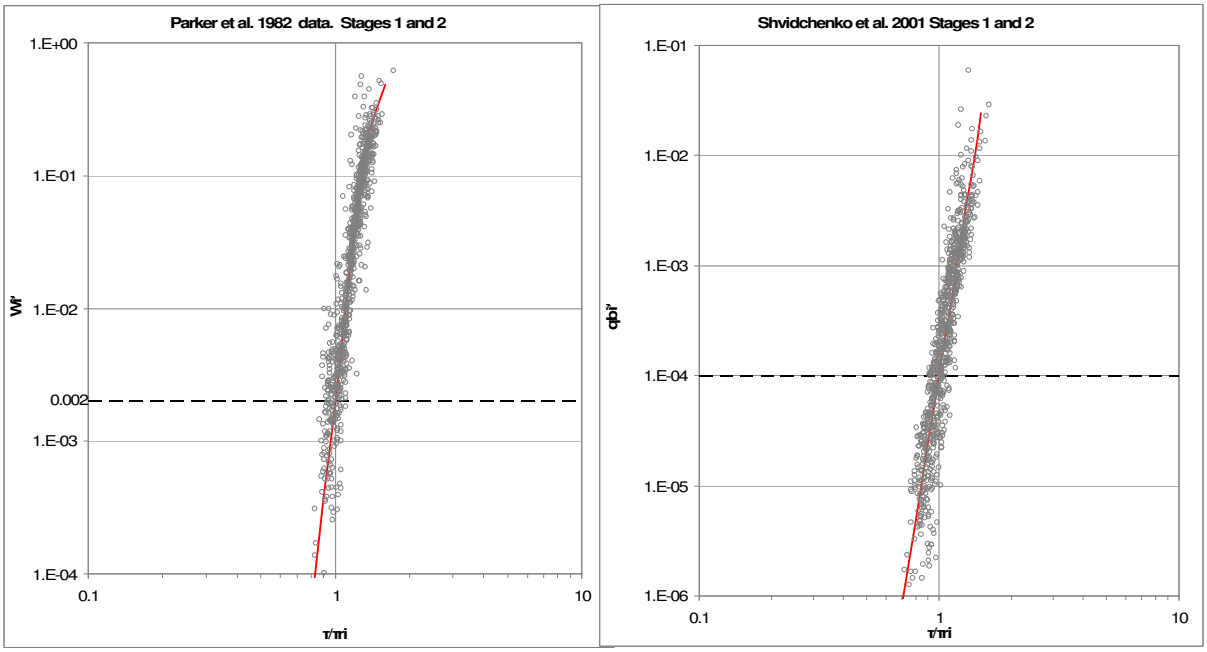

Fig. 3-24. Collapsed dimensionless transport rate data and fitting of equations developed.

3.5 *Experimental programme*

A total of 76 experiment runs (Table 3-12, Appendix 2) were undertaken for this thesis. They can be divided in three main series depending on equipment available and experimental complexity:

1) Preliminary analysis of the effect of antecedent conditions using a near-uniform gravel (Pilot Runs). These were based on particle movement counts only
2) Flume experiments using a unimodal sand-gravel mix, these were further sub-divided in Stage1 and Stage 2 as means of studying the separate effects of flow magnitude and time exposure. Both particle entrainment counts and bedload samples were available.
3) Repetition of Pilot Runs with steeper slope and collecting particle movement counts and bedload samples simultaneously.

In addition to particle movement count, bedload samples and bed surface composition data (complete runs), velocity data was also collected. Since the time necessary to obtain a full velocity data profile (30-45 min.) was incompatible with the short duration of the successive increase of flows used in

the experiment runs, additional partial experiments were carried out whenever velocity data was required. These consisted of the repetition of the run until the flow required was achieved, collecting velocity data and stopping the experiment when finished. No other data (eg. bed surface composition or bedload) were collected during these partial experiments. These replicates of the runs have implicitly associated the correspondence of the conditions recorded in the complete runs with velocity data recorded for the partial runs. Table 3-12 below contains a summary of the experiment series and the data collected in each of them. Appendix 3 contains a full list of the experiment run characteristics and hydraulic conditions.

Series	Slope	Grain size range (D_{50}) (mm)	Duration of acceleration rates (h)	Data collected	Experiment no.
Pilot Runs (near-uniform gravel)					
Complete run	1/200	2-8 (4.8)	0.5, 1, 2, 4, 6	PMV	[1] to [18]
Partial run	1/200	2-8 (4.8)	0.5, 1, 2, 4, 6	ADV	[19] to [30]
Unimodal mix					
Stage 1					
Complete run	1/150	1-16 (6.6)	0.5, 1, 2, 4, 6, 10	BIW, BIUV, BLS, PMV	[31] to [49]
Partial run	1/150	1-16 (6.6)	0.5, 2, 6	ADV	[50] to [54]
Stage 2					
Complete run	1/150	1-16 (6.6)	0.5, 1, 2, 6	BIW, BIUV, BLS, PMV	[55] to [66]
Uniform gravel					
Complete run	1/150	4-5.6 (4.8)	0.5, 2, 6	BLS, PMV	[67] to [75]
Partial run	1/150	4-5.6 (4.8)	0.5, 2, 6	ADV	[76] to [79]

BIW: bed images (white light); BIUV: bed images (UV light); BLS: bedload sample; PMV: particle movement video; ADV: velocity data using ADV.

Table 3-12. Summary of experimental runs and data collected in each group.

3.5.1 Data sampling scheme

The four main data sets collected were (Table 3-12): (1) Bed particle movement, (2) bed surface composition, (3) bedload samples amounts and composition and , 4) velocity data. Bed particle movements were recorded in video (3.4.1) of intermittent segments of 3 minutes at the beginning of each flow period monitored. Photographs of the bed surface (UV and white light) were taken immediately after video recording, taking approximately 30 seconds for each of the four locations (3.4.3). Bedload collection was continuous, with systematic replacement of the collection box at the end of each flow stage (section

3.2.2.3), thus, ensuring the full collection of the material transported during the specific flow duration. In the case of Stages 1 and 2, the entire cycle of data collection for each flow took 5-6 minutes. As mentioned above, obtaining profiles of velocity data required specific partial runs for which only such data was collected at the specified discharge. Appendix 3 contains details of flow steps and sampling sequences.

3.5.1 Definition of hydrographs

The test hydrographs used in this study can be divided in two main components:

- Antecedent conditions and,
- Stability test

Antecedent conditions were defined by increasing flows contained between a certain initial low flow Q_{ini} and what is here called target flow Q_t. This initial low flow (approx. 1/3 of critical flow for the bed) was run for 30 minutes as a common settling period to eliminate air pockets and the influence of the bed preparation procedure. The target flow was the maximum flow reached in the antecedent conditions, and had three possible values: Reference flow Q_{ref}, defined as the critical entrainment flow of the bed when subject to no antecedent conditions; and Q_L and Q_H, target flows that were 8% lower and higher than Q_{ref} respectively (section 4.2.1.2). This ±8% is the result of a compromise between a meaningful change of Q_{ref} and avoiding overlapping with the flow steps already established for Stage 1. Once the target flows were defined, the acceleration rates of the antecedent conditions were determined by a range of durations: 0.5, 1, 2, 4, 6 and 10 hours. The maximum duration was limited by the ability to complete a full experiment without running the flume overnight. The lines joining Q_{ini} and Q_t separated by the specified durations provided the theoretical antecedent conditions and the acceleration rates (Fig. 3-25). These idealised continuously increasing flows were in practical terms segmented into a series of steady flow steps, each under uniform flow conditions.

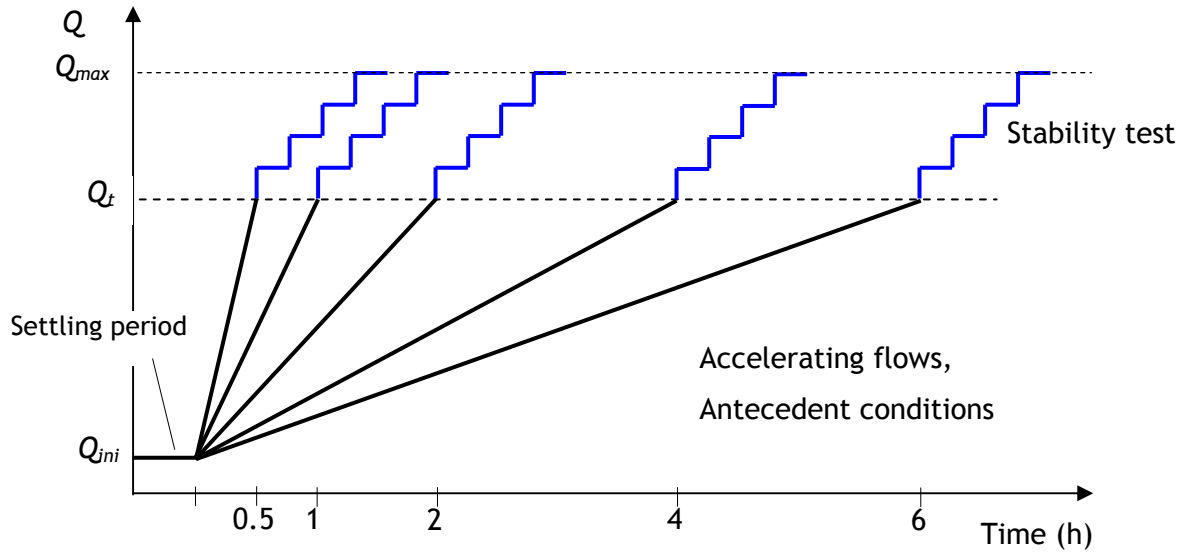

Fig. 3-25. Sketch of test hydrographs

	Near-uniform gravel (Pilot Runs)	Unimodal sand-gravel (Stage 1)	Unimodal sand-gravel (Stage 2, L)	Unimodal sand-gravel (Stage 2, H)	Uniform gravel
Bed slope	1/200	1/150	1/150	1/150	1/150
Q_{ini}	12.7	12	12	12	12
Q_{ref},	35.6	31.5	-	-	29.2
Q_L	-	-	29	-	-
Q_H	-	-	-	34	-
Q_{max}	56	50	50	50	50
Antecedent conditions					
No. of steps [1]	24	6	6	6	6
Flow step (l/s)	0.93	3.25	2.8	3.7	2.9
Duration of step (min.)[2]	1.25, 2.5, 5, 10, 15, -	6, 12, 24, 48, 72, 120	6, 12, 24, -, 72, -	6, 12, 24, -, 72, -	6, -, 24, - , 72, -
Stability test					
No. of steps	8	4	4	4	4
Flow step (l/s)	3.2	5	5	5	5
Duration of step (min.)	4	6	6	6	4

[1] *The number of flow steps for Stages 1 and 2 and the uniform gravel experiments were reduced in order to increase their duration and have sufficient time to sample bed surface composition and bedload.*
[2] *Durations correspond consecutively for AccRate1, AccRate2, AccRate3, AccRate4, AccRate5, and AccRate6 (L or H where applicable).*

Table 3-13. Summary of key flows used for the definition of test hydrographs and acceleration rates.

The stability test was conceptually the same for all experiments. A series of increasing flows of fixed duration that produced general mobility of the bed for the largest flow magnitudes. The duration of the stability test for the Pilot Runs

and uniform gravel experiments was 4 minutes; whereas the corresponding duration for Stages 1 and 2 was 6 minutes. This difference was due to the longer data collection period required for the sand-gravel bed that involved photographing the bed surface. Flows for the stability test ranged from Q_{ref}, to a maximum flow that ensured bed mobilisation, Q_{max} (Fig. 3-25). Table 3-13 shows a summary of the main characteristics of all the hydrographs used in this research. Extended information on Stages 1 and 2 and uniform gravel tests is presented in Appendix 3.

Chapter 4
Experimental results

"This river will teach you everything you need to learn…"
- James F. Twyman.

Experimental results

As documented in Chapter 3, three bed compositions were used: a near-uniform gravel, a unimodal sand-gravel mix, and a uniform gravel. This sequence corresponds to both the time line of the research work and the level of complexity of the experiments and analyses. The same structure is followed in this chapter for the presentation of results.

4.1 *Near uniform gravel: Pilot Runs*

4.1.1 Bed configuration and summary of procedure

The flume bed was set-up as follows: the most upstream section of bed (1.5 m) was made of coarse gravel (D_{50} = 12 mm) to ensure rough turbulent flow. The 1 m^2 test section contained a very well sorted gravel (Hoey, 2004) (D_{50} = 4.8 mm, σ_g = 1.45) and was located between 4 m and 5 m from the flume inlet. The remainder of the bed comprised gravel fill of D_{50} = 7.5 mm. The bed slope was set at 1/200 and the sediment bed depth was approximately 40 mm.

Experimental variables are shown in Table 4-1. Each experiment followed a similar procedure of flooding, settling period, antecedent conditions and stability test (section 3.5).

Name	Duration	Acceleration rate	Range of flows	Range of depths
	(h)	(l/s/s)	(l/s)	(mm)
Reference[(1)]	0	---	11-56	37.5-93.1
AccRate1	0.5	0.0129	9-56	34.4-93.1
AccRate2	1	0.0064	10-57	36.0-94.1
AccRate3	2	0.0032	10-57	36.0-94.1
AccRate4	4	0.0016	9-56	34.4-93.1
AccRate5	6	0.0011	9-56	34.4-93.1

(1) This series included incremental flows in order to find the reference threshold flow.

Table 4-1. Summary of experimental runs for the near-uniform gravel

Critical flow of the bed with no antecedent conditions was estimated by fitting an exponential curve to particle movement data averaged for four replicates. The intersection of the fitted line with the criterion of N = 10 movements provided a critical flow of Q_{ref} = 35.6 l/s for the bed. Values of the individual replicates ranged from 34.5 to 39.6 l/s. Five acceleration rates were applied to the bed, ranging from 0.0011 l/s/s to 0.0129 l/s/s, corresponding to antecedent durations of 6h to 0.5h, respectively, between the end of the bedding-in phase and a target flow $Q_t = Q_{ref}$ (Table 4-1). Three repetitions of each acceleration rate run were undertaken, determining the new threshold flow using the same procedure as Q_{ref}.

The bed shear stress values at entrainment were calculated from measured velocity profiles in the centre of the flume over the test area, for each of the new critical flows. These data were obtained from additional repetitions (x2) of the experiment runs carried out until the new threshold flow was reached, at which velocity u data was collected, stopping the experiment immediately afterwards, as the velocity sampling phase introduced inadequate duration of flow exposure to the bed. A Nortek 3D Vectrino velocimeter (ADV) was used to measure velocity at 7 or 8 heights between 0.09 to 0.95 z/h, with z = distance from the bed and h = water depth. The logarithmic profile expression of equation 2-8 was used to estimate the value of shear velocity u_*; with $d = 0.2\ k_s$ (Graf, 1998), k_s was equal to D_{50} = 4.8 mm and κ = 0.4. Shear stress values were obtained using $\tau = \rho \cdot u_*^2$. The velocity data is contained in Appendix 7. The velocity data were averaged for the two repetitions before estimating u_*;

between-repetition differences of *u* were minimal (typically, within ±2% of the average value).

4.1.2 Results

Particle movements increase rapidly with increase in discharge, with trends well represented by exponential curves (Fig. 4-1). Repeatability is shown by the vertical error bars, which define the range of values obtained for the three repetitions. Absolute values of the range limits generally increased with flow magnitude, although the ratios given by the range maximum and minimum generally decreased with higher flows (Fig. 4-2). Critical flows were obtained after averaging grain detachments for the three repetitions.

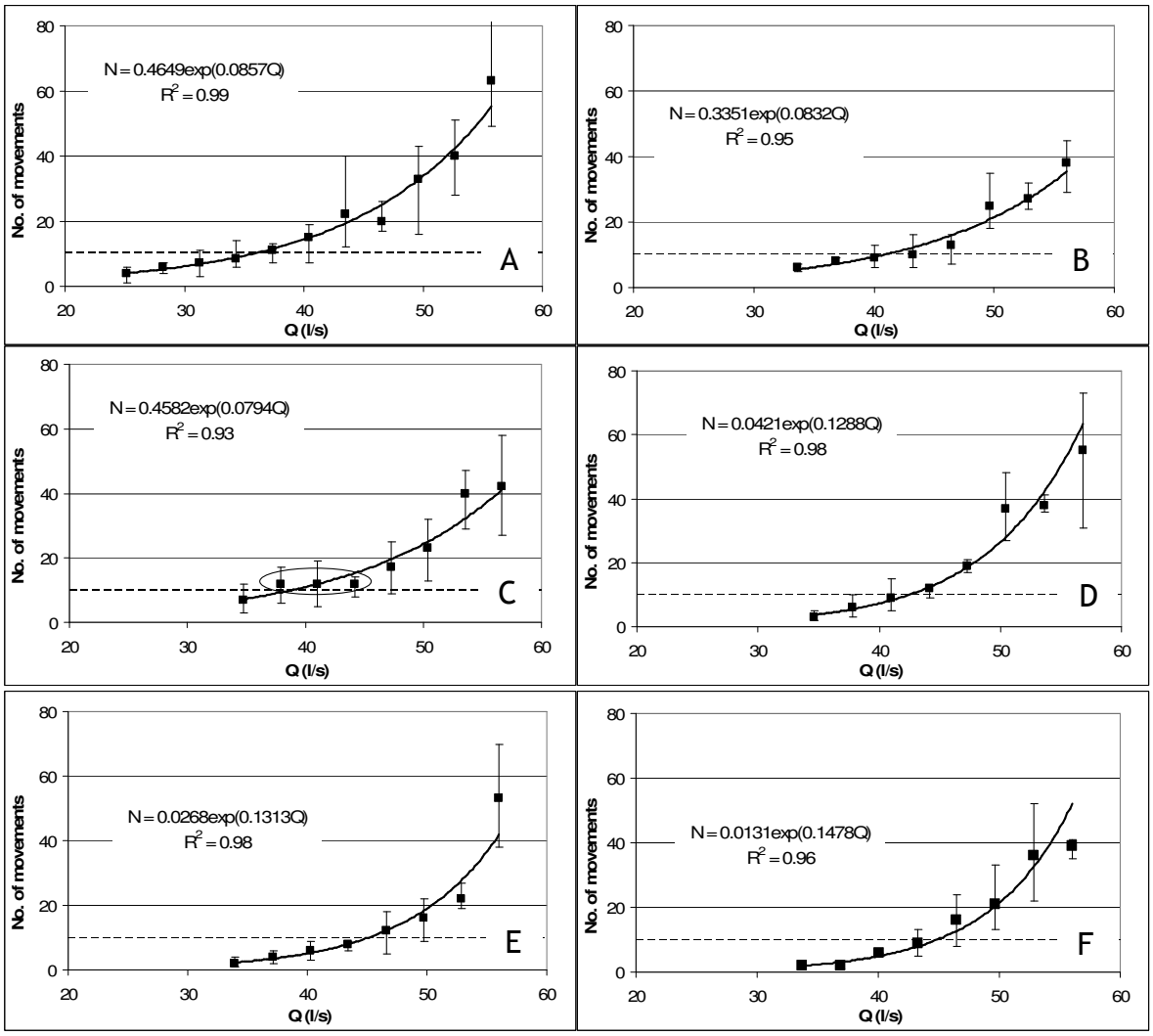

Fig. 4-1. Number of observed grain movements as a function of flow for near-uniform gravel bed. A) Reference; B) AccRate1; C) AccRate2; D) AccRate3; E) AccRate4; F) AccRate5.

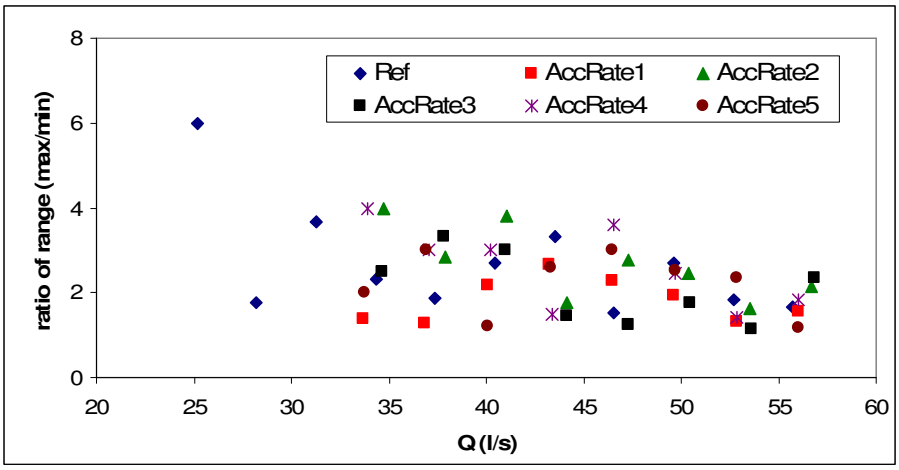

Fig. 4-2. Ratios of range (max/min) of the particle count scatter.

In general, resistance to entrainment increases with the length of exposure to increasing flows (smaller acceleration rates), from τ_{cr} = 4.07 Pa for no antecedent conditions to τ_{cr} = 6.70 Pa for the 6h run; with very similar values for the two longest durations, τ_{cr} = 6.96 Pa and τ_{cr} = 6.70 Pa for 4 and 6h respectively, (Table 4-2). Data from AccRate2, whose critical flow is lower than that for AccRate1, are inconsistent with the overall trend. The correlation coefficient of the best-fit exponential curve, R^2, of AccRate2 is the lowest in all cases. Additionally, Fig. 4-1C shows that the particle movement data have the same average values for three consecutive flows N = 12 (circled data points). This is likely to affect the entrainment data obtained and may explain the smaller values of Q_{cr} and R^2 for this particular duration.

Series	*Duration of increasing flows (h)*	Q_{cr} (l/s)	Q_{cr}/Q_{ref}	τ_{cr} (Pa)	u_*/u_{*ref}
Reference	-	35.6	1	4.07	1.00
AccRate1	0.5	40.8	1.15	5.48	1.16
AccRate2	1	38.8	1.09	5.18	1.13
AccRate3	2	42.5	1.19	6.63	1.28
AccRate4	4	45.1	1.27	6.96	1.31
AccRate5	6	44.9	1.26	6.70	1.28

Table 4-2. Summary of results using averaged particle movements.

Data in Fig. 4-1 suggests that the antecedent conditions delay the onset of full transport conditions until higher discharges, shown by the general horizontal displacement of the exponential curve along the x-axis, with values of critical

bed shear stress increasing by over 20% when durations are increased from 0.5h to 6h. This is also shown by the reduction of particle movements at the same Q_{ref} with increasing hydrograph duration (Fig. 4-3), where the initial N = 10 decreases to N = 3 for the 6h run.

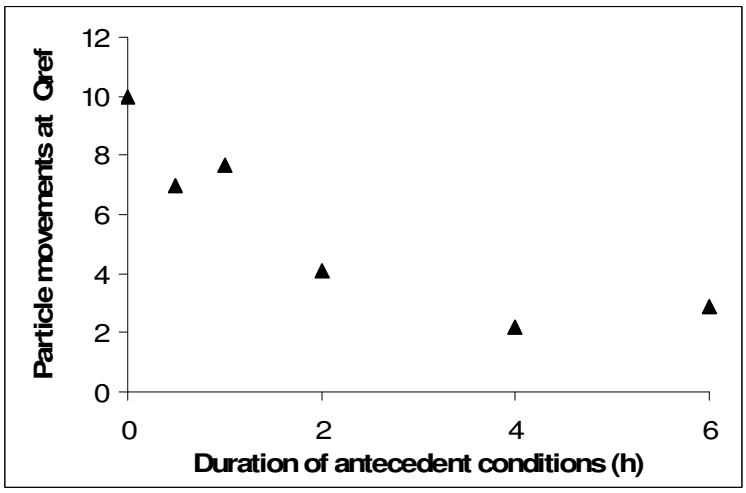

Fig. 4-3. Reduction of particle movements at the reference critical flow with increasing antecedent flow duration.

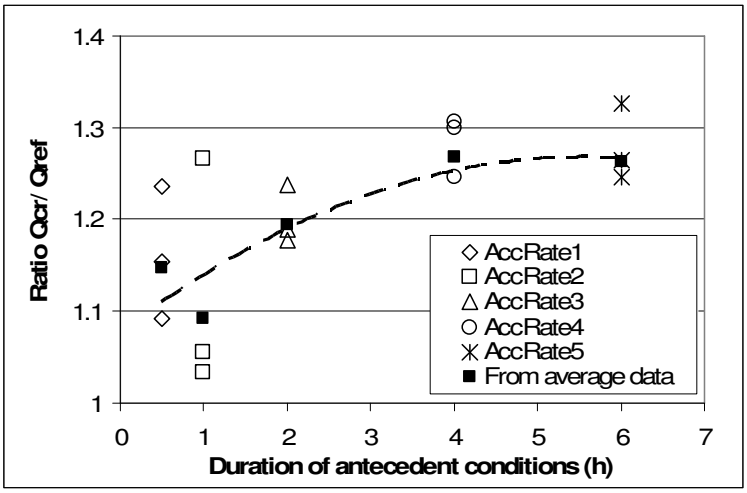

Fig. 4-4. Ratio of new critical flow (Q_{cr}) to reference critical flow (Q_{ref}) with flow duration for each of the three repetitions undertaken. Values obtained from fitting exponential curve to average N data are shown in Table 4-2.

The effect of the acceleration rates and flow durations can be assessed using the ratio Q_{cr}/Q_{ref} obtained for each acceleration rate (Fig. 4-4). Compared to Q_{ref}, all the runs that include antecedent flows lead to an increase of critical flow and shear stress. Critical flow values increase by over 26% over Q_{ref} for the two lowest acceleration rates 0.0016 and 0.0011 l/s/s (Table 4-2). In general, data indicates an inverse relationship between critical flow and acceleration rates; i.e. beds subject to higher acceleration rates have lower flows and shear

stresses at entrainment than those subjected to longer periods of increasing flows (Table 4-2). Fig. 4-4 demonstrates that the positive correlation between Q_{cr}/Q_{ref} and duration progressively weakens for longer durations. This suggests convergence to an upper limit of antecedent-generated stabilisation for durations between 4h and 6h (acceleration rates 0.0016-0.0011 l/s/s).

4.1.3 Discussion

Data show a positive relationship of entrainment thresholds with the duration of sub-threshold flows (longer rising limbs), with an apparent limit to the stability achieved by antecedent conditions (45 l/s approximately). Paphitis and Collins (2005), using the visual method for estimating entrainment conditions, also found the bed entrainment threshold increased with the duration of the sub-threshold flow exposure. They recorded an increase of shear velocity at etrainment of up to 27%, very similar to the reported increase of entrainment flows (26%).

The potential deficiencies of the visual method have been documented (Wilcock, 1988; Buffington and Montgomery, 1997), so precautions were taken to minimise uncertainties and operator errors (section 3.4.1). The variability of the determination of entrainment using the visual method was already highlighted by McEwan and Heald (2001), who linked this variability to the distribution of shear stresses. The data scatter between repetitions is linked here to the stochastic nature of particle movement, as spatial variability of granular displacements is related to flow turbulence and the protrusion, orientation and exposure of individual particles (Miller *et al.*, 1977; Carling *et al.*, 1992). Bottacin-Busolin *et al.* (2008) showed that particle movements correlated to changes in the flow velocity field and that particle movements were closely related to streamwise velocities. Thus, since flow turbulence is more intense for higher flows, flows may produce different movement counts between runs of the same experiment, as local turbulence differ from run to run, affected in turn by the bed surface topography and composition (Carling *et al.*, 1992; Papanicolaou *et al.*, 2001; Carollo *et al.*, 2005), which are randomly reset for each repetition. Increased scatter of counts for higher discharges may also be caused by collisions

between transported particles and those still on the bed, which was noted during counting, where moving particles impacted others which were then entrained. Grain impacts were also reported by Drake *et al*. (1988). Therefore, scatter shown by the data was mainly related to the physical processes and not to the experimental procedure or operator error (see section 3.3.8). Although certain scatter due to miscounting may be expected for large values of *N*, the scatter presented and discussed above refers to between-runs variability not within the same experiment.

Support for these findings is provided by previous studies. Saadi (2002) used similar test hydrographs to those applied here (for a bimodal sand-gravel mixture - D_{50} = 5.2 mm σg = 3.45) with flow accelerations of 0.0031, 0.0016 and 0.0010 l/s/s, followed by a common 3h receding flow phase. Two of these acceleration rates are very similar to those used in this study (0.0016 and 0.0011 l/s/s, Table 4-1). Saadi's (2002) results showed a decrease of transport rate with antecedent flow duration (lower acceleration rates) which could be associated with increased bed resistance. Paphitis and Collins (2005) tested the influence of the magnitude and duration of constant antecedent sub-threshold flows (no acceleration rates were considered) on bed threshold using Yalin's criterion and sand-sized sediment. The results presented in this thesis show a similar trend to Paphitis and Collins (2005) (Fig. 4-5): an increase of the critical threshold with antecedent flow duration and a slight decrease for the longest durations.

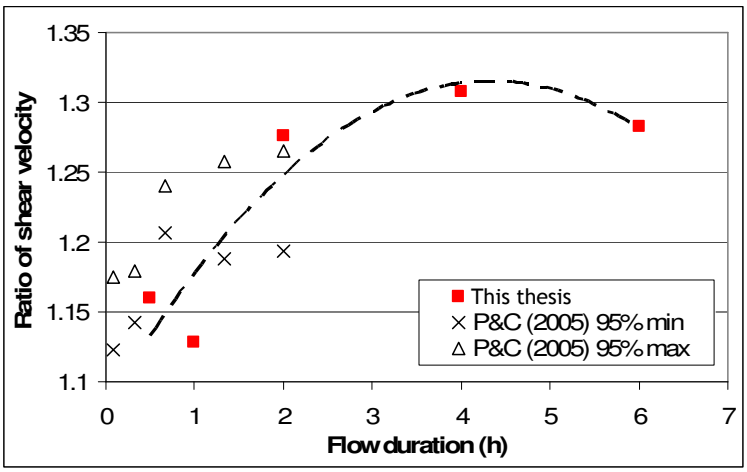

Fig. 4-5. Ratio of critical shear velocity with flow duration. Paphitis and Collins (2005) data (maximum and minimum) for 95% pre-threshold velocity included.

Although Paphitis and Collins (2005) used much finer sediment (0.194-0.774 mm) and shorter durations (5-120 min.), their largest increase in critical shear velocity, of around 25-30%, is similar to that obtained in the work presented here (around 25%, Table 4-2). In their work using constant flows Monteith and Pender (2005) and Haynes and Pender (2007) also reported increased bed stability with duration of sub-threshold flows. Their work used graded bed material, where the influence of hiding was suggested in partial explanation, the increase of bed stability with longer antecedent durations was also linked to packing density and stronger imbrication. The results presented here also indicate that there is a convergence of the data to a maximum limit of antecedent-linked stability, with similar threshold values for 0.0016 l/s/s (4h duration) and 0.0011 l/s/s (6h duration). This is in agreement the concept of a maximum critical flow suggested by Haynes and Pender (2007).

The results presented here demonstrate the effect of antecedent conditions on non-cohesive granular beds, specifically, on near-uniform gravel. However, bed compositions of natural rivers include large variety of sizes and therefore, findings based on uniform gravel may not be applicable to them (Carling, 1983; Bathurst, 2007; Recking, 2010). The study by Haynes and Ockelford (2008) underlines the need to analyse granular beds with different grain size distributions. Thus, the next series of experiments continued the investigation of the impact of sub-thresholds antecedent conditions on natural beds.

4.2 *Unimodal sand-gravel bed: Stages 1 and 2*

4.2.1 Reference critical flow and test hydrographs

The estimation of the critical discharge of the sand-gravel bed subject to no antecedent conditions was required for the creation of test hydrographs. A series of increasing flows, from 15 l/s to 50 l/s (τ = 2.41-4.74 Pa) in steps of 6 minutes duration were applied to the bed. Particle movement measurements and bedload samples were taken at each step.

4.2.1.1 Stage 1

Typically, two repetitions of each acceleration rate were carried out. In the case of the determination of Q_{ref} for Stage 1, the critical shear stresses determined from the first two repetitions were considerably different (Table 4-3); and an additional run was carried out. The critical flow value for this third repetition was nearly identical to the value for repetition 2 (Table 4-3), and thus, the first run was discarded. It is possible that the bed preparation procedure produced an unusually unstable bed in the first case, explaining this discrepancy of entrainment values. Variability of experimental results, in terms of entrainment thresholds, was anticipated; nonetheless, the consistency of the values of Q_{ref} obtained for the last two repetitions supports the procedure followed. Carrying out a higher number of repetitions for each experiment would assist in the definition of the range of variability to be expected and presence of outliers in experimental work similar to the one described in this thesis. However, multiple repetitions are unusual in laboratory work, with single runs being frequent (Wilcock and McArdell, 1993; Shvidchenko *et al.*, 2001; Saadi, 2002) and clearly unattainable in field work. Thus, the three runs carried out here are sufficient.

Criterion	Repetition		
	R1	R2	R3
Shvidchenko *et al.*, 2001	31.3 (3.62)	37.7 (4.03)	38.4 (4.07)
Parker *et al.*, 1982	20.6 (2.85)	31.8 (3.65)	31.1 (3.60)
Yalin (1977)	21.9 (2.95)	27.9 (3.38)	28.3 (3.41)

Table 4-3. Summary of initial entrainment thresholds for Stage 1. Main figures are flows (l/s), shear stress (Pa) in brackets.

A consistent methodology and entrainment criterion was necessary to define critical flows and define the test hydrographs. Observations of particle movements suggested an entrainment threshold in the region of 30 l/s. This was similar to those using Parker's (RTM-P) and Yalin's (VM) methods, whereas critical flows determined using Shvidchenko *et al.*'s (2001) method (RTM-S) were considerably higher. Entrainment thresholds determined from physical sampling of bedload material were considered by the author of this thesis more robust and reliable than visual observation of individual particle movements whose random character affects the results (see section 4.1). The value of critical flow

based on VM is inherently variable due to the small number of grain displacements (N = 4) used to define bed mobility. Therefore, Parker *et al.*'s (1982a) method is used to determine the entrainment thresholds, although both VM and RTM-S thresholds were determined throughout the experiments. The average critical flow from repetitions 2 and 3 of RTM-P provided the adopted value of Q_{ref} = 31.5 l/s for the unimodal bed. Test hydrographs were then constructed following the guidelines in 3.4.11. The resulting acceleration rates are shown in Table 4-4.

	Stage 1		**Stage 2**			
Q_t (l/s)	**31.5**		**34**		**29**	
Duration (h)	Series	AccRate (l/s/s)	Series	AccRate (l/s/s)	Series	AccRate (l/s/s)
0.5	AccRate1	0.01083	AccRate1H	0.0122	AccRate1L	0.0094
1	AccRate2	0.00542	AccRate2H	0.0061	AccRate2L	0.0047
2	AccRate3	0.00271	AccRate3H	0.0031	AccRate3L	0.0024
4	AccRate4	0.00135				
6	AccRate5	0.0009	AccRate5H	0.0010	AccRate5L	0.0008
10	AccRate6	0.00054				

Table 4-4. Summary of characteristics of test hydrographs for Stage 1 and Stage 2

A later review of the RTM methodology, after the Stage 1 runs had been completed, confirmed the value of Q_{ref} previously determined, providing a value of Q_{ref} = 30.7 l/s for RTM-P. This figure is only about 2.5% smaller than the original 31.5 l/s and within the variability expected in the measurements. Since Q_{ref} only applies to the very last stage of the antecedent conditions phase, the effect of the reviewed Q_{ref} on flow history is negligible. Thus, experiments continued to use Q_{ref} = 31.5 l/s.

4.2.1.2 Stage 2

The test hydrographs in Stage 1 inevitably include two variables, the duration of the antecedent conditions and the target flow. In combination these provide the overall effect of antecedent conditions. Stage 2 was designed to separate the effects of time of exposure and flow magnitude. The same durations of antecedent conditions were applied with discharges slightly larger and smaller (H and L) than the reference. This approach was based on the hypothesis that test hydrographs with higher target flows would result in larger effects on the

bed composition/structure and bed entrainment flows than those with the lower target flow. Hydrographs for Stage 2 were constructed using 4 of the durations tested in Stage 1 (0.5, 1, 2 and 6h) and target flows defined as ±8% of Q_{ref} (Q_H = 34 l/s, Q_L = 29 l/s). These values were symmetrical over Q_{ref} without overlapping the last flow step of the flow history (28.3 l/s) and the first one of the stability test (35 l/s). The resulting acceleration rates were then slightly higher and lower than those of Stage 1 (Table 4-4). Appendix 3 contains details of the test hydrographs.

4.2.2 Entrainment threshold results

4.2.2.1 Stage 1

Results using all three methods for determining critical flow are presented, although, as discussed earlier, results using the RTM-P method form the basis for the calculations and assessments presented here. Critical flows using all three criteria for all experiment runs of Stage 1 are in Appendix 4. These use the modal size class (5.6-8 mm), which contained D_{50}. Appendix 4 also shows critical bed shear stress values for all size fractions (RTM-P only). Data for the visual method (Yalin, 1977) in Appendix 4 is given for each repetition after fitting an exponential line to the particle movement data for comparison with RTM results. The methodology followed for the visual method was the same as the one presented for the Pilot Runs (section 4.2). The calculated critical flows (Table 4-5; Fig. 4-6) indicate that the bed becomes more resistant to entrainment with increasing antecedent durations up to around 2h (using RTM data), with bed entrainment thresholds decreasing for longer durations (and lower acceleration rates; Fig. 4-7). The increase of the duration of the antecedent conditions from 2h to 6h reduces critical flow by over 16%.

	Duration (h)	AccRate (l/s/s)	Q_{cr} (l/s)	τ_{cr} (Pa)
AccRate1	0.5	0.0108	29.5	3.49
AccRate2	1	0.0054	27.8	3.38
AccRate3	2	0.0027	30.7	3.58
AccRate4	4	0.0014	30	3.53
AccRate5	6	0.0009	26.5	3.29
AccRate6	10	0.0005	25.7	3.23

Table 4-5. Summary of flow entrainment thresholds (Q_{cr} and τ_{cr}) for Stage 1

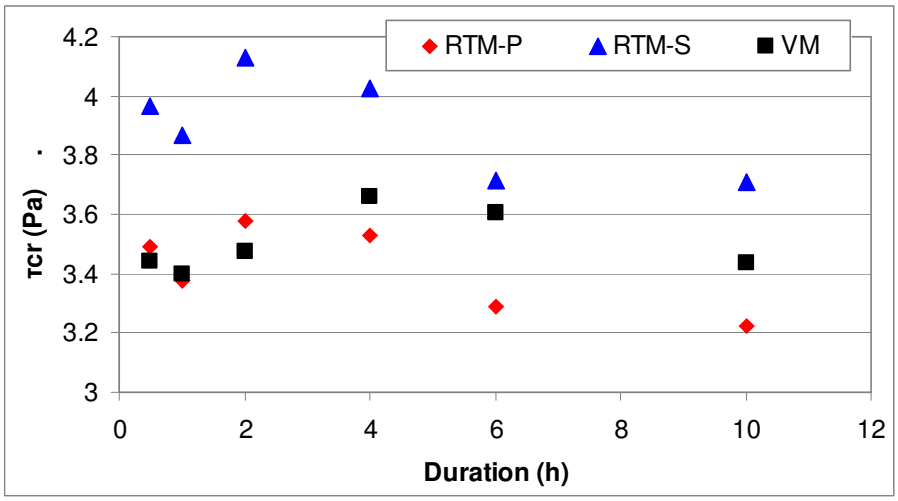

Fig. 4-6. Relationship of entrainment thresholds with antecedent durations for Stage 1. Parker et al.'s (1982a) Reference Transport method (RTM-P); Shvidchenko et al's. (2001) Reference Transport method (RTM-S); Yalin's (1977) Visual method of (VM).

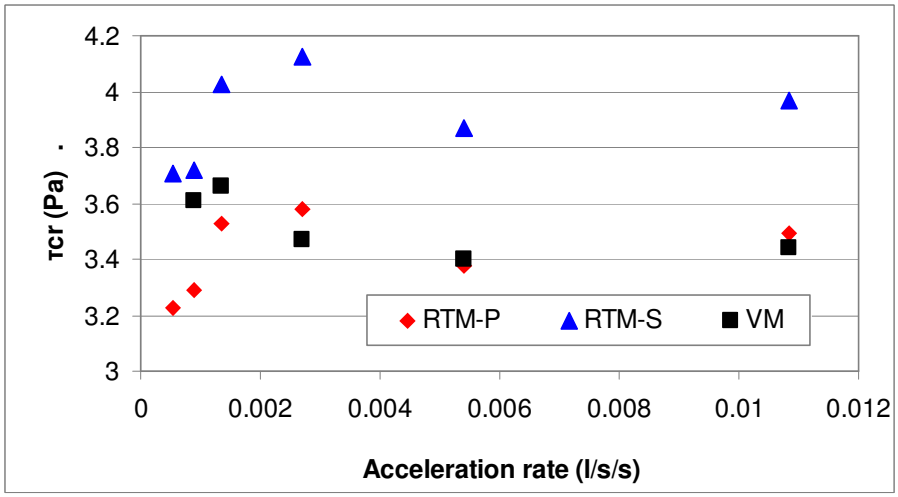

Fig. 4-7. Relationship of entrainment thresholds with acceleration rates for Stage 1. See Fig. 4-6 for legend details.

In general the three threshold criteria used show consitent trends, although the actual values differ. Bed shear stress values using the RTM-S are approximately 15% larger than those by RTM-P throughout the acceleration rates, reflecting the more demanding threshold set by Shvidchenko *et al*. (2001). As both criteria are based on the same bedload samples, these differences are a consequence of the thresholds proposed by the authors. Indeed, Shvidchenko *et al*. (2001) already established the following relationship between critical Shields parameters (θ_{cri}): $\theta_{cri}Parker = 1.20\theta_{cri}Shvidchenko^{1.09}$. This relationship was confirmed by the present work, where data for Stage 1 and Stage 2 resulted in a similar expression: $\theta_{cri}Parker = 1.24\theta_{cri}Shvidchenko^{1.10}$. Results from the visual method

also indicate a progressive bed strengthening with duration up to 4h, with a decrease of bed stability after a maximum is reached for this duration. However, the reduction of bed shear stress is smaller than that shown by RTM data with a ratio of the maximum over minimum shear stress of 0.94 for the VM and 0.9 for both RTM-P and RTM-S. Also, the largest critical shear stress obtained by the visual method corresponds to duration of 4h as opposed to 2h found using both reference transport methods. The reason for these discrepancies is unclear but it is speculated that are due to intrinsic methodological issues. These are discussed further in this chapter.

4.2.2.2 Stage 2

Entrainment threshold data for Stage 2 (Table 4-6, Fig. 4-8 and Fig. 4-9; Appendix 4) show a very similar pattern to the Stage 1 results. There is a progressive increase of critical shear stress with duration of antecedent conditions, reaching a maximum of τ_{cr} = 3.5 Pa (RTM-P) at 2h, with a decrease for longer durations (τ_{cr} = 3.1-3.2 Pa for 6h). As in the case of Stage 1, both RTM-P and VM methods show similar trends, in this case coinciding over the range of durations for which the bed is most stable (around 2h). RTM-S data is approximately 15% larger than RTM-P throughout the range of acceleration rates, which is consistent with the data obtained in Stage 1.

	Duration (h)	AccRate (l/s/s)	Q_{cr} (l/s)	τ_{cr} (Pa)
AccRate1H	0.5	0.0122	25.8	3.23
AccRate1L	0.5	0.0094	25.9	3.24
AccRate2H	1	0.0061	29.0	3.46
AccRate2L	1	0.0047	28.9	3.46
AccRate3H	2	0.0031	29.6	3.50
AccRate3L	2	0.0024	27.1	3.33
AccRate5H	6	0.0010	24.4	3.13
AccRate5L	6	0.0008	25.2	3.19

Table 4-6. Summary of flow entrainment thresholds (Qcr and τcr, based on RTM-P) for Stage 2.

The data on the effect of target flow Q_t on bed stability are inconclusive as values of τ_{cr} do not display a consistent pattern (Fig. 4-10). Critical stresses for series Q_H and Q_L for RTM-P are nearly identical in most cases (Fig. 4-8), which limit the assessment of the impact of flow magnitude on entrainment. It is possible that the target flows set for AccRatesH and AccRatesL (Q_H and Q_L),

whose differences reduce progressively as the flow steps approach the minimum flow Q = 12 l/s, were insufficient to cause a distinct effect on the bed, and consequently, on entrainment thresholds.

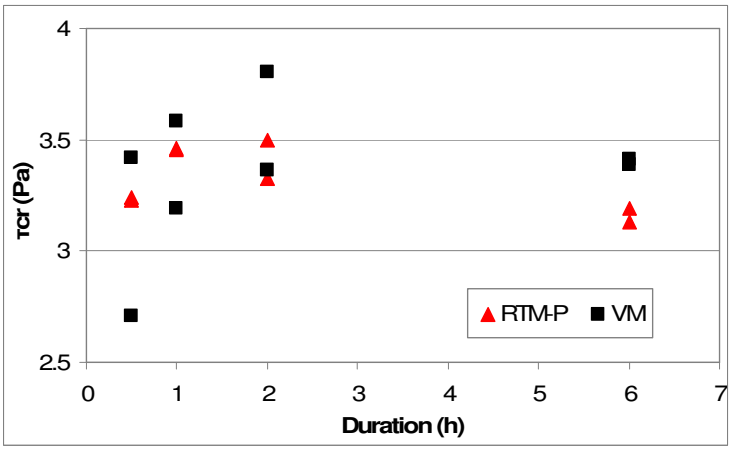

Fig. 4-8. Comparison of τ_{cr} obtained using RTM-P and VM methods. RTM-S data is not shown to improve clarity of the plot, with values from RTM-S approximately 15% higher than those from RTM-P.

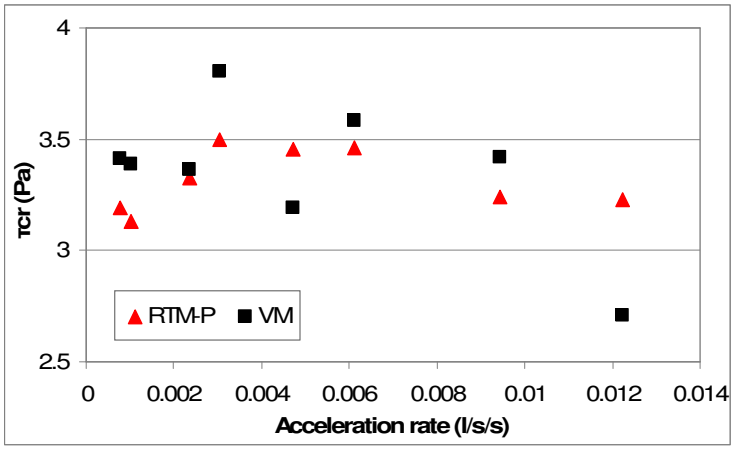

Fig. 4-9. Comparison of τ_{cr} obtained using RTM-P and VM. RTM-S data is not shown, see caption in Fig. 4-8 for explanantion.

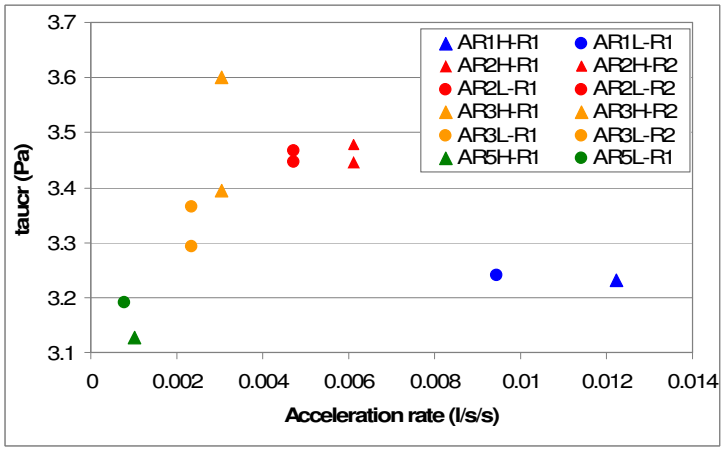

Fig. 4-10. Effect of target flows on entrainment.Legend nomenclature corresponds to the acceleration rate run shown in Table 4-6 followed by the repetition number after the dash.

The comparison of results for Stage 1 and Stage 2 shows a similar relationship between acceleration rates and bed stability (*Fig. 4-11*). The two data sets display ranges of critical bed shear stress between 3.1 Pa and 3.6 Pa approximately, with maximum values for acceleration rates between 0.004 and 0.006 l/s/s. However, data also show larger scatter between experiments of the same acceleration rates for Stage 1 than Stage 2. Nonetheless, values of τ_{cr} confirm similar behaviour of the bed under the tested sub-threshold antecedent conditions.

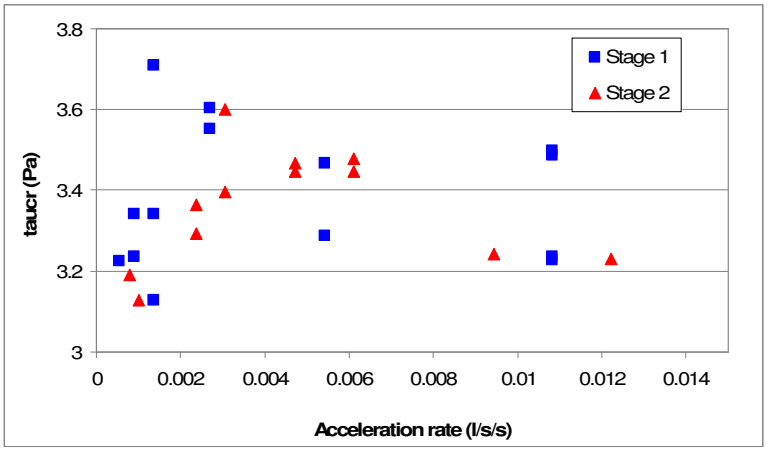

Fig. 4-11. Comparison of critical bed shear stresses obtained using the RTM-P method for Stages 1 and 2.

4.2.3 Bed surface composition

Bed surface composition was measured for two main purposes: (1) to obtain grain size distributions to input into the reference transport method calculations (section 3.4.6.2); and, (2) to explore the relationship between entrainment values and bed surface composition. This section will present and discuss the possible link between bed stability and bed size composition and evolution. The main hypothesis was: the variation of bed stability may be related to changes of bed surface composition during exposure to sub-threshold flows, in which coarsening, fining or the presence or absence of certain grain sizes may affect general particle entrainment. In this section, the relationship between bed surface composition and entrainment thresholds is assessed in three ways:

- Bed surface grain size evolution and comparison between initial bed and bed at target flow (end of antecedent conditions),
- Representative bed diameters (D_x) and sorting of the bed surface in relation to entrainment and,
- Specific contents of coarse or fine grains and observed Q_{cr}.

The proportions of size classes in the bed surface (f_i) initially and at the end of the antecedent period were analysed. This data set is too large and complex to be presented individually for each run so a reduced analysis is developed. Entrainment thresholds are related to the ratios of representative bed sizes, D_{16}, D_{50}, and D_{90}, and sorting parameter σ_g for beds at target flow Q_t (end of antecedent conditions) and initial beds (Fig. 4-12). Data are in Appendix 5.

4.2.3.1 Bed evolution during antecedent conditions

There is no apparent correspondence between the ratios of key bed particle diameters for post- and pre-antecedent conditions with critical flows for either Stage 1 or Stage 2 (Fig. 4-12). Changes of bed surface composition during the antecedent periods were minimal, with the majority of the ratios of particle diameters (D_{16}, D_{50} and D_{90}) pre- and post-antecedence ranging from 0.95 to 1.1.

Bed surface compositions after antecedent periods were very slightly coarser than those of the initial beds, with ratios of both D_{90} and D_{50} generally larger than 1 (average ≈ 1.02, range = 0.95-1.1). Values of the ratio of D_{16} show the largest relative increase, with most data in the range > 1 and maximum ratio > 1.1, indicating a loss of fines from the bed surface. This bed surface behaviour is also seen when average size distributions and key bed diameters for the initial bed and bed at the end of the antecedent conditions are compared (Fig. 4-13 and Table 4-7). There is a reduction of the presence of sizes smaller than 4 mm (from 4.6% to 3.6%) and an increase of the sizes larger than 5.6 mm (on average, 64.6% of bed surface composition is made up of grains larger than 5.6 mm for the initial bed and 69.9% for the bed after antecedent conditions) for Stage 1 runs (Fig. 4-13); producing a slight coarsening of the entire size distribution (from D_{50} = 6.41 mm for the initial bed to D_{50} = 6.61 mm for the post-antecedent

conditions beds, ratio of 1.03), more pronounced for the finer classes, with the ratio of D_{16} for pre- and post-antecedent conditions of 1.06. Differences between bed compositions for Stage 2 are minimal, with all size ratios in the range 0.99-1.03, suggesting very little bed evolution during the antecedent phase.

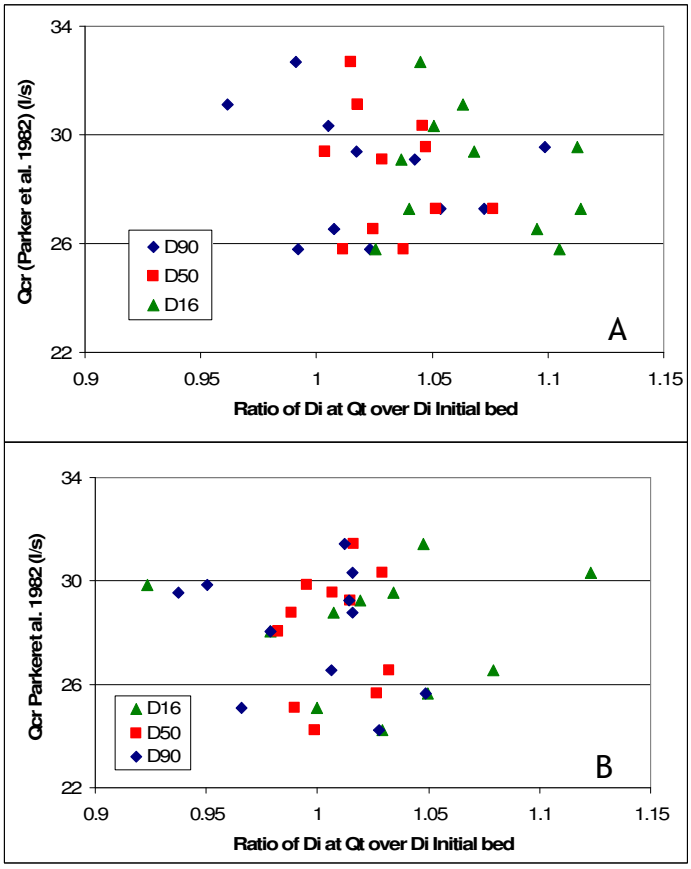

Fig. 4-12. Relationship between bed evolution and entrainment thresholds. Ratios refer to key diameters of beds after antecedent conditions were applied (beds at target flow Q_t) and those for beds before accelerations rates were applied (initial beds). A) Stage 1, B) Stage 2.

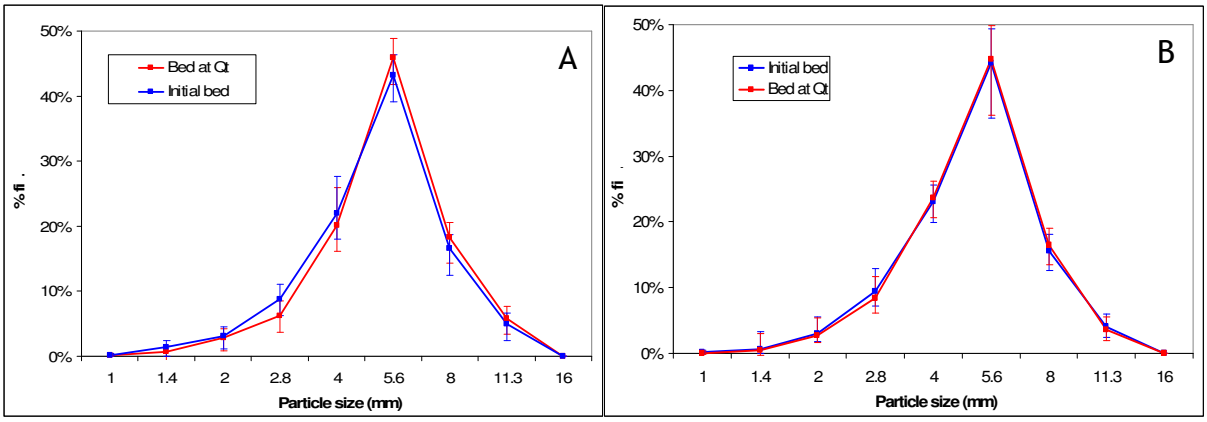

Fig. 4-13. Bed surface compositions of initial bed and bed at target flow Q_t. Values shown are averaged f_i of all runs. Error bars indicate range of results. A) Stage 1, B) Stage 2.

	Stage 1			Stage 2		
	Initial beds	Beds at Q_t	Ratio	Initial beds	Beds at Q_t	Ratio
D_{16}	4.19	4.47	1.06	4.19	4.29	1.03
D_{50}	6.41	6.61	1.03	6.34	6.39	1.01
D_{84}	9.05	9.39	1.03	8.74	8.78	1.01
D_{90}	10.27	10.50	1.02	10.03	10.00	1.00
σ_g	1.47	1.45	0.98	1.44	1.43	0.99

Table 4-7. Average key sizes (mm) of beds pre and post antecedent conditions. Stage 1 and Stage 2.

4.2.3.2 Relationship between Dx and critical flows

Since the resistance of granular beds can be related to their size distributions (percentage of large and fine material), a possible relationship between bed resistance and bed surface size distribution was explored. The comparison of representative particle sizes D_x, (x = % of bed particles finer) and sorting ($\sigma_g = \sqrt{D_{84}/D_{16}}$) of beds pre and post antecedent conditions with entrainment thresholds did not show any noticeable correlation (Fig. 4-14 and Fig. 4-15). The range of Q_{cr} appears unaffected by values of D_{16}, D_{50} or sorting, with only values of D_{90} displaying a very weak positive relationship.

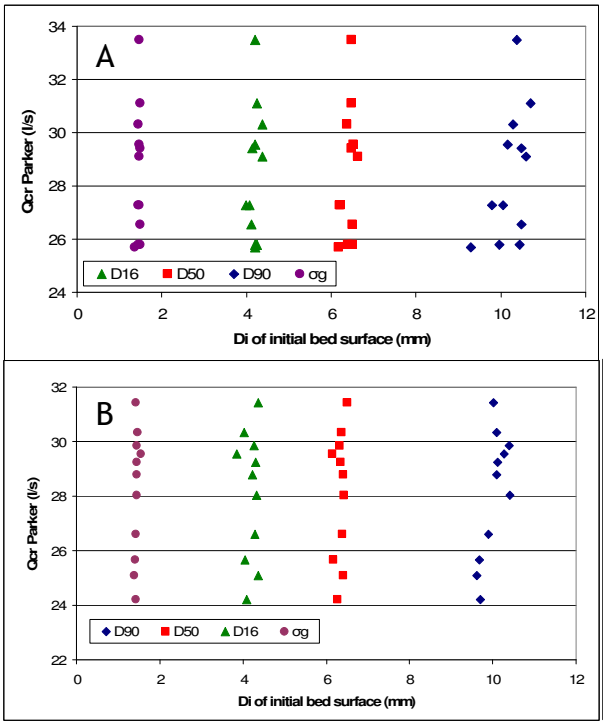

Fig. 4-14. Relationship between parameters of initial bed surfaces and entrainment thresholds. A) Stage 1, B) Stage 2.

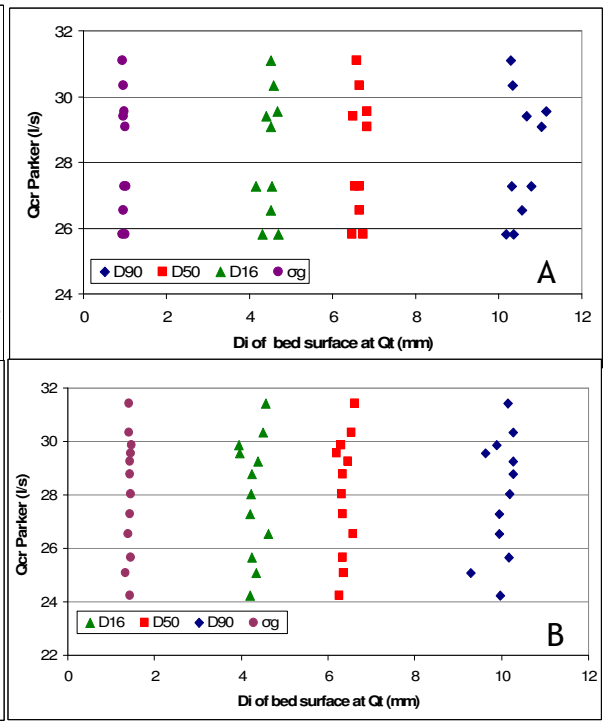

Fig. 4-15. Relationship between bed surface representative sizes and sorting of bed at target flow Q_t (end of antecedent conditions) and entrainment thresholds. A) Stage 1, B) Stage 2.

4.2.3.3 Content of coarse and fine grains

A positive correlation between bed stability and coarse fraction is expected as the abundance of large particles on the bed surface would strengthen the bed. The coarse fraction is represented here by D_{90}, and is plotted against entrainment thresholds in Fig. 4-16. The data supports the above hypothesis but the correlations are very weak (R^2 = 0.002 to 0.55). The lowest correlation associated with D_{90} at Q_t for Stage 1 (0.002) is significantly improved to R^2 = 0.73 when the apparent outliers are excluded (circled points in Fig. 4-16B). However, no indication of why these points might not follow the general trend was found. Nevertheless, there is no clear correlation of critical flows with coarse material. Fig. 4-17 shows the relationship between entrainment thresholds and changes in the abundance of fines in the bed surface (taken as D < 4 mm) during antecedent conditions. Results for Stage 1 suggest that there is a value of the ratio of fines of the Q_t bed over the initial bed in the region of 0.8 for which critical flow is maximised; with both smaller and larger ratios leading to weaker beds. Although this would suggest a link between fine content and bed stability, results for Stage 2 are inconclusive.

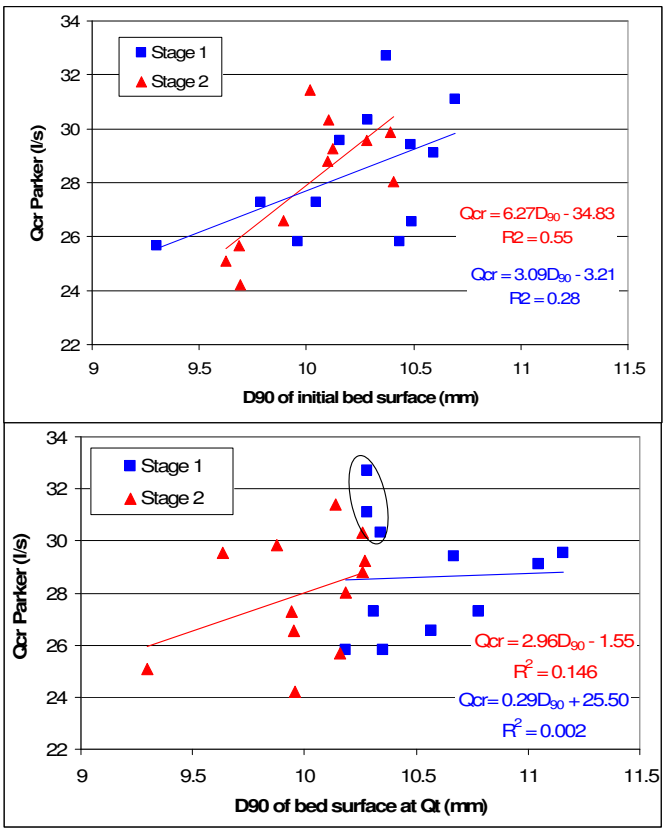

Fig. 4-16. Relationship between coarse fraction (D_{90}) and entrainment thresholds. A) Initial beds, B) Beds after flow exposure.

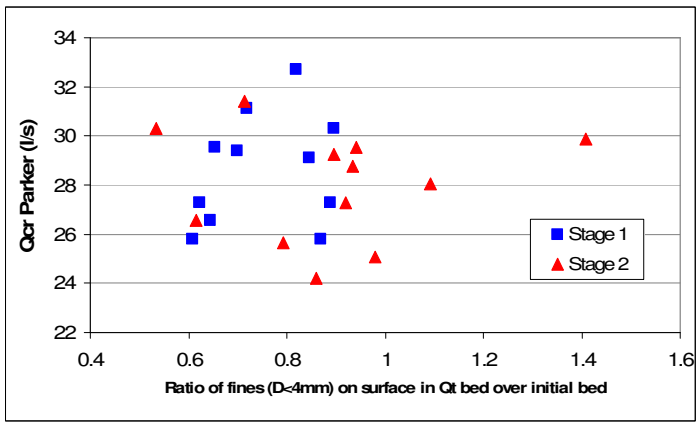

Fig. 4-17. Relationship between fines and entrainment threshold. Horizontal axis represents the ratio of the content of fines (D<4mm) of the bed at target flow Q_t over the initial bed, as a measure of the evolution of fine content during the antecedent period.

4.2.4 Bedload size composition

Bedload size composition was assessed using values of p_i/f_i, with p_i being the proportion of each size class in the bedload sample and, f_i the proportion of the same size class on the bed surface. Due to the large data set generated for the individual runs; the analysis focuses on average values of p_i and f_i (Fig. 4-18).

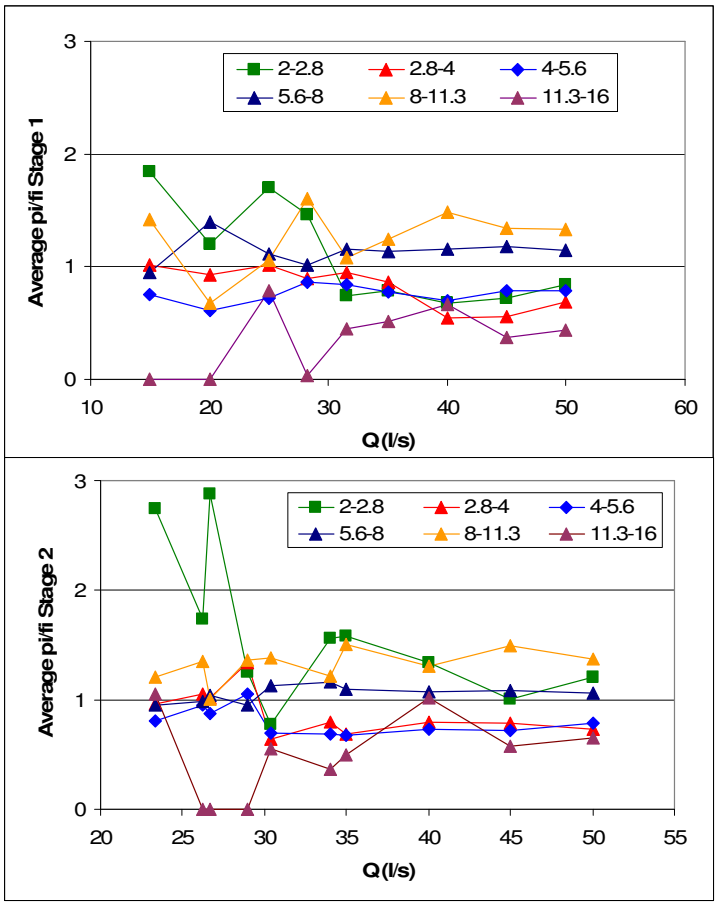

Fig. 4-18. Average values of p_i/f_i for Stage 1 and Stage 2. Note that values of p_i =0 for the size classes < 2mm for most of the bedload samples; thus, data is not plotted.

Values show that there is a significant variability of p_i/f_i at low flows. Data for all size classes cross p_i/f_i = 1 at lower flows, appearing to stabilise for flows larger than approximately 30 l/s. This behaviour of the bedload composition may reflect the randomness of the entrainment process (Miller *et al.*, 1977; Carling, 1983, Andrews and Parker, 1987; Papanicolaou *et al.*, 2002; van Rijn, 2007), especially at flows below threshold. As flows increase, the direct action of hydraulic forces come to dominate the entrainment process (Grass, 1970; Kirchner *et al.*, 1990), stabilising the values of p_i/f_i (Kuhnle, 1992). The observed scatter of p_i/f_i for low flows may also be a consequence of sampling errors of p_i at low transport rates (see section 3.2.2.3). The threshold of approximately 30 l/s for stabilisation of grain-size behaviour is close to the entrainment threshold of the bed (31.5 l/s). This correspondence may reflect a reduction of the stochasticity of entrainment and a more direct link between average flow magnitude and particle entrainment for flows similar or above Q_{ref}, stabilising values of p_i/f_i.

For flows > 30 l/s general patterns of p_i/f_i can be described. For the 5.6-8 mm and 8-11.3 mm classes, p_i/f_i values were > 1 for the flow range 30-50 l/s, with values for 5.6-8 mm just above 1. These coarser classes are therefore over-represented in the bedload relative to their abundance in the bed surface. The remaining grain sizes have ratios below 1, except the 2-2.8 mm size class in Stage 2. The proportion of the largest size class 11.3-16 mm in bedload remained considerably below 1, especially for low flows, confirming the expected low mobility of this particle size due to its submerged weight.

Values of p_i and f_i for the two finest classes 1-1.4 mm and 1.4-2 mm were often 0 and thus, could not be included in this analysis. However, the behaviour of size class 1.4-2 mm, together with the other particle sizes, can be indicatively studied by plotting values of p_i/F_i , with F_i = composition of the bulk mix (values of F_i were larger than 0 for all size classes so p_i/F_i provides information about the evolution of bedload size distribution without the effect of changes in surface composition f_i). Fig. 4-19 shows the results. The behaviour of the finer size classes 1.4-2 mm, 2-2.8 mm and 2.8-4 mm is very similar: a progressive reduction of the values of p_i/F_i with increasing flows up to 30 l/s approximately

(Kuhnle, 1992) and a levelling off for the remaining flows, reaching a state of pseudo-equilibrium during the stability test period.

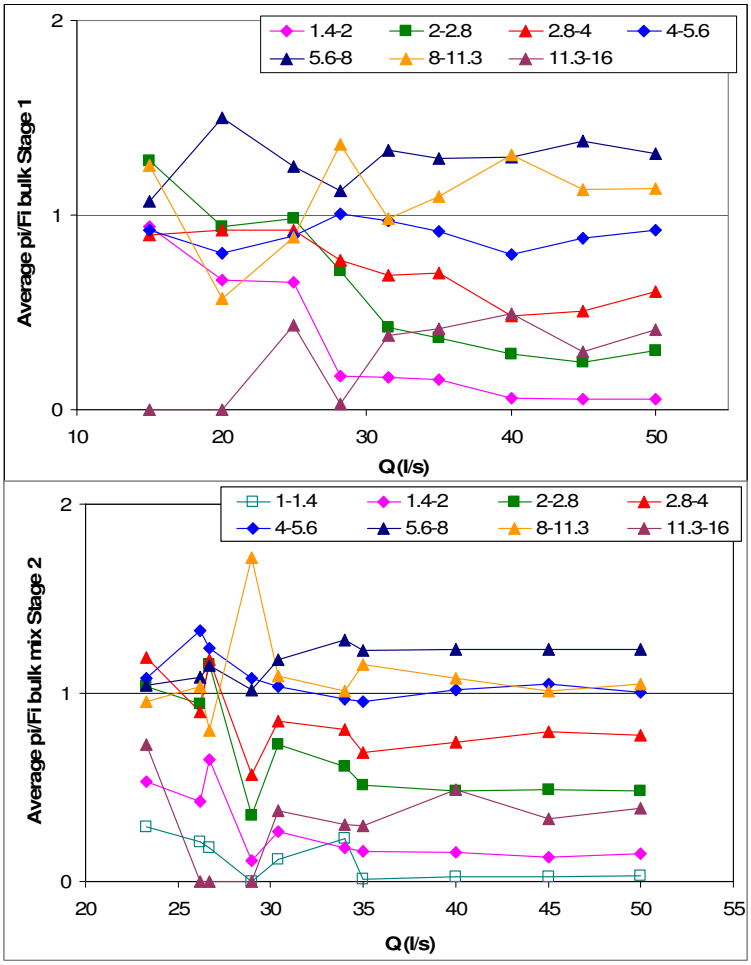

Fig. 4-19. Average values of p_i/F_i (F_i for the bulk mix) for Stages 1 and 2.

Further exploration of the size composition of the bedload consisted of a similar analysis of bedload composition to that of Powell *et al.* (2001), carried out for Stage 1 runs. Average representative particle percentiles D_x (16^{th}, 50^{th} and 90^{th}) of the bedload were obtained for all runs (Fig. 4-20A). Results show how all size percentiles increase with rising flows during the antecedent conditions phase (15 l/s < Q < approx. 28 l/s), with clear stabilisation of the D_x values during the stability test. Fig. 4-20B shows the ratios of D_x over the average value of the corresponding D_x for the entire flow range of each run. Results show how for flows approximately below 28 l/s all size percentiles are below 1, indicating that bedload size composition is finer than the run-average. However, the ratios of all three representative sizes appear to be reasonably stable above 1 for Q > 28-30 l/s, with D_{50} and D_{90} being closer to 1. Values of D_{16} sit furthest above and

below the line = 1 due to the larger relative effect of a smaller average D_x. Ratios indicate that bedload samples were finer than the average bedload sample at the initial stages of the runs, becoming increasingly coarser with rising discharges. Once the entrainment flow was overcome, relative percentages of particles classes remained constant throughout the stability test. These results could be interpreted similarly to Powell *et al.* (2001), in the sense that size selectivity appears to be present for lower flows, approaching equal entrainment for larger flows (Parker *et al.*, 1982b; Wilcock, 1992; Wilcock and McArdell, 1997). However, the threshold for which this switch occurs is approximately $\tau/\tau_{cr} \approx 1$, much lower than the one reported in Powell *et al.* (2001) of $\tau/\tau_{cr} = 4.5$.

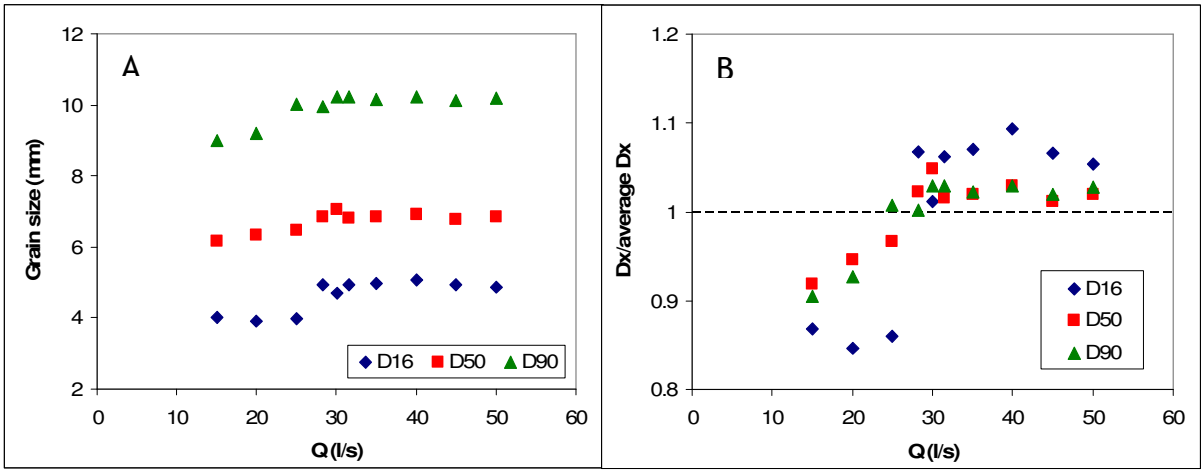

Fig. 4-20. A) Evolution of representative bedload diameters with flow, and B) ratio of D_x at each flow stage over the average D_x for the entire run. Data for Stage 1 only.

The observed fractional transport rates (p_i/f_i) can be related to grain mobility. Table 4-8 and Fig. 4-21 show the values of τ_{cri}/τ_{cr50} in relation to the relative particle size D_i/D_{50}, with D_{50} = the average of the median sizes of the initial beds. All size classes except 5.6-8 mm and 8-11.3 mm have an average τ_{cri}/τ_{cr50} above 1; with $\tau_{cri}/\tau_{cr50} = 1$ for size class 5.6-8 mm (as it contains D_{50}) and $\tau_{cri}/\tau_{cr50} < 1$ for 8-11.3 mm reflecting the relatively higher mobility of this size class, ($p_i/F_i > 1$). The smallest size classes show the largest scatter of τ_{cri}/τ_{cr50} values, which may explain the unclear pattern showed by p_i/f_i values.

	Stage 1		Stage 2	
Size class (mm)	D_i/D_{50} (1)	average τ_{cri} / τ_{cr50}	D_i/D_{50} (1)	average τ_{cri} / τ_{cr50}
1-1.4	0.19	-	0.19	-
1.4-2	0.26	1.10	0.27	1.03
2-2.8	0.37	1.03	0.38	1.01
2.8-4	0.53	1.04	0.54	1.03
4-5.6	0.75	1.04	0.77	1.03
5.6-8	1.06	1.00	1.08	1.00
8-11.3	1.50	1.00	1.54	0.98
11.3-16	2.12	1.09	2.18	1.06

(1) D_i = arithmetic mean of size class. D_{50} for Stage 1 and Stage 2 were obtained as average D_{50} for each initial bed; hence, values of D_i/D_{50} are slightly different for the two stages.

Table 4-8. Average mobility values for each size class.

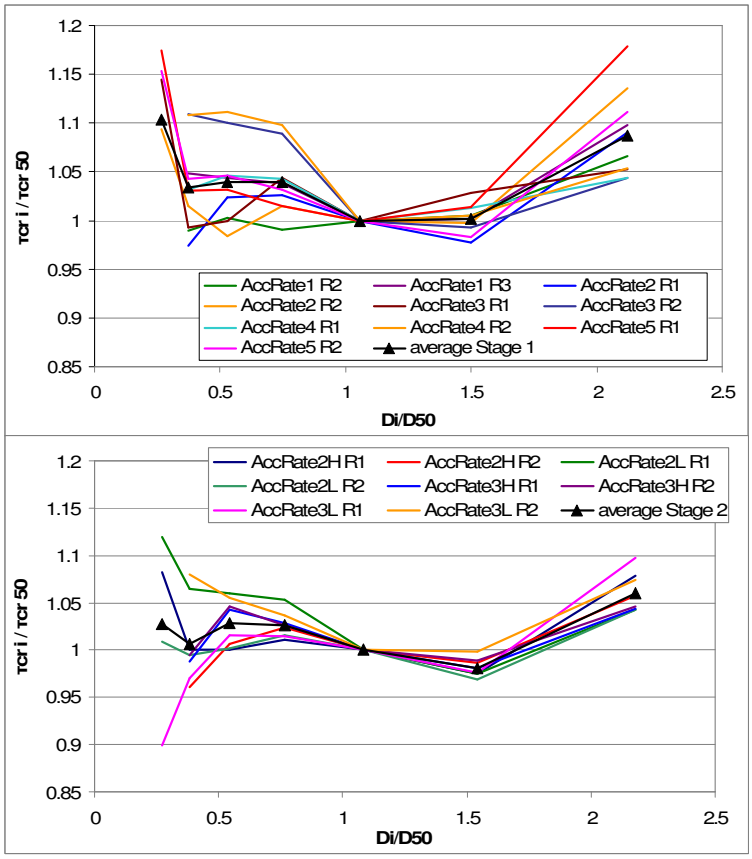

Fig. 4-21. Mobility of size classes in relation to average initial bed surface D_{50} for Stage 1 and Stage 2.

In general, finer particles than the median size appear more resistant to movement ($\tau_{cri}/\tau_{cr50} > 1$), possibly linked to the relative size interactions, i.e. hiding effects, (Parker and Klingeman, 1982; Reid and Frostick, 1986; Andrews and Parker, 1987; Van Rijn, 2007b). Whereas the increased stability of the

coarsest fraction (11.3–16 mm) is likely linked to its size and submerged weight (Parker and Klingemann, 1982; Wilcock and McArdell, 1997).

4.2.5 Bedload quantities

4.2.5.1 Bedload and flow acceleration rates

Bedload rates q_b were measured in kg/m/s by dividing the dry weight of the collected sample by the width of the sediment trap opening (0.45 m) and by the sampling period, which was the duration of the flow step for antecedent conditions (Appendix 6) or every 6 minutes within the stability test. A summary of all bedload transport rates is presented in Appendix 6.

The relationship between average bedload rates, flows and acceleration rates is shown in Fig. 4-22. In general, solid transport rates increase with flow magnitude, although this pattern is less clear for Stage 2, possibly due to the effect of increased sample sizes due to air bubbles at low flows (section 3.2.2.3). Data show that, within the same flume discharge, there is a reduction of bedload transport rates at acceleration rate 0.0027 l/s/s for Stage 1 and 0.0031-0.0047 l/s/s for Stage 2. In both cases these are the acceleration rates that produce the most stable beds (section 4.2.2). This is consistent as more resistant beds will result in smaller transported material. Patterns appear more consistent when average bedload transport rates for the duration of the stability test are plotted against acceleration rates (Fig. 4-23). Values show that minimum rates (2e-3 - 3e-3 kg/m/s) correspond to acceleration rates 0.002-0.004 l/s/s in Stage 1 and Stage 2 data sets. Data show that there are consitent results between these two experiment groups and that the combination of duration and target flow that produces an acceleration rate in the region of 0.003 l/s/s results in the most stabe bed. Saadi (2002) also reported a reduction of bedload transport during the stability test for his intermediate duration of increasing flows (6h), with average transport rates of 0.0845, 0.3455 and 0.507 g/m/s for durations 3, 6 and 9h respectively. He related these measurements to improved bed stability that the 6h experiment appeared to produce over the shorter and longer durations of flow exposure.

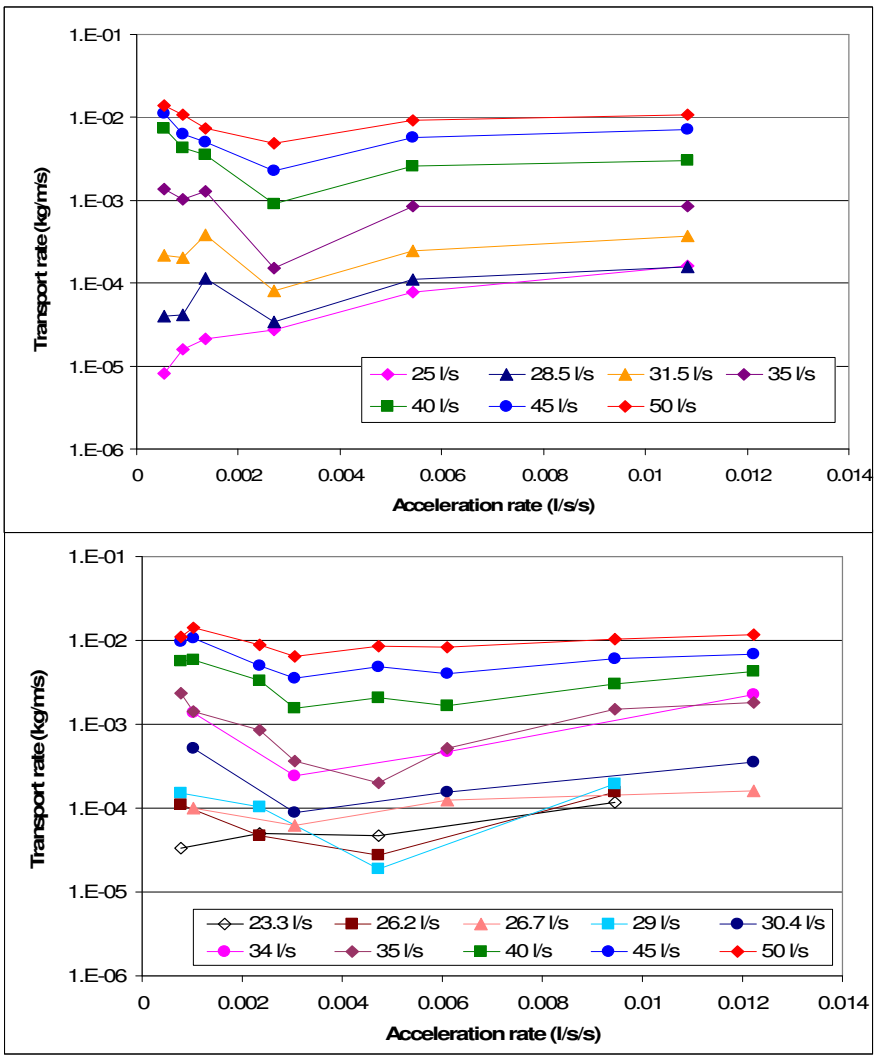

Fig. 4-22. Average bedload transport rates for each flow and acceleration rate. Vertical axes are in logarithmic scale

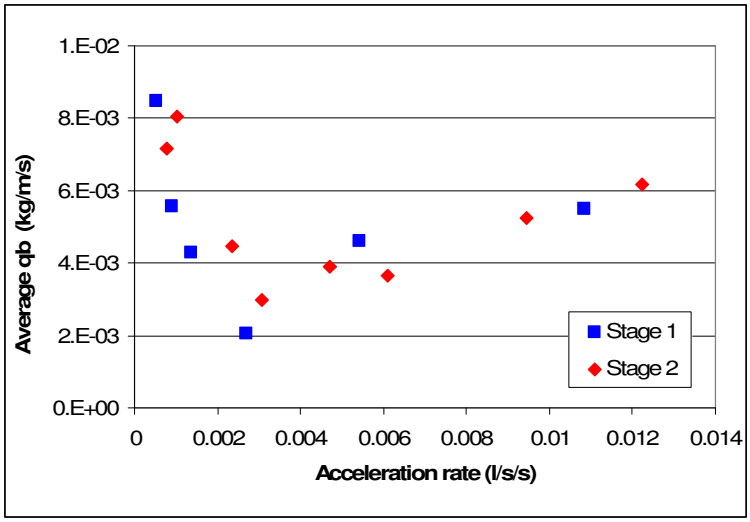

Fig. 4-23. Average bedload transport rate during stability test periods for Stage 1 and Stage 2. Average transport rate defined as the total bedload weight collected during the stability test over the total duration of the stability test (24 minutes). Since the stability test is the same for all experiments in Stage 1 and Stage 2the data represent the effect of antecedent conditions on bed mobility.

A complementary analysis of this ratio of bedload transport in terms of shear stress is shown in Fig. 4-24. An increase of bed shear stress from 3.18 Pa to 4.71 Pa (approximately 50% increase) produced bedload transport rates 2-3 orders of magnitude larger. Data in Fig. 4-24 also shows a clear hierarchy of bedload ratios with flow acceleration rates, with the ratios being consistently larger with lower acceleration rates.

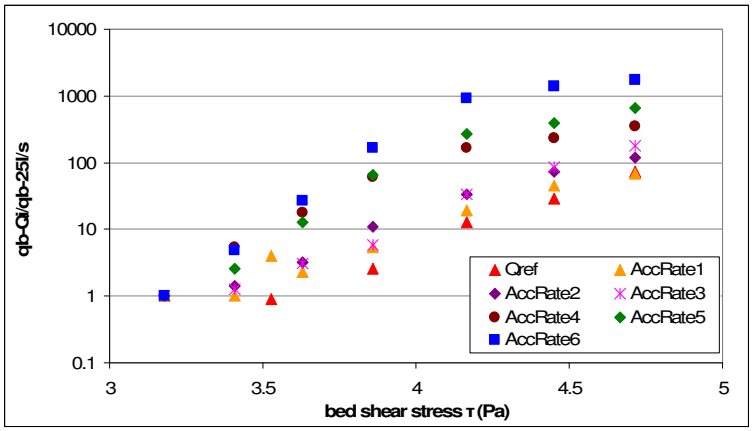

Fig. 4-24. Effect of flow acceleration rates on bedload transport rate as a function of bed shear stress. Stage 1.

The effect of acceleration rates can be further explored by analysing total bedload transport during the stability test in relation to the critical bed shear stress obtained for each run. Since flow magnitudes and durations in the stability test are the same for all runs, this comparison is related directly to the influence of the antecedent conditions. The results (Fig. 4-25) show a reduction of the total bedload (kg/m) produced during the stability test with increasing critical bed shear stress, indicating increased bed stability. This implies that acceleration rates affect the bed during the antecedent periods and that these effects continue after entrainment occurs; with this effect persisting to the maximum flows tested, over 50% larger than Q_{ref}. Negative power laws fitted to the data show a better fit of Stage 2 data (R^2 = 0.9) than Stage 1 values (R^2 = 0.65), although both exponential curves are very close to each other. The values of both data sets overlap, suggesting a common response of bedload to the tested antecedent conditions.

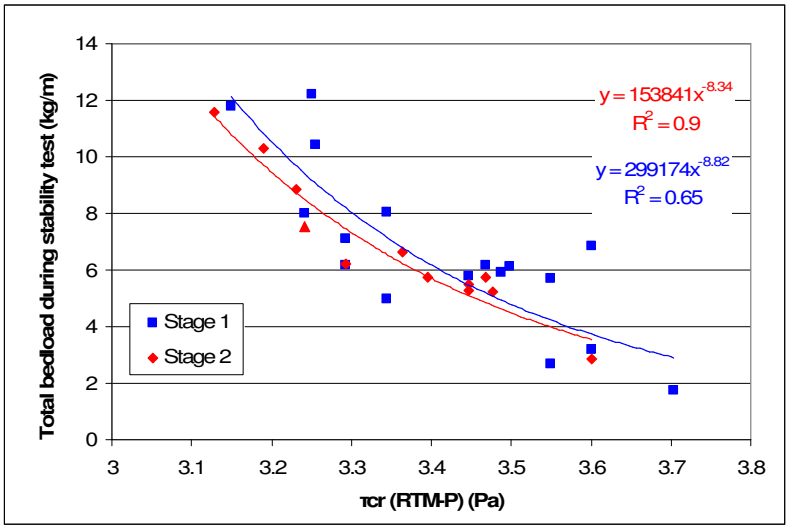

Fig. 4-25. Relationship between new entrainment threshold (bed shear stress) and total bedload (kg/m) during the stability test.

4.2.5.2 Total bedload transport rates and bedload equation

Fractional transport rates were used during the application of the reference transport methods for the estimation of τ_{cr}. Here, the total bedload amounts transported at each discharge are analysed. Fig. 4-26 shows that total bedload rates (kg/m/s) collapse into a approximately single curve when plotted against τ/τ_{cr}; with τ = bed shear stress and τ_{cr} = critical bed shear stress obtained using RTM-P for each run. The best-fit line shown in Fig. 4-26 has two components:

$$q_b = A\,(\tau/\tau_{cr})^B \qquad \text{for } (\tau/\tau_{cr}) \le 1.3 \qquad \textit{Eq. 4-1}$$

$$q_b = C\,(\tau/\tau_{cr}) + D \qquad \text{for } (\tau/\tau_{cr}) > 1.3 \qquad \textit{Eq. 4-2}$$

with q_b = total bedload transport rate in kg/m/s, and the constants have the following values: $A = 8.0\text{x}10^{-5}$; $B = 16$; $C = 0.047$ and $D = -0.056$.

Parameter values were obtained after visual optimisation of the best-fit line for the full data set of Stage 1 and Stage 2 combined. This procedure avoids bias towards larger transport rates that would occur with automatic optimisation based on least-squares regression over several orders of magnitude (Ferguson, 1986 and 1987; Walling and Webb, 1988) and reduces the effect of scatter and data outliers on the equation fit. A smooth transition between equations 4-1 and 4-2 was also achieved by this procedure. Fig. 4-26 shows that the largest scatter

occurs around τ/τ_{cr50} = 1, possibly due to instability of the bed close to the threshold.

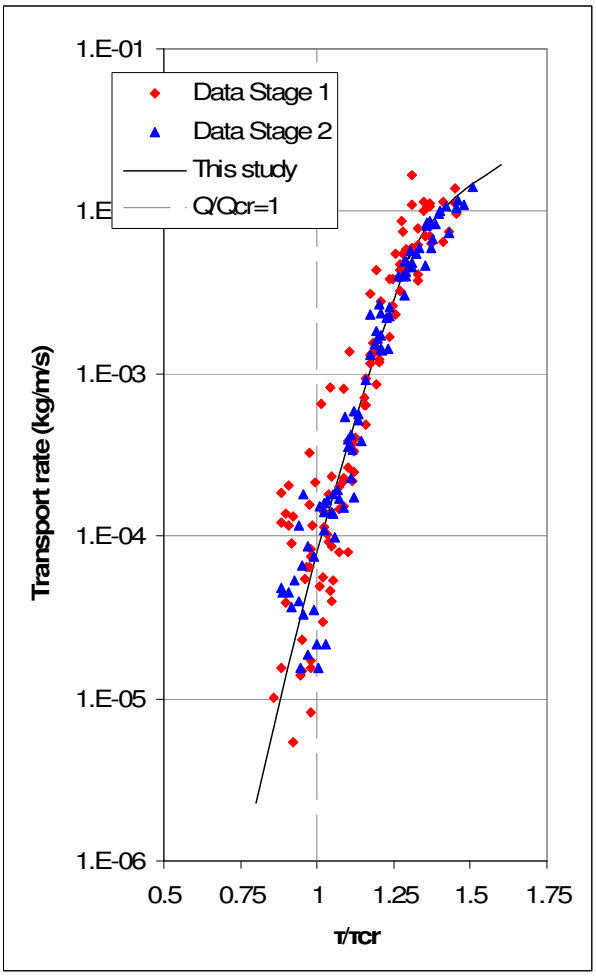

Fig. 4-26. Collapsed bedload transport rates showing fitting of the proposed bedload equations. Total bedload measured in kg/m/s. Note the scatter around τ/τ_{cr50} =1.

When flows are clearly below threshold (τ/τ_{cr50} < 0.8) there is very little particle movement and therefore little scatter of the data (narrower range of values). At the other end of τ/τ_{cr50}, when flows are above threshold (τ/τ_{cr50} > 1.1 approximately), grain movement is dominated by the flow strength and therefore there is little scatter on the relationship between the bedload data and excess bed shear stress. Conversely, under near-threshold conditions, particle mobility is more sensitive to flow turbulence and local grain characteristics such as imbrication, orientation and protrusion (Carling, 1983; Andrews and Parker, 1987; Church *et al.*, 1998), therefore, uncertainty on particle mobility is greater, increasing the range of q_b in Fig. 4-26 to about 1-2 orders of magnitude, more noticeable for the values of Stage 1. It is noted that Fig. 4-26 shows data from both Stages 1 and 2, and that both show consistent values and trends. Hence, there appears to be a common response of bedload and resulting entrainment thresholds for both groups of experiments.

The proposed best-fit of equations 4-1 and 4-2 can be used to estimate critical bed shear stress if bedload samples are available. Unlike reference transport methods, no fractional transport rates are necessary for creating Fig. 4-26 and applying equations 4-1 and 4-2, making this an alternative method when fractional transport rate data are unavailable, as is often the case with field

data. In the next section a method for predicting bedload transport rates and entrainment thresholds is proposed.

4.2.6 Proposed method for prediction of transport rates and τ_{cr}

It was demonstrated above that bedload transport rates for the same flows decrease with increasing entrainment thresholds (Fig. 4-25). Fig. 4-27 shows that the reduction of transport rates for each flow step follows a power law when plotted against bed entrainment thresholds (τ_{cr}) obtained with the reference transport method (RTM-P) (section 4.2.2):

$$q_b = A\,\tau_{cr}^{\;B} \qquad \text{Eq. 4-3}$$

where *A* and *B* parameters that vary with the bed shear stress corresponding to each flow stage (τ) as shown in Fig. 4-28.

$$A = A_1 \cdot \tau^{A_2} \qquad \text{Eq. 4-4}$$

$$B = B_1 \cdot \tau^2 + B_2 \cdot \tau + B_3 \qquad \text{Eq. 4-5}$$

where A_1, A_2, B_1, B_2 and B_3 are parameters, optimised for the present data set (Table 4-9), and τ = bed shear stress corresponding to each flow step.

Parameters for equations 4-4 and 4-5			
A_1	1.15E+61	B_1	-3.632
A_2	-88.91	B_2	50.8
		B_3	-164.97

Table 4-9. Values of parameters used to generate curves on Fig. 4-27.

The parameters in Table 4-9 were then used to generate theoretical bedload transport rates (dashed lines in Fig. 4-27). However, these predictions rely on previous knowledge of critical stress. In order to use this procedure for estimating entrainment thresholds, the data in Fig. 4-27 must be read vertically to produce a series of transport rates for a range of flows for a given τ_{cr}. This produces a series of curves that depend on the values of τ_{cr}, such as the ones shown in Fig. 4-29.

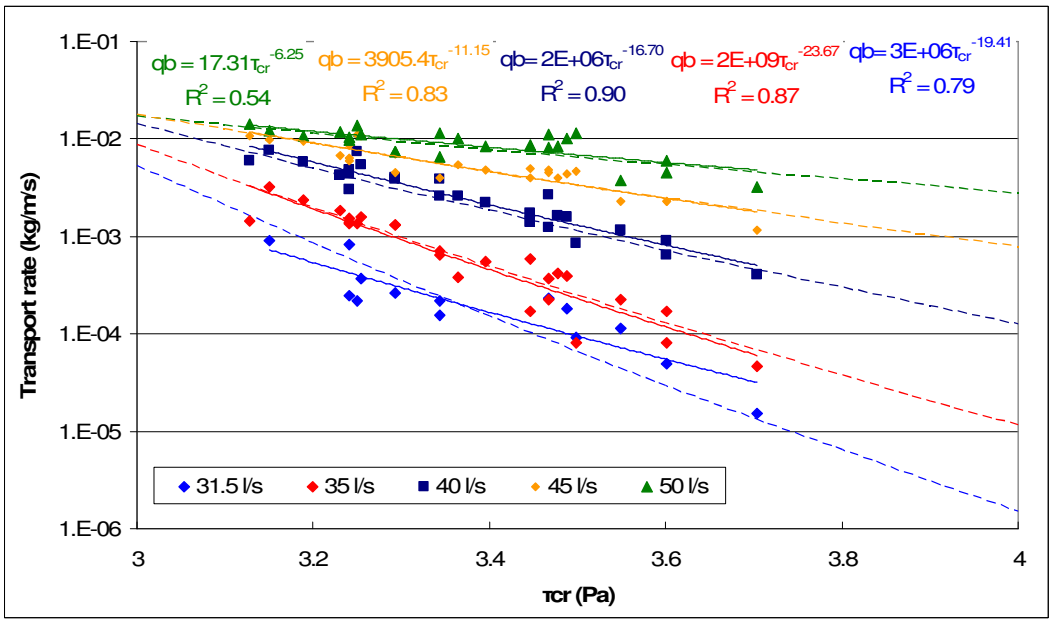

Fig. 4-27. Evolution of bedload rates with critical bed shear stress. Stages 1 and 2 data combined. Only data from the stability test are plotted, as this phase of the experiments provides sufficient data points for adequate curve fitting.Lines correspond to ordinary east squares fit (solid lines) and generated by equation 4-3 (dashed lines).

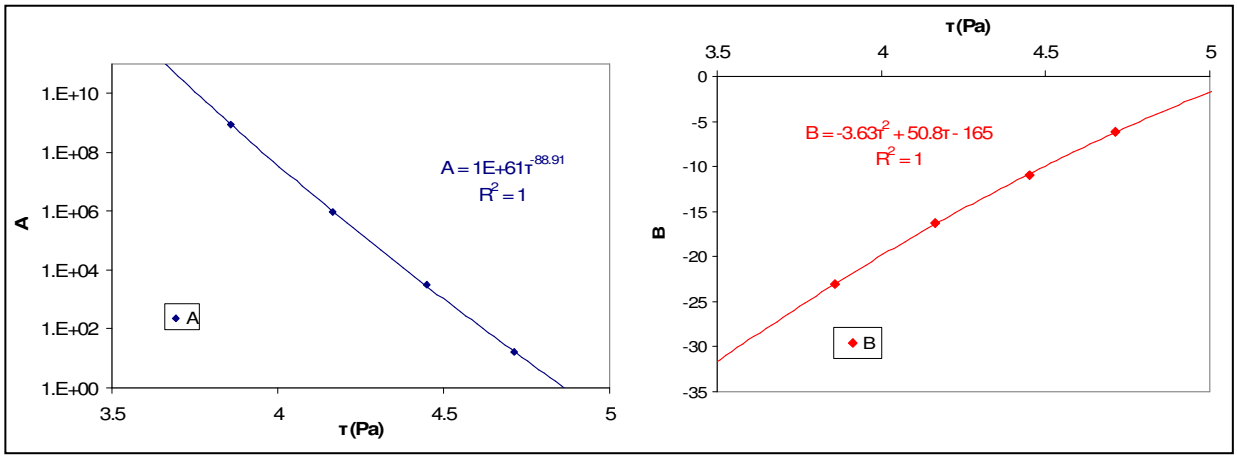

Fig. 4-28. Relationship of Parameters A and B in eq 4-3 with bed shear stress

It is noted that data points in Fig. 4-29 deviate from the predictive lines at low shear stresses, with deviations increasing below the estimated critical stress. This may indicate a relationship between entrainment thresholds and bedload transport rates that can be used for defining a transport rate equation divided in two stages: the first one, of approximately constant low transport rate, $q_b \approx 8x10^{-5}$ kg/m/s for sub-threshold flows, and a second one, following the described curves for flows above threshold. The deviation observed for the lower values of τ could also be associated with (1) the sampling issues discussed in 4.2.2 (oversampling due to air bubbles) and (2) the effect of randomness of entrainment for flows near the threshold (Carling, 1983; van Rijn, 2007a). As bed

shear stress values increase, solid transport is dominated by flow strength, largely reducing scatter in Fig. 4-29. The comparison of the theoretical curve for the series τ_{cr} = 3.6 Pa and the corresponding experimental data (τ_{cr} = 3.58 Pa) suggests that the curve should be shallower, producing higher q_b for the low range of τ (τ < 4.2 Pa) and smaller q_b for τ > 4.4 Pa. This deviation may be reduced if future additional data is available for the revision of the parameters adopted.

The value of the parameter A_1 in Table 4-9 is particularly large, with the results of eq. 4-3 being very sensitive to its value. A change of units (g/m/h) of the bedload transport rates and a change of equation form of eq. 4-3 [exponential form $q_b = AxExp(\tau_{cr} B)$, maintaining the power and polynomic forms of eqs. 4-4 and 4-5] were tested to check the sensitivity of the parameters in Table 4-9. Since the change of units produces a shift of scale without altering the trends (larger values of q_b) in Fig. 4-27, the values of B_1, B_2 and B_3 are very similar (within the uncertainty of the fitting) to those initially obtained, with the value of A_1 reflecting the higher coefficient A required by the new units (Table 4-10). When an exponential expression is used instead the power law in eq. 4-3 the parameters reduce (Table 4-10); however, the coefficient A_1 remains very large, effectively of a similar order of magnitude to the initial value.

Alternative parameters for equations 4-4 and 4-5		
	Using g/m/h	Using $q_b = AxExp(\tau_{cr} B)$ in eq.4-3
A_1	9.00E+69	3.6E+56
A_2	-92.5	73.2
B_1	3.7	-1.1
B_2	52.1	15.4
B_3	169.4	-50.1

Table 4-10. Alternative parameters used in eq. 4-4 and 4-5 using a change of units (g/m/h) and an exponential expression of eq. 4-3.

The reported large figures obtained for A_1 are likely to originate from the large reduction of bedload rates (several orders of magnitude) for a very small increase of critical bed shear stress τ_{cr} (ca. 3.2 to 3.7 Pa) (Fig. 4-27). This results in large gradients of the coefficient A both in the power and exponential forms of eq. 4-3; which are propagated to A_1, requiring very large values. Thus, the

figures obtained for A_1 A_2, B_1, B_2 and B_3 do not change substantially with different q_b units of equation form, since they result from the steep reduction of transport rates with entrainment thresholds.

The equation presented here (equation 4-3) can be used to assess entrainment thresholds, even when antecedent conditions are present as the procedure relies on actual sampled data. The entrainment threshold can be determined iteratively. In the case of eq. 4-3, no fractional transport rates are required. This makes it a very fast and easy method to apply, especially for field data, where sample sieving may be impractical.

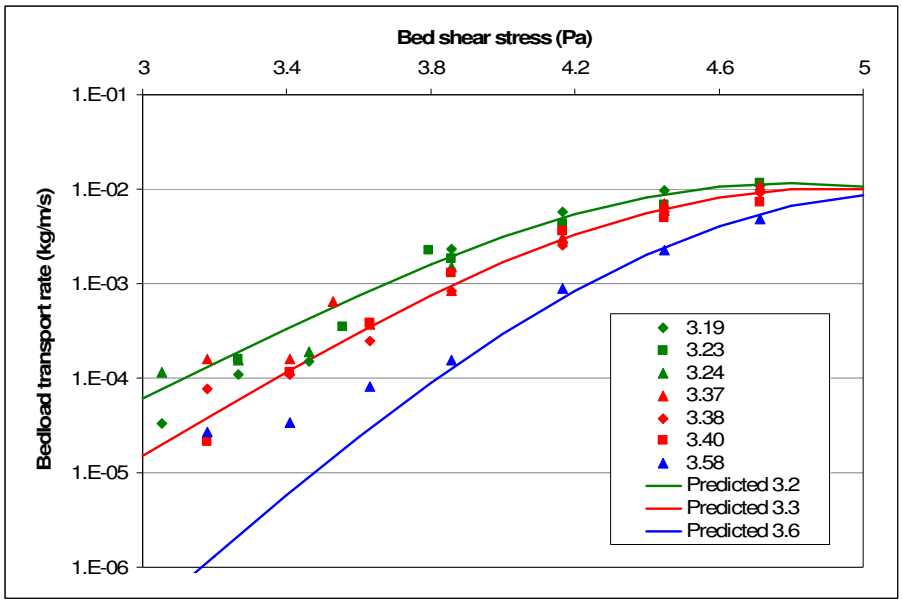

Fig. 4-29. Comparison of measured bedload transport rates with predictions using the method proposed in the text. Red line represents predicted transport rates when τ_{cr}.= 3.3 Pa. The comparison of this line with the data for the initially estimated τ_{cr}.≈ 3.4 Pa (using RTM-P) suggests that this latter value may be slightly overestimated, and critical bed shear stress for these runs should be 3.3 Pa.

A reassessment of the entrainment thresholds determined previously using RTM-P was carried out using the method described above. Fig. 4-30 shows the comparison with the previous τ_{cr} obtained with RTM-P. The results show very close correspondence between data sets, with average ratio of τ_{cr} obtained using the new method over τ_{cr} obtained with RTM-P equal to 0.99 (range 0.96-1.02). These results confirm the suitability of the proposed procedure, providing near identical results to those obtained using Parker *et al.*'s (1982a) RTM. It is noted however, that since the procedure presented was developed based on the values

of critical shear stress obtained by RTM-P in the first place, this reported similarity of the results is to certain extent expected. Nonetheless, results highlight the suitability of the new methodology, which is considerably easier and faster to apply than the visual method and the reference transport methods, with fewer requirements of data acquisition and calculations.

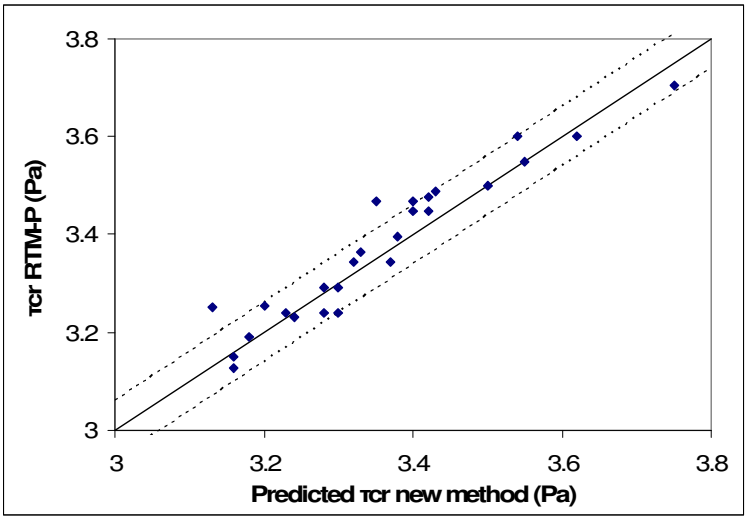

Fig. 4-30. Comparison of τcr from RTM-P and values obtained from the proposed method. Solid line shows a 1:1 correspondence, with dashed lines indicating the interval defined by ±1 standard deviation.

The data of entrainment thresholds and bedload presented suggest a number of issues:

- Bedload transport rates for the same flow magnitude reduce with increasing critical bed shear stress, with this reduction extending to the stability test. This confirms the influence of antecedent conditions on not just entrainment thresholds but also on subsequent bed mobility.

- A new methodology is developed to estimate bed entrainment thresholds solely based on total bedload transport, overcoming the need for data of bed surface composition and fractional transport rates.

- The results of the described new methodology are very similar to those obtained by Parker *et al.*'s (1982a) reference transport method (Fig. 4-30). Indicating that this new simpler procedure provides estimates of critical bed shear stress comparable to those from a well established method.

- Fractional data indicates that size classes 5.6–8 mm and 8–11.3 mm are proportionally more mobile than the others. For coarser grains, submerged weight is likely to be the main factor for their reduced mobility; whereas values of $p_i/f_i < 1$ reported for $D < 5.6$ mm may be influenced by hiding effects (Parker and Klingeman, 1982; Reid and Frostick, 1986; Andrews and Parker, 1987; Wilcock and McArdell, 1997; Van Rijn, 2007b).

4.2.7 Velocity data and bed roughness

One way in which exposure to antecedent flows could affect entrainment is by changing bed surface roughness (Church *et al.*, 1998; Haynes and Pender, 2007; Recking *et al.*, 2008), as mechanisms such as rearrangement of particle position and orientation and disappearance of fines from the surface take place during exposure to sub-threshold flows (Allan and Frostick, 1999; Haynes and Pender, 2007; Frey and Church, 2009). The logarithmic law of the wall (equation 4-6) contains the parameter z_0, which describes the hydraulic roughness of the bed (Monin and Yaglom, 1971; Yaglom, 1979; Wilcock, 1996). The value of z_0 can be obtained from velocity data and the application of the logarithmic law (equation 4-6) (Graf, 1998; Dey and Raikar, 2007; Piedra *et al.*, 2009).

$$\frac{u}{u_*} = \frac{1}{\kappa}\ln\left(\frac{z+d}{z_0}\right) \qquad \textit{Eq. 4-6}$$

Streamwise velocity profiles were obtained using a Vectrino acoustic velocimeter (section 3.3.1). The Clauser method (Graf, 1998; Cooper *et al.*, 2008; Piedra *et al.*, 2009) was applied to obtain bed shear velocity u_* and bed roughness length z_0. Individual measurements at each elevation took 120 s, with a full profile taking approximately 30 minutes. Therefore, it was impossible to take these measurements simultaneously with the flow steps used during antecedent conditions; thus, partial repeats of specific runs, corresponding to Stage 1 conditions, were conducted separately to obtain velocity data.

The effect of antecedent conditions on bed roughness was assessed by comparing velocity data and the resulting parameters of the log-law at the beginning and end of the antecedent conditions. Three acceleration rates were selected: AccRate1, AccRate3 and AccRate5, corresponding to durations of 0.5, 2 and 6h respectively. These durations were adopted as they showed the largest effect on entrainment thresholds (section 4.2.2). Two profiles were obtained for each run at Q = 12 l/s for: a) the initial bed prior to application of test hydrographs; and, b) the bed after exposure to the antecedent conditions; (*Fig. 4-31*).

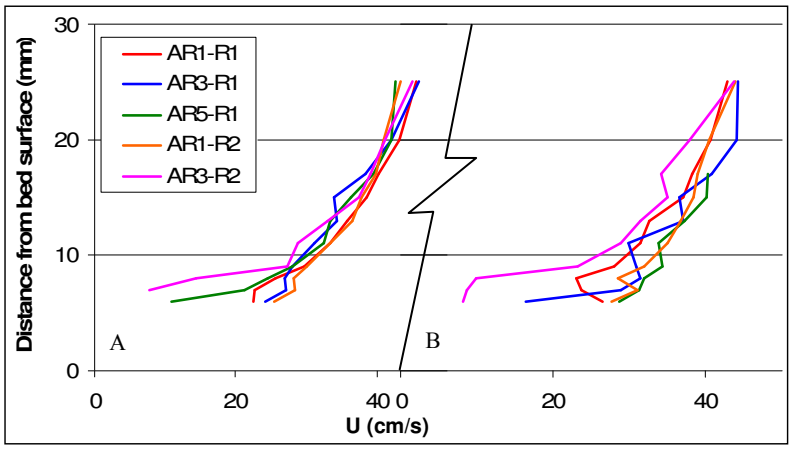

Fig. 4-31. Comparison of velocity profiles A) pre and B) post antecedent conditions. Note that 2 replicates were carried out for AccRates 1 and 3.

A considerable volume of literature suggests that the application of the Clauser method is restricted to approximately the lowest 20% of the flow depth (Monin and Yaglom, 1971; Nezu and Nakagawa, 1993; Graf, 1998; Oertel *et al.*, 2004). However, extensive ADV data collected over a greater range of flow depths suggests that the logarithmic law may apply to a much larger proportion of the flow depth, up to 0.5-0.8 z/h (Smart, 1999; Lamarre and Roy, 2005; Piedra *et al.*, 2009). Thus, the flow depth range used for the line fitting required for the application of the Clauser method was individually selected based on specific data, similarly to Wilcock (1996) and Smart (1999). This range was generally 0.3-0.8 z/h. Appendix 7 shows a summary of the velocity data and the parameter values obtained.

Roughness appears to increase by an average or 20% with antecedent duration up to 2 h, but reducing for the longest duration to approximately 30% of the initial bed value (*Fig. 4-32*A). This trend of increase and decrease of roughness with

the maximum found for the duration of 2h is similar to that showed by the entrainment thresholds (section 4.2.2). This is confirmed when the ratio of bed roughness is plotted against critical stress (*Fig. 4-32*B). Bed roughness after application of antecedent flow periods appears to increase for the beds with largest entrainment thresholds.

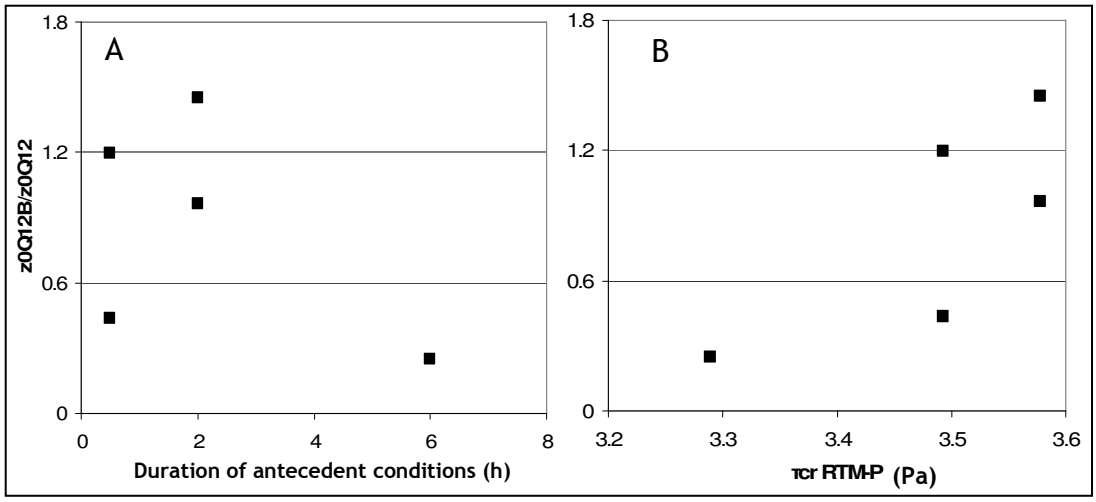

Fig. 4-32. Relationship between the ratio of bed roughness post-(z_0Q12B) and pre-(z_0Q12) antecedent conditions and: A) Duration of antecedent flow, B) Critical stress. Q12 and Q12B correspond to data for Q = 12 l/s pre and post antecedent conditions respectively.

Data in *Fig. 4-32*B suggest that hydraulically rougher beds are more difficult to entrain; yet, theory would suggest that their increased grain protrusion and exposure might make these beds more mobile. To resolve this potential conflict the findings may be explained by dividing total bed shear stress into form drag and skin friction directly applied to grains (Einstein and Banks, 1950; Robert, 1990; Petit, 1990; Buffington and Montgomery, 1997), with the first increasing with the appearance of bed forms (Wiberg and Smith, 1989; Buffington and Montgomery, 1999a). Thus, the magnitude of the bed shear stress acting to entrain particles reduces with bed forms (Knighton, 1998). No apparent or macro-scale bed forms (eg. dunes) were observed for any of the runs. However, as the estimation of the effect of flow history was based on velocity data taken at a single location, i.e. at the micro-scale, small changes in the bed, such as grain reorientation, grain removal or replacement by a different-size particle could act in a way equivalent to micro bed forms. Their presence might reduce the proportion of the bed shear stress dedicated to entrainment, explaining the apparent increased stability of the bed with hydraulically rougher beds.

A possible effect of flow history could be inferred from the comparison of velocity data at Q = 12 l/s. Measured velocities for profiles taken after antecedent periods display more noticeable deviations from a single-curve profile than those taken at the beginning of the run (Fig. 4-31). This may reflect disruption of the bed during sub-threshold flows, producing increased turbulence as a reflection of increased roughness. Pender *et al*. (2001) reported larger Manning's roughness parameters after beds were exposed to constant flows for durations in the region of 5000 minutes. These autors also showed evidence (laser bed topography data) of increased irregularities in the bed surface elevations as the experiments progressed. These measurements are consistent with those presented in this thesis for graded beds of increased bed roughness resulting from exposure to flows. However, the practical limitations of both the Clauser method and the velocity data, make a more robust assessment of bed roughness unachievable with the present data set. Nonetheless, this limited analysis of velocity profiles and bed roughness lengths indicates the following:

- Beds appear hydraulically rougher at the end of the test hydrograph as the new bed entrainment threshold increases (Fig. 4-32).

- In the absence of noticeable changes of bed surface composition (section 4.2.3) small-scale changes of particle position and orientation may be responsible for the observed increase in bed roughness.

- Calculations are based on single velocity profiles and assessment of the impact of test hydrographs on general bed characteristics will require velocity data at multiple locations.

4.2.8 Particle clustering analysis

Structural changes of the bed have been suggested in the previous two sections as responsible for the observed link between antecedent conditions and values of the bed critical shear stress and hydraulic roughness. So this section tries to study these structural changes quantitatively. The analysis of the effect of flow

history on bed surface was extended by considering both the abundance and spatial distribution of particles in the 8-11.3 mm class (section 3.4.4). This grain size class, containing D_{90} of the bed (10.6 and 10.3 mm for the bulk mix and initial beds repectively), was painted in ultra violet blue paint. The results and discussion presented below can be interpreted as a compositional and structural study of bed surfaces under antecedent conditions. The analysis of grain clustering also provided information about the mobility of the 8-11.3 mm size class. UV photographs were taken coinciding with bedload and bed surface composition sampling for eight acceleration rates during Stage 2, including two replicates for AccRates 2H, 2L, 3H and 3L (section 3.5). In addition, for four of those experiments UV images were taken throughout the antecedent flow period. The methodology followed was detailed in section 3.3.2.

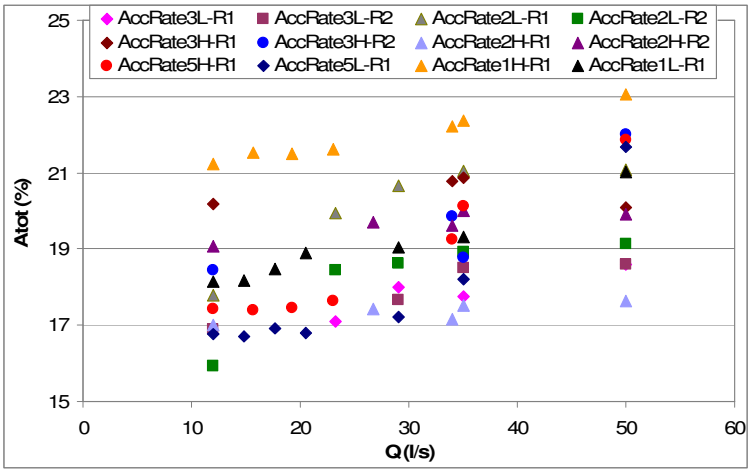

Fig. 4-33. Total area of 8-11.3mm particles on the bed surface during increasing flows.

The total area occupied by 8-11.3 mm particles A_{tot} (Fig. 4-33) remains reasonably unchanged for flows below 20-25 l/s, after which A_{tot} increases with discharge. *Fig. 4-34* shows that average element area a_i and total number of clusters or elements N_e also remain reasonably stable during antecedent conditions. Once this apparent threshold of 20-25 l/s is overcome, a_i and N_e show a very large increase and decrease with flow, respectively. These results suggest that these coarse particles group together, producing fewer individually larger *elements*, i.e. clustering.

It is possible that observed increases of A_{tot} might be due to additional particles coming into the area of observation, as more grains are mobilised during large

flows, and/or to exposure of blue-painted particles from the subsurface layer after surface grains are entrained. However, the relative changes of both a_i and N_e are lager than the increase of total surface area, as indicated by data in *Fig. 4-35*. If the increase of A_{tot} was due to additional 8-11.3 mm grains being exposed, the average cluster size would remain approximately stable, and N_e would increase. This is not the case, with a_i and *Ne* becoming substantially larger and smaller respectively with flow. Thus, it can be concluded that existing coarse particles on the bed surface group with increasing flows. Clustering appears to persist during the stability test, as shown by the continuous increase of a_i and decrease of N_e with higher flows (*Fig. 4-34*).

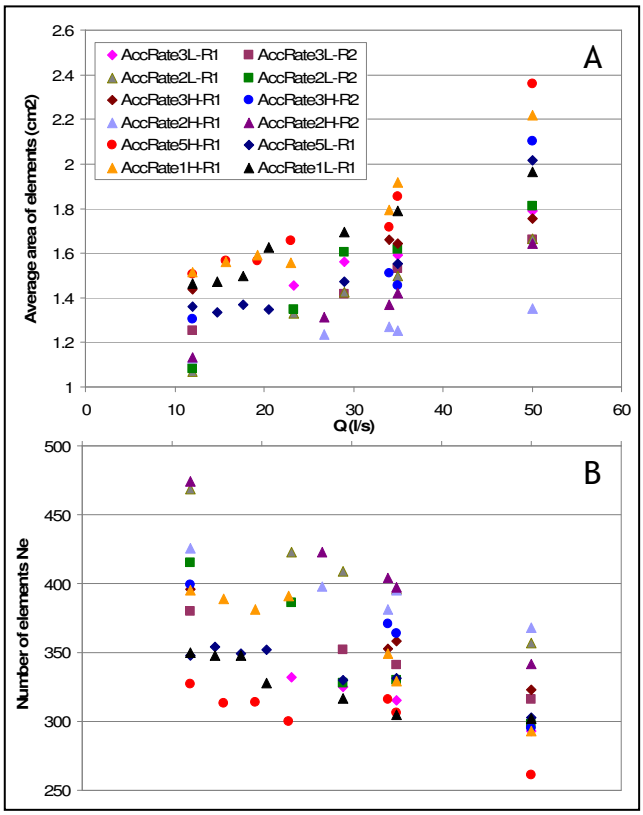

Fig. 4-34. Evolution of cluster characteristics with discharge. A) Average area of cluster/element, B) Total number of elements.

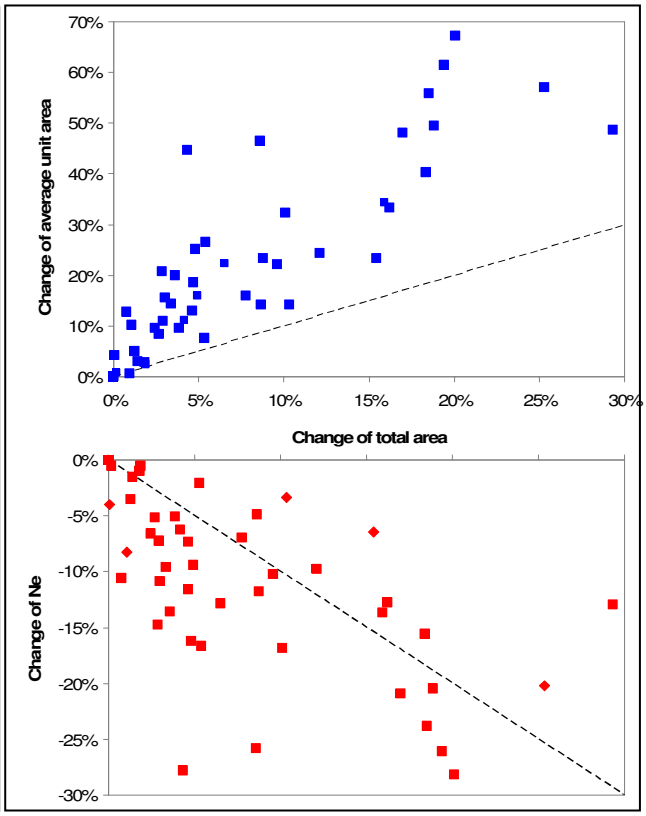

Fig. 4-35. Comparison of change of a_i and N_e relative to the evolution of A_{tot}. Dashed lines indicate equal rates of change.

The smaller value of Q_{cr} of the 8-11.3 mm class than Q_{cr50} noted here (around 25 l/s) is confirmed by the earlier analysis of entrainment thresholds (4.2.2), where the ratio τ_{cri}/τ_{cri50} is < 1 for the 8-11.3 mm class ($D_i/D_{50} \approx 1.5$), indicating movement of this size class at lower discharges. Increased grain exposure of the

coarser grains has been shown before to cause particle entrainment at lower thresholds than finer fractions (Parker *et al.*, 1982b; Wilcok and McArdell, 1993; McEwan *et al.*, 2004; van Rijn, 2007b). The results presented indicate similar mechanisms of entrainment for particles of size class 8-11.3 mm. Results of bed surface evolution using colour thresholding also show changes in bed resistance to entrainment. Fig. 4-36 shows a positive correspondence between bed entrainment thresholds and the number of groups (N_e) formed by 8-11.3 mm particles found on the bed surface pre (IB) and post antecedent conditions (Q_t). This indicates that beds with larger number of elements are more stable. Alternatively, it could also be the case that more stable beds are consequence of larger percentage of coarse particles on the bed surface. However, Fig. 4-37 shows that there is no correspondence between entrainment thresholds and the total area occupied by 8-11.3 mm particles.

The question arises then whether N_e is a reflection of a higher percentage of size class 8-11.3 mm on the bed. Fig. 4-38 shows that N_e does not have a clear correspondence with total bed surface area occupied by the 8-11.3 mm class. Therefore, a large value of N_e is not linked to a large proportion of the 8-11.3 mm size class on the bed. It would appear then that increased bed stability is not related to the total area occupied by coarse grains, but reflects the abundance and how these grains are distributed over the bed surface. It is noted that critical shear stress decreases with larger average area of clusters present on the bed surface (Fig. 4-39). This would indicate an apparent contradiction, as one might conclude that larger clusters of coarse particles would lead to stronger beds (Hassan and Reid, 1990; Hassan and Church, 2000; Frey and Church, 2009). Thus, it is proposed here that the stability of the unimodal bed tested is partially due to the surface distribution of 8-11.3 mm particles over the bed. Fig. 4-39 shows two processes: i) antecedent conditions appear to cause similar effect on a_i for all runs, and ii) critical shear stress is largest for the smallest values of a_i.

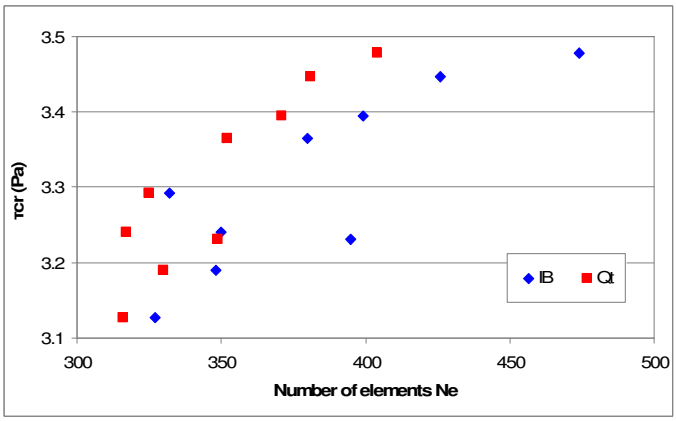

Fig. 4-36. Relationship between Ne and bed entrainment threshold.

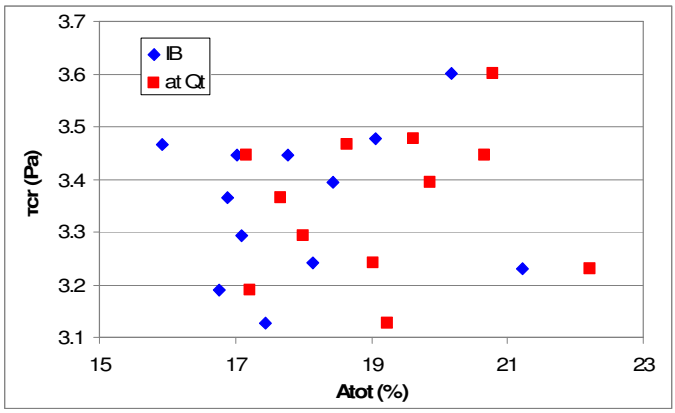

Fig. 4-37. Variation of τ_{cr} with total surface area occupied by particles of size class 8-11.3mm.

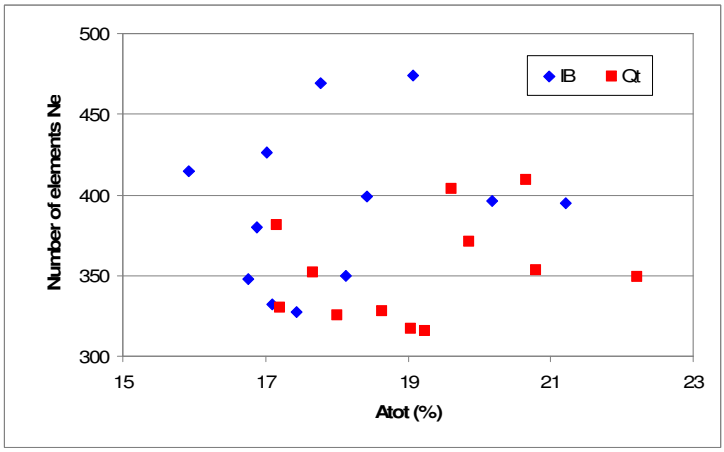

Fig. 4-38. Relationship between total percentage area of size class 8-11.3mm measured under UV light (A_{tot}) and number of elements on the bed surface (N_e)

The correspondence between bed stability and the surface distribution of coarse particles is further reinforced by the inverse relationship between the percentage change of N_e during antecedent conditions and N_e in the initial bed (Fig. 4-40). The largest change of N_e corresponds to initial beds with the largest number of unconnected coarse particle groups. As high values of N_e are not necessarily linked to large presence of 8-11.3 mm particles, this can be

interpreted as vulnerability to movement of coarse grains. As established here, high values of N_e indicate a more scattered distribution of coarse particles over the bed, while low values of N_e suggest that particles are clustered. Fig. 4-40 suggests that coarse particles are more vulnerable to movement when they are isolated, with the opposite occurring for particles that belong to a group of the same size grains. This increased resistance of clusters was highlighted by Reid *et al.* (1984), Marion *et al.* (1997) and Church *et al.* (1998).

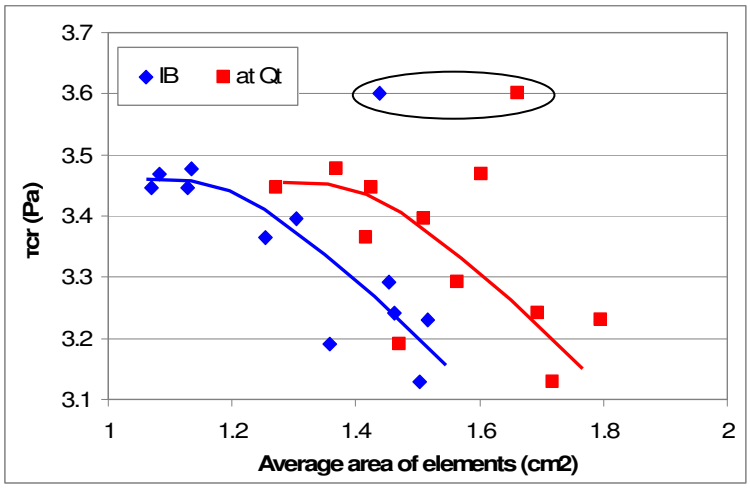

Fig. 4-39. Variation of bed entrainment thresholds with average area of elements of initial bed (IB) and bed at target flow (Q_t). Note the near-parallel trend lines, indicating a reasonably uniform effect of antecedent conditions on a_i. Trend lines, drawn by eye, are indicative only. Circled data points correspond to outliers of the same run.

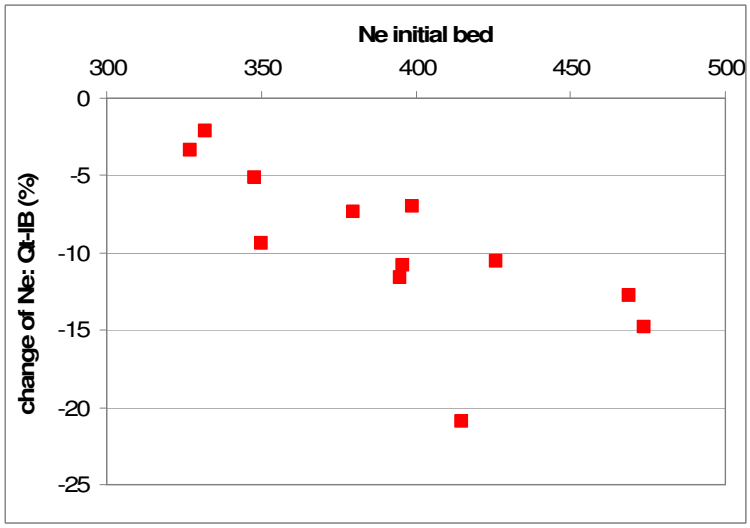

Fig. 4-40. Sensitivity of cluster formation to Ne of initial beds.

This observed sensitivity of the 8-11.3 mm particles may be related to the strength of individual elements on the bed. The same total bed surface area occupied by particles of size 8-11.3 mm can be achieved by either a large number of individual particles scattered over the bed surface, or concentrated

in smaller number of elements of larger surface area. The analysis above suggests that the bed as a whole will be weaker in the second case; however, the elements themselves will be more stable when grouped in clusters. This would explain why beds with most numerous elements appear to result in more resistant beds, at the same time as being the ones that show the largest percentage changes in both N_e and a_i.

Finally, the relationship between antecedent conditions and bed evolution, based on size class 8-11.3 mm, is further demonstrated in Fig. 4-41. Bed stability increases with larger changes of N_e during antecedent periods. As demonstrated above, beds that experience the largest coarse grain activity are those with highest value of N_e (directly related here to the surface distribution of 8-11.3 mm grains), which in turn, appears to produce the strongest beds. This link between bed resistance and spatial distribution of coarse grains is an important finding as it introduces yet another factor in bed stability assessment. These results imply that in order to understand entrainment it is insufficient to know bed surface grain size distribution or a representative grain size, eg. D_{50} or D_{90} (Cooper *et al.*, 2008). The distribution of coarse particles on the surface appears to influence bed stability from the outset. It is noted, however, that this suggestion is based on a limited number of experiments and a single particle size.

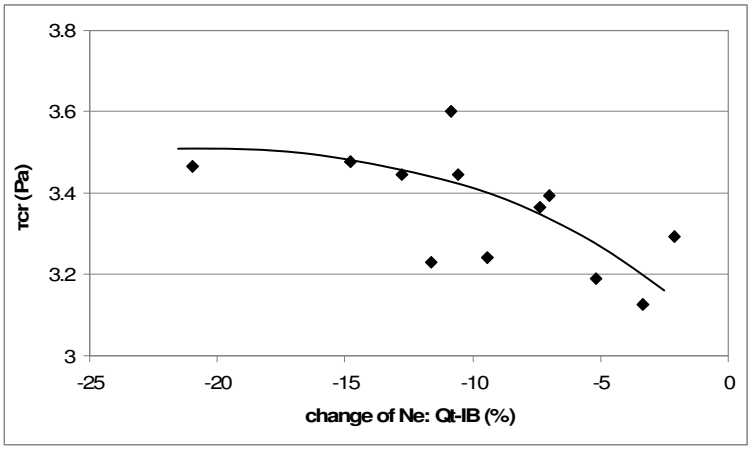

Fig. 4-41. Relationship between bed entrainment threshold and reduction of Ne during antecedent conditions.

To summarise the analysis of clustering and mobility carried out, below are the main findings:

1. The analysed particle size class (8-11.3 mm) moves for lower flows than the bed median size, confirming the effects of hiding proposed by previous authors (section 2.2.4).
2. Numerical data on cluster size and discharge values were obtained for the first time, clearly demonstrating that coarse particles gather together under increasing flows.
3. Data suggest that the proportion of coarse particles contained on the bed surface has a secondary role on bed stability and beds with slightly larger contents of 8-11.3 mm grains are not necessarily more resistant to entrainment.
4. There appears to be a positive relationship between the number of unconnected coarse grains (D_{90}), their spatial distribution over the bed surface and the stability of the mixed bed, provided that the proportion of this size class on the bed surface (A_{tot}) remains reasonably unchanged.

This final point is relevant when estimating entrainment thresholds and connects with the changes that antecedent conditions have on bed structure. If the coarser sizes in granular beds are active during what may be considered sub-threshold flows, their surface distribution may be altered and thus, the resistance of the bed. This is evidence of the importance of studying the impact of antecedent conditions and the shape of hydrographs on the stability of gravel beds.

4.3 *Uniform gravel 4-5.6 mm*

The data set, analysis and discussion of the effect of acceleration rates on entrainment using a near-uniform gravel bed were somewhat incomplete as entrainment thresholds were estimated using the visual method only. Given that this method has a number of uncertainties, both in the definition of the criterion and practicalities of its application (section 4.4.1), a selection of experiments carried out for the Pilot Runs were repeated to permit comparative bedload data analysis for threshold studies. In addition, since the bed slope was changed from 1/200 for the Pilot Runs to 1/150 for these runs using uniform gravel, results can also address the effect of bed slope on entrainment.

The procedure followed was similar to the Pilot Runs and Stages 1 and 2 and the method selected to provide the main data set was Parker *et al.*'s (1982a) method (complemented by Wilcock and Crowe's, 2003 equation). The reference entrainment threshold of the bed for the new conditions was estimated as Q_{ref} = 29.2 l/s (RTM-P); which was then used to construct test hydrographs for durations 0.5, 2 and 6 h. These were selected since they were those that showed largest effect on critical flows in Stages 1 and 2 and encompass the main range of flow history durations tested during the Pilot Runs. As in the cases of the unimodal bed runs, visual method (Neill and Yalin, 1969), RTM-P (Parker *et al.*, 1982a) and RTM-S (Shvidchenko *et al.*, 2001) data were collected and analysed.

4.3.1 Entrainment thresholds

Appendix 4 contains a summary of values of entrainment thresholds for the single size bed tested. Entrainment flows determined using the visual method increase from 21 l/s to 24.7 l/s as antecedent durations increase from 0.5h to 2h, followed by a slight increase of the entrainment flow (25.8 l/s) for the longest duration (Fig. 4-42). This confirms the results of the Pilot Runs. However, critical flows obtained by RTM-P show a distinctly different picture. Values of Q_{cr} slightly reduce from 0.5h to 2h (28.6 l/s to 28.0 l/s), increasing again to $Q_{cr} \approx Q_{ref}$ = 29.2 l/s for the longest duration. It is also noted that the range of Q_{cr} for RTM-P is considerably smaller than that of the VM, 1.3 l/s and 4.1 l/s respectively. Thus, if the results of RTM-P are followed, antecedent conditions have little effect on the uniform gravel bed.

Discrepancies between the results obtained using different entrainment criteria affect both the trends and absolute values of critical flow. Q_{ref} for RTM-P is 1.4 times higher than Q_{ref} (VM), with ratios between critical flows of 1.36, 1.12 and 1.17 for AccRates 1, 3 and 5 respectively. Differences of values were also reported for the sand-gravel mix (section 4.2.2), although general trends were similar to one another. The reasons for these contradictory results are uncertain but are expected to be related to the concept and methods used by the different entrainment criteria, (Wilcock, 1998; Buffington and Montgomery,

1997), eg. local particle mobilisation versus bedload sample, small inspection area versus the width of the sediment trap (4.4.1).

It is noted that the application of the RTM-P and RTM-S methods to the uniform gravel bed continued to show consistently larger values of critical flows for RTM-S (9-11%). Also, the parameters of the Shvidchenko *et al.* (2001) equation used for fitting the transport rates to obtain critical shear stress had to be adjusted, as the equation depends on θ_{cr50}, which is different for the unimodal and uniform gravels tested. However, the parameters of the modified Wilcock and Crowe (2003) equation fitted to the unimodal gravel data remained the same for the uniform gravel. This is an advantage of the latter method as the application of the criterion and comparison between data sets does not depend on mixture size. Table 4-11 shows the comparison between parameters of Shvidchenko *et al.*'s (2001) equation for the unimodal and uniform beds.

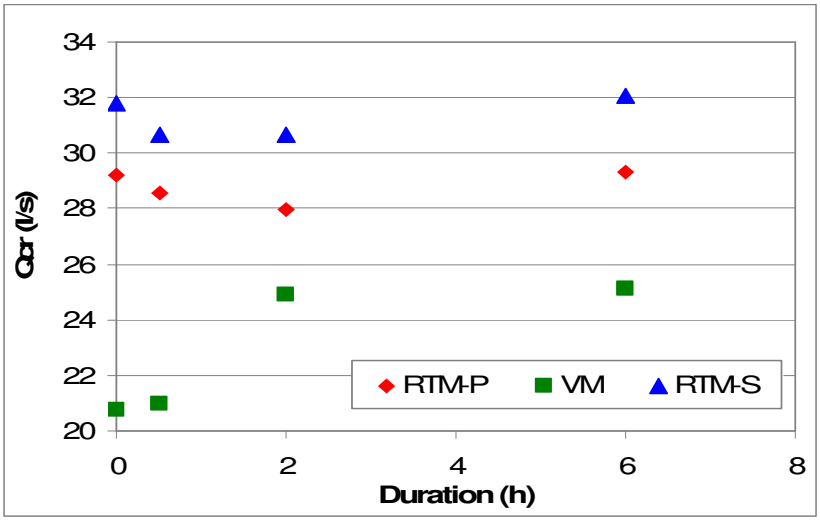

Fig. 4-42. Effect of duration of antecedent conditions on entrainment for the single size runs.

Parameter	Unimodal	Uniform
θ_{cr50}	0.0384	0.0445
B	13.5	13
C	3.96	3.34

Table 4-11. Comparison of parameters of Shvidchenko et al.'s (2001) equation for estimation of critical shear stress

4.3.2 Effect of slope on entrainment thresholds

Critical flow data for the visual method show similar trends to the Pilot Runs (Fig. 4-43): a general increase of Q_{cr} with durations and an apparent maximum bed resistance achieved by antecedent conditions. The ratios of average values of Q_{cr} for the Pilot Runs over those for the uniform gravel for each duration are all approximately 1.7, except for the duration 0.5 h, where the ratio is 1.94 (Table 4-12). This discrepancy of the ratio for 0.5h could be due to the very small increase of Q_{cr} for this case, contrary to the same duration in the Pilot Runs, or to the already discussed discrepancies between results of durations 0.5 h and 1 h of the Pilot Runs (section 4.1.2). Since the particle sizes of both beds are nearly identical (D_{50} = 4.8 mm for both beds) the observed differences of Q_{cr} between Pilot Runs and uniform gravel data sets are likely to be due to bed slope (Table 3-13). The main reason for changing the bed slope from the original 1/200 to 1/150 was the lack of mobility of the unimodal bed; which increased considerably under the steeper slope. Shvidchenko *et al.* (2000) noted an increase of critical shear stress with steeper slope for the same grain size. Comparison of data between experimental series shows that relative depths for the Pilot Runs are 1.2-1.3 times larger than those for the uniform bed, which would lead to lower critical flows according to Shvidchenko *et al.* (2000). However, despite bed sizes being very similar, critical flows for the Pilot Runs were higher than those for the uniform gravel in the experiments presented here (Fig. 4-43).

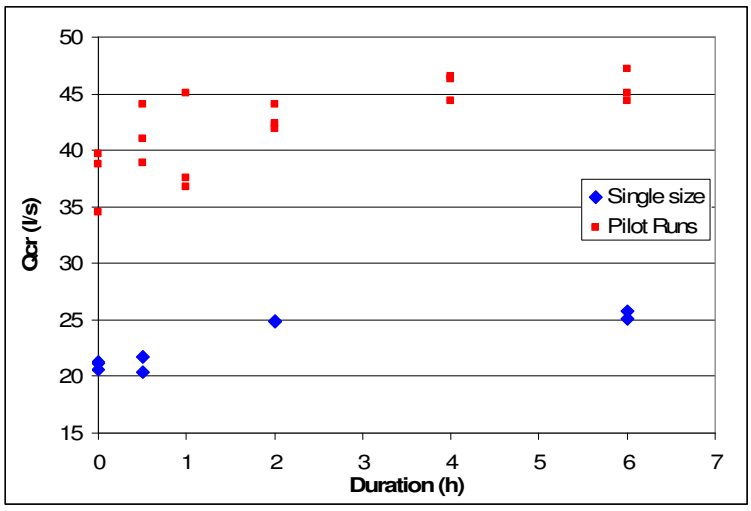

Fig. 4-43. Comparison of Q_{cr} from Pilot Runs and single size runs.

Shvidchenko *et al.* (2000) suggest greater resistance of the grains caused by reduced relative depth as the reason for the observed results. Recking (2010) also reported larger entrainment thresholds for the same particle size on steeper beds, although no detailed explanation was given. As relative depth reduces with steeper beds for the same discharge, an increase of slope will generally produce larger velocities and bed shear stresses for the same flow. As grain position, hiding and bed surface composition will not be affected by a change of slope, it is difficult to see how greater entrainment resistance can be achieved by steeper beds. Thus, the higher entrainment flows found for the shallower slope experiments are linked here to the larger flows required to produce sufficient destabilising forces to entrain the grains.

	Qref	AccRate1	AccRate2	AccRate3	AccRate4	AccRate5
Duration (h)	0	0.5	1	2	4	6
			Pilot Runs			
R1	38.8	41.1	37.6	41.9	46.3	44.4
R2	34.5	44.0	36.8	42.3	44.4	45.0
R3	39.6	38.9	45.1	44.1	46.5	47.2
Q_{cr} (1)	35.58	40.8	38.83	42.47	45.1	44.9
			Single size			
R1	21.2	20.4		24.9		25.1
R2	20.6	21.7		24.9		25.8
R3	21.1					
Q_{cr} (2)	20.8	21.0		24.7		25.8
(1)/(2)	1.71	1.94		1.72		1.74

Table 4-12. Comparison of results of Q_{cr} from the visual method.

The relative effect of antecedent conditions appears to be similar for both experimental series when the results of the visual method are considered. *Fig. 4-44* shows that values of the ratio Q_{cr}/Q_{ref} are very similar except for 0.5 h; suggesting that the effect of acceleration rates on very well sorted beds is different to that shown by the sand-gravel bed. However, as discrepancies between methods persist, this conclusion is only applicable to the data sets presented here. It is clear that in the case of the uniform gravel, critical flow values, and therefore the interpretation of the data, depend on the methodology adopted.

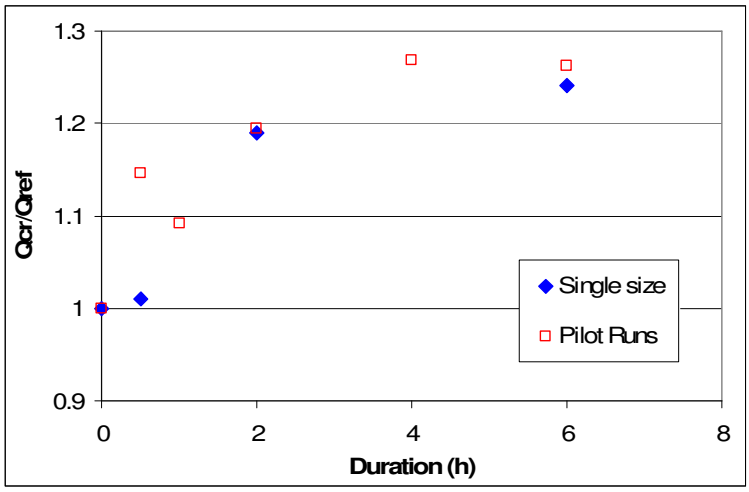

Fig. 4-44. Values of Q_{cr}/Q_{ref} for Pilot Runs and single size runs using the visual method.

4.3.3 Bedload transport

Transport rate values are shown in Appendix 6. The combination of power and linear laws developed for Stages 1 and 2 relating total bedload transport and τ/τ_{cr} (equations 4-1 and 4-2) can also be applied to the uniform gravel. The final parameter values (section 4.2.5.2) were obtained after visually fitting the proposed curve to the full data set corresponding to sand-gravel and uniform beds. *Fig. 4-45* shows the comparison between the theoretical equation and the data for the uniform gravel bed. Thus, equations 4-1 and 4-2 appear to be applicable for the full range of τ/τ_{cr}. However, scatter is observed for values of q_b in the region of τ/τ_{cr} = 1. This again, may be related to the stochasticity of entrainment at near-threshold flows and the possible excess bedload samples due to air bubbles in the sediment trap.

The methodology for the prediction of the transport rates and the estimation of entrainment threshold was tested against data for the uniform bed. Equation 4-3 was applied using the same parameter values determined for Stages 1 and 2. The comparison of the four data series shows good fit between predicted and recorded transport rates for the upper shear stress range (Fig. 4-46). This is consistent with the results for the sand-gravel mix (section 4.2.6). Critical bed shear stresses estimated by the proposed method are within ± 1% of those by RTM-P. These results confirm that the critical shear stresses estimated by RTM-P for the uniform gravel are consistent. More significantly, the results suggest that

the method and equations developed to predict transport rates and estimate critical shear stresses appears to work well for different bed compositions.

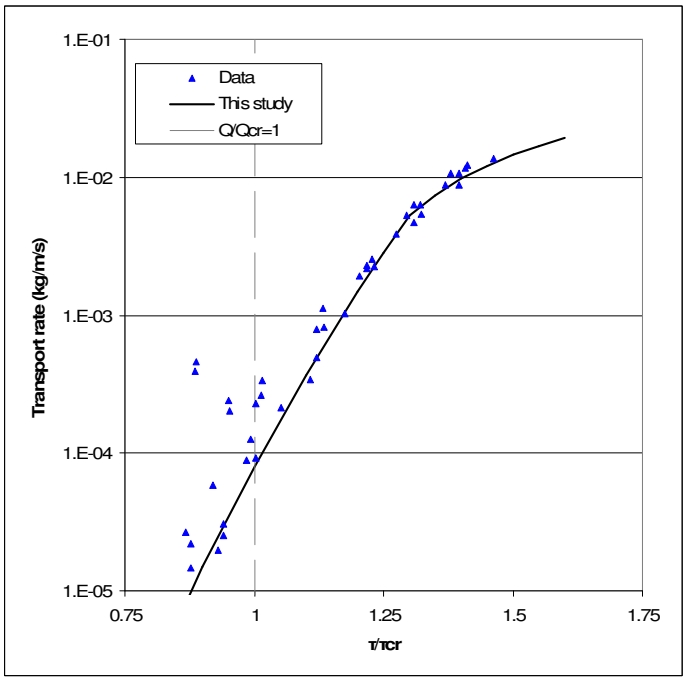

Fig. 4-45. Fitting of the transport rate equations for the uniform gravel bed data set.

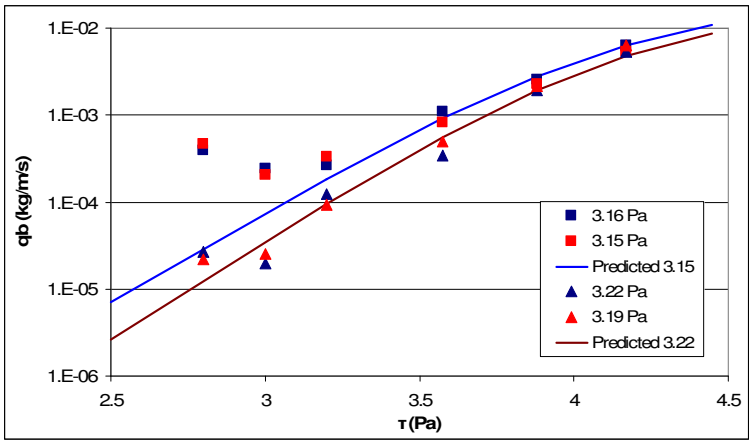

Fig. 4-46. Comparison of actual and predicted transport rates using eq.4-3 for the uniform gravel runs. Deviation of data for series 3.15 and 3.16 for τ/τ_{cr} < 3.2 Pa suggest oversized bedload samples due to air bubbles.

Finally, the effect of antecedent conditions on average transport rates for the duration of the test hydrographs (Fig. 4-47) shows that transport rates reduce from 1.59e-4 kg/m/s for the 0.5h duration to 2.28e-5 kg/m/s when antecedent duration increases to 6h, suggesting a reduction of bed mobility and transport as flows continue to act over the bed. This reduction of bedload rates could be

interpreted as strengthening of the bed with increasing exposure to flow; and therefore, in agreement with critical flows obtained by the visual method.

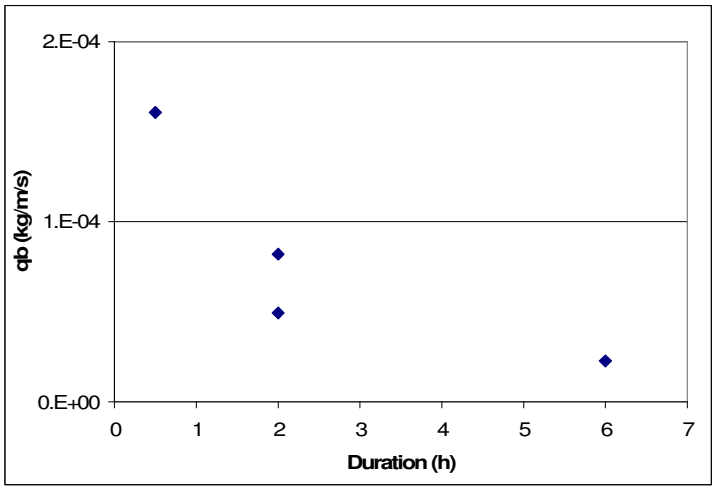

Fig. 4-47. Bedload rates for antecedent conditions phase for uniform gravel runs.

4.3.4 Velocity profiles and bed roughness

A similar analysis of bed hydraulic roughness to that of the unimodal mix bed was carried out for the uniform gravel. Roughness appears to reduce with the duration of the antecedent conditions (Fig. 4-48); while the relationship between critical bed shear stress and the ratio of the hydraulic roughness value of the bed after exposure to the antecedent conditions (z_0Q12B) over that of the initial bed (z_0Q12) at a common discharge Q = 12 l/s (z_0Q12B/z_0Q12) reaches a maximum (3.44) for τ_{cr} = 3.16 Pa (AccRate1) (Fig. 4-49).

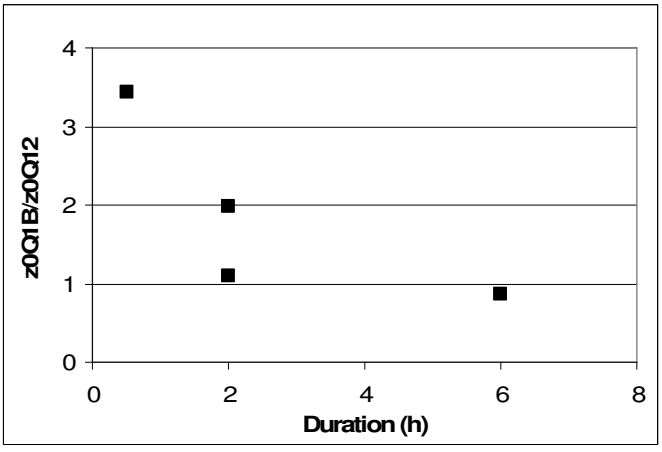

Fig. 4-48. Effect of the duration of the antecedent conditions on the ratio of bed roughness post and pre antecedent conditions (z0Q12B/z0Q12).

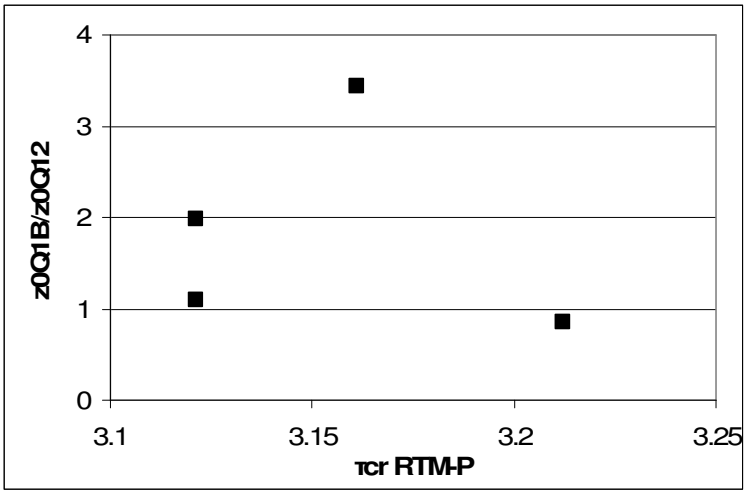

Fig. 4-49. Relationship between the ratio of bed roughness post and pre antecedent conditions (z0Q12B/z0Q12) and estimated entrainment thresholds.

These results appear to contradict the earlier data for the unimodal bed, which showed an increase of roughness length with bed resistance. This difference may be due to a different response of the uniform and graded gravels to flow history (Ockelford *et al.*, 2010), by which prolonged exposures of the bed to increasing flows make the well sorted bed surface hydraulically smoother. In their experiments with a graded mixture Pender *et al.* (2001) found that bed surface became rougher (expressed by the increase of Manning's roughness parameter *n* of c. 18%). In addition, their bed elevation frequency distributions (deviations over average bed elevation) for the beds at 20 and 80 hours into the run expanded at the range limits, reducing their peak frequency with respect to the distribution curve of the initial bed (Fig. 11 in Pender *et al.*, 2001). These results indicate that the bed surface compacted and became more irregular, with the consequent increase of hydraulic roughness. Saadi (2002) also recorded an increase of a bimodal bed surface peaks and troughs after antecedent conditions. Haynes and Pender (2007) deduced that increased bed roughness results from greater rearrangement of the bed surface caused by longer antecedent durations. Ockelford *et al.* (2010) showed how the range of bed surface elevations for the uniform gravel decreased (smoother bed), whereas the same parameter increased for the bimodal bed, effectively making the bed rougher (van Rijn, 2007b). Unimodal beds, like the one tested here, contain a variety of sizes. The interaction between different particles may favour small grain movement and the formation of troughs and crests, resulting in increased roughness. However, the limited geometric variability of grains in the well

sorted beds, both vertically and spatially, is smaller than that of the unimodal gravel. This, combined with the homogeneity of voids in the uniform gravel reduces the range of possible bed surface changes by size segregation or structural changes. In the uniform gravel bed there are two ways that the surface may be modified: a) grain rearrangement to become less exposed to fluid actions or achieve increased imbrication/friction; or, b) grain entrainment removing the more exposed, protruding grains. Following this, those grains that are not entrained lead to hydraulically smoother beds.

The reduced degree of freedom of movement of particles in uniform gravel may also explain the small range of critical shear stress observed with RTM-P. As the options for bed surface evolution are smaller than those of a multi-size bed, differences between reference entrainment thresholds and those after flow history are smaller than the ones observed for the unimodal bed, with ranges of Q_{cr} values of around 1 l/s and over 4 l/s for the uniform and unimodal material respectively. This also has consequences for the study of sediment transport generally; as the compositional and textural changes undergone by each type of bed mixture will depend on their size distribution (Haynes and Ockelford, 2008, Ockelford *et al.*, 2010). Hence, findings and results obtained using uniform gravels may not be directly applicable to a particular size class when it is included within a multi-size bed (van Rijn, 2007b).

4.4 *Discussion*

4.4.1 Evaluation of the visual method

A number of authors have applied the visual method to estimate the threshold of motion of granular beds (Neill and Yalin, 1969; Wilcock, 1988; Paphitis and Collins, 2005; Haynes and Pender, 2007). Its relatively simple application, where only visual observation is needed and potentially no equipment is required, makes this method very attractive for sediment entrainment studies. The practical application of the procedure is progressively complicated if the area of observation is large, moving grains are small or analyses of count repeatability are required. In these cases, recording and magnifying the images require using video equipment (VCR, TV, video camera, etc.), although these are devices

easily available nowadays. In the case presented in this thesis, video recording was used to increase reliability of the particle count, where the same counting period was replayed twice to ensure counting of all movements (section 3.4.1). Results obtained from the visual method appear to represent the changes of bed resistance produced by antecedent conditions discussed in this chapter. Indeed, trends of entrainment threshold values provided by the visual method agree with the findings of Paphitis and Collins (2005), Haynes and Pender (2007) and Haynes and Ockelford (2008) in the sense that bed resistance appears to increase with the duration of antecedent conditions, reaching a maximum, and remaining approximately constant or slightly lower for longer durations (results corresponding to well sorted material). However, when the results from the visual method are compared to those obtained with the reference transport method, a number of discrepancies appear, particularly in the case of well sorted sediment. These observed differences of values and especially of trends are likely to be related to the conceptual and practical definitions of these two entrainment criteria (Buffington and Montgomery, 1997). These authors pointed out at the subjectivity of the definition of how much movement constitutes initial motion (weak, medium, general movement of Kramer, 1935) as one of the causes of the uncertainty of the method. Neill and Yalin (1969) and Wilcock (1988) suggested formulae to reduce this uncertainty based on the adoption of a fixed parameter (10^{-6}). However, there appears to be no dedicated study on the effect of the constant used as the threshold criterion on the visual method.

Thus, estimating entrainment thresholds from observation of particle movements has a number of limitations that restrict its accuracy, reliability and repeatability:

- Movement counts are made over a small area, which may not be representative of the behaviour of a larger bed area, since bed surface size composition and texture may vary over the full bed extent. Thorough remixing of the bed material prior to each experiment attempted to minimise this effect. However, a small area of observation is necessary if appropriate grain definition and visual identification are to be achieved. Larger areas would reduce the number of pixels on the video image and

most importantly, would reduce the size of the grains on the screen, making movement counts impractical.

- Secondly, particle movements, especially in a small area, are affected by the random character associated with grain distribution, orientation and movement under turbulent flows (Miller *et al.*, 1977; McEwan *et al.*, 2004; van Rijn, 2007a). Differences of grain position or orientation may result in more mobile grains under the same acting forces than if the same grains had slight different geometrical configurations. The bedding-in period applied to the bed in all experiment runs is partially aimed at eliminating this factor, as it reduces the influence of bed construction. Quantification of the influence of the size and location of the area of observation will require repeating measurements of particle movement at different locations of a range of areas of visual inspection. However, this was not the focus of the research presented in this thesis.

- An important factor affecting grain movement counts is the fact that all movements occurring within the observation area are considered, regardless whether they originate from the observation area itself or not. This is due to the extreme difficulty of visually differentiating the source of moving grains, especially at high flows, when tens of particle movements, many of them simultaneously, occur in a short period of time. Other authors that used the visual method did not specify the origins of particle movement (eg. Monteith, 2001; Paphitis and Collins, 2005) and so it is assumed here that a similar approach was followed.

- The counting procedure followed also has an influence on the results. The entire method relies on the identification of particle movements, which in the case of this research work was based on visual observation. Operator ability to distinguish grain detachments is essential. However, human errors and limitations are intrinsically associated to this method. Operator's eyesight, concentration and ability to focus on the entire observation area are to be considered. The procedure followed in this research minimised the effect of these factors by splitting the observation

area in two during the review stage (section 3.4.1); the single observer was placed at an appropriate distance to ensure adequate coverage and focus over the screen; particle counts were not performed live but recorded and then replayed twice (one per count area on the screen), and lighting conditions in the laboratory and the bed itself were regulated to maximise image contrast. A small number of particle movements might have been missed out during the counting process, especially at high transport rates. However, this is unlikely to affect entrainment results, which are based on smaller particle movement rates and whose accurate count was ensured. Thus, resulting values of critical flows are likely to remain unaffected by this human factor.

These are some limitations of the visual method, some of them were addressed and minimised during the experimental work to make the process as efficient as possible. Others are intrinsically associated to the method. As discussed earlier, bedload trap samples provided physical quantities of actual solid transport collected for the duration of the flow stage and therefore, the methods based on these data (RTM) are preferred. However, the comparison of results from the visual method and reference transport methods highlight the different results obtained with each approach and agree with the comparative analyses carried out by researchers such as Wilcock (1988) and Buffington and Montgomery (1997).

4.4.2 Discussion of results

The data sets presented throughout this thesis relate to a range of aspects of the effects of antecedent conditions on entrainment of non-cohesive sediments, covering both uniform and unimodal gravel beds. In addition, data corresponding to entrainment thresholds using three different methodologies (VM, RTM-P and RTM-S), bed surface composition, bedload transport characteristics, clustering of coarse grains and hydraulic roughness were also analysed. This section includes detailed discussions of these results, which are compared and contrasted to previous work by other authors.

4.4.2.1 Entrainment thresholds

Data presented clearly demonstrates that flow acceleration rates do have an effect on entrainment thresholds. However, calculated critical flows show different values and trends depending on the bed composition used and the methodology applied. For well sorted beds (uniform and near-uniform gravels) the visual method indicates an approximately continuous increase of stability with duration of antecedent conditions up to approximately 25% of the reference flow estimated for the bed under no antecedent conditions; also suggesting a limit to bed strengthening achieved by flow exposure. These trends are similar to those found by Paphitis and Collins (2005), Haynes and Pender (2007) and Haynes and Ockelford (2008). Paphitis and Collins (2005) and Haynes and Ockelford (2008) also reported maximum increases of around 25% for their uniform beds; these were measured based on shear velocity at entrainment and bed shear stress respectively. These similarities occur despite the maximum durations of sub-threshold flows for these two previous references being 120 and 60 min respectively, compared to the 6h of he experiments presented in this thesis. However, the application of the reference transport methods by Parker *et al*. (1982a) and Shvidchenko *et al*. (2001) to the same experimental runs suggest an inverse trend, with values of τ_{cr} showing very little sensitivity of uniform sediments to the antecedent conditions tested, with average values of τ_{cr} remaining within the range 3.12-3.21 Pa.

In the case of the sand-gravel bed, both visual and reference transport methods suggest a similar trend of increase of τ_{cr} with hydrograph duration to a maximum value of 3.50-3.60 Pa for the rising limb with a duration of 2h (RTM-P) and 3.6-3.8 Pa for a duration of 4h (VM), with subsequent reduction of τ_{cr} for longer durations (maximum duration 10h) (Appendix 4). However, actual values of entrainment thresholds show disparity (Fig. 4-8 and Fig. 4-9). Contrary to Buffington and Montgomery (1997) who found entrainment thresholds obtained by the visual method lower than those from the reference transport method, results from this thesis do not display a particular trend (Fig. 4-50). The ratio of τ_{cr} from these two methods has an average value of 1.0; however, data show considerable scatter, with half of the data points in Fig. 4-50 outside the range ±1 standard deviation. These results indicate that there is no systematic under-

or over-estimation introduced by the methods used and the comparison between entrainment criteria is affected by inherent uncertainty of the results.

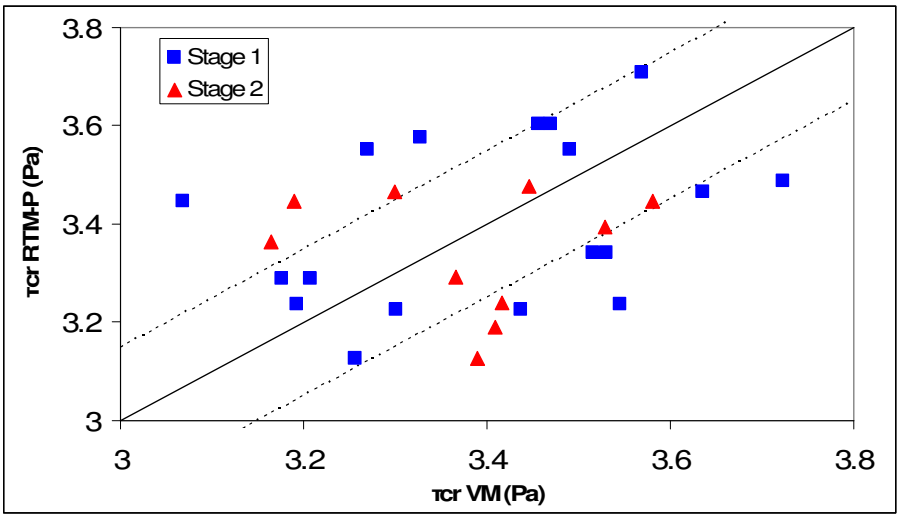

Fig. 4-50. Correlation of critical bed shear stress values obtained using RTM-P and VM for Stage 1 and Stage 2. Solid and dashed lines correspond to the equal values (1:1) and ±1 standard deviation respectively.

It is also noted that values of Q_{ref} provided by VM were the lowest values of entrainment thresholds; contrary to results from RTM, where Q_{ref} values do not correspond to minimum critical flows for any of the experimental series presented. All this adds complexity to the assessment of the suitability of each method. Since the study presented here is, to the author's knowledge, the only one that systematically and concurrently applied both the visual method and reference transport methods to the same experiments, it is difficult to contextualise the observed results. The work by Garde and Ranga Raju (1977), Wilcock (1988), Buffington and Montgomery (1997), Paphitis (2001) and Shvidchenko *et al*. (2001) already indicates that different results of entrainment thresholds may be obtained depending on the methodology and criterion followed.

It is accepted here that since the visual and the reference transport methods, in any of its variations, are based on very different data, i.e. local particle movements and bedload collected, discrepancies between results are likely. However, the explanation of the inconsistency of trends shown by each method for the well sorted beds remains difficult. It is speculated here that two main aspects of the visual method may be partly responsible: (1) some particle

movements within the area of observation might be due to random instabilities of individual particles, not necessarily related to general bed mobility. Indeed, observations of grains being dislodged and transported over short distances, eg. 1 or 2 grain diameters, were recorded as movements, since they fall into the category of particle dislodgement used to define movement in the visual method (section 3.4.6.1). (2) the threshold of particle movements set to define entrainment was small, and the above random movements may produce particle counts not representative of the bed mobility, resulting in critical flows being defined for lower values than appropriate. This is especially applicable to the unimodal bed, for which minimum movements associated to the threshold condition were particularly small (N = 4). This value of N resulted from limiting the observation interval to 180 seconds (similarly to Haynes and Ockelford, 2008) to reduce the potential impact of data collection periods on flow history, and to a size of observation area that allowed reliable identification of moving particles (section 3.4.1).

Entrainment threshold values obtained with both reference transport methods Parker *et al*. (1982a), complemented by the equation proposed by Wilcock and Crowe (2003), and Shvidchenko *et al*. (2001) follow the same trends (Fig. 4-7), although values for the second entrainment criterion are consistently higher than RTM-P. The similarities of trends are due to the fact that both methodologies are based on the same data sets, bedload transport rates. In the case of RTM-P calculations are based on volumetric rates, whereas for RTM-S they are based on mass rates. However, the values of τ_{cr} result from the application of the entrainment criteria set by each procedure (W_i^* = 0,002 and q_{bi}^* = 0.0001 for RTM-P and RTM-S respectively) and thus, critical shear stresses are an average of 12-15% higher for the RTM-S than for the RTM-P. Shvidchenko *et al*. (2001) expressed this differences in the entrainment values using the equation θ_{cri} *Parker* = 1.20 [θ_{cri} *Shvidchenko*]$^{1.09}$, obtained theoretically when the dimensionless bedload transport rates W_i^* and q_{bi}^* are combined together with their corresponding threshold limits (0.002 and 0.0001). The data from this study produced the empirical expression θ_{cri} *Parker* = 1.23 [θ_{cri} *Shvidchenko*]$^{1.10}$ for the combined data from Stage 1 and Stage 2. The small differences in the parameters are due to the variability introduced by the visual fitting of the

equations used in this thesis. It is re-stated that visual fitting has been used for the application of the reference transport method by Shvidchenko *et al*. (2001), Saadi (2002), Wiclcok and Crowe (2003), and thus, the procedure used in this thesis is consistent with previous authors.

Although the RTM-P has been selected here as the main procedure/criterion for the estimation of entrainment conditions and calculations, methods based on analysis of bedload samples (RTM) are not exempt from challenges. Dimensionless transport rates are calculated using actual sample sizes and compositions; which are entirely based on collected material. However, as pointed out by Hassan *et al*. (1991) and Church and Hassan (1992), there is a size-preferred component in grain travel distances. They suggested that, at near threshold flows, finer particles tend to be trapped in the bed, reducing differences in travel distances among grain sizes; whereas distances of coarser material depend mainly on size and inertia. At high flows, when general bed mobilisation occurs, particles are freer to move and smaller grains outrun larger ones. Allan and Frostick (1999) also discussed the overpassing of coarser material farther downstream than finer classes. Thus, all grains mobilised by certain flow may not reach the trap during the time that flow acts over the bed. As a consequence, the next sample may contain particles that were entrained and transported by the smaller flow but could not reach the trap during the previous flow step. The process described by Hassan *et al*. (1991) and Church and Hassan (1992) would produce size segregated samples, with the consequent distortion of bedload composition. Although these effects are less likely to occur in short flumes like the one used in this research, the use of equally spaced sediment traps along flumes, especially long ones, would provide distributed samples and will aid to quantify the effect of particle travelling times on entrainment definition. The extra effort by this division of the flume would be offset by the additional data directly related to the variation of bed composition and particle travelling distances. To the author's knowledge, no such experiments have been conducted to date.

As a consequence of the uncertain trends recorded for threshold flows (sections 4.2.1 and 4.3.1), predicting bed entrainment thresholds after certain

acceleration rates have been applied over granular beds, similarly to Paphitis and Collins (2005), is currently unachievable. However, both the values and durations of flow history do have a considerable effect on bed mobility, both, in terms of entrainment flows and the amount of solid transport produced (sections 4.2.5 and 4.3.3). This last aspect is of particular relevance, as it appears to generally apply regardless the bed composition.

4.4.2.2 Critical shear stress and bed surface composition

Bed surface composition data was obtained by counting coloured grains over a fixed bed surface area, which is equivalent to bulk sampling (Kellerhaus and Bray, 1971). The method was first developed by Wilcock and McArdell (1993). Here, a sensitivity analysis to the minimum number of grain counts was undertaken (section 3.4.3), showing that 100 counts per image provided consistent results. The method was further contrasted against two different procedures: a) digitations of b-axis and b) surface sampling using soft plasticine. Results from these comparative studies also showed the suitability of the method proposed. An extensive data set was then produced, with surface grain size distributions available for a range of water discharges. Thus, the evolution of the bed surface composition could be analysed.

Although by definition, antecedent conditions were made up of sub-threshold flows, the antecedent periods were hypothesised to affect surface composition, especially towards the fine end of the distribution. It would appear that the test flow histories applied were not sufficient to produce noticeable changes of bed composition, similarly to Marion *et al*. (1997), Pender *et al*. (2001), Haynes and Pender (2007) and Haynes and Ockelford (2008). The observed small changes in size composition of the unimodal bed during antecedent conditions could be explained as follows: Q_{ref} was defined based on the modal size class, containing D_{50} (Wilcock *et al.*, 1996), and therefore, other particles sizes may be mobilised during the flow history period at lower discharges (Paphitis, 2001; McEwan *et al*. 2004). This is demonstrated by the ratios of τ_{cri}/τ_{cr50} (Fig. 4-21), showing how 8-11.3 mm class moves at lower discharges than D_{50}, and that finer classes are proportionally more resistant to mobilisation, suggesting hiding effects (Parker and Klingeman, 1982; Andrews and Parker, 1987; Wu *et al.*, 2000). The observed

reduction of fine content in both, bed surface and bedload samples (sections 4.2.3 and 4.2.4), leads to conclude that fines penetrate below the surface (Allan and Frostick, 1999; Frey and Church, 2009).

Some of the results suggest that there might be a link between critical flows and fine content of the bed (section 4.2.3.3), possibly related to an optimum content of fines on the bed surface (Fig. 4-17). Authors like Haynes and Pender (2007) already suggested this link. However, data did not show a consistent pattern between fine contents and entrainment thresholds. It is possible that the content of fines of the mixture used was too small (D < 2 mm 4%, D < 4 mm 17% of bulk mix, Table 4-13) to provide sufficient data on the link between bed resistance and bed size composition during sub-threshold antecedent flows. Wilcock and Crowe (2003) showed that the sand content affects the entrainment threshold of the bed median size, which reduces as the sand content increases. The sand (D < 2 mm) content of Saadi's (2002) bimodal mixture was 25% and that of D < 4 mm was 35%, the same percentages for the unimodal bed used by Haynes and Ockelford (2008) were 7.5% and 30% respectively. In contrast, the coarse mixture used by Shvidchenko *et al*. (2001) was of similar composition to the unimodal sediment used in this thesis (D_{16} = 3.8 mm, D_{50} = 6.4 mm, D_{84} = 9.1 mm and σ_g = 1.5). It is possible that the unimodal mixture used in this thesis may not have sufficient fines to support a strong link of bed composition and stability.

Reference	D < 2 mm	D < 4 mm
Shvidchenko *et al*. (2001)	3%	12%
Saadi (2002)	25%	35%
Haynes and Pender (2007)	20%	47%
Haynes and Ockelford (2008)	7.5%	30%
This thesis	4%	17%

Table 4-13. Summary of fine content of sediments used by other researchers.

The analysis of fine content based on the values of p_i/f_i was also affected by the very small percentage of small size classes on the bed, where values of p_i or f_i were often zero or near zero, limiting the extent of the analysis for these fine classes. A larger proportion of fines (D < 4 mm) may have produced clearer

correspondence between fine content and bed stability (Kuhnle, 1993; Wilcock and McArdell, 1997).

It is interesting to note that other studies on the effect of antecedent conditions on bed mobility using graded mixtures also showed a reduction of bed resistance due to antecedent conditions when the duration of exposure to flow increased beyond that which produced the highest entrainment thresholds (Saadi, 2002; Monteith and Pender, 2005; Haynes and Pender, 2007) (section 4.2.1); a consistency that it is remarkable since these studies include constant and time-varying flows, and entrainment values were estimated using the reference transport and the visual methods, although not simultaneously. This behaviour may be related to a continuous loss of fines from the bed surface and the effect of finer particles on the resistance of individual coarser grain (Andrews and Parker, 1987; Kuhnle, 1993; Church *et al.*, 1998; Saadi, 2002; van Rijn, 2007b).

4.4.2.3 Resistance to entrainment and bed structure

Since bed surface composition, the presence/absence of fines or the general slight coarsening of the bed surface of the unimodal bed do not show clear correspondences with thresholds, other forms of bed reorganisation may be responsible for the changes in entrainment flows observed. Pender *et al*. (2001) reported fine percolation as one of the mechanisms occurring during their experiments. McEwan *et al*. (2004) suggested that particle rearrangements increased bed stability, and that bed restructuring dominated over changes of bed surface composition; hence, supporting the suggested link between antecedent conditions, entrainment and grain orientation. Paphitis and Collins (2005) and Haynes and Pender (2007) pointed at small-scale grain reorientation and increased imbrication as responsible for higher bed stability. Cooper *et al*. (2008) showed that the same bed composition resulted in different bed hydraulic characteristics (higher roughness) and flow conditions (lower velocity values) after a rotation of 90º of the bed without any changes of bed surface composition or elevation. Thus, bed structure and grain orientation affect entrainment under constant grain size distribution.

The results of bed surface structure based on coarse grains (section 4.2.8) presented here suggest a link between the areal distribution of coarse particles and entrainment thresholds, with a secondary role of the abundance of these grains on the bed surface. These results are interpreted as follows: granular beds with more scattered coarse particle distribution are more resistant to mobilisation than those with the same proportion of coarse particles but with groups of grains already formed. These results appear to contradict Hassan and Reid (1990), Hassan and Church (2000) and Frey and Church (2009), who reported increased bed stability with the presence of clusters. It is suggested here that the abundance, size and concentration of these clusters may influence bed stability. This point may be illustrated by an idealised example. If all grains corresponding to D_{90} were collected over a small area of the bed surface, this coarse patch will be very stable; however, the rest of the bed surface will be unprotected and thus easily mobilised. If instead, the same number of D_{90} particles were distributed evenly over the bed surface, they may be more moveable as individual grains but the bed will be better protected against entrainment due to the sheltering and hiding effects that these coarse grains have over finer particles (Parker and Klingeman, 1982; Reid and Frostick, 1986; Andrews and Parker, 1987; Church *et al.*, 1998; Wu *et al.*, 2000). If we considered the smaller, more spatially distributed 8–11.3 mm grains in this study as scaled down field cluster units, the more numerous they are, the more resistant the bed is. Thus, the findings of this study and those by Hassan and Reid (1990), Hassan and Church (2000) and Frey and Church (2009) are in agreement. It is also noted that, in the case of the flume data presented in this thesis, clusters were considered formed by a single size class (8 – 11.3 mm), whereas in the above references they are composed of a variety of sizes. This differentiation is determined by the single class painted in UV paint studied.

In the case of uniform and near-uniform gravels, local rearrangement may be responsible for the observed bed strengthening, as the possible effects of fine content do not apply to well sorted beds. This process may also be linked to the monotonic increase of bed resistance with flow exposure duration (smaller acceleration rates) shown by the VM results followed by an approximately stable value (Fig. 4-43). The increased imbrication of individual particles occurring in

well sorted gravels suggested here (Paphitis and Collins, 2005; Ockelford and Haynes, 2008) is unlikely to be reversed by a large extent due to the continuous action of fluid forces. This may explain the differences in τ_{cr} based o the visual method observed between the graded and well sorted beds tested.

Based on the results of this thesis and the findings of previous researchers, there appears to be two common actions of sub-threshold antecedent conditions on granular beds: (1) small scale vibration of grains and (2) in-situ particle reorientation (Allan and Frostick, 1999; Paphitis and Collins, 2005; Haynes and Pender, 2007, Ockelford *et al.*, 2010). However, the impacts of these effects depend on bed size composition. If beds have a variety of sizes, fines will penetrate into the bed aided by the vibrations and reorientation of larger particles, which create the spaces and paths for the fines to travel down into sub-surface layers (Frey and Church, 2009). If this process continues, bed stability increases, with the bed reducing its fine content to a possible optimum proportion. If sub-threshold flows continue either longer duration or in higher magnitude, increasing amounts of fines disappear from the bed surface. Coarser grains will then loose the support that fines provide by direct contact and filling the interstices and coarser grains will be more easily entrained (Kuhnle, 1993; Haynes and Pender, 2007), resulting in a reduction of the general bed stability found in the experiments using graded bed material (Fig. 4-6). If beds are well or very well sorted, the presence of finer sizes is minimal, and only the process of local particle rearrangement takes place during the antecedence phase, which will likely increase imbrication and compactation (Saadi, 2002; Paphitis and Collins, 2005; Ockelford *et al.*, 2010). If flow action continues, this strengthening process continues until a limit is reached by which all the potential imbrication and interlocking is achieved, resulting in no additional bed stability for longer antecedent conditions (Haynes and Ockelford, 2008), consistent with the levelling off of τ_{cr} observed for this type of bed (based on VM).

4.4.2.4 Bed roughness

Changes in entrainment thresholds and bed surface hydraulic roughness were analysed in relation to bed surface composition and flow antecedency. After

demonstrating that bed surface composition did not change noticeably (section 4.2.3), similarly to Pender *et al*. (2001) and Haynes and Ockelford (2008), it is argued that changes of bed structure, eg. particle reorientation, may be responsible for the observed changes of threshold flows and roughness. Cooper *et al*. (2008) showed that roughness parameter k_s, obtained from applying the Clauser method to spatially-averaged velocity profiles recorded with PIV, increased between 50-60% when beds were rotated 90º, i.e. bed particles were reoriented without any change of bed surface composition or bed elevation. It is possible then, as suggested by Paphitis and Collins (2005), Haynes and Pender (2007) and Haynes and Ockelford (2008), that the action of sub-threshold antecedent conditions, represented in this research work by flow acceleration rates of hydrograph rising limbs, affect particle position characteristics in such a way that alter entrainment conditions. These possible particle reorientations may also affect grain imbrication and friction angle, which in turn are related to bed stability (Ashworth and Ferguson, 1989; Church *et al*., 1998; Paphitis and Collins, 2005). The link between bed resistance to entrainment and structural changes of the bed is more likely to be of primary importance for uniform beds, where changes of grain size composition are not possible (Ockelford *et al*., 2010). However, since detailed bed surface structure data is not available for this study, the above explanation remains to be confirmed for the experiments presented.

The bed hydraulic roughness z_0 data obtained from the velocity profiles indicates that there are differences in behaviour between bed grades. In the case of the unimodal bed, values of the ratio of z_0 after and before antecedent conditions are applied are approximately 0.8, 1.2 and 0.25 for the durations of 0.5h, 2h, and 6h respectively; whereas in the case of the uniform gravel the same ratios are approximately 3.4, 1.5 and 0.9. These results suggest that beds are hydraulically smoother for the longest periods of sub-threshold flows (resulting from particle reorientation), while the effect of short durations of antecedent conditions is less consistent and depends on bed sorting. A common result is that both bed compositions produce rougher beds (20-50%) when increasing sub-threshold flows act for 2h.

The assessment of the evolution of bed roughness with antecedent conditions was based on a small data set and extraction of general conclusions might be premature. Of particular relevance is the difficulty of capturing small changes of velocity data near the bed, as the quality of the data, defined by the velocimeter correlations, were lower than the widely used threshold of 70% (section 3.3.1); excluding these data points form the calculations. This limitation of the data available often reduced the data range to a minimum of approximately $0.3z/h$, above the commonly used limit of applicability of the logarithmic profile, $0.2z/h$ (Nezu and Nakagawa, 1993, Graf, 1998; Dey and Raikar, 2007). This minimum elevation conditioned by the ADV correlations eliminated velocity data that is most likely to reflect changes of bed roughness as they are closest to the bed. Therefore, the analysis of the impact of antecedent conditions on bed roughness presented here is inconclusive and the question whether acceleration rates make the bed rougher or smoother and therefore impact on bed entrainment remains unanswered. However, the analysis of bed topography undertaken by Pender *et al*. (2001) shows that the frequency distribution of bed elevations expands its tails and reduces its peak with the duration of flow exposure. This indicates that bed surface becomes more irregular, with larger troughs and crests, resulting in higher Manning's roughness parameters found by these authors (Ockelford *et al*., 2010).

4.4.2.5 Bedload composition and grain mobility

The disappearance of fines from the bed surface is suggested as one of the elements affecting bed stability and entrainment values. Those fine particles can either be entrained and transported as bedload, being collected in the trap, or, as discussed, penetrate further into the bed aided by the small in-situ movement of larger particles that create paths for fines to reach the bed sub-surface layers (Allan and Frostick, 1999; Frey and Church, 2009). Fig. 4-51 shows the ratio of bedload fine content (D < 4 mm) for each flow step over the average proportion of fines across the corresponding run. Generally, the experimental data display a decreasing trend for low-medium flows (up to 35-40 l/s), changing to an upwards trend for the largest flows. This could be interpreted as a general reduction of fine content of bedload samples during antecedent conditions, increasing again for flows applied during the stability test.

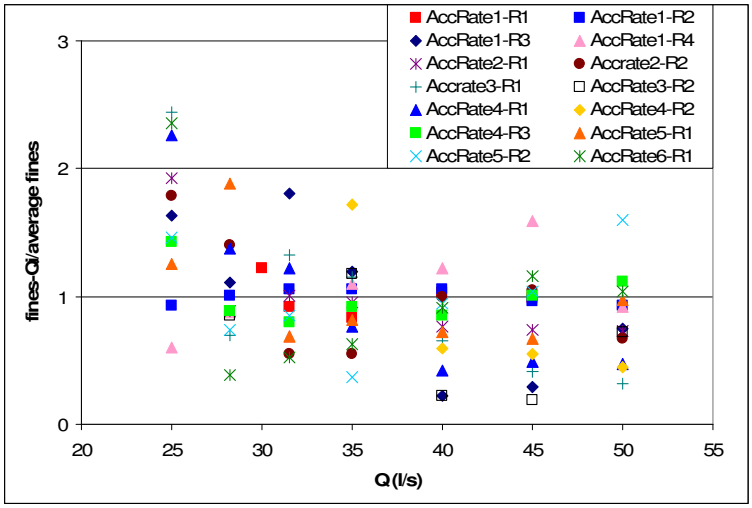

Fig. 4-51. Ratio of fine content of bedload for each flow step over the average fine content throughout the entire run. Stage 1 only.

The continuous reduction of the ratio of fines of the bedload samples with increasing discharges indicated in Fig. 4-51 suggests a progressive exhaustion of fines available for transport during antecedent conditions, either by entrainment and transport of the most unstable grains or by particle percolation below the bed surface, or a combination of these two (Parker *et al.*, 1982b; Allan and Frostick, 1999; Pender *et al.*, 2001; Frey and Church, 2009). As flows continue to increase during the stability phase, when the entrainment threshold is overcome, larger particles are mobilised, uncovering the fines below (Parker *et al.*, 1982b; Ashworth and Ferguson, 1989; Bathurst, 2007), thus, increasing back the proportion of fines on the bedload samples (Fig. 4-51).

It is noted that the values of this ratio of fine content are around 2 for 25 l/s, indicating a proportionally large percentage of fines for this flow and possibly for previous lower flows during the test hydrographs. Authors such as Wiclcok and McArdell (1997), Church *et al.* (1998), Hassan and Church (2000), Haynes and Pender (2007) and Bathurst (2007) showed that bedload composition tends to be proportionally finer than the bed surface size distribution during sub-threshold flows, where size selectivity dominates bedload, with solid transport approaching equal mobility as flows increase and coarser size classes are entrained (Ashworth and Ferguson, 1989).

The analysis of the values of p_i/f_i indicated that for flows larger than approximately 30 l/s (value very close to the bed reference entrainment flow Q_{ref} = 31.5 l/s) the mobility of the size classes is clearly identifiable, with 5.6-8 mm and 8-11.3 mm classes having proportionally larger presence on the bedload samples than their percentages of the bed composition (p_i/f_i > 1). The remaining size classes are under-present in the bedload samples, suggesting that hiding effects act to reduce the mobility of the classes finer than 5.6 mm and the submerged weight of the largest size 11.3-16 mm makes this class largely immobile, particularly during flows < 30 l/s (Fig. 4-18). Data of D_x/averageD_x contained in Fig. 4-20 shows that bedload composition becomes coarser as flows increase during the antecedent conditions, reaching approximately constant values (1-1.1) for the stability test period. These results indicate that finer classes were initially mobilised during the sub-threshold antecedent periods and once the bed became mobile all size classes were mobilised in similar proportions throughout the stability test.

4.4.2.6 Bedload predictions

The reduction of total bedload transport during the stability test with entrainment threshold is a key finding of this research, as it highlights that the change of bed entrainment threshold does not only affect the beginning of particle movement but also the subsequent mobility of the bed under larger flows. This has considerable consequences for river managers as it clearly demonstrates a reduction of the solid transport of beds that have been stabilised through flow history (Reid *et al.*, 1985 and Reid and Frostick, 1986). One might assume that total bedload transport would be the same once critical conditions are reached. However, data presented here demonstrate that solid transport can be over one order of magnitude lower for the same flows if the bed has been strengthened by flow history (Fig. 4-27). Thus, there is an argument for bedload transport equations to consider this effect of antecedent conditions in their expressions (Paphitis and Collins, 2005; Monteith and Pender, 2005).

The proposed new set of equations for the estimation of transport rates and entrainment thresholds (section 4.2.6) could be used to estimate the values of τ_{cr} to input in the proposed bedload equation (Chapter 5), as only total bedload

data is required. It is noted however, that the curves of bedload rates predicted here approach a common value for $\tau_{cr} \approx 5$ Pa (Fig. 4-29); so for large flows the effect of flow history on bed mobility appears to decrease. Equation 4-3 can be used to estimate entrainment thresholds without using any of the more complex stability criteria available, particularly the reference transport methods, which require difficult to obtain values of bed surface composition and fractional transport rates, especially in the field. The power law method for estimating τ_{cr} proposed here (section 4.2.6) relies only on the quantification of total solid transport rates (kg/m/s) for each discharge, which in field is much easier to assess using calibrated weighing cells (Reid and Frostick, 1986). Plotting values of total bedload transport rate q_b against τ will allow the estimation of τ_{cr} that provides the best fit of the data (Fig. 4-29). The results obtained have been demonstrated to be equivalent to those by the extensively used Parker *et al.*'s (1982a) reference transport method. However, the proposed method must be tested under a much wider variety of conditions, scales and bed compositions than those available through this PhD alone to be accepted as universally applicable.

A summary of the main findings so far is below:

- The effect of sub-threshold antecedent conditions on the stability of granular beds has been demonstrated, with entrainment threshold being affected by the duration and intensity of the test flow hydrographs.

- There appears to be a dependency of the results of τ_{cr} on the methodology used.

- Data indicates that there are differences in the response of granular beds to antecedent conditions depending on their size composition and sorting, with increased imbrication for the well sorted beds and winnowing of fines and grouping of some larger, proportionally more mobile grains for the graded bed tested.

- A relationship between fine content of the bed surface with stability of grains has been suggested, although the characteristics of the bed (insufficient fines) and inconclusive data prevent this link to be confirmed.

- The sub-threshold antecedent conditions tested reduce bedload quantities due to their strengthening effect on granular beds. This influence of antecedent conditions continues to act for flows during the larger discharges of the stability test; the result of this influence is lower bedload transport rates q_b for the same discharges as the entrainment threshold of the bed increases due to the acceleration rates tested.

- A new method for the estimation of entrainment threshold τ_{cr} based on total bedload transport rates has been developed. Its results are comparable to Parker *et al.*'s (1982a) reference transport method with the key advantage that no bedload composition data is required.

All the above collection of results and the subsequent analyses contained in this chapter are aimed at studying the link between sub-threshold antecedent conditions, as rising limbs, and bed entrainment, with the goal of improving bedload transport estimates. The following chapter compares the solid transport predictions from a number of bedload transport equations and analyses the impact that different entrainment thresholds have on equation performance. Since it has been demonstrated that sub-threshold flow characteristics affect values of τ_{cr}, Chapter 5 will study the influence of the values of τ_{cr} on bedload predictions.

Chapter 5
Comparison of bedload transport equations

"One finger cannot lift a pebble" -
American Indian Proverb.

Comparison of bedload transport equations

5.1 *Introduction*

Results presented in Chapter 4 showed the bedload transport rates for the same flows vary depending on the degree of bed stability, defined by the new critical bed shear stress, achieved by antecedent conditions. A new method for assessing critical conditions based on total bedload transport data was also presented and discussed. This method had the major advantage of easy applicability with minimal data and calculation requirements.

In this chapter, the performance of a number of well known bedload transport equations will be tested against a proposed new formulation obtained based on the laboratory data presented in this thesis. Since bedload rates have been shown to vary depending on the magnitude and duration of antecedent conditions (section 4.2.5), this chapter is dedicated to test how close some equations available in literature represent the laboratory data set. Since entrainment threshold in these equations is estimated solely based on bed grain size distribution data and bed slope without accounting for antecedent conditions, their ability to reproduce the flume data is a benchmark for the proposed equation, this new formulation allows the input of τ_{cr} that is not based

on grain size distributions but on estimations of τ_{cr}, like those obtained using equation 4-3. As an example, Fig. 5-1 shows 3 data series covering the range of entrainment threshold obtained for the sand-gravel mixture under different test hydrographs. Data clearly show that for the same bed shear stress τ total bedload transport rates q_b reduce as the entrainment threshold τ_{cr} increases, with values of q_b approximately 1 order of magnitude smaller when τ_{cr} increases from 3.13 Pa to 3.71 Pa (Fig. 5-1). Data collapse into a single curve when plotted against the ratio τ/τ_{cr}. It is noted that transport conditions for the experiments carried out and presented here correspond to marginal and partial transport, with relatively low transport rates and where size selectivity may apply (Wilcock, 1997; Powell *et al.*, 2001).

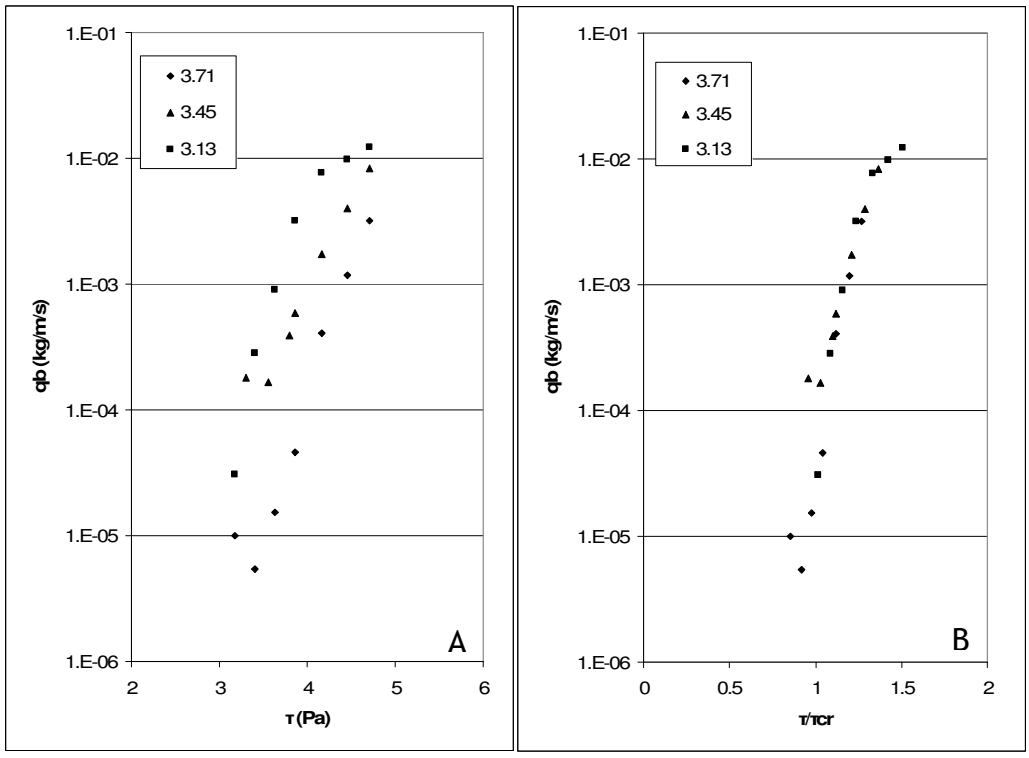

Fig. 5-1. Differences of bedload transport with critical bed shear stress τcr (Pa). A) Plotted against τ and, B) Plotted against τ/τcr. Note the collapse of the data and equation results in B). X-axis in linear scale in both cases.

The aim of this section is not so much postulating a new bedload transport as to explore the effect of changing critical shear stress on equation results. The equation proposed in this study shares some characteristics with existing formulations (eg. Parker, 1990, Wilcock and Crowe, 2003, Recking, 2010) in terms of structure; i.e. the division of the equations in two "sections", one for low/moderate q_b and another for large transport rates (section 5.3). This

common equation structure suggests a general expression of the bedload transport equation may be adopted. However, the equation proposed is a simplified form in the sense that τ_{cr} is defined by the user and not by bed characteristics like, for example, the equations proposed by Wilcock and Crowe (2003) and Recking (2010) (section 5.3).

5.2 *Available equations*

A wide variety of bedload transport equations has been developed, based on laboratory and field observations. Common to all formulae is a functional relationship between bedload rate, hydraulic forces and a representative bed particle size (Ackers and White, 1973; Carson and Griffiths, 1985, 1987; van Rijn, 2007a; Yadav and Samtani, 2008). Different approaches have been used to develop transport equations: (1) empirical relationships between bedload and flow intensity (Q, τ or θ) (Meyer-Peter & Müller, 1948; Wilcock and Crowe, 2003), (2) based on dimensional considerations (eg. Shields, 1936), and (3) semi-theoretical schemes based on particle mechanics (Einstein, 1950; Garde and Ranga Raju, 1977; Wiberg and Smith, 1989). Here only the first group will be considered, since it is the most widespread type of equation available.

The approaches based on mean flow intensity use a wide variety of measures of that intensity, including: total or unit discharge Q or q (Hassan and Woodsmith, 2004; Barry *et al.*, 2008); stream power ω (Bagnold, 1980; Ashmore, 1988); bed shear stress τ (Parker, 1990; Wilcock and Crowe, 2003); and, Shields parameter θ (Meyer-Peter & Müller, 1948; Zhang and McConnachie, 1994; Recking, 2010). Many of these equations include a threshold term to represent the minimum amount of hydraulic force acting on the grains required to initiate motion. It is generally considered that below this threshold sediment transport does not occur in measurable quantities (Wilcock and Crowe, 2003) or at all (Meyer-Peter & Müller, 1948). The excess force can be expressed as difference [eg. ω- ω_0 (Bagnold, 1977, 1980)], as a ratio [eg. τ/τ_{cr} (Wilcock and Crowe, 2003), $\theta/\ \theta_{cr}$ (Parker, 1990; Recking, 2010)], or a combination of both [eg $(\tau-\tau_{cr})/\tau_{cr}$ (Yalin, 1963)]. Equations that consider excess flows (or stress) as a difference, eg. Bagnold (1980), are not applicable below the threshold; however, as discussed

by Reid and Frostick (1986), McEwan *et al.* (2004) and Vericat *et al.* (2008), sediment transport occurs well below the bed entrainment threshold, albeit in small quantities (marginal transport); while equations that express excess forces as a ratio, eg. Parker (1990), are capable of producing bedload at shear stresses below threshold.

The threshold of motion is a key parameter in many bedload equations. As Buffington and Montgomery (1997) discuss, small errors in τ_{cr} due to uncertainty caused by the method applied can cause significant errors in bedload transport rate estimates. However, a single value of flow intensity at particle entrainment is not just a disputed concept (Lavelle and Mofjeld, 1987), it is also difficult to define (Buffington and Montgomery, 1997) and measure (Carsons and Griffiths, 1985; Reid and Frostick, 1986; Bathurst, 2007; Recking, 2010), and its value depends on a range of particle parameters such as shape, size distribution, armouring, imbrication, etc. (Parker *et al.*, 1982a; Carsons and Griffiths, 1985; Carling *et al.*, 1992; Buffington and Montgomery, 1997; Church *et al.*, 1998) (Chapter 2); and on the methodology and criterion followed (Buffington and Montgomery, 1997) (Chapter 4). Furthermore, entrainment thresholds are not a fixed characteristic of a certain bed size distribution and flow condition, but they change depending on flow history (Reid and Frostick, 1986; Paphitis and Collins, 2005; Haynes and Pender, 2007; Haynes and Ockelford, 2008). Thus, bedload predictions based on a single estimate of τ_{cr} calculated for a particular bed size, eg. D_{50}, may not be appropriate.

Despite considerable effort over nearly a century, bedload transport equations have often been reported to have limited success when tested against materials and conditions different to those for which these equations were developed. Large under- and over-predictions are both found (Reid and Frostick, 1986; Wiberg and Smith, 1989; Batalla, 1997; Gomez and Church, 1989; Wilcock and Crowe, 2003; Frey and Church, 2009). Added to this, is the difficulty of extending results obtained using uniform beds to multi-sized sediment, even when they share particle median sizes (Wu *et al.*, 2000; van Rijn, 2007b; Recking, 2010) as particle interaction, imbrication, hiding effects and size-selective transport affect grain mobility. Thus, there is still no bedload transport

formulation universally applicable to a range of bed compositions and flow conditions (Bathurst, 2007).

One of the aims of this research is to suggest ways of improving predictions of entrainment and sediment transport quantities. Data in Chapter 4 show a link between flow history and entrainment threshold; however, these data did not show a sufficiently well defined trend to allow consistent predictability of τ_{cr} with antecedent conditions. Thus, an alternative approach to correcting existing formulae was adopted here. Instead, a new simplified formula was explored. It was based on the equation fitted to W_i^* data, which collapsed to a single line when plotted against τ/τ_{cr} (Chapter 4). During the analysis of bedload samples, an equation was developed that appeared to accurately represent total sediment transport with the ratio τ/τ_{cr} (section 4.3.5). In this chapter, the predictions of such equation are tested against other formulations and additional data collected from past publications (Bagnold, 1980; Reid and Frostick, 1986). The procedure suggested is easy to apply. Crucially, it is not intrinsically associated to any particular representative bed particle size, but to a general entrainment threshold of the bed. This feature eliminates the need for complex and time consuming bed composition data collection and analysis. However, the equation only provides values of total bedload transport rates, and cannot be used to generate fractional rates. Nonetheless, bulk rates are often sufficient for a range of environmental and engineering applications.

5.3 *Equations used*

Six equations were selected for this comparative study, ranging from those obtained based on uniform and non-uniform beds and those providing predictions of total and fractional transport rates. These were, in chronological order:

- Meyer-Peter & Müller (1948)
- Shvidchenko *et al*. (2001)
- Wilcock and Crowe (2003)
- Recking (2010) for uniform gravel
- Recking (2010) for non-uniform beds
- The equation proposed in this study

Each equation was selected based on a range of reasons (Table 5-1).

Equation	Equation in this thesis	Excess forces	2-part equation	Hiding term	Slope term (1)	Antecedent conditions correction
Meyer-Peter & Müller (1948)	*Eq. 5-1*	θ-θ_{cr}	No	No	No	No
Shvidchenko *et al*. (2001)	*Eq. 5-3*	θ/θ_{cr50}	No	Yes	Yes	No
Wilcock and Crowe (2003)	*Eq. 5-7*	τ/τ_{cri}	Yes	Yes	No	No
Recking (2010) eq. 5	*Eq. 5-13*	θ/θ_{cr}	Yes	No	Yes	No
Recking (2010) eq. 12	*Eq. 5-15*	θ/θ_{cr84}	Yes	Yes	Yes	No
This study	*Eq. 5-18*	τ/τ_{cr} (2)	Yes	No	No	Yes (3)

(1) Inclusion of a slope correction term in any component of the formulation
(2) Although no specific particle size diameter is proposed, data was obtained after applying reference transport method to the bed modal size class, which included D_{50}; therefore, strictly, values of τ_{cr} *correspond* to D_{50}.
(3) Correction for antecedent conditions is not explicitly expressed on the equation; however, the complete methodology includes assessment of τ_{cr} after antecedent conditions were applied as discussed in Chapter 4. Values of τ_{cr} are modified by the user in order to fit the resulting curve; hence, including a correction for antecedent conditions.

Table 5-1. Comparison of main features of bedload transport equations tested.

Meyer-Peter & Müller (1948) was selected due to its historical relevance and because it expresses excess hydraulic forces as difference (θ-θ_{cr}). Shvidchenko *et al*. (2001) developed their bedload transport formulation based on laboratory data with a range of bed compositions among which was a coarse skewed, whose size characteristics were very similar to the unimodal sand-gravel mixture used in this thesis (D_{16} = 3.8 mm, D_{50} = 6.4 mm and σ_g = 1.5). This equation also included an explicit term for bed slope. Using a simpler formulation than Parker (1990) Wilcock and Crowe (2003) provides fractional transport rates with τ/τ_{cr} as independent variable. Despite being partly based on Parker (1990), Wilcock and Crowe (2003) provided fractional transport rates without the need to eliminate sand classes from bed composition, as Parker (1990) requires. Recking's (2010) equations were tested since they were based on a large flume and field data set, which strengthened their potential wider applicability; Recking proposed two different equations for uniform or non-uniform beds. Equation 5 in Recking (2010) applies to uniform gravel sediments only; it does not include a slope term explicitly on the formulation but the value of θ_{cr} depends on bed slope. Equation 12 in Recking (2010) does include a term of slope in addition to correcting values

of θ_{cr} with slope. Table 5-1 contains a summary of the main characteristics of the tested equations. Other equations such as Ackers and White (1973) and van Rijn (2007b) were available; however, the study presented here was constrained by the extent and objectives of this thesis.

5.3.1 Meyer-Peter & Müller (1948)

This well known equation has a basic form:

$$\Phi = \chi(\theta - \theta_{cr})^{3/2} \qquad \text{Eq. 5-1}$$

where $\Phi = q_{bvol} / \left[g(\rho_s/\rho - 1)D^3\right]^{0.5}$ is the volumetric Einstein dimensionless bedload parameter (Einstein, 1950), θ, θ_{cr} = Shields dimensionless shear stress of the flow and entrainment threshold respectively. A standard value of the coefficient χ = 8 is often used; however, it has been noted that this value increases with shear stress, varying from 5-15 (Wiberg and Smith, 1989). Wong and Parker (2006) revised the original Meyer-Peter & Müller (MPM) equation using uniform gravels with arithmetic mean diameters D_m = 3.2-28.7 mm, suggesting χ = 4.93 and an exponent 1.6 instead of 3/2, with χ = 3.97 if an exponent equal to 3/2 was retained.

The formulation of the traditional MPM equation given in Recking (2010) was used here. It explicitly includes a correction of the bed shear stress applied over the grains, provided by the ratio n'/n; with $n' = D_{90}^{1/6}/26$ particle roughness and n = total roughness calculated from Manning's equation.

$$q_b\left[kg/m/s\right] = 8\rho_s\sqrt{g(\rho_s/\rho - 1){D_{50}}^3}\left(\left(\frac{n'}{n}\right)^{3/2}\theta - 0.047\right)^{3/2} \qquad \text{Eq. 5-2}$$

5.3.2 Shvidchenko et al. (2001)

Shvidchenko *et al.* (2001) analysed the effect of slope on a range of bed granular compositions. They developed an alternative reference transport method and entrainment criterion based on the concept of probability and intensity of grain mobilisation. Based on visual fitting of their data they obtained the following expression for the Einstein bedload parameter for fraction *i*:

$$q_{bi}* = \left(\frac{a\theta_i}{\varepsilon_i} \right)^{18} S^{-5.0} \qquad \text{Eq. 5-3}$$

where $a = -1.1[\log(D_{50})]^3 + 4.8[\log(D_{50})]^2 - 5.0[\log(D_{50})] + 4.6$, θ_i = dimensionless bed shear stress, ε_i = hiding function (equation 5-4), S = bed slope; and particle diameters D_i, D_{50} in mm.

$$\varepsilon_i = \frac{\theta_{cri}}{\theta_{cr50}} = \begin{cases} \left(\frac{D_i}{D_{50}} \right)^{-e} ; if \frac{D_i}{D_{50}} \le 1 \\ \left[\log\left(10 \frac{D_i}{D_{50}} \right) \right]^{-2.2} ; if \frac{D_i}{D_{50}} \ge 1 \end{cases} \qquad \text{Eq. 5-4}$$

$$e = 2.0\sigma_g^{-0.10} \left\{ \begin{matrix} 0.049[\log(D_{50})]^3 - 0.26[\log(D_{50})]^2 + \\ 0.33[\log(D_{50})] + 1.20 \end{matrix} \right\} - 1.4 \qquad \text{Eq. 5-5}$$

With σ_g = mixture geometric standard deviation.

Bedload transport rate in mass units is then:

$$q_{bi}(kg/m/s) = q_{bi}^{*} f_i \rho_s \sqrt{(\rho_s/\rho - 1) g D_i^{\,3}} \qquad \text{Eq. 5-6}$$

5.3.3 Wilcock and Crowe (2003)

Wilcock and Crowe (2003) analysed fractional transport rates and entrainment thresholds, based on the application of Parker *et al.*'s (1982a) reference transport method, to obtain a bedload transport equation capable of producing fractional transport rates. This equation included a hiding function and a correction for bed sand content. They used 5 different sand-gravel beds with sand content between 6% and 34%. Their equation was partly based on Parker (1990) but differed from it in that it only had two sections, depending on the value of τ/τ_{cr}, as opposed to three in Parker (1990), and it did not require separation of the sand classes. They proposed the following set of equations for estimating dimensionless fractional transport rates W_i^* based on volumetric transport rate q_{bivol}.

$$W_i^* = 0.002 \cdot \phi^{7.5} \qquad \text{for } \phi < 1.35$$

$$W_i^* = 14\left(1 - \frac{0.894}{\phi^{0.5}}\right)^{4.5} \cdot \qquad \text{for } \phi \geq 1.35 \qquad \textit{Eq. 5-7}$$

where $\phi = \tau/\tau_{cri}$; $W_i^* = \dfrac{(\rho_s/\rho - 1)g \cdot q_{bi\ vol}}{f_i \cdot u_*^{0.5}}$

$$\frac{\tau_{cri}}{\tau_{cr50}} = \left(\frac{D_i}{D_{50}}\right)^b \qquad \textit{Eq. 5-8}$$

$$b = \frac{0.67}{1 + \exp\left(1.5 - \frac{D_i}{D_{50}}\right)} \qquad \textit{Eq. 5-9}$$

$$\theta_{cr50} = 0.021 + 0.015\exp(-20Fs) \qquad \textit{Eq. 5-10}$$

Fs = proportion of sand on bed surface

$$\tau_{cr50} = \theta_{cr50}(\rho_s - \rho)gD_{50} \qquad \textit{Eq. 5-11}$$

It is noted that Wilcock and Crowe (2003) defined *Fs* as "*percent sand on the bed surface*". However, their Fig. 5 shows that *Fs* is actually the proportion of sand, not percent.

The procedure for calculating solid transport begins with the estimation of θ_{cr50} and τ_{cr50} using equations 5-10 and 5-11 respectively. The values of exponent *b* is calculated using equation 5-9, which is then used to estimate τ_{cri} for each size class using the mean class diameter D_i. Values of W_i^* are then calculated (equation 5-7) for each ϕ. Finally, total mass transport rates are obtained using:

$$q_b weight(kg/m/s) = \sum_i q_{bi} weight = \rho_s \cdot \sum_i q_{bi} vol \qquad \textit{Eq. 5-12}$$

5.3.4 Recking (2010)

In his comprehensive analysis of field and flume bedload transport data (over 7000 bedload values), Recking (2010) proposed two equations, one for uniform

sediment (eq.5 in Recking, 2010) and the other for graded material (eq.12 in Recking, 2010). These equations are presented here.

5.3.4.1 Uniform gravel

$$\Phi = 0.00005\left(\frac{\theta}{\theta_{cr}}\right)^{12.9} \quad \text{for } \theta/\theta_{cr} < 2.3 \cdot S^{0.08}$$

$$\Phi = 14\theta^{2.45} \quad \text{for } \theta/\theta_{cr} > 2.3 \cdot S^{0.08} \qquad \text{Eq. 5-13}$$

where $\Phi =$ Einstein dimensionless volumetric transport rate (Einstein, 1950) and

$$\theta_{\mathrm{cr}} = 0.15S^{0.275} \quad \textit{(eq.3 in Recking, 2010)} \qquad \text{Eq. 5-14}$$

5.3.4.2 Non-uniform gravel

$$\Phi = 0.0005\left(\frac{D_{84}}{D_{50}}\right)^{-18\sqrt{S}}\left(\frac{\theta_{84}}{\theta_{cr84}}\right)^{6.5} \quad \text{for } \theta_{84}/\theta_{cr84} < L$$

$$\Phi = 14\theta_{84}{}^{2.45} \quad \text{for } \theta_{84}/\theta_{cr84} > L \qquad \text{Eq. 5-15}$$

$$\theta_{cr84} = (1.32S + 0.037)\left(\frac{D_i}{D_{50}}\right)^{-0.93} \qquad \text{Eq. 5-16}$$

Equation 5-15 corresponds to eq.4 in Recking (2010), who recommends calculating *L* iteratively so the two parts of equation 5-15 have the same value at $\theta_{84}/\theta_{cr84} = L$. Therefore, the mass transport rate is:

$$q_b(kg/m/s) = q_{bvol} \cdot \rho_s = \rho_s \cdot \left[g(\rho_s/\rho - 1)D^3\right]^{0.5}\Phi \qquad \text{Eq. 5-17}$$

Note that the second parts of equations 5-13 and 5-15 are the same, with D_{84} defining the bed size in the latter. Note also that the exponent in the first part of equation 5-13 is smaller than the equivalent exponent in equation 5-15. Although there is a correction factor representing hiding effects, $(D_{84}/D_{50})^{-18\sqrt{S}}$, this is constant for each bed grain-size distribution and slope, and therefore, the rate of increase of Φ is much smaller in equation 5-13 than 5-15.

5.3.5 This study

The equation obtained for fitting dimensionless transport rates W_i^* during the estimation of critical flows (section 4.3.5) was used to predict transport rates. This takes the form:

$$q_b(kg/m/s) = A_1\left(\frac{\tau}{\tau_{cr}}\right)^{B_1} \qquad \text{if } \tau/\tau_{cr} \leq 1.3$$

$$q_b(kg/m/s) = A_2\left(\frac{\tau}{\tau_{cr}}\right) + B_2 \quad \textit{if } \tau/\tau_{cr} > 1.3 \qquad \textit{Eq. 5-18}$$

where, A_1 = 8e-5, B_1 = 16.0, A_2 = 0.047 and B_2 = 0.056. The values of the parameters were optimised for the data set presented.

5.4 *Methodology*

The analysis here is based on a comparison of the predictions provided by the equations presented above with the transport rate data set collected during the experimental phase. Equation results were obtained by applying the presented equations with the original parameters recommended by their authors. Thus, a test of the comparability of the present flume data with the data sets used by the cited authors is implicit. Transport rate data were plotted against the ratio τ/τ_{cr}, where τ_{cr} is considered the bed entrainment threshold (this corresponds to D_{50}). The use of τ/τ_{cr} results in the collapse of the transport data, making comparison easier. In the case of equation 5-18 were a single value of τ_{cr} was required in the collapsed plot, the average critical bed shear stresses obtained in Stage 1 and Stage 2 τ_{cr} = 3.38 Pa was used. Similarly to Recking (2010), the performance of the best four performing equations was tested by calculating: (1) relative differences between observed data and equation results, and (2) the number of predictions that differ from the observed data more than ± 1 order of magnitude. Data for the Elbow River contained in Bagnold (1980) (originally collected by A. B. Hollingshead, 1968) and data from the Turkey Brook (Reid and Frostick, 1986; Ian Reid, *pers comm.* 2005) were also used to test equation performance. The comparison of flume and field transport rates and trends

provide a context of the data collected. All bedload transport rates are in kg/m/s.

5.5 *Results*

Results are presented here sequentially in the same order as the equations above. Equation predictions are initially qualitatively assessed, with a comparative quantitative analysis of their performance contained in the section 5.6.

5.5.1 Previous equations

The Meyer-Peter & Müller (MPM) equation performs very poorly, with low transport rates particularly underestimated (τ/τ_{cr} < 1.5) (Fig. 5-2). Conversely, MPM appears to overestimate the highest rates (τ/τ_{cr} > 1.5); however, since the values of τ/τ_{cr} produced by the MPM equation are largely above those of the flume data set, the numerical assessment of this overestimation of hindered.

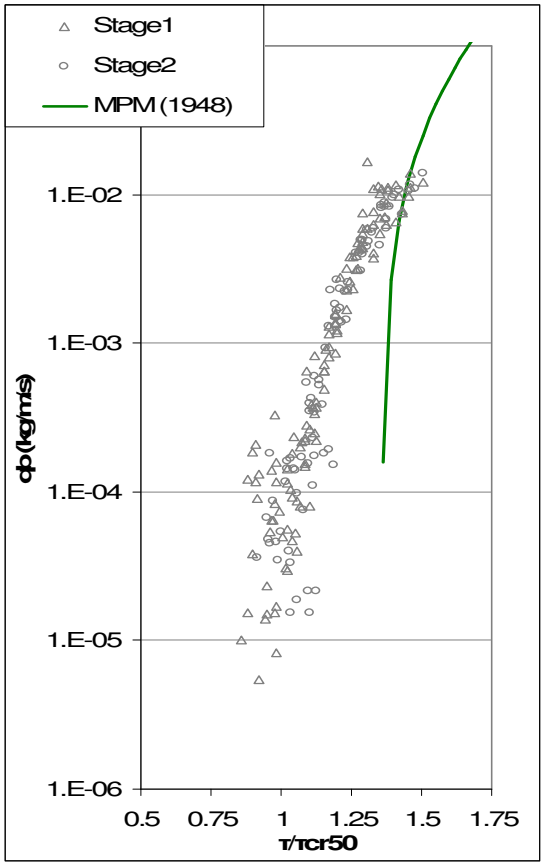

Fig. 5-2. Comparison of data (Stages 1 and 2) and results of Meyer-Peter & Müller (1948).

The large deviation between observed and predicted sediment transport rates for low excess stresses is a consequence of the values of the Shields parameter given for the initiation of movement (θ = 0.047) and the general formulation of the equation, which does not produce solid transport until relatively large stresses (τ/τ_{cr} > 1.25), increasing transport rates very rapidly thereafter. Poor performance of MPM has also been reported before (Reid and Frostick, 1986; Gomez and Church, 1989; Recking, 2010), partly because MPM equation

was developed using uniform material and the adoption of a single grain size that is representative of graded beds is difficult (Recking, 2010). Wong (2003) revised the parameters in the MPM equation, with 4.93 and 1.6 instead of 8 and 3/2 for the coefficient and exponent, respectively. This revised formulation produced little improvement over the original results (Appendix 8).

Results from Shvidchenko *et al*. (2001) show that their equation underestimates bedload transport rates by approximately 1 order of magnitude. Equation results were drastically improved when the exponent of the slope term in equation 5-3 is changed from -5.0 to -4.96 and the exponent of shear stress reduced from 18 to 16. Shvidchenko (2000) say that bedload rates are "*reasonably well represented*" by his equation 4.11, which includes exponent = 18. Since eye fitting was carried out by Shvidchenko (2000), it is possible that the exponent may be sensitive to subjective fitting. Inspection of the graphs presented in Shvidchenko (2000) indicates that fitting of the lines is subject to author judgement. Therefore, a revised exponent 16 is adopted here.

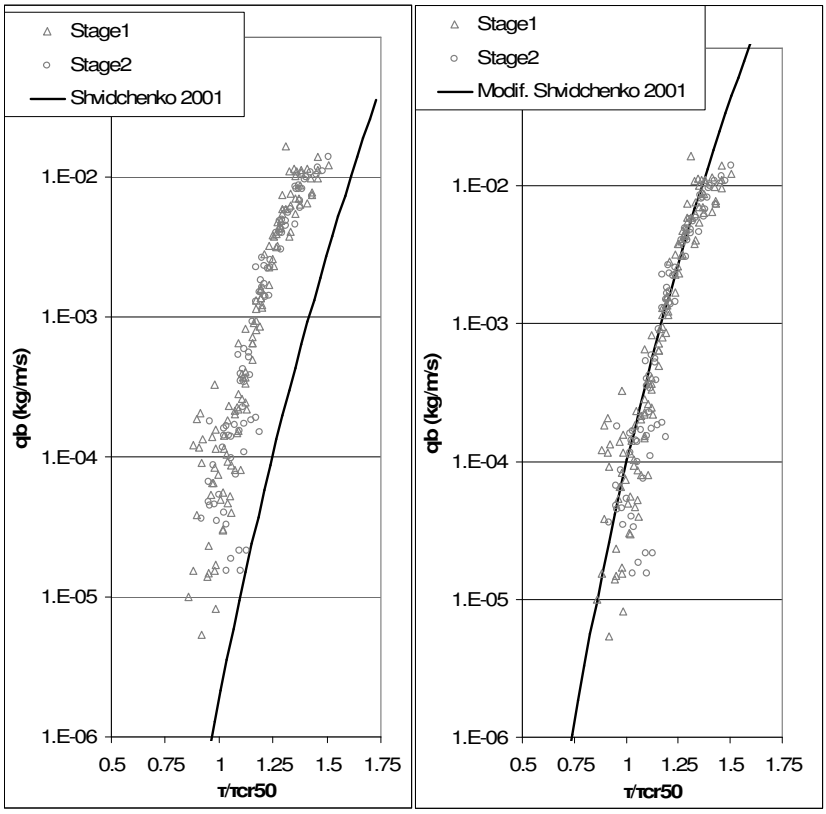

Fig. 5-3. Comparison of bedload transport data for the sand-gravel mixture and results from Shidchenko et al. (2001) with A) slope exponent -5.0 and, B) slope exponent -5.7.

Wilcock and Crowe's (2003) equation determines fractional transport rates, which were added for the eight size classes in the bed to obtain total transport rates. Results from the original Wilcock and Crowe (2003) equation were comparable to the data for a narrow range of values of τ/τ_{cr} between 0.9 and 1.1; with over and underestimations for $\tau/\tau_{cr} < 0.9$ and $\tau/\tau_{cr} > 1.1$ (Fig. 5-4) due to the low rate of increase of transport rates expressed by the exponent 7.5.

Parameters	Original (W&C, 2003)	Modified W&C, 2003
C_1	0.002	0.002
C_2	7.5	16
C_3	14	14
C_4	0.894	1.029
C_5	0.5	0.5
C_6	4.5	2
Split	1.35	1.3

Table 5-2. Original and modified (this study) parameters of Wilcock and Crowe (2003) equation for bedload transport rates. Split corresponds to the value of $\Phi = \tau/\tau_{cr}$ that defines the use of each section in equation 5-7. The factor 0.002 must be preserved if the criterion $W_i^* = 0.002$, set by Parker et al. (1982a), is to be maintained.

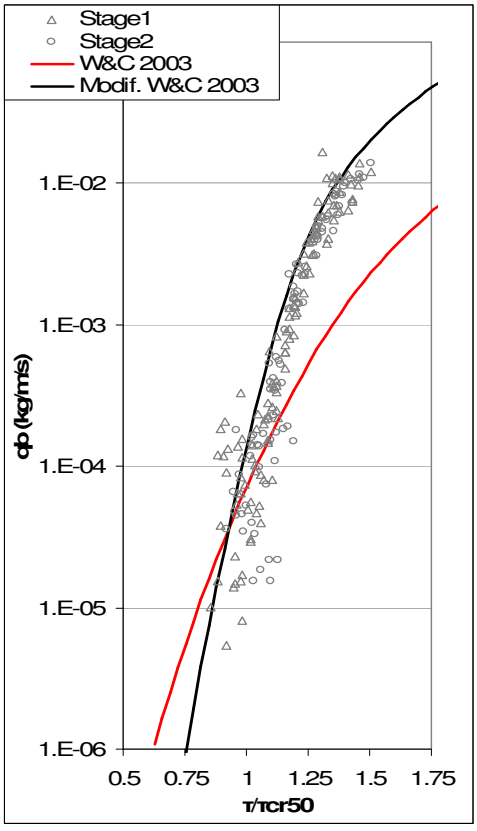

Fig. 5-4. Comparison of results from original Wilcock and Crowe (2003) set of equations and the same equation set modified in this study.

A considerable improvement in the prediction of transport rates was achieved (Fig. 5-4) by using the modified parameter values (Table 5-2) determined when applying the Parker *et al.* (1982a) reference transport criterion to the flume data (Chapter 4). The under-predictions of > 1 order of magnitude for $\tau/\tau_{cr} > 1.25$ of the original W&C (2003) equation are eliminated by the equation with the revised parameters. The exponent $C_2 = 16$ in equation 5-7 provided better representation of the rate of solid transport increase with $\tau/\ \tau_{cr}$ shown by the data.

Cui (2007) also modified the original Wilcock and Crowe (2003) parameter values and proposed a value of 14.2 for the exponent when ϕ < 1 in order to increase the rate of growth of the curve for smaller excess shear stresses. Adjustments of C_4, exponent C_6 and the limit ϕ defining the ranges of application of each equation (called *split* in Table 5-2) were also necessary.

Recking (2010) introduced specific equations for uniform and non-uniform granular beds. Previous workers have also shown the need to take account of sediment sorting in bedload equations (eg. Wilcock and Crowe, 2003; van Rijn, 2007b), or have introduced parameters designed to account for the degree of sorting (eg. Parker, 1990). Equations 5-13 and 5-14 were used to estimate bedload transport rates for the sand-gravel bed using D_{50} of the mixture 6.38 mm (average bed surface composition at the start of the antecedent conditions of Stages 1 and 2). Equations 5-15 and 5-16 were applied using the average of initial beds of Stages 1 and 2 to represent the bed, giving D_{50} = 6.38 mm and D_{84} = 8.88 mm. Values of θ_{cr} in all cases were obtained following Recking's (2010) method applied to the experimental data.The results in Fig. 5-5 show that the application of Recking's uniform bed equation outperforms the equation for graded material, with the uniform equation values and trend closer to the data, particularly for larger excess shear stresses. The latter produces large overestimations of q_b up to 2 orders of magnitude as the ratio τ/τ_{cr} decreases. It is noted that median size D_{50} was used for the uniform gravel equation, whereas the equation for non-uniform material uses D_{84} as representative bed size;

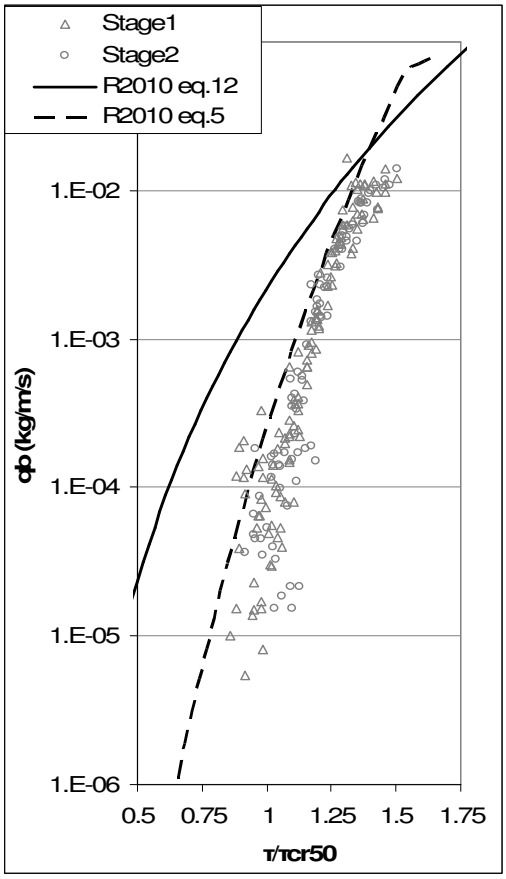

Fig. 5-5. Comparison of data and results from Recking (2010) equation 5-13 applied to the unimodal sand-gravel bed using D_{50} and equation 5-15 using θ_{cr84} from equation 5-16.

and thus, it may be the case that D_{84} is not as representative of the bed behaviour as D_{50}. Critical dimensionless bed shear stress obtained as the average of all runs for Stage 1 and 2 was 0.031 whereas θ_{cr} obtained with equation 5-14 and D_{50} was 0.0378, approximately 14% higher. On the other hand, θ_{cr84} from equation 5-16 was 0.0337, 45% higher than the experimental average of 0.0232. This larger discrepancy in entrainment threshold may be partly responsible for the differences observed. Further, the higher exponent (12.9) in the equation 5-13 appears to be more adequate than the lower exponent (6.5) in equation 5-15. As in the case of the Wilcock and Crowe (2003) equation, a higher exponent represented the rate of increase of *qb* with $\tau/\ \tau_{cr}$ more accurately.

5.5.2 New equation

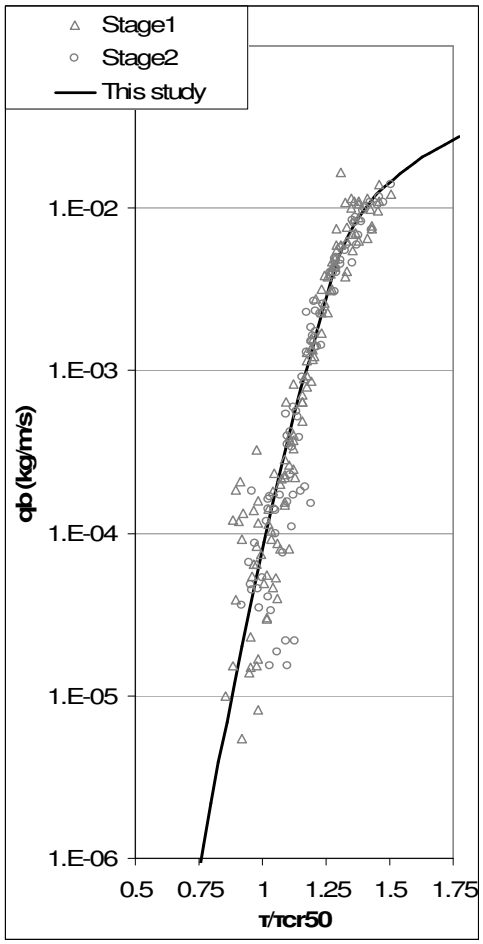

Fig. 5-6. Comparison of data and results from equation 5-18 in this study.

Transport rates calculated by the new equation 5-18 fit the data set better than any of the previous equations (Figures 5-2 to 5-5) (see section 5.6), particularly for τ/τ_{cr} > 1.1 (Fig. 5-6). This good fit is expected however, since the equation parameters were optimised for this data set. It is noted that τ_{cr} represents the general bed entrainment threshold, taken in this case as $\tau_{cr} = \tau_{cr50}$. The parameters proposed for this equation were optimised to fit the entire data set, including both the uniform and unimodal beds (Table 5-3). Fig. 5-7 shows the comparison between data and all the equations tested above.

Equation 5-18 produces the best fit to the data, followed by Shvidchenko *et al.* (2001) with modified slope exponent (see section 5.6 for a comprehensive assessment of the performance of the equations).

Parameter	Unimodal bed	Uniform gravel
A_1	0.00008	0.00008
B_1	16	16
A_2	0.047	0.047
B_2	-0.056	-0.056
Split	1.3	1.3

Table 5-3. Optimised parameters (fitted visually) for the proposed bedload equation.

Equation 5-13 generally follows the data but it would appear that a higher rate of bedload increase (curve slope) would be required. It is noted that the equations by Shvidchenko *et al.* (2001) and this study contain the highest exponent for the independent variable τ/τ_{cr} or θ/θ_{cr} (mathematically these ratios produce the same values), with values of 18 and 16 respectively. The corresponding exponent in equation 5-13 (eq. 5 in Recking, 2010) is 12.9, followed by 7.5 in Wilcock and Crowe (2003) and 6.5 for equation 5-15 (eq. 12 in Recking, 2010). When the exponent of Wilcock and Crowe (2003) equation was increased to 16, its performance improved noticeably. This clearly suggests that higher exponents are more adequate to represent the laboratory data presented.

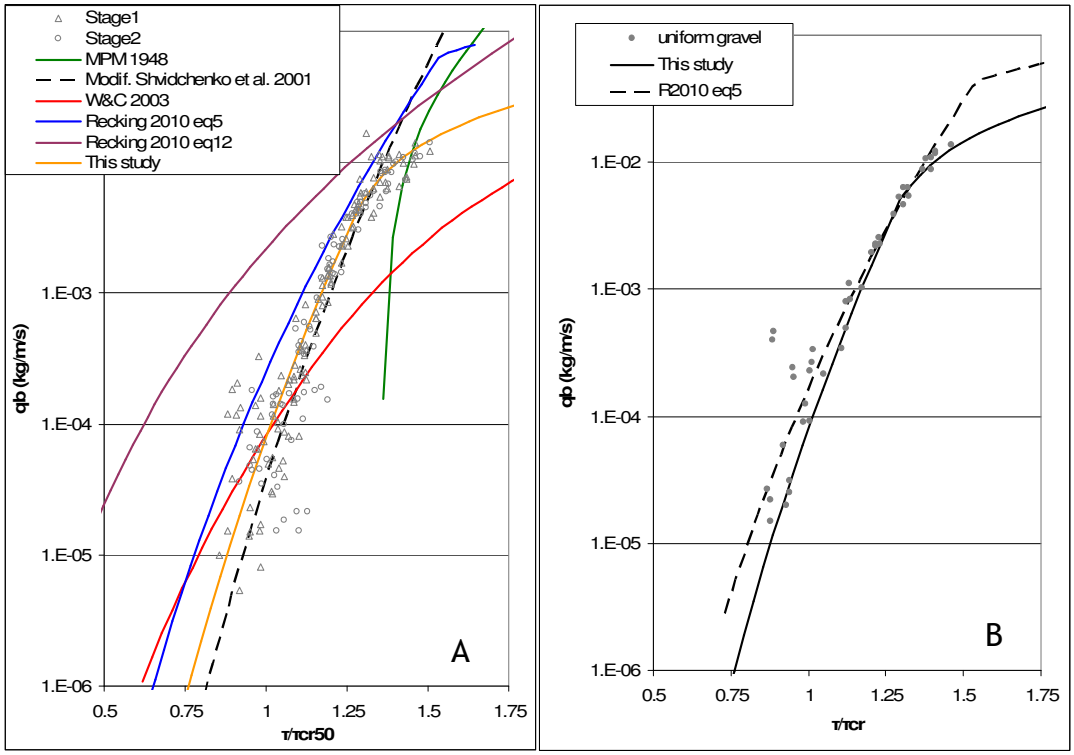

Fig. 5-7. Comparison of bedload transport data and results from all the equations tested for A) Sand-gravel mixture and, B) Uniform gravel

Fig. 5-7 also shows the bedload transport rate data of the uniform gravel and the results produced by equations 5-13 and 5-18 using D = 4.8 mm. As before, entrainment thresholds θ_{cr} and τ_{cr} were calculated with equation 5-14 and average of relevant runs, with values 0.0378 and 3.16 Pa respectively. Results of equation 5-18 appear to produce best fit.

5.6 *Comparison of equation performance*

Comparison of the performance of the formulations tested was restricted to those equations that provided the closest representation of the data (Fig. 5-7). These were, for the unimodal mix:

- Shvidchenko *et al*. (2001) with slope exponent equal to -5.7.
- Wilcock and Crowe (2003) with modified parameters.
- Recking (2010) eq.5 with $D = D_{50}$.
- Equation 5-18 (τ_{cr} = 3.38 Pa).

And for the uniform gravel:

- Recking (2010) eq.5
- Equation 5-18 (τ_{cr} = 3.16 Pa).

Following Recking (2010), calculated and observed transport rates ($q_b$cal, $q_b$obs) were compared (Fig. 5-8 and Fig. 5-9) so the accuracy of the bedload predictions could be quantified . The percentage of data points falling within a range of ±1 order of magnitude ($0.1 < q_b\text{cal}/q_b\text{obs} < 10$) and $0.5 < q_b\text{cal}/q_b\text{obs} < 2$ were also calculated (Table 5-4).

For both types of bed composition, equations 5-13 and 5-18 (see caption of Fig. 5-8) provided the best estimates of total transport rates, closely followed by the modified Shvidchenko *et al*. (2001) (Table 5-4). The first two equations have the same formulation structure: a constant factor multiplying the ratio θ/θ_{cr} or τ/τ_{cr} powered to exponents 12.9-16 respectively. Again, the ratios θ/θ_{cr} and τ/τ_{cr} are numerically the same. This common power law replicates observed data well for most of the bed stress range. However, the values and change of curvature of q_b are more closely represented by equation 5-18, with equation 5-13 producing overestimates of q_b (Fig. 5-7).

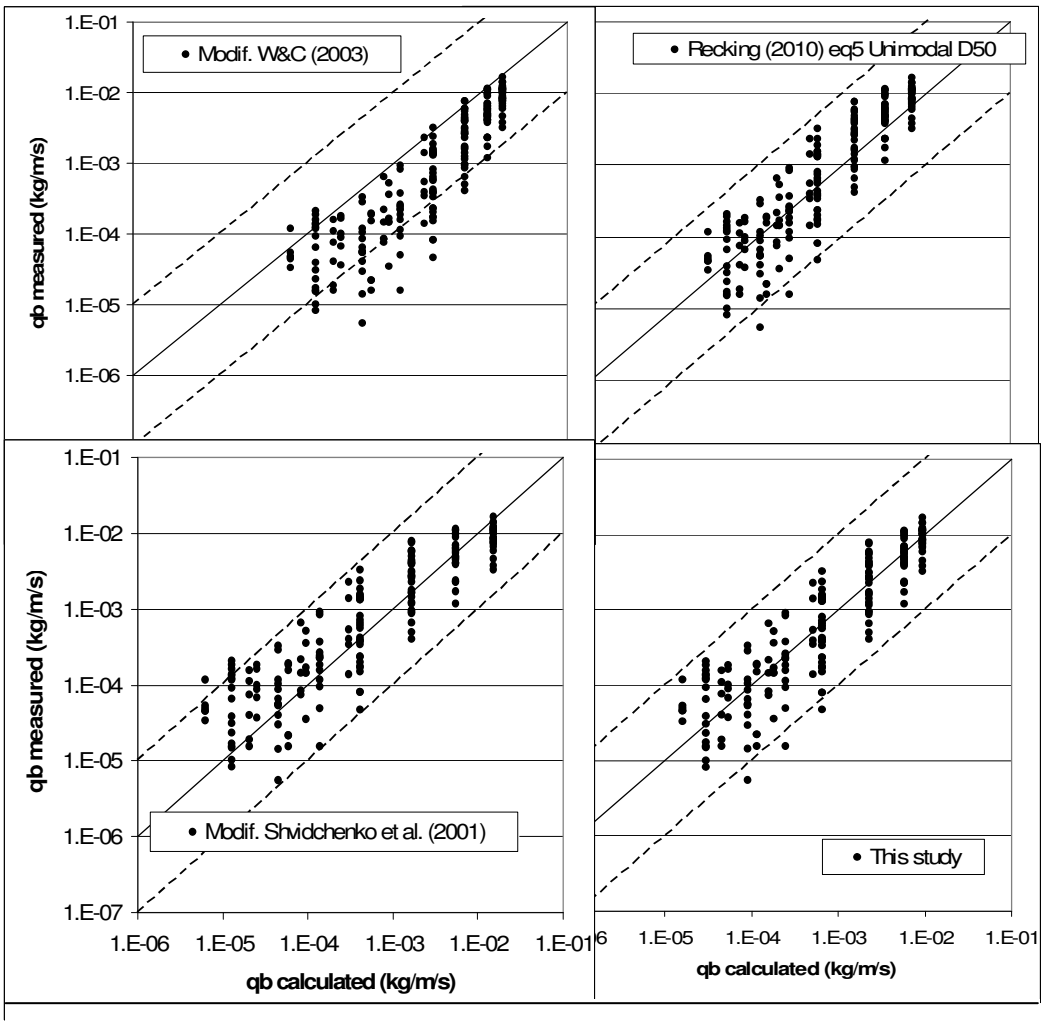

Fig. 5-8. Comparison of calculated and measured bedload transport rates for the four equations selected for the unimodal sand-gravel bed. Equation labelling is as follows: Modif. W&C (2003): equation 5-7 with modified parameters as described in section 5.5; Recking (2010) eq5 Unimodal D_{50}: equation 5-13 using D_{50} of the bed; Modif. Shvidchenko et al. (2001): equation 5-3 with modified parameters as described in section 5.5. This study: equation 5-18.

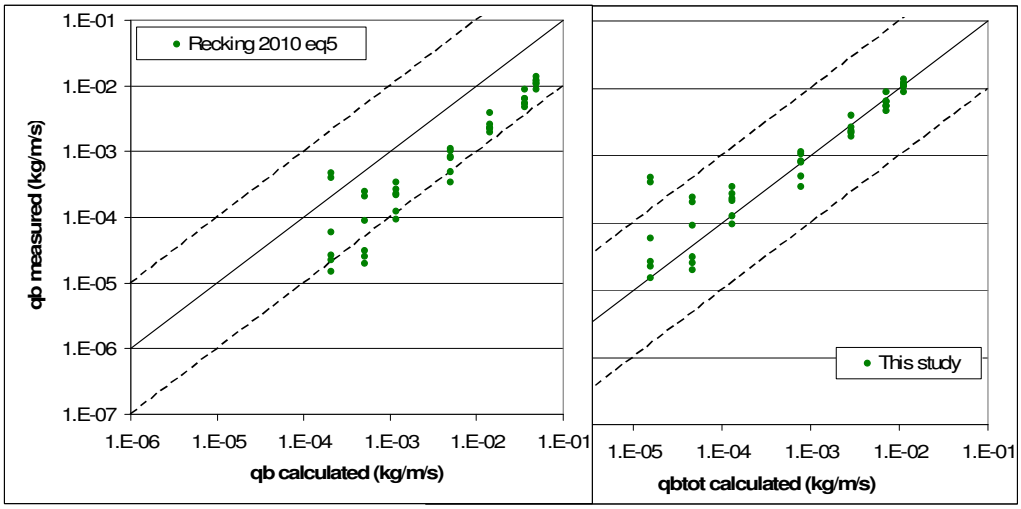

Fig. 5-9. Comparison of calculated and measure bedload transport rates for uniform gravel. A) Recking (2010) eq.5 and B) This study.

Formulation	% of data (1)	% of data (2)
Unimodal sand-gravel bed		
Modif. W&C (2003)	84.8	33.3
Recking (2010) eq.5 $D = D_{50}$	98.5	54.9
Modif. Shvidchenko *et al.* (2001)	97.1	52.9
This study (τ_{cr} = 3.38 Pa)	98.5	58.8
Uniform gravel bed		
Recking (2010) eq.5	83.3	2.4
This study (τ_{cr} = 3.16 Pa)	95.2	73.8

Table 5-4. Percentage of calculated bedload transport rates for which (1) 0.1 < $q_b cal/q_b obs$ < 10 and (2) 0.5 < $q_b cal/q_b obs$ < 2.

The modifications introduced in the equations by Wilcock and Crowe (2003) and Shvidchenko *et al.* (2001), chiefly increase of exponents, dramatically improved the performance of the equations but was insufficient to outperform equation 5-18. Values of residual errors $q_b calc/q_b obs$ (similarly to Fig. 7 in Wilcock and Crowe, 2003) were analysed for each of the four equations tested in Fig. 5-8. Data confirms the above assessment and shows that discrepancies between calculated and observed bedload rates decrease with τ/τ_{cr} (Appendix 8). The new equation proposed here outperformed all of the others, except Recking's (2010) equation for uniform material; with Shvidchenko *et al.*'s (2001) and Wilcock and Crowe's (2003) equations requiring modification of some of their parameters to fit the data more closely. The percentages of the data within ±1 order of magnitude were over 95% for best performing equation sets. Recking (2010) reported values of 83-86% for his eq. 12 when applied to a large field data set from 33 streams in Idaho (King *et al.*, 2004) and a second field data set collected from available literature (17 rivers). This equation could not reproduce the flume bedload transport values obtained for this research as closely as equation 5-18. The superior performance of equation 5-13 for uniform beds over equation 5-15 suggests that mobility of the beds tested here can be represented by a single particle size D_{50}.

All the tested equations predict a rapid increase in transport rates with shear stress for approximately τ/τ_{cr} < 1.5 (in the semi-log plot) and a drastic reduction of the rate of increase of q_b for approximately τ/τ_{cr} > 1.5. This reinforces the adoption of formulations that include two parts, one for each range of τ/τ_{cr}.

Parker (1990), Wilcock and Crowe (2003), and Recking (2010) all include this separation. Hassan and Woodsmith (2004) report transport rates increasing rapidly close to threshold, but then increasing more slowly for flows above a higher break point in the curve, which they identified as bankfull discharge. Bathurst (2007) also described similar trend of q_b; with steep lines following data near threshold values (lower flows or shear stresses) when q_b is plotted on a log-scale. This steeply rising line corresponds to the power laws of the first part of the bedload transport equations. For higher shear stresses, a more pronounced curvature is visible on the q_b log-axis, reflecting a change of the form of the transport law, represented by the second equation part. The proposed bedload transport equation (equation 5-18) includes these elements in its formulation.

It is noted here that this change of the rate of increase of q_b with τ is not related to a reduction of transport rates, but slower rates of increase of q_b with τ. Indeed, as bed shear stress rises bedload amounts will also increase but at a slower pace than when τ/τ_{cr} < 1.3-1.5 approximately. This value of the breaking point of the bedload equations may be related to the condition of partial-full transport, commonly reported to be $\tau/\tau_{cr} \approx 2$ (Church *et al.*, 1998; Lisle *et al.*, 2000). When bedload rates are plotted in linear axes (Fig. 5-14 and Fig. 5-15) transport rates for τ/τ_{cr} < 1.3-1.5 approx. are insignificant compared to those for τ/τ_{cr} > 1.5. The range between τ/τ_{cr} = 1.5 and 2 could be related to the transition of the bed from partial to full transport modes. The change between partial and full transport has been associated to breaking the armour layer (Wilcock, 1992; McEwan *et al.*, 2004 and Bathurst, 2007), entraining not just larger amounts of particles but also coarser heavier grains, which, since q_b is measured in mass units, contribute relatively more than finer classes to bedload quantities. In the case of the flume results presented, well developed armouring was not observed (although reduction of fines and a degree of bed surface coarsening was measured, section 4.2.3); thus, this increase of the bedload transport rates is associated to flows reaching the bed entrainment threshold, for which all grain sizes are mobilised.

5.7 *Comparison with field data*

The equation proposed in this study was formulated and parameterised based on the data collected and reported in Chapter 4, hence its performance would be expected to be optimal against this data set. To provide an independent test of the best performing equations: Recking's (2010) eq.5 and the one proposed here, these were tested against field bedload transport data from Turkey Brook (Reid and Frostick, 1986) and from Elbow River (reported by Bagnold, 1980). Turkey Brook data set is one of the very few that has been directly associated to the effects of antecedent conditions and flow history. A reduced section (approx. 55% of the total data set) of the Turkey Brook data was analysed. The data included mean unit bedload transport rate (kg/m/s, submerged mass), water discharge, average depth, average water surface slope S and hydraulic radius R_h collected during the period December 1978 - February 1979. Water surface slope and hydraulic radius data were used to estimate bed shear stress using $\tau = \rho g R_h S$ (Fig. 5-10). Bedload rates were converted from submerged mass to dry mass for the analysis presented here.

Estimates of q_b (kg/m/s) were obtained from equations 5-13 and 5-18 using the median size of the surface layer D_{50} = 22 mm and average water surface slope S = 0.0083 (Reid and Frostick, 1986). Equation 5-14 was used to obtain an initial value of θ_{cr}, (0.0406) which was later corrected to test its influence on the results. The threshold for initiation of motion reported by Reid and Frostick (1986) was ω_0 = 3.74 kg/m/s, which corresponds to $\tau_{cr} \approx$ 21 Pa (θ_{cr} = 0.059). This value resulted in large underestimations (about 2 orders of magnitude) for $\tau/\tau_{cr} <$ 1 and large overestimations for $\tau/\tau_{cr} >$ 1. When the value of ω_0 = 3.74 kg/m/s was used, only 18% of the field flow data was above this entrainment threshold, so it is likely that the reported value of ω_0 is excessively high. Alternatively, a value of θ_{cr} = 0.03 (Newson and Sear, 1998; Powell *et al.*, 2001; Barry *et al.*, 2008) was adopted, resulting in $\tau_{cr} \approx$ 10.7 Pa. Fig. 5-10 shows the comparison of the data and equation results.

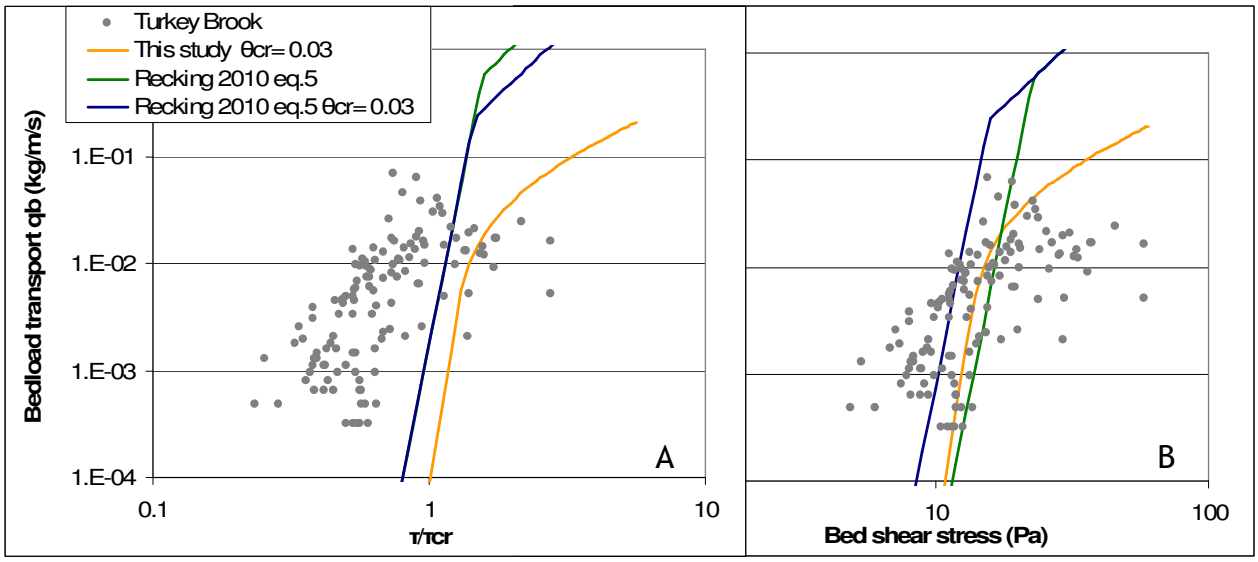

Fig. 5-10. Comparison of Turkey Brook data and results from Recking (2010) eq.5 using θcr = 0.0406 from eq.10 and optimised θcr = 0.03, and values from eq. 13 with θcr = 0.03. A) using excess shear stress τ/τ_{cr} and, B) using bed shear stress only.

Equations 5-13 and 5-18 with θ_{cr} = 0.03 produce predictions that are comparable to data for only a very narrow range around $\tau/\tau_{cr} \approx 1$ (Fig. 5-10A), but over- and under-predict measured bedload transport rates outside this range, with significantly larger overpredictions by Recking's (2010) equation. The initial value of θ_{cr} = 0.0406 provided by equation 5-14 produces smaller transport rates that the revised θ_{cr} = 0.03 (the value used by Parker, 1979, Wu *et al.*, 2000 and Barry *et al.*, 2008). Values from the equation proposed here produce the closest fit to the data, with 60.6% of the data within ±1 order of magnitude from the field data. Figures for the other two equations are 33.1% (θ_{cr} = 0.0406) and 39.4% (θ_{cr} = 0.03) (Fig. 5-10B).

It is worth noting that using τ or τ/τ_{cr} on the x-axis produces different visual assessments of the performance of the equations (Fig. 5-10). When τ/τ_{cr} is used, the adoption of certain entrainment threshold shifts data along the x-axis. In the case of the Turkey Brook, θ_{cr} = 0.059 obtained from the suggested ω_0 in Reid and Frostick (1986) is nearly twice as high as the one tested; producing the separation between data and equation results observed in Fig. 5-10A. However, when absolute values of shear stress are used in the plot, there is no effect of critical bed shear stress and data and equation results overlap. In addition, equation 5-13 curves collapse below the breaking point in the graph when using

τ/τ_{cr}, with an apparent vertical shift for larger values of q_b; whereas when τ is used, equation values show the effect of θ_{cr}: lower θ_{cr} produces an increase of bedload transport provided by the first section of equation 5-13, clearly reflected in Fig. 5-10B, as it depends on θ/θ_{cr},; however, as equation 5-13 only depends on θ for $\theta/\theta_{cr} > 2.3S^{0.08}$ (Recking, 2010), the second section of the equation is not affected by θ_{cr}. This makes the equation results appear to change with the variable used in the x-axis.

Data for the Elbow River, Alberta (Hollingshead, 1968), reported by Bagnold (1980)[8], was also used to test equations 5-13 and 5-18 (Fig. 5-11). The Elbow River had similar characteristics to Turkey Brook: S = 0.0075, D_{50} = 25 mm, and S = 0.0086 and D_{50} = 22 mm respectively. Calculations of shear stress were based on $\tau = \rho g R_h S$ with R_h estimated from width B and depth h data (calculations confirmed $R_h \approx$ depth h for wide channels, average B/h = 25-30 for the Elbow River data used).

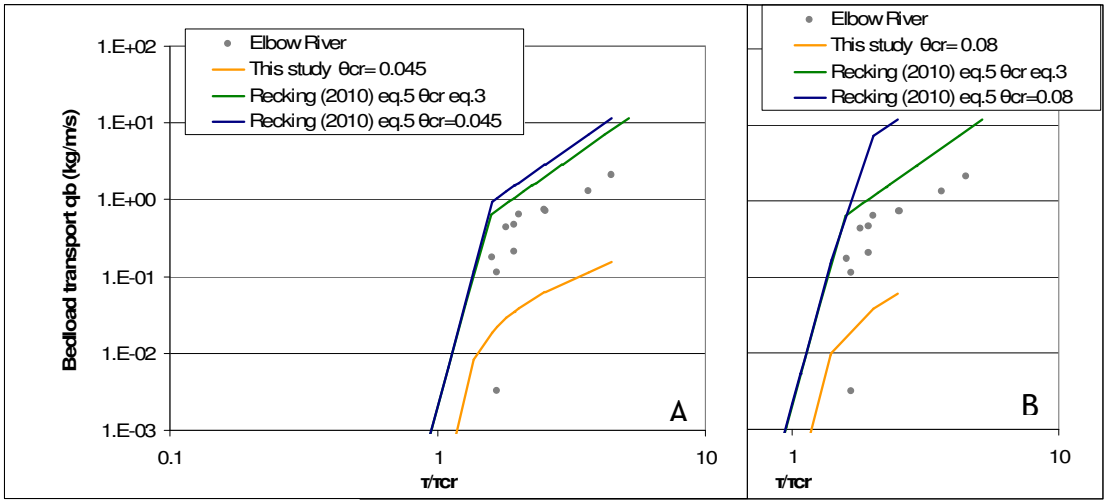

Fig. 5-11. Comparison of bedload transport rates of the Elbow River and results from equations 10 and 13. A) θ_{cr} = 0.045 obtained from ω_0 = 3.1 kg/m/s (Bagnold, 1980) and, B) θ_{cr}= 0.08 (Ashmore, 1988).

Fig. 5-11 shows that Recking's (2010) equation appear to perform better than equation 5-18 for larger transport rates with θ_{cr} = 0.045 (from ω_0 = 3.1 kg/m/s in

[8] Two of the values of width B that appeared to be wrong in Bagnold (1980) were corrected before being used herein. The effect of this correction on the trends in the full data set was minimal.

Bagnold, 1980). Bedload data falls between Recking's (2010) equations and the one proposed in this study, with the latter approaching the data with lower θ_{cr}. Ashmore (1988) fitted Parker's (1990) bedload equation to the Elbow River and Oak Creek transport data with θ_{cr} = 0.08. Using such value results in larger underestimations by equation 5-18 and overestimations with equation 5-13 (Fig. 5-11B); indicating that the parameters proposed by the original formulation of Recking's (2010) equation 5 provide the best results for this case.

It is seen then that finding a single equation and parameter set that fits well the field data used is extremely difficult. Whereas equation 5-18 appears to perform better in the Turkey Brook case, Recking's (2010) formulation provides closer values of q_b for the Elbow River. This comparison also shows that it is likely that the threshold for initiation of motion given by Reid and Frostick (1986) for the Turkey Brook is overestimated. The equations tested did not appear to confirm the suitability of θ_{cr} = 0.08 for the Elbow River, as implied by Ashmore (1988), with considerably lower values of θ_{cr} producing better fit to the data.

The difficulty of finding a universal bedload equation has been demonstrated here using a relatively small field and flume data set of bedload transport. Although this data set has been implicitly enlarged by including other bedload transport equations developed based on a combination of flume and field data. It would appear that the variable selected to present and assess equation results has a considerable impact. Fig. 5-12A would indicate that data from the flume experiments and field are not comparable, with seemingly different trends. However, when bedload transport data are plotted against dimensionless shear stress, data points collapse and a general trend, defined by the flume and Elbow River data, appears. The equation proposed here follows the trend of the flume and Turkey Brook data (the large scatter present in the latter is noted), while it underestimates values of q_b for the Elbow River, however equations appear to reflect the rate of increase of q_b with θ (Fig. 5-12B). Gomez and Church (1989) presented the results of 12 different bedload transport formulations for the Elbow River, where none of them replicated the data satisfactorily. Fig. 5-12 clearly shows the differences of data trend for the Turkey Brook set; which appears to produce larger and lower transport rates than expected for θ < 0.04

and θ > 0.06 respectively. Turkey Brook data has considerable scatter and a descriptive pattern is more difficult to establish. Reid and Frostick (1986) pointed to observed bedload pulses in Turkey Brook, independent of hydrograph shape, as a main cause of the scatter.

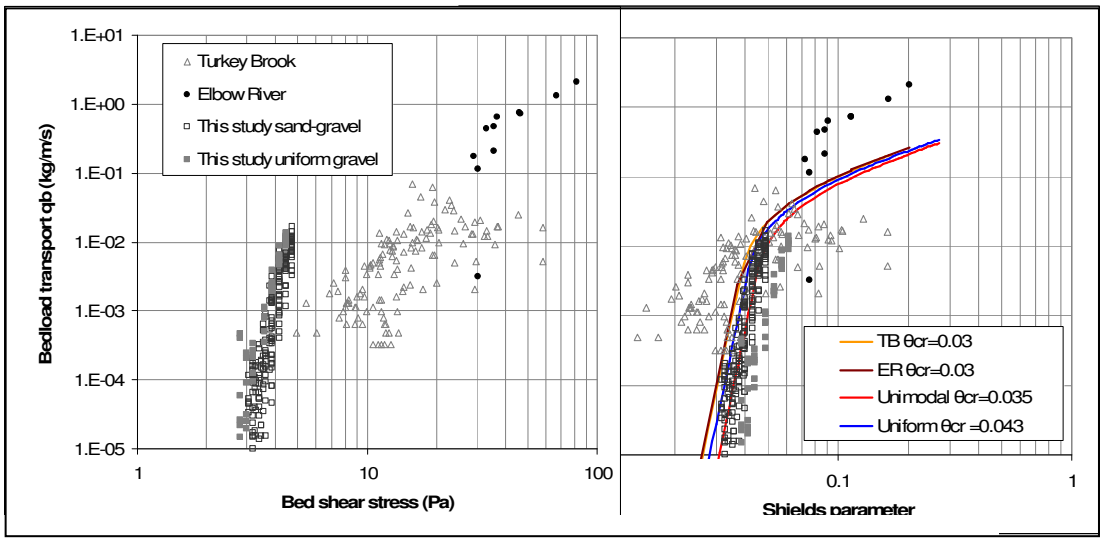

Fig. 5-12. Comparison between bedload transport data from this study (flume) and field data for Turkey Brook and the Elbow River plotted against A) τ and, B) θ. Curves correspond to results of equation 13 for the different data sets.

It would appear that the adoption of a standard variable representing fluid forces is necessary so a unified procedure for assessing bedload equation performance can be achieved. Fig. 5-13 shows how the same q_b data and equation results can appear very different depending on the independent variable used. When Shields stress θ is used flume data appears to follow a straight line on Fig. 5-12. Elbow River data then appear to follow the trend described by equation 5-13 but approximately 1 order of magnitude higher. It is speculated here that a more comprehensive formulation may be achieved if a single independent variable is adopted. Visual assessment of equation performance is also subject to plot type, with differences between equations being most evident when plotted against bed shear stress (Fig. 5-13).

Interestingly, all equations except 5-18 cannot reproduce the horizontal shift that q_b data displays when bed entrainment values θ_{cr} or τ_{cr} are defined by channel bed characteristics (eg. particle size, hiding and slope). Only equation 5-18 has the flexibility to integrate new values of entrainment threshold and therefore, quantify bedload transport rates more accurately (Fig. 5-13).

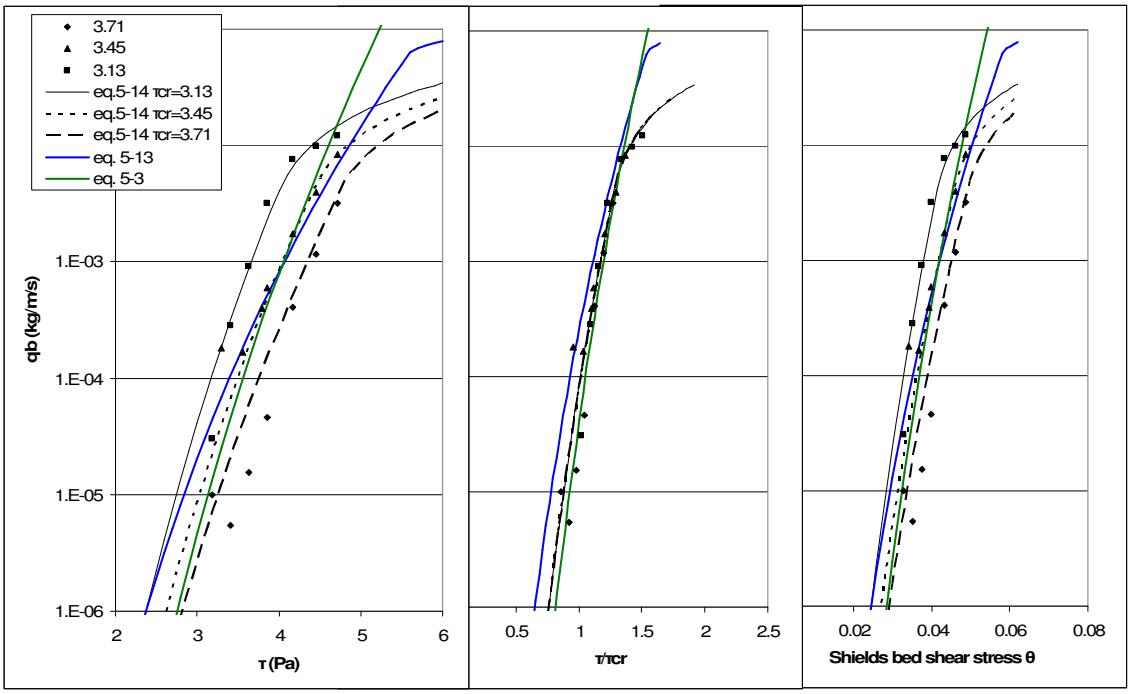

Fig. 5-13. Comparison of data and equation results plotted against three different independent variables. Note how equation 5-18 can closely replicate changes of qb with bed entrainment threshold.

5.8 *Conclusions*

The data and calculations presented here highlight that there are a number of conceptual formulations for sediment transport in gravel bed rivers that include the two stages of rapid increase of q_b followed by a smaller rate of increase of q_b with τ (in the semi-log plot) observed in the data (Wiberg and Smith, 1989 Hassan and Woodsmith, 2004; Bathurst, 2007). However, the comparison between the selected bedload equations and bedload data, from both flume experiments and two completely independent field data sets (Turkey Brook and Elbow River) suggests that there is no unique equation (fixed parameters) capable of describing bedload transport behaviour for gravel channels with differing environmental conditions (Gomez and Church, 1989). Local factors such as bed size and composition, slope, particle shape and particle interactions play an important role in determining grain mobility. Shvidchenko *et al.*'s (2001) attempt to include hiding and bed slope deserves appropriate praise; however, it has been demonstrated that parameterisation may have to be revised. Successful formulations of bedload sediment transport must aspire to pseudo-universal applicability at the same time as be flexible enough to include local

particularities. The similarity of the formulations proposed by Parker (1990), Wilcock and Crowe (2003), Recking (2010) and equation 5-18 in this thesis supports this idea. The equations put forward by these authors have a common structure: (1) division of equation in at least 2 sections applicable to ranges of τ/τ_{cr} or θ/θ_{cr} < 1.3-1.5, likely related to partial transport (Church *et al.*, 1998), characterised by a power law with an exponent varying between authors; (2) a second section for larger values of excess bed shear stress where the rate of increase of q_b (steepness of curve in logarithmic axis) reduces. The specific formulation of this second section varies among authors, with Parker (1990) and Wilcock and Crowe (2003) using a power law of θ/θ_{cr} and τ/τ_{cr} respectively, Recking (2010) using another power law but depending only on θ, and the one suggested here, a straight line equation with τ/τ_{cr}. It is noted that a linear relationship is not generally found in literature; however, both flume data and values for the Elbow River strongly suggest a linear relationship between bed shear stress and total bedload transport rates when plotted against τ/τ_{cr} (Fig. 5-14 and Fig. 5-15).

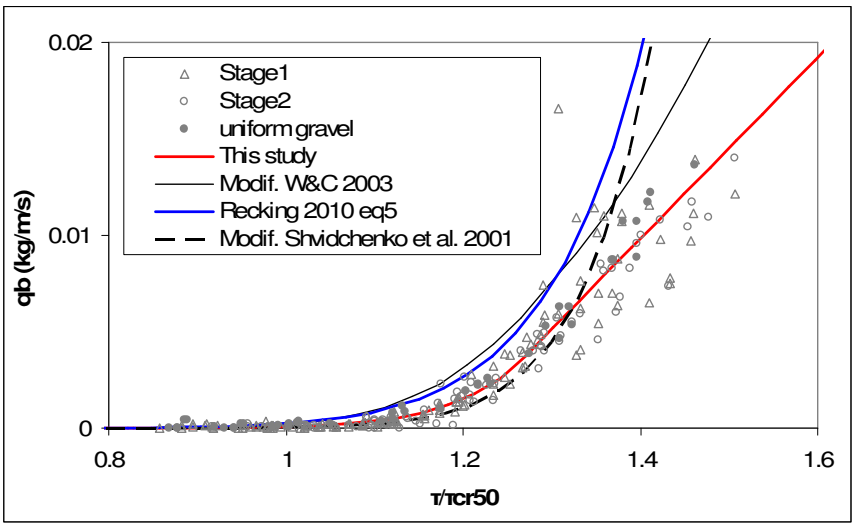

Fig. 5-14. Bedload transport rates in relation to τ/τ_{cr} showing linearity of data for τ/τ_{cr} > 1.3. Y-axis in linear scale.

The determination of an appropriate ratio of τ/τ_{cr} or θ/θ_{cr} , i.e. τ_{cr}, has been shown to be an important element for the accuracy of equation results. Where values of critical bed shear stress are determined based on bed particle size distribution and/or slope without including the effect of antecedent conditions theoretical curves cannot fully represent the variations of q_b observed on the flume data presented (Fig. 5-13).

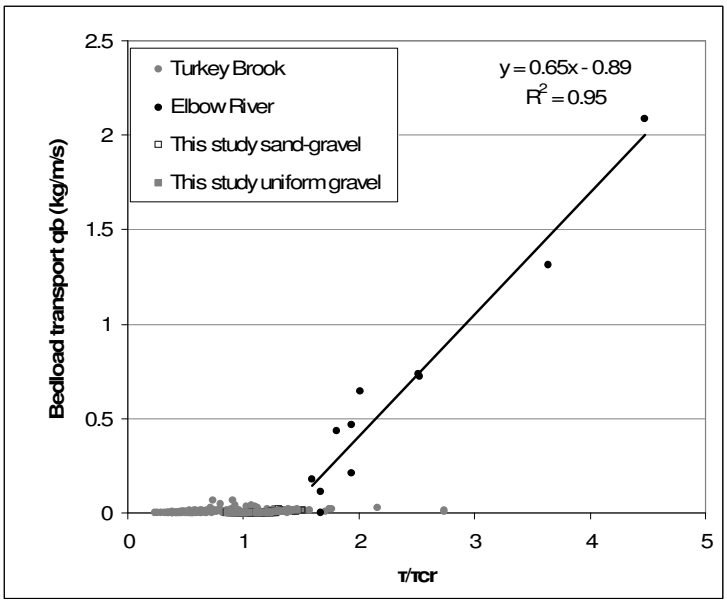

Fig. 5-15. Field and flume bedload transport rate data on linear axes. Note how the Elbow River data follows a straight line.

Only when the equation of bedload transport includes flexibility on the definition of τ_{cr} these reported variations of transport rates can be replicated. Equation predictions may be further complicated by the adoption of a characteristic threshold of motion. Reid and Frostick (1986) suggested considering two thresholds of motion when predicting sediment transport, one for initiation of movement and another lower value for cessation of transport, which they related to the rising and falling limbs of hydrographs respectively. These two values, given by Reid and Frostick, were tested during the calculations presented. It would appear that the true entrainment threshold, based on results from equation 5-18, is somewhere between these two. In this study, only rising limbs have been considered, therefore, the assessment of different entrainment and settling conditions could not be carried out. Future experiments including both rising and falling limbs should help in this matter. The work by Saadi (2002) is possibly the only one dedicated to this subject.

The differences between field data and values of q_b provided by equation 5-18 reported here might indicate that the formulation obtained based on laboratory experimentation may not be directly applicable to the rivers tested. Ackers and White (1973) proposed an exponent m = 1.5 for coarse material in their equation relating bedload rates with mean velocity of flow, with m > 1.5 for finer material. Ashmore (1988) showed that dimensionless bedload transport data for

his model of braided river are several orders of magnitude larger than those from the Oak Creek and Elbow River for the same dimensionless bed shear stress. Ashmore referred to the lower ratio D_{90}/D_{50} of the model (2.2) than those of the Oak Creek and Elbow River (3.3 and 3.8 respectively) to explain increased mobility of the model bed. Thus, sorting appears to be inversely related to bedload quantities. This is supported by the form of Parker (1990) equation, in which a hiding function reduces W_i^* with larger values of D_i/D_{50}. Recking (2010) reported that transport rates in flume experiments were larger that those recorded in the field for the same value of θ. On the contrary, Vericat *et al.* (2008) showed that flume bedload transport rates were approximately 2 orders of magnitude smaller that field data of the same bed composition and the same excess shear stress τ-τ_{cr}. Thus, a) the findings obtained with flume data may not be directly applicable to field data and vice-versa, and; b) careful examination of the material and methods used when developing and applying bedload equations should be considered.

Since the trends showed by the flume and Elbow River data appear to follow a continuous curve whose shape (but not values) is followed by equation 5-18 (Fig. 5-12), it may be possible to introduce a scaling factor $\pi(D_{ip}/D_{im})$ as a function of the ratio of the prototype and model representative bed sizes D_{ip} and D_{im}. However, it is highlighted that the bed material composition and channel characteristics (eg. slope) used in the laboratory were not intended to replicate either the Elbow River or Turkey Brook; hence, the extension of the equation to these cases was unlikely. Nonetheless, the promising representation of some of the bedload transport data of the Turkey Brook and the trend (not the actual values) of the Elbow River is encouraging.

It is emphasised that the comparison of bedload data and formulations presented here was mainly intended to show how an equation developed from flume experimentation, simpler than many found in literature (Shvidchenko *et al.*, 2001; Wilcock and Crowe, 2003, Recking, 2010), can not only outperform other more established equations for the flume data but it does so with a simplistic account of bed entrainment threshold; which, at the same time, provides the necessary flexibility to reproduce the variation of bedload with bed stability

shown in this thesis. The equation introduced here produces values of total bedload transport rate only; if fractional transport rates are required other functions must be adopted.

It would appear that a universal expression capable of producing accurate predictions of bedload rates under all conditions in gravel-bed rivers without changing parameter values, may not be currently achievable. On the contrary, a template formula with adaptable parameters appears to be more viable, providing the flexibility required to represent the high variability of key attributes, such as bed particle sizes, slopes, relative submergence, and antecedent conditions, present in river environments, at the same time as maintaining a common structure.

Comparison of the formulations that provided the most accurate bedload transport rate estimates resulted in a number of common elements:

- The basic equation for low excess bed shear stress is a power law with the main independent variable being θ/θ_{cr} or τ/τ_{cr}.
- The exponent of the power law ranges from 13 to16.
- The threshold determining the change of equation or curvature for larger transport rates is θ/θ_{cr} (or τ/τ_{cr}) ≈ 1.3-1.5 depending on the equation.

Expressions for q_b when θ/θ_{cr} (or τ/τ_{cr}) > 1.3-1.5 differ among authors. Wilcock and Crowe (2003) proposed a power law based on the inverse of the ratio τ/τ_{cr}, whereas Recking (2010) suggested a power law with θ as independent variable for all bed compositions, using θ_{84} for non-uniform beds. A linear relationship between τ/τ_{cr} and q_b (kg/m/s) is proposed here for τ/τ_{cr} > 1.3. Linearity between shear stress and solid transport is not common; however, as Fig. 5-14 shows, the equation proposed here was the only one closely predicting transport rates in that region; with general overestimation by the other equations tested. Bathurst (2007) also showed bedload rates that appeared to follow a straight line for larger flows, although he plotted q_b against unit discharge Q/B. However, it is noted that transport conditions in the experiments carried out for this study were within the range of marginal and partial transport (Wilcock and McArdell, 1993; Wilcock, 1997; Pender *et al.*, 2001), with ratios τ/τ_{cr} not extending far

enough to confirm the selected formulation. Hence, equation 5-18 should be tested against higher transport rates. Data from the Elbow River may prove convenient for this purpose. Fig. 5-12 would suggest that the breaking point defined by τ/τ_{cr} should be around 1.7 for the Elbow River data, and that parameters for the second part of equation 5-18 should be such that higher transport rates are predicted while maintaining the general shape of the curve. This suggests that a general formulation with user defined parameter may achieve the required universality. However, the definition of adequate parameters for each case will have to be based on existing and future data sets, which may result in a database relating channel and bed characteristics to equation parameters. Maybe then, more reliable predictions of bedload transport might be achievable without bedload data for the site.

It is likely that accomplishing this goal is still some years from now and further research in the inclusion of a range of parameters representing bed conditions is required. The use of an appropriate calibrated bedload transport rate equation will considerably enhance predictions of sediment transport in gravel bed rivers, with immediate application in areas such as computer hydraulic models. The assumption of similar bed characteristics used for predicting bedload rates based on existing data sets (past and current conditions) may be challenged by the high variability of the multitude of factors affecting bedload mobility. This can however be turned into an opportunity to use a reliable bedload equation to evaluate the sensitivity of the river channel to changes in bed or hydrological conditions. Thus, aiding the management of natural and man-induced changes in fluvial catchments.

Chapter 6
Further research and improvements

Beware of silent dogs and still waters.
– Proverb.

Further research and improvements

Gathering scientific knowledge during this PhD was often coupled with the realisation of the limitations associated with a particular technique or its application, sometimes due to equipment issues. Often, these realisations resulted in actual improvements during the research; in other occasions these developed into lessons and skills to be applied in future work. Some of these are summarised below. This chapter contains a critical assessment of the limitations of the methods and equipment used, together with future improvements to some of the techniques or data collection used. There are also a number of proposed further research areas that follow on from the present work, these are highlighted below.

6.1 *Unifying entrainment criteria*

The application of techniques for entrainment estimation highlighted that there is considerable scope for analysing the definition and performance of the entrainment criteria used here, specifically: (1) revising the reference transport rates of either Parker *et al*. (1982a) or Shvidchenko *et al*. (2001), or both, so critical flows are coincident whether calculations are based on volumetric or

mass transport rates; and, (2) refining the reference transport and visual methods so these also provide similar values of entrainment.

Reducing Shvidchenko *et al.'s* (2001) reference transport rate $q_{bi}^{*} = 10^{-4}$, so values of critical bed shear stress τ_{cr} are the same for RTM-P and RTM-S is proposed. This revision of RTM-S instead of RTM-P is based on the more extensive use of $W_i^{*} = 0.002$ and the similarity of τ_{cr} found with visual method results (section 4.2.2). In addition, it was already noted in Chapter 4 that entrainment thresholds for RTM-S appeared to be unrealistically high compared to observations made during experiments.

The discrepancies of values and trends between VM and RTM-P (or RTM-S) observed here remain to be appropriately explained. Practicalities of each method (eg. stochasticity of grain entrainment, uncertainty in grain movement count and visual fitting, Chapter 4) are unlikely to fully explain these differences, which are expected to originate from the conceptual definition of each entrainment criterion (Buffington and Montgomery, 1997) and from the adopted thresholds of N, W_i^{*} and q_{bi}^{*} proposed by the authors of each methodology (Chapter 4). A comparative analysis of the results provided by the three methods used here will be pursued by the author in future publications.

6.2 *Effect of area of observation*

As discussed in Chapter 4, the visual method may be affected by the size and location of the area of observation of particle movements (Buffington and Montgomery, 1997). A series of experiments in which the grain movements on a number of areas (of a range of sizes placed at different locations over the sediment bed) are simultaneously recorded should be conducted. These measurements can then be related to local bed surface grain size distribution and texture, and thus, could potentially provide very useful data sets for assessing the sensitivity of the visual method results to the characteristic of the observation area. Multiple sediment traps (section 6.10) will complement this study in connection to the reference transport method results.

6.3 *Effect of slope on entrainment*

Shvidchenko *et al*. (2001) and Recking (2010) showed that entrainment thresholds increase with steeper bed slopes. The work carried out for this thesis only includes one slope for the non-uniform bed and a partial analysis of the effect of slope on uniform gravel. Data from the visual method for the latter showed that absolute entrainment thresholds for the steeper bed S = 1/150 are smaller than those of S = 1/200. This would contradict the findings of Shvidchenko *et al*. (2001) and Recking (2010). However, values of Q_{cr}/Q_{ref} are comparable between the two slopes (section 4.3), indicating that the effects of antecedent conditions on bed characteristics (eg. particle rearrangement and imbrication) and entrainment may be consistent for different bed slopes. A more comprehensive analysis of the effect of bed slope on entrainment when acceleration rates are applied would clarify the above contradicting results in two ways: (1) confirm whether, for the types of experiments undertaken, entrainment thresholds increase with bed slope; and, (2) analyse whether the trends observed between acceleration rates and critical bed shear stress are consistent throughout a range of slopes. Additional experiments that include these elements are required.

6.4 *Using different bed compositions*

Since bed grade characteristics (grain size compositions and sorting) appear to produce different response to sub-threshold antecedent conditions (Chapter 4), a natural extension of the work presented here is the repetition of similar experiments using a range of bed compositions, maintaining the range of particle sizes and median bed size, changing bed bimodality, similarly to the work initiated by Haynes and Ockelford (2008). This proposal is reinforced after the possible effect of fine content on bed behaviour during antecedent conditions (section 4.4.2.2). This extended experimental work will build up a data set of entrainment thresholds and bedload transport that would be essential to develop knowledge of the relationship between antecedent conditions using increasing flows, and confirm the suitability of the bedload equation proposed. For the case of constant flows such data sets have been generated over the years (eg. Wilcock and McArdell, 1993; Buffington and Montgomery, 1997, Haynes and

Ockelford, 2008), evidencing that bed composition characteristics affect grain mobility and therefore, providing further support to the extension of the research proposed here.

6.5 *Testing full hydrograph*

The work presented focussed on the effect of increasing flows as antecedent conditions. These can be considered as the rising limbs of hydrographs. Powell *et al*. (2001), Hassan *et al*. (2006) and Parker *et al*. (2008) considered the effects of full hydrographs on bed composition and mixing and bedload during mobilising flows. Saadi (2002) showed that the duration and magnitude of falling limbs also have an effect on entrainment values. This, considered together with the suggestion by Reid and Frostick (1986) that thresholds for the cessation of motion during falling limbs may be useful descriptive parameters for bedload prediction, leads to the need to extend the present research to full hydrographs. Bed mobility, bed surface composition, grain clustering and bedload amounts and composition should be included in order to study the effect on hydrograph magnitude and duration on bed mobility.

6.6 *Feed and recirculation*

Authors such as Hassan and Church (2000) and Wilcock and Crowe (2003) have shown that solid transport rates/composition and bed size distribution change with feeding rates and composition (same size composition as the transported material or the bulk mix). Feeding was not considered in this PhD as sub-threshold flows, which produce very low transport rates, were the main focus of the research. However, feeding may represent a range of natural and man-made events (eg. bank collapse, sediment release downstream of a dam or mining activities) that may affect bed stability and river bed composition, for which the inclusion in experiments similar to those presented in this thesis is necessary. It is proposed here that further research including feed or recirculation is studied after the link between flow history and entrainment is better understood.

6.7 *Image quality*

Digital photographs were extensively used throughout this research work for the assessment of bed surface composition and bed evolution. Other authors have cyclically reduced the water depth in the flume at a number of stages during the runs in order to sample the bed, increasing flows back up again afterwards (Hassan and Church, 2000). This procedure was incompatible with the main objective of this research, i.e. analysing the effect of flow history on bed entrainment, as these cycles of high-low flows would introduce unwanted flow history. Thus, images had to be collected under flowing water. Image quality reduced with stronger flows, caused by disturbances on the bed surface and fast running flows, which reduced the clarity of the images. Results are unlikely to be noticeably affected by this issue, since bed surface composition was based on colour identification not on particle boundary definition (an advantage of the technique used). However, improved image quality would be desirable. Tests using a glass plate were undertaken during the early stages of the research work; however, adjusting the position of the glass plate took too long, making it incompatible with the limited time available to collect data during the flow steps applied. Thus, the use of the glass plate was discarded. A robust system for underwater image recording (eg. quick-release single-pulley plate adjustment or floating plate) will be of major benefit to future experiments.

6.8 *Use of UV light*

The analysis of surface cluster formation, coarse particle mobility and bed stability using UV light provided very informative results. Carrying out simultaneous measurements under UV light of painted grains with improved image quality (see above) has the potential to provide essential data to understand individual and collective particle evolution and its relation with bed resistance. The technique used is simple and appeared to provide suitable quantitative data for mathematical analyses (section 4.2.8). Painting other size classes in UV paint must also be considered for optimising the information available. However, paint colours must be sufficiently distinguishable under UV light by the software used. For instance, blue and red UV colours have been shown to be clearly identified by ImageJ (sections 3.4.4 and 4.2.8).

6.9 *Bedload sampling optimisation*

Slight over-sampling of bedload due to air bubbles destabilising grains on the avalanche slope around the trap opening was reported, especially for low flows. This issue was related to the design of the sediment trap. Thus, the presence of air bubbles is unavoidable with the current system. Successive changes of the collection box reduced the number of grains destabilised and collected in the box. These samples coincided with larger flows and hence, larger transport rates. Consequently, the impact of excess grains on later samples within the same experiments was minimal. Therefore, calculations of critical bed shear stress remain valid, as those transport rates that were artificially high were not considered during the visual fitting of the curves for estimating τ_{cr} (section 4.2.5), taking full advantage of the visual fitting used. The same occurred when developing the proposed method for estimating τ_{cr} (section 4.2.6), for which only the most reliable data sets, often corresponding to the stability test, were included.

A new sediment trap design that eliminates the presence of air bubbles would likely require a more complex double shaft system, where all the trap elements are filled with water prior to opening the connection to the flume channel. The experience gathered during the execution of the experiments reported here will help the author to better design and manage sediment traps in the future.

6.10 *Using multiple sediment traps*

In section 4.4.2.1 the benefits of installing multiple sediment traps were discussed. In particular, the effect of spatial heterogeneity of the bed surface composition and texture on bedload quantities could be assessed. In large flumes, where this heterogeneity is more likely, the installation of multiple sediment traps would be advantageous. In short flumes, like the use used in this thesis (7m) is not practical, as it would shorten the sections of the flume associated to each trap to inappropriately short lengths. The author will propose the use of multiple traps in his future research positions whenever suitable.

6.11 *Velocity data: ADV vs. PIV*

The analysis of the effects of antecedent conditions on bed and flow characteristics is somewhat inconclusive (sections 4.2.7 and 4.3.4). The limited velocity data taken using ADV faced the difficulties of reduced data reliability where it is most needed, near the bed (section 3.3.1). Since the application of the logarithmic Law of the Wall is often restricted to the lowest 20% of the flow depth (Nezu and Nakagawa, 1993; Graf, 1998; Pokrajac *et al.*, 2006; Dey and Raikar, 2007), this limiting range poses a contradiction difficult to solve: the most relevant values of velocity are those least reliable. In addition, the time required for collecting a full velocity vertical profile (around 30-40 minutes for 8-10 data points) was incompatible with the continuous running of the described experiments, forcing the repetition of partial runs. Thus, an alternative method for obtaining velocity data would have been ideally used. Particle Imagery Velocimetry (PIV) can collect large amounts of data in a matter of seconds, providing a high number of data points per profile, overcoming the issue of data reliability near the bed surface. PIV can also help analyse flow structures and study the forces that act over small areas of the bed (Nelson *et al.*, 1995; McLelland *et al.*, 1999; Campbell *et al.*, 2005; Hager, 2007), contributing to assess lift/drag forces involved in particle entrainment (Dittrich *et al.*, 1996; Wu and Chou, 2003). The increased data density and reliability provided by PIV will also result in more robust analyses of velocity profiles, bed shear stress obtained from the Clauser method and Reynolds stresses (section 3.4.5), and bed roughness parameter (sections 4.2.7 and 4.3.4).

A PIV system was purchased by the Department of Civil Engineering in 2008, however, it could not be fully installed in time to be used for this research work. Further research work should include the use of PIV data for a more robust assessment of the impacts of sub-threshold flows on bed characteristics and flow properties.

6.12 *Estimation of u_*, τ and roughness*

The analysis of streamwise velocity profiles has the primary objective of estimating bed shear stress, bed shear velocity and bed roughness

characteristics. The limitations of the methods available for doing so are added to the constraints of data capturing discussed above. Two of the three main methods for estimating τ (Clauser method and Reynolds stresses) are based on velocity data at a single location (section 3.4.5), the remaining one (depth-slope) includes the average cross sectional properties of the flow. Therefore, they are likely to provide different results (Dey and Raikar, 2007; Piedra *et al.*, 2009). Thus, the estimation of bed shear stress and roughness length should include all three procedures whenever possible, for which velocity data and continuous water depth data are required. This is directly connected to the use of PIV discussed above.

In addition, the suitability of the Law of the Wall and the formulations of the logarithmic profile may be questioned. Reported variability of the von Kárman constant, i.e. not constant, suggested that its value reduces with increasing transport conditions (Dey and Raikar, 2007). Using one formulation or another also has theoretical and practical consequences. Using equation 2-8, which includes k_s and B (section 2.6.1), results in one additional parameter over that of using z_0 (equation 2-9). Grain equivalent roughness k_s is usually determined based on a representative particle size D_{50}, D_{84} or D_{90}, fixing B = 8.5, (Cheng and Chiew, 2003; Recking, 2009), or assuming a value of k_s and obtaining B from data (Stone and Hotchkiss, 2007). However, Graf (1998) and Dey and Raikar (2007) reported values of B within the range 8.5±15% and 6.8-9.62 respectively. These values are rarely considered by researchers when using k_s and B. The use of z_0 is preferred by the author here as its value comes from imposing boundary conditions on the logarithmic law, hence can be directly connected to physical conditions of the flow/bed (Piedra *et al*. 2009), unlike k_s and B that are artificial parameters with no direct physical meaning. Furthermore, the correction for displacement of the zero-plane is often ignored by researchers (Pokrajac *et al*. 2006, Piedra *et al*. 2009). Placing the origin of vertical distance at the bed surface or grain crests may be appropriate for relatively small material where bed surface is approximately uniform; however, for multi-sized poorly sorted beds with large gravels and cobbles this is unlikely. The application of the log-law is further complicated in such beds as velocity data and therefore, parameter derivation, will vary depending on the location of the profile. As data

and parameters are often used to characterise bed and flow conditions, a single profile measurement may not be sufficient. Work on double-averaging (Nikora *et al*. 2007) aims at including spatial variability of velocity data. However, it is still based on relatively small-scale measurements.

The author believes that there is still considerable confusion and uncertainty on the application of the log-law (Bauer *et al*. 1992). Additional work on the range of applicability of the logarithmic profile and a suitable procedure and parameters is required. It is the intention of the author to include this subject in his future work. In particular, continuing with the study of the effect of the depth range used for the application of the log-law ($z/h > 0.2$) initiated during this PhD, which was presented in the 2009 IAHR Congress in Vancouver (Canada). The extension of this work to the relationship between bed grain size characteristics and the velocity range z/h and the link between depth average velocity U and bed shear velocity u_* are also part of the author's research plan.

6.13 *Bed surface composition*

The application of both the visual method and the reference transport methods requires knowledge of bed size distribution: a representative size for the first method and the full size distribution for the second. The method used here, i.e. painting each size class in a different colour, has also been used by others (eg. Wilcock and McArdell, 1993). However, painting and sieving all size classes is completely impractical in the field, and obtaining reliable large-scale spatially distributed bed size distribution data is laborious (Mosley and Tindale, 1985; Fripp and Diplas, 1993; Rice and Church, 1996; Church *et al*., 1987). Thus, painting size fractions is restricted to laboratory experimentation. A number of methodologies and software packages for obtaining automated particle size distribution have been developed over the past few years with apparent success (Lane *et al*., 2001; Carbonneau *et al*., 2003; Sime and Ferguson, 2003; Rubin, 2004; Graham *et al*., 2005a,b; Carbonneau *et al*., 2005). These automated techniques appear to be more appropriate to field work where larger clasts may be more effectively treated by image analysis. One of these packages (Digital Gravelometer, Graham *et al*., 2005a,b) was tested in this research, with

inadequate results. Automated identification of particle sizes using digital images has a major limitation: the bed surface must be dry (Sime and Ferguson, 2003). This makes the methodology inadequate during a large proportion of the year or if continuous sampling is required. Thus, innovative methodologies must be used for obtaining bed size distributions in the field and laboratory. In flume experimentation, the method used in this thesis of painting all size classes and counting a selected number of randomly chosen grains (section 3.4.3) may be combined with the success of the thresholding of grains painted in UV paint to attempt colour thresholding of multiple size classes in the bed to obtain semi-automated grain size distributions of the bed surface.

6.14 *Validating the proposed sediment transport equation*

The analysis of bedload sediment transport equations presented in Chapter 5 showed that the new equation proposed herein outperformed all but one of the selected equations against both flume and field data (only Recking's, 2010 eq. 5 provided similar bedload predictions, section 5.6). However, the range of sediment transport rates tested did not extend far enough into larger transport rates for the linear expression used for the second term of the equation 5-18 to be confirmed. However, comparison of equation results and field data for the Elbow River offered encouraging results. Future flume experiments, similar to the ones carried out for this research, should include larger flows during the stability test in order to generate higher solid transport rates. However, larger transport rates will likely be accompanied by noticeable degradation of the test bed and recirculation/feed set-ups may have to be considered (section 6.6).

In any case, the proposed sediment transport equation should be validated using as many data sets as possible, both flume and field data. Data sets such as those by Shvidchenko (2000) may prove very useful. One considerable advantage of the proposed method is that it does not require previous knowledge of flow history or bed size composition, which, as discussed above, is costly and time consuming. Thus, data sets that only include coupled transport rates and shear stresses are also valid.

6.15 *Using field data*

As noted earlier in the thesis, validating the range of issues discussed herein will require detailed field data. However, this may not be easily attainable, especially the application of flow acceleration rates. Natural rivers are highly variable and replicates of experiments are unlikely. Nonetheless, similar hydrological events may be sufficient to represent the different flow increase rates assessed in the laboratory. Alternatively, larger flumes could be used to scale a range of river channel geometries and bed compositions. Nevertheless, flume experimentation appears to be the most cost-effective approach for the immediate future of studying the effect of acceleration rates and hydrograph shape on entrainment.

6.16 *Unifying bedding-in periods and flow history*

A final issue to be considered is of prime relevance given the evidence of the impact of flow history on entrainment values. As mentioned in this thesis, little experimental work has detailed the history of discharges to which beds were subject prior to entrainment. This may be partly responsible for the scatter observed in the Shields' curve (Chapter 2) and other past data sets, in particular field data sets. Reporting and standardising sub-threshold flows will contribute to better comparison between research data sets and identify the effect of pre-entrainment flows on the mobility of granular beds (Monteith and Pender, 2005).

Chapter 7
Conclusions

"I got this powdered water - now I don't know what to add".-Steven Wright

Summary and Conclusions

The work presented in this thesis, together with previous research (Saadi, 2002; Paphitis and Collins, 2005; Haynes and Pender, 2007; and Haynes and Ockelford, 2008) clearly demonstrates the effect of sub-threshold antecedent flow conditions on the initiation of motion of granular bed entrainment and the changing values of entrainment flows depending on flow history, as suggested by Reid *et al*. (1985) and Reid and Frostick (1986). With this in mind, the way in which sediment transport studies are carried out in the future should consider the flow history element in them. Authors should then report the full flow history of their experiments (including intra-experimental flow reductions for sampling/measurements) in order to determine the comparability of their data to other data sets. More relevant is the implication that past sediment transport studies were likely to have been carried out with different flow magnitudes and durations, which are largely unreported. These differences in experimental procedures may account for some of the scatter frequently found in entrainment threshold values, such as Shields' graph.

Of the four initial research objectives set out in Chapter 1, the first three (quantifying the effect of increasing sub-threshold antecedent flows on bed

stability, studying entrainment mechanisms and investigating the relationship between flow duration and magnitude with changes in τ_{cr}) have been achieved. In the case of the fourth one (correction for bedload equations), entrainment threshold data did not provide a robust enough trend to create a suitable correction due to flow history for bedload transport equations. However, the comparative analysis of bedload equations does suggest that there is potential for the inclusion of values of τ_{cr} that originate from actual solid transport rates, implicitly including the effect of antecedent conditions.

The research presented here focussed only on increasing flow values and durations, which can be associated with rising limbs of river hydrographs of different magnitudes and durations. It is suggested further similar work be carried out using both: (1) other sediment mixtures and full hydrographs; and, (2) multiple hydrographs. The extension to other mixtures should pay particular attention to the different reaction of the same grain size to antecedent conditions, whether it belongs to a uniform, unimodal or bimodal bed. Of particular interest is the further study of the differences between methodologies for entrainment estimation observed in this research.

In summary, the importance of flow history on the entrainment of granular beds has been clearly established, with the effects of flow exposure appearing to be influenced by bed composition and the technique used for estimating critical conditions. Since hydrological regimes are ever changing in most rivers, present and future bed stability must be increasingly related to flow history, particularly when hydrological patterns are likely to be altered by human river regulation and climate change. The consequences of the findings exposed in this thesis are far reaching, affecting future research and current consideration of sediment transport mechanics, as well as policy and river management practices. For instance, predictions of bedload amounts may have to be reviewed if the event studied occurs at the end of the summer, where river beds may have undergone the strengthening process discussed here during periods of low flows. Linked to this effect of seasonality are river engineering works, such as river restorations, where the mobility of the newly laid bed/bank material may be naturally enhanced if the channel is opened at the beginning of the summer. In turn,

these practical elements may be included in related legislation and consideration by regulatory bodies of the timeline of the works proposed. This connection of the research presented here with legislation and guidance provided by regulatory bodies played an important role in the funding agreement with Scottish Natural Heritage (SNH).

Further, as discussed in Chapter 2, the prospects of changes in hydrological patterns due to climate change and river regulation can affect the shape of hydrographs. As demonstrated here, the rates of flow increase and durations of rising limbs will modify the stability of the river bed, which in turn, will alter the amounts of bedload produced (Chapter 4). Thus, potential changes of river channel geometry and solid transport may not only relate to the geomorphological status of river channels, of prime relevance for bodies such as SNH, but can also impact on other more pragmatic areas of river engineering and management such as bridge blocking, reduction of capacity of flood control reservoirs and the success and durability of river diversions and restorations. Thus, this research has ramifications in theoretical and practical research, policy and river practices.

Appendices

Appendices

Appendix 1. Tests with Digital Gravelometer and ImageJ

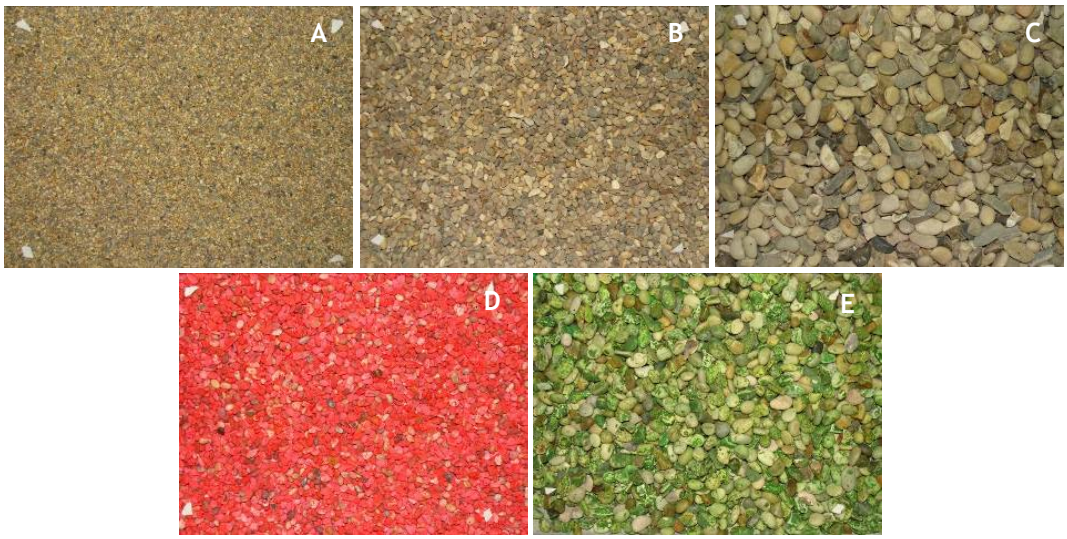

Fig. A-1. Sample images used for testing Digital Gravelometer. A) 1.4-2mm; B) 4-5.6mm; C) 8-11.3mm; D) 4-5.6mm UV red; E) 8-11.3mm UV green. The area marked by white markers on the images corresponds to approx. 200 x 163 mm^2.

Sieve size	Actual composition			Digital Gravelometer results				
(mm)	1.4-2	4-5.6	8-11.3	1.4-2	4-5.6	4-5.6 red	8-11.3	8-11.3 green
0.06				0	0	0	0	0
0.09				0.05	0	0.01	0	0
0.13				0.02	0	0	0	0
0.18				0.08	0.01	0.01	0.01	0.02
0.25				0.43	0.03	0.03	0.03	0.08
0.35				1.66	0.07	0.09	0.07	0.15
0.5				4.17	0.13	0.19	0.18	0.39
0.71				10.42	0.28	0.45	0.32	0.94
1				22.45	0.79	1.19	0.79	2.33
1.41				35.82	2.36	2.75	1.30	4.06
2	100			22.66	5.94	6.46	1.96	6.38
2.83				2.25	15.21	16.31	4.03	12.79
4					40.68	31.56	7.89	17.34
5.66		100			30.30	34.94	14.43	29.07
8					3.91	5.67	24.47	23.88
11.31			100		0.30	0.35	37.80	2.58
16							6.71	

Table A-1. Actual composition for each sediment sample and results of the particle size distribution obtained with DG after parameter optimisation (values from Grid-by-number settings). Values correspond to percentage of total weight in each size class (mm).

Size class (mm)	**1-1.4**	**1.4-2**	**2-2.8**	**2.8-4**	**4-5.6**	**5.6-8**	**8-11.3**	**11.3-16**
Colour	Yellow	White	Light blue	Green	Lilac	Red	Blue	Black
Bulk mix	1	3	5	8	17	40	20	6
Test bed #1								
100 count A	1	6	5	12	21	38	13	4
100 count B	0	4	8	11	25	36	13	3
200 count A	1	4	7	14	24	37	12	2
200 count B	1	4	6	10	25	38	13	4
Test bed #2								
100 count A	0	1	5	8	21	42	17	6
100 count B	0	2	5	8	19	40	20	6
200 count A	0	1	2	8	23	44	16	5
200 count B	1	2	3	9	20	45	16	5
Test bed #3								
100 count A	0	4	4	9	22	41	17	3
100 count B	0	3	6	11	20	41	15	4
200 count A	0	2	5	10	24	39	15	5
200 count B	0	2	5	10	21	40	17	4

Table A-2. Values of f_i for 100 and 200 particle counts.

Appendix 2. Test hydrographs and sampling sequences

					AccRate1	AccRate2	AccRate3	AccRate4	AccRate5
				Duration (h)	0.5	1	2	4	6
Phase	Sampling	Hz	Q (l/s)[1]	Depth (mm)	time step (sec)	time step (sec)	time step (sec)	time step (sec)	time step (sec)
Flume filling		14	4.1	23.7	180	180	180	180	180
Settling period		16	10.4	35.2	1800	1800	1800	1800	1800
Antecedent Conditions hydrograph		16.3	11.4	36.8	75	150	300	600	900
		16.6	12.3	38.5	75	150	300	600	900
		16.9	13.3	40.1	75	150	300	600	900
		17.2	14.2	41.7	75	150	300	600	900
		17.5	15.2	43.3	75	150	300	600	900
		17.8	16.1	44.9	75	150	300	600	900
		18.1	17.1	46.4	75	150	300	600	900
		18.4	18.0	47.9	75	150	300	600	900
		18.7	19.0	49.5	75	150	300	600	900
		19	19.9	51.0	75	150	300	600	900
		19.3	20.9	52.4	75	150	300	600	900
		19.6	21.8	53.9	75	150	300	600	900
		19.9	22.8	55.4	75	150	300	600	900
		20.2	23.7	56.8	75	150	300	600	900
		20.5	24.7	58.2	75	150	300	600	900
		20.8	25.6	59.6	75	150	300	600	900
		21.1	26.6	61.0	75	150	300	600	900
		21.4	27.5	62.3	75	150	300	600	900
		21.7	28.5	63.7	75	150	300	600	900
		22	29.4	65.0	75	150	300	600	900
		22.3	30.4	66.3	75	150	300	600	900
		22.6	31.3	67.6	75	150	300	600	900

		22.9	32.3	68.9	75	150	300	600	900
		23.2	33.2	70.1	75	150	300	600	900
	PMV	23.5	34.2	71.3	240	240	240	240	240
Mobility test sequence	PMV	24.5	37.4	75.3	240	240	240	240	240
	PMV	25.5	40.5	79.1	240	240	240	240	240
	PMV	26.5	43.7	82.7	240	240	240	240	240
	PMV	27.5	46.9	86.1	240	240	240	240	240
	PMV	28.5	50.0	89.4	240	240	240	240	240
	PMV	29.5	53.2	92.4	240	240	240	240	240
	PMV	30.5	56.4	95.2	240	240	240	240	240

PMV: particle movement video.

Table A-3. Test hydrograph and sampling sequences for Pilot Runs.

(1) Flow steps were controlled by the programming of the signal inverter controlling the pump and therefore, smooth rising limbs were achieved. Once the self-control pump system was installed (section 3.2.3) programming of flow stages was no longer possible and the number of flow steps was reduced for manual control in the remaining of the experimental work.

Phase	Sampling			AccRate1	AccRate2	AccRate3	AccRate4	AccRate5	AccRate6
			Duration (h)	0.5	1	2	4	6	10
		Q (l/s)	depth (mm)	t (min)	t (min)	t (min)	t (min)	t (min)	t (min)
Settling period		12	33.8	0	0	0	0	0	0
	BIW	12	33.8	30	30	30	30	30	30
Antecedent conditions hydrograph		15.25	38.1	30	30	30	30	30	30
		18.5	42.3	36	42	54	78	102	150
		21.75	46.3	42	54	78	126	174	270
	BIW, BLS, PMV	25	50.2	48	66	102	174	246	390
	BIW, BLS, PMV	28.25	54.0	54	78	126	222	318	510
Mobility test sequence	BIW, BLS, PMV	31.5	57.6	**60**	**90**	**150**	**270**	**390**	**630**
	BIW, BLS, PMV	35	61.3	66	96	156	276	396	636
	BIW, BLS, PMV	40	66.4	72	102	162	282	402	642
	BIW, BLS, PMV	45	71.1	78	108	168	288	408	648
	BIW, BLS, PMV	50	75.6	84	114	174	294	414	654

BIW: bed images (white light); BIUV: bed images (UV light); BLS: bedload sample; PMV: particle movement video.

Table A-4. Test hydrograph sequence for Stage 1.

Phase	Sampling					AccRate 1H-1L	AccRate 2H-2L	AccRate 3H-3L	AccRate 5H-5L
		Duration (h)				0.5	1	2	6
		QH (l/s)	depth (mm)	QL (l/s)	depth (mm)	t (min)	t (min)	t (min)	t (min)
Settling period		12	33.8	12	33.8	0	0	0	0
	BIW, BIUV	12	33.8	12	33.8	30	30	30	30
Antecedent conditions hydrograph	BIUV	15.7	38.7	14.8	37.5	30	30	30	30
	BIUV	19.3	43.3	17.7	41.3	36	42	54	102
	BIUV	23.0	47.8	20.5	44.8	42	54	78	174
	BIW, BIUV, BLS, PMV	26.7	52.2	23.3	48.2	48	66	102	246
	BIW, BIUV, BLS, PMV	30.4	56.4	26.2	51.6	54	78	126	318
Mobility test sequence	BIW, BIUV, BLS, PMV	34	60.3	29.0	54.8	**60**	**90**	**150**	**390**
	BIW, BIUV, BLS, PMV	35	61.3	35	61.3	66	96	156	396
	BIW, BIUV, BLS, PMV	40	66.4	40	66.4	72	102	162	402
	BIW, BIUV, BLS, PMV	45	71.1	45	71.1	78	108	168	408
	BIW, BIUV, BLS, PMV	50	75.6	50	75.6	84	114	174	414

BIW: bed images (white light); BIUV: bed images (UV light); BLS: bedload sample; PMV: particle movement video

Table A-5. Test hydrograph sequence for Stage 2.

Phase	Sampling		AccRate1	AccRate3	AccRate5
		Duration (h)	0.5	2	6
		AccRate (l/s/s)	0.0096	0.0024	0.0008
		Q (l/s)	t (min)	t (min)	t (min)
Settling period		12	0	0	0
		12	30	30	30
Antecedent conditions hydrograph		14.9	30	30	30
		14.9	36	54	102
		17.7	42	78	174
		20.6	48	102	246
	BLS, PMV	23.5	54	126	318
	BLS, PMV	26.3	60	150	390
Mobility test sequence	BLS, PMV	29.2	60	150	390
	BLS, PMV	35	64	154	394
	BLS, PMV	40	68	158	398
	BLS, PMV	40	72	162	402
	BLS, PMV	45	76	166	406
	BLS, PMV	50	80	170	410

BLS: bedload sample; PMV: particle movement video

Table A-6. Test hydrograph sequence for Uniform gravel.

Appendix 3. Summary of experimental runs and hydraulic conditions

Exp. No.	Exp. series	Test group	Duration of antecedent conditions (h)	Acceleration rate (l/s/s)	Rep.	QADV (l/s) [1]
Pilot Runs						
1		Q_{ref}	-	-	1	
2					2	
3					3	
4		AccRate1	0.5	0.0129	1	
5					2	
6					3	
7		AccRate2	1	0.0064	1	
8					2	
9					3	
10		AccRate3	2	0.0032	1	
11					2	
12					3	
13		AccRate4	4	0.0016	1	
14					2	
15					3	
16		AccRate5	6	0.0011	1	
17					2	
18					3	
Repetition of partial run to obtain velocity data at threshold flow						
19		Q_{ref}	-		1	35.6
20					2	
21		AccRate1	0.5		1	40.8
22					2	
23		AccRate2	1		1	38.8
24					2	
25		AccRate3	2		1	42.5
26					2	
27		AccRate4	4		1	45.1
28					2	
29		AccRate5	6		1	44.9
30					2	
Stage 1						
31		Q_{ref}	-	-	1	
32					2	
33					3	
34		AccRate1	0.5	0.01083	1	
35					2	
36					3	
37		AccRate2	1	0.00542	1	
38					2	
39		AccRate3	2	0.00271	1	
40					2	
41		AccRate4	4	0.00135	1	
42					2	
43					3	
44		AccRate5	6	0.0009	1	

45				2	
46	AccRate6	10	0.00054		
	Repetition of partial run to obtain velocity data				
47	AccRate1			1	12A, 12B, 31.5
48				2	12A, 12B, 31.5
49	AccRate3			1	12A, 12B, 31.5
50				2	12A, 12B, 31.5
51	AccRate5			1	12A, 12B, 31.5
	Stage 2				
52	AR1H	0.5	0.0122	1	
53	AR1L	0.5	0.0094	1	
54	AR2H	1	0.0061	1	
55				2	
56	AR2L	1	0.0047	1	
57				2	
58	AR3H	2	0.0031	1	
59				2	
60	AR3L	2	0.0024	1	
61				2	
62	AR5H	6	0.001	1	
63	AR5L	6	0.0008	1	
	Uniform gravel				
64	Q_{ref}	-	-	1	
65				2	
66				3	
67	AccRate1	0.5	0.0096	1	
68				2	
69	AccRate3	2	0.0024	1	
70				2	
71	AccRate5	6	0.0008	1	
72				2	
	Repetition of partial run to obtain velocity data				
73	AccRate1		0.0096	1	12A, 12B, 29.2
74	AccRate3		0.0024	1	12A, 12B, 29.2
75				2	12A, 12B, 29.2
76	AccRate5		0.0008	1	12A, 12B, 29.2

(1) Discharge (l/s) at which velocity data were obtained with ADV
(2) Hydraulic conditions of each experiment are summarised in the table below due the multiplicity of flow stages in each run.

Table A-7. Summary of experimental runs.

Inverter freq. (Hz)	*Q* (l/s)	Slope (m/m)	aver*H* (m)	*V* (= Q/wet area) (m/s)	τ (Pa)	u_* (m/s)
Pilot Runs						
16	10.4	0.005	0.035	0.33	1.69	0.041
17.5	15.1	0.005	0.043	0.39	2.07	0.046
19.6	21.8	0.005	0.054	0.45	2.56	0.051
21.7	28.4	0.005	0.064	0.50	3.01	0.055
22.6	31.3	0.005	0.068	0.51	3.19	0.057
23.2	33.2	0.005	0.070	0.53	3.31	0.058
23.5	34.1	0.005	0.071	0.53	3.36	0.058
24.5	37.3	0.005	0.075	0.55	3.55	0.060
25.5	40.5	0.005	0.079	0.57	3.72	0.061
26.5	43.6	0.005	0.083	0.59	3.88	0.062
27.5	46.8	0.005	0.086	0.60	4.03	0.064
28.5	50.0	0.005	0.089	0.62	4.17	0.065
29.5	53.1	0.005	0.092	0.64	4.31	0.066
30.5	56.3	0.005	0.095	0.66	4.43	0.067
Stage 1						
-	12	0.0067	0.034	0.40	2.16	0.047
-	15	0.0067	0.038	0.44	2.41	0.049
-	20	0.0067	0.044	0.50	2.80	0.053
-	25	0.0067	0.050	0.55	3.18	0.056
-	28.25	0.0067	0.054	0.58	3.41	0.058
-	30	0.0067	0.056	0.60	3.53	0.059
-	31.5	0.0067	0.058	0.61	3.63	0.060
-	35	0.0067	0.061	0.63	3.85	0.062
-	40	0.0067	0.066	0.67	4.16	0.065
-	45	0.0067	0.071	0.70	4.44	0.067
-	50	0.0067	0.076	0.74	4.71	0.069
Stage 2						
-	12	0.0067	0.034	0.39	2.16	0.047
-	14.8	0.0067	0.038	0.44	2.39	0.049
-	15.7	0.0067	0.039	0.45	2.47	0.050
-	17.7	0.0067	0.041	0.48	2.63	0.051
-	19.3	0.0067	0.043	0.50	2.75	0.053
-	20.5	0.0067	0.045	0.51	2.84	0.053
-	23	0.0067	0.048	0.53	3.03	0.055
-	23.3	0.0067	0.048	0.54	3.05	0.055
-	26.2	0.0067	0.052	0.56	3.26	0.057
-	26.7	0.0067	0.052	0.57	3.30	0.057
-	29	0.0067	0.055	0.59	3.46	0.059
-	30.4	0.0067	0.056	0.60	3.56	0.060
-	34	0.0067	0.060	0.63	3.79	0.062
-	35	0.0067	0.061	0.63	3.86	0.062
-	40	0.0067	0.066	0.67	4.17	0.065
-	45	0.0067	0.071	0.70	4.45	0.067
-	50	0.0067	0.076	0.74	4.71	0.069
Uniform gravel						
-	15	0.0067	0.034	0.50	2.13	0.021
-	17.7	0.0067	0.037	0.53	2.35	0.023
-	20	0.0067	0.040	0.56	2.53	0.025
-	20.6	0.0067	0.041	0.56	2.58	0.026
-	23.5	0.0067	0.044	0.59	2.80	0.028
-	25	0.0067	0.046	0.60	2.91	0.029

-	26.3	0.0067	0.048	0.61	3.00	0.030
-	29.2	0.0067	0.051	0.64	3.20	0.032
-	30	0.0067	0.052	0.64	3.26	0.033
-	35	0.0067	0.057	0.68	3.59	0.036
-	40	0.0067	0.062	0.71	3.89	0.039
-	45	0.0067	0.067	0.74	4.18	0.042
-	50	0.0067	0.072	0.78	4.44	0.044

Table A-8. Hydraulic conditions of all runs.

Appendix 4. Entrainment threshold data sets

AccRate	Duration (h)	AccRate (l/s/s)	Q_{cr} (l/s)			Q_{cr} [(1)] (l/s)	Q_{cr} [(2)] (l/s)	diff [(3)] (%)
			Rep.1	Rep.2	Rep.3			
Reference	--	--	38.77 [1]	34.50 [2]	39.63 [3]	37.41	35.6	5.14
AccRate1	0.5	0.0127	41.05 [4]	44.01 [5]	38.87 [6]	41.31	40.8	1.26
AccRate2	1	0.0064	37.55 [7]	36.77 [8]	45.07 [9]	39.80	38.8	2.49
AccRate3	2	0.0032	41.89 [10]	42.34 [11]	44.06 [12]	42.77	42.5	0.70
AccRate4	4	0.0016	46.28 [13]	44.38 [14]	46.50 [15]	45.72	45.1	1.38
AccRate5	6	0.0011	44.39 [16]	45.04 [17]	47.21 [18]	45.54	44.9	1.44

[(1)] Average all repetitions
[(2)] Fitting to average data
[(3)] Difference between (1) and (2)

Table A-9. Entrainment flows for Pilot Runs. Numbers between square brackets are the run number (Table A-7).

	Qref	AccRate1	AccRate2	AccRate3	AccRate4	AccRate5	AccRate6
Duration (h)	0	0.5	1	2	4	6	10
AccRate (l/s/s)	--	0.01083	0.00542	0.00271	0.00135	0.0009	0.00054
	Parker *et al.* (1982a)						
	Critical flow (l/s)						
R1	26.5 [31]	25.8 [34]	29.1 [37]	30.3 [39]	27.3 [41]	25.8 [44]	25.7 [46]
R2	30.3 [32]	29.4 [35]	26.5 [38]	31.1 [40]	32.7 [42]	27.3 [45]	
R3	31.1[33]	29.6 [36]					
Adopted	30.7	29.5	27.8	30.7	30.0	26.5	25.7
	Critical bed shear stress (Pa)						
R1	3.29	3.24	3.47	3.55	3.34	3.24	3.23
R2	3.55	3.49	3.29	3.60	3.71	3.34	
R3	3.60	3.50			3.13		
Adopted	3.58	3.49	3.38	3.58	3.52	3.29	3.23
	Shvidchenko *et al.* (2001)						
R1	34.3	34.3	37.7	39.4	34.3	32.2	32.7
R2	36.0	35.6	32.7	39.4	41.1	33.4	
R3	42.9	37.8			30.4		
Adopted	39.4	36.7	35.2	39.4	37.7	32.8	32.7
	Yalin (1977)						
R1	25.0	--	31.6	29.4	29.8	30.2	28.7
R2	26.3	25.2	25.4	29.1	30.6	30.0	
R3	28.9	32.9					
Adopted	27.6	29.1	28.5	29.3	30.2	30.1	28.7
Fitting to average data	28.4	28.7	28.1	29.2	31.9	31.2	28.7

Table A-10. Entrainment flows and bed shear stress (RTM-P only). Stage 1. Numbers between square brackets are the run number (Table A-7).

	Qref				AccRate1			AccRate2		
Size class (mm)	R1 [31]	R2 [32]	R3 [33]	average	R2 [35]	R3 [36]	average	R1 [37]	R2 [38]	average
1-1.4	(1)	(1)	(1)	(1)	(1)	(1)	(1)	(1)	(1)	(1)
1.4-2	3.47	3.60	3.34	3.47	3.22	3.99	3.60		3.60	3.60
2-2.8	3.38	3.60	3.63	3.61	3.45	3.67	3.56	3.38	3.34	3.36
2.8-4	3.40	3.60	3.86	3.73	3.50	3.65	3.58	3.55	3.24	3.40
4-5.6	3.38	3.63	3.78	3.70	3.46	3.63	3.54	3.56	3.34	3.45
5.6-8	3.29	3.55	3.60	3.58	3.49	3.50	3.49	3.47	3.29	3.38
8-11.3	3.29	3.53	3.58	3.56	3.50	3.50	3.50	3.39	3.29	3.34
11.3-16	3.61	3.61	3.72	3.67	3.72	3.84	3.78	3.78	3.74	3.76

	AccRate3			AccRate4			AccRate5			AccRate6
Size class (mm)	R1 [39]	R2 [40]	average	R1 [41]	R2 [42]	average	R1 [44]	R2 [45]	average	R1 [46]
1-1.4	(1)	(1)	(1)	(1)	(1)	(1)	(1)	(1)	(1)	(1)
1.4-2	4.06	(1)	4.06	3.68	(1)	3.68	3.81	3.86	3.83	(2)
2-2.8	3.52	3.99	3.76	3.45	4.10	3.78	3.34	3.49	3.41	(2)
2.8-4	3.55	3.96	3.76	3.50	4.12	3.81	3.34	3.50	3.42	(2)
4-5.6	3.70	3.92	3.81	3.49	4.07	3.78	3.29	3.45	3.37	(2)
5.6-8	3.55	3.60	3.58	3.34	3.76	3.55	3.24	3.34	3.29	3.23
8-11.3	3.65	3.58	3.61	3.39	3.72	3.56	3.29	3.29	3.29	(2)
11.3-16	3.74	3.76	3.75	3.49	3.90	3.70	3.82	3.72	3.77	(2)

(1) Bedload was zero for this size class and run.
(2) Only bed shear stress for the modal class was obtained.

Table A-11. Critical bed shear stress for all size classes (RTM-P only). Stage 1. Numbers between square brackets are the run number (Table A-7).

	AccRate1H	AccRate1L	AccRate2H	AccRate2L	AccRate3H	AccRate3L	AccRate5H	AccRate5L
Duration (h)	0.5	0.5	1	1	2	2	6	6
Target flow Q_t (l/s)	34	29	34	29	34	29	34	29
AccRates (l/s/s)	0.0122	0.0094	0.0061	0.0047	0.0031	0.0024	0.0010	0.0008
Parker *et al*. (1982a)								
Q_{cr} (l/s)								
R1	25.8 [52]	25.9 [53]	28.8 [54]	28.8 [56]	31.1 [58]	26.6 [60]	24.4 [62]	25.2 [63]
R2			29.2 [55]	29.1 [57]	28.1 [59]	27.6 [61]		
Average all repetitions	**25.8**	**25.9**	**29.0**	**28.9**	**29.6**	**27.1**	**24.4**	**25.2**
τ_{cr} (Pa)								
R1	3.23	3.24	3.45	3.45	3.60	3.29	3.13	3.19
R2			3.48	3.47	3.40	3.36		
Average all repetitions	3.23	3.24	3.46	3.46	3.50	3.33	3.13	3.19
Shvidchenko *et al*. (2001)								
Q_{cr} (l/s)								
R1	33.1	31.6	31.1	36.3	37.2	33.6	27.2	31.2
R2			35.6	35.5	34.4	35.2		
Average all repetitions	33.1	31.6	33.3	35.9	35.8	34.4	27.2	31.2
Yalin (1977)								
Q_{cr} (l/s)								
R1	18.7	28.4	30.8	25.2	34.1	27.6	28.0	28.3
R2			28.8	26.7	30.0	24.8		
Average all repetitions	18.7	28.4	29.8	25.9	32.1	26.2	28.0	28.3
Fitting to average data	18.7	28.4	29.7	25.9	31.1	25.8	28.0	28.3

Table A-12. Entrainment flows and bed shear stress. Stage 2. Numbers between square brackets are the run number (Table A-7).

	AccRate1H	AccRate1L	AccRate2H			AccRate2L		
Duration (h)	0.5	0.5	1			1		
Acceleration rate (l/s/s)	0.0122	0.0094	0.0061			0.0047		
Size class (mm)	R1 [52]	R1 [53]	R1 [54]	R2 [55]	**average**	R1 [56]	R2 [57]	**average**
1-1.4	(1)	(1)	(1)	(1)	(1)	(1)	(1)	(1)
1.4-2	(1)	(1)	3.73		**3.73**	3.86	3.50	**3.68**
2-2.8	2.72	3.20	3.45	3.34	**3.40**	3.67	3.45	**3.56**
2.8-4	3.34	3.19	3.45	3.50	**3.47**	3.65	3.47	**3.56**
4-5.6	3.34	3.27	3.49	3.56	**3.52**	3.63	3.52	**3.58**
5.6-8	3.23	3.24	3.45	3.48	**3.46**	3.45	3.47	**3.46**
8-11.3	3.14	3.21	3.36	3.43	**3.39**	3.36	3.36	**3.36**
11.3-16	3.37	3.41	3.72	3.68	**3.70**	3.59	3.61	**3.60**

	AccRate3H			AccRate3L			AccRate5H	AccRate5L
Duration (h)	2			2			6	6
Acceleration rate (l/s/s)	0.0031			0.0024			0.0010	0.0008
Size class (mm)	R1 [58]	R2 [59]	**average**	R1 [60]	R2 [61]	**average**	R1 [62]	R1 [63]
1-1.4	(1)	(1)	(1)	(1)	(1)	(1)	(1)	(1)
1.4-2	(1)	(1)	(1)	2.96	(1)	**2.96**	(1)	(1)
2-2.8	3.56	3.38	**3.47**	3.20	3.63	**3.41**	3.05	3.01
2.8-4	3.76	3.55	**3.65**	3.34	3.55	**3.45**	3.22	3.19
4-5.6	3.70	3.49	**3.60**	3.34	3.49	**3.41**	3.27	3.27
5.6-8	3.60	3.40	**3.50**	3.29	3.36	**3.33**	3.13	3.19
8-11.3	3.53	3.36	**3.45**	3.21	3.36	**3.29**	3.12	3.21
11.3-16	3.76	3.55	**3.66**	3.61	3.61	**3.61**	3.10	3.45

(1) Bedload was zero for this size class and run

Table A-13. Critical bed shear stress for all size classes (RTM-P only). Stage 2. Numbers between square brackets are the run number (Table A-7).

	Q_{ref}	AccRate1	AccRate3	AccRate5
Duration (h)	0	0.5	2	6
Acc rates (l/s/s)	--	0.0096	0.0024	0.0008
	Critical flow RTM (Parker *et al.*, 1982a) (l/s)			
R1	30.1 [64]	28.6 [67]	29.0 [69]	29.6 [71]
R2	28.5 [65]	28.5 [68]	26.9 [70]	29.0 [72]
R3	29.0 [66]			
Average	29.2	28.6	28.0	29.3
	Critical shear stress RTM (Parker *et al.*, 1982a) (Pa)			
R1	3.27	3.16	3.19	3.23
R2	3.16	3.16	3.05	3.19
R3	3.19			
Average	3.21	3.16	3.12	3.21
	Critical flow RTM (Shvidchenko *et al.*, 2001) (l/s)			
R1	32.3	31.2	32.3	32.3
R2	31.2	31.2	31.2	32.3
R3	31.8			
Average	31.8	31.2	31.8	32.3
	Critical flow (Yalin, 1977) (l/s)			
R1	21.2	20.4	24.9	25.1
R2	20.6	21.7	24.9	25.8
R3	21.1			
Fitting average values	20.8	21.0	24.9	25.1

Table A-14. Entrainment thresholds for uniform gravel runs. Numbers between square brackets are the run number (Table A-7).

Appendix 5. Bed surface composition data sets

	Qref			AccRate1			AccRate2		AccRate3		AccRate4		AccRate5		AccRate6
	R1 [31]	R2 [32]	R3 [33]	R1 [34]	R2 [35]	R3 [36]	R1 [37]	R2 [38]	R1 [39]	R2 [40]	R1 [41]	R2 [42]	R1 [44]	R2 [45]	R1 [46]
Size range (mm)	**Bed surface composition of initial beds (% finer than)**														
1-1.4	0%	0%	0%	0%	0%	0%	0%	0%	0%	0%	0%	0%	0%	0%	0%
1.4-2	0%	0%	0%	0%	0%	0%	0%	0%	0%	0%	0%	0%	0%	0%	0%
2-2.8	1%	2%	2%	1%	2%	2%	2%	1%	1%	2%	2%	2%	2%	2%	1%
2.8-4	5%	6%	6%	4%	5%	5%	3%	5%	3%	5%	5%	6%	5%	6%	4%
4-5.6	14%	13%	15%	13%	14%	14%	12%	15%	10%	13%	16%	13%	13%	15%	13%
5.6-8	38%	36%	33%	35%	34%	32%	30%	33%	37%	35%	39%	34%	34%	40%	37%
8-11.3	78%	79%	77%	80%	77%	78%	76%	78%	77%	75%	83%	79%	76%	80%	78%
11.3-16	94%	96%	94%	97%	94%	96%	94%	94%	96%	93%	96%	94%	95%	96%	94%
16-22	100%	100%	100%	100%	100%	100%	100%	100%	100%	100%	100%	100%	100%	100%	100%
	Key particle sizes (mm)														
D_{16}	4.14	4.19	4.09	4.20	4.13	4.20	4.37	4.12	4.37	4.24	4.00	4.21	4.24	4.07	4.23
D_{50}	6.32	6.38	6.54	6.39	6.48	6.53	6.64	6.50	6.37	6.48	6.21	6.47	6.49	6.19	6.38
D_{84}	9.29	8.98	9.42	8.76	9.30	9.05	9.46	9.20	9.23	9.58	8.30	9.11	9.37	8.87	9.21
D_{90}	10.54	10.10	10.58	9.96	10.49	10.16	10.59	10.49	10.29	10.69	9.79	10.37	10.44	10.05	10.43
σ_g	1.50	1.46	1.52	1.44	1.50	1.47	1.47	1.49	1.45	1.50	1.44	1.47	1.49	1.48	1.48

Table A-15. Bed surface composition of Initial bed. Stage 1. Numbers between square brackets are the run number (Table A-7).

	Qref [1]			AccRate1			AccRate2		AccRate3		AccRate4		AccRate5		AccRate6
	R1 [31]	R2 [32]	R3 [33]	R1 [34]	R2 [35]	R3 [36]	R1 [37]	R2 [38]	R1 [39]	R2 [40]	R1 [41]	R2 [42]	R1 [44]	R2 [45]	R1 [46]
Size range (mm)	**Bed surface composition of bed at Q = 31.5 l/s (% finer than)**														
1-1.4				0%	0%	0%	0%	0%	0%	0%	0%	0%	0%	0%	0%
1.4-2				0%	0%	0%	0%	0%	0%	0%	0%	0%	0%	0%	0%
2-2.8				1%	0%	0%	1%	0%	1%	1%	1%	2%	1%	1%	0%
2.8-4				4%	4%	4%	3%	3%	3%	3%	5%	6%	2%	5%	2%
4-5.6				11%	10%	9%	10%	9%	9%	9%	14%	11%	8%	9%	11%
5.6-8				35%	33%	26%	28%	30%	29%	31%	32%	31%	27%	29%	36%
8-11.3				77%	78%	73%	71%	75%	77%	77%	78%	78%	76%	76%	81%
11.3-16				96%	93%	91%	92%	94%	95%	96%	95%	95%	96%	93%	95%
16-22				100%	100%	100%	100%	100%	100%	100%	100%	100%	100%	100%	100%
	Key particle sizes (mm)														
D_{16}				4.31	4.41	4.67	4.53	4.51	4.59	4.51	4.16	4.40	4.69	4.53	4.30
D_{50}				6.46	6.50	6.84	6.83	6.66	6.66	6.59	6.53	6.57	6.74	6.66	6.34
D_{84}				9.15	9.36	10.05	10.09	9.52	9.26	9.21	9.16	9.17	9.37	9.59	8.68
D_{90}				10.19	10.67	11.16	11.04	10.57	10.34	10.28	10.31	10.28	10.35	10.78	10.05
σ_g				1.46	1.46	1.47	1.49	1.45	1.42	1.43	1.48	1.44	1.41	1.45	1.42

[1] No data as this series did not include Q = 31.5 l/s

Table A-16. Bed surface composition of beds at target flow Q_t. Stage 1. Numbers between square brackets are the run number (Table A-7).

	AccRate1H	AccRate1L	AccRate2H		AccRate2L		AccRate3H		AccRate3L		AccRate5H	AccRate5L
	R1 [52]	R1 [53]	R1 [54]	R2 [55]	R1 [56]	R2 [57]	R1 [58]	R2 [59]	R1[(1)][60]	R2 [61]	R1 [62]	R1 [63]
Size range (mm)	**Bed surface composition of initial beds (% finer than)**											
1-1.4	0%	0%	0%	0%	0%	0%	0%	0%	-	0%	0%	0%
1.4-2	0%	0%	0%	0%	0%	0%	0%	0%	-	0%	0%	0%
2-2.8	0%	0%	1%	1%	3%	1%	0%	1%	-	0%	0%	0%
2.8-4	2%	2%	7%	4%	7%	3%	2%	5%	-	2%	4%	2%
4-5.6	15%	12%	17%	11%	16%	12%	11%	13%	-	11%	15%	11%
5.6-8	39%	35%	42%	37%	36%	37%	32%	35%	-	35%	38%	33%
8-11.3	84%	81%	77%	79%	81%	79%	80%	80%	-	79%	82%	83%
11.3-16	96%	97%	96%	96%	95%	94%	96%	96%	-	94%	98%	98%
16-22	100%	100%	100%	100%	100%	100%	100%	100%	-	100%	100%	100%
	Key particle sizes (mm)											
D_{16}	4.05	4.28	3.84	4.31	4.02	4.27	4.36	4.22	-	4.32	4.09	4.35
D_{50}	6.18	6.38	6.15	6.36	6.36	6.34	6.50	6.42	-	6.43	6.27	6.41
D_{84}	8.11	8.67	9.19	8.96	8.71	9.03	8.79	8.88	-	9.10	8.42	8.31
D_{90}	9.69	9.89	10.28	10.12	10.10	10.39	10.02	10.10	-	10.41	9.69	9.63
σ_g	1.41	1.42	1.55	1.44	1.47	1.45	1.42	1.45	-	1.45	1.43	1.38

(1) No images available

Table A-17. Bed surface composition of Initial bed. Stage 2. Numbers between square brackets are the run number (Table A-7).

	AccRate1H	AccRate1L	AccRate2H		AccRate2L		AccRate3H		AccRate3L		AccRate5H	AccRate5L
	R1 [52]	R1 [53]	R1 [54]	R2 [55]	R1 [56]	R2 [57]	R1 [58]	R2 [59]	R1 [60]	R2 [61]	R1 [62]	R1 [63]
Size range (mm)	**Bed surface composition of initial beds (% finer than)**											
1-1.4	0%	0%	0%	0%	0%	0%	0%	0%	0%	0%	0%	0%
1.4-2	0%	0%	0%	0%	0%	0%	0%	0%	0%	0%	0%	0%
2-2.8	0%	0%	2%	0%	1%	0%	0%	0%	0%	0%	0%	0%
2.8-4	5%	0%	7%	2%	2%	5%	3%	4%	4%	4%	1%	2%
4-5.6	12%	7%	16%	10%	8%	17%	8%	12%	13%	12%	13%	11%
5.6-8	37%	30%	39%	35%	32%	37%	30%	37%	37%	38%	38%	34%
8-11.3	79%	79%	83%	78%	78%	82%	77%	80%	80%	79%	81%	85%
11.3-16	96%	98%	98%	96%	96%	96%	97%	95%	97%	96%	96%	98%
16-22	100%	100%	100%	100%	100%	100%	100%	100%	100%	100%	100%	100%
	Key particle sizes (mm)											
D_{16}	4.25	4.62	3.97	4.39	4.51	3.94	4.57	4.25	4.21	4.23	4.21	4.35
D_{50}	6.34	6.59	6.19	6.45	6.54	6.31	6.61	6.34	6.33	6.31	6.26	6.35
D_{84}	9.00	8.89	8.32	9.17	9.16	8.54	9.14	8.88	8.77	9.03	8.68	7.79
D_{90}	10.16	9.95	9.64	10.27	10.26	9.88	10.14	10.26	9.94	10.19	9.96	9.30
σ_g	1.46	1.39	1.45	1.44	1.42	1.47	1.41	1.45	1.44	1.46	1.44	1.34

Table A-18. Bed surface composition of beds at target flow Q_t. Stage 2. Numbers between square brackets are the run number (Table A-7).

Appendix 6. Bedload rates

	τ_{cr} (Pa)	Q (ls)	Total transport rate (kg/m/s)						
			Qref	AccRate1	AccRate2	AccRate3	AccRate4	AccRate5	AccRate6
Repetition 1	3.18	25	1.39E-04		9.10E-05	3.86E-05	2.31E-05	1.70E-05	8.18E-06
	3.41	28.25			1.16E-04	5.40E-05	5.56E-05	5.30E-05	3.98E-05
	3.53	30	2.16E-04	6.48E-04					
	3.63	31.5		8.27E-04	2.33E-04	1.14E-04	2.19E-04	2.47E-04	2.19E-04
	3.86	35	8.02E-04	1.38E-03	3.67E-04	2.28E-04	6.45E-04	1.36E-03	1.35E-03
	4.17	40	3.13E-03	4.35E-03	1.22E-03	1.15E-03	2.62E-03	4.85E-03	7.46E-03
	4.45	45	5.46E-03	8.79E-03	4.54E-03	2.30E-03	4.06E-03	6.34E-03	1.12E-02
	4.71	50	7.77E-03		1.10E-02	3.77E-03	6.49E-03	9.73E-03	1.39E-02
Repetition 2	3.18	25	1.85E-04	2.07E-04	6.48E-05	1.54E-05	1.00E-05	1.49E-05	
	3.41	28.25		3.27E-04	1.03E-04	1.39E-05	5.40E-06	2.96E-05	
	3.53	30	7.41E-05						
	3.63	31.5		1.82E-04	2.62E-04	4.94E-05	1.54E-05	1.54E-04	
	3.86	35	1.48E-04	3.89E-04	1.31E-03	8.02E-05	4.63E-05	7.16E-04	
	4.17	40	9.41E-04	1.59E-03	3.93E-03	6.45E-04	4.04E-04	3.83E-03	
	4.45	45	3.80E-03	4.33E-03	6.98E-03	2.28E-03	1.17E-03	6.24E-03	
	4.71	50	1.09E-02	1.01E-02	7.49E-03	5.90E-03	3.21E-03	1.15E-02	
Repetition 3	3.18	25	1.20E-04	1.17E-04			3.05E-05		
	3.41	28.25		6.48E-05			2.82E-04		
	3.53	30	8.33E-05						
	3.63	31.5		9.26E-05			9.04E-04		
	3.86	35	2.01E-04	8.02E-05			3.20E-03		
	4.17	40	4.91E-04	8.55E-04			7.65E-03		
	4.45	45	1.70E-03	4.72E-03			9.80E-03		
	4.71	50	1.66E-02	1.14E-02			1.22E-02		

Table A-19. Bedload transport rates. Stage 1. For run number refer to Table A-7.

	τ_{cr} (Pa)	Q (l/s)	Total transport rate (kg/m/s)			
			AccRate1H	AccRate2H	AccRate3H	AccRate5H
Repetition 1	3.30	26.7	1.60E-04	1.81E-04	3.63E-05	9.85E-05
	3.56	30.4	3.52E-04	1.67E-04	3.47E-05	5.20E-04
	3.79	34	2.29E-03	3.95E-04	1.39E-04	1.39E-03
	3.86	35	1.84E-03	5.93E-04	1.70E-04	1.43E-03
	4.17	40	4.24E-03	1.73E-03	9.20E-04	5.91E-03
	4.45	45	6.82E-03	4.00E-03	2.28E-03	1.08E-02
	4.71	50	1.17E-02	8.30E-03	4.51E-03	1.40E-02
Repetition 2	3.30	26.7		6.64E-05	8.72E-05	
	3.56	30.4		1.42E-04	1.42E-04	
	3.79	34		5.37E-04	3.40E-04	
	3.86	35		4.23E-04	5.59E-04	
	4.17	40		1.64E-03	2.23E-03	
	4.45	45		4.02E-03	4.81E-03	
	4.71	50		8.48E-03	8.31E-03	
	τ_{cr} (Pa)	Q (l/s)	AccRate1L	AccRate2L	AccRate3L	AccRate5L
Repetition 1	3.05	23.3	1.17E-04	4.48E-05	5.32E-05	3.32E-05
	3.26	26.2	1.54E-04	1.54E-05	7.48E-05	1.09E-04
	3.46	29	1.91E-04	1.54E-05	1.82E-04	1.51E-04
	3.86	35	1.51E-03	1.73E-04	1.30E-03	2.34E-03
	4.17	40	3.06E-03	1.42E-03	4.01E-03	5.75E-03
	4.45	45	5.97E-03	4.94E-03	4.60E-03	9.58E-03
	4.71	50	1.04E-02	8.72E-03	7.36E-03	1.09E-02
Repetition 2	3.05	23.3		4.78E-05	4.55E-05	
	3.26	26.2		4.01E-05	1.85E-05	
	3.46	29		2.16E-05	2.16E-05	
	3.86	35		2.28E-04	3.86E-04	
	4.17	40		2.67E-03	2.56E-03	
	4.45	45		4.89E-03	5.53E-03	
	4.71	50		8.15E-03	1.00E-02	

Table A-20. Bedload transport rates. Stage 2. For run number refer to Table A-7.

			Total transport rate (kg/m/s)		
	AccRates (l/s/s)		0.0096	0.0024	0.0008
	τ_{cr} (Pa)	**Q (ls)**	**AccRate1**	**AccRate3**	**AccRate5**
Repetition 1	2.80	23.5	3.95E-04	1.48E-05	2.65E-05
	3.00	26.3	2.41E-04	3.09E-05	1.98E-05
	3.20	29.2	2.64E-04	2.27E-04	1.25E-04
	3.57	35	1.11E-03	7.96E-04	3.43E-04
	3.88	40	2.57E-03	2.29E-03	1.94E-03
	4.17	45	6.27E-03	4.67E-03	5.29E-03
	4.45	50	1.17E-02	8.83E-03	1.07E-02
Repetition 2	2.80	23.5	4.63E-04	5.86E-05	2.21E-05
	3.00	26.3	2.04E-04	8.95E-05	2.52E-05
	3.20	29.2	3.33E-04	2.13E-04	9.26E-05
	3.57	35	8.24E-04	1.03E-03	4.91E-04
	3.88	40	2.26E-03	3.88E-03	2.18E-03
	4.17	45	5.39E-03	8.74E-03	6.32E-03
	4.45	50	1.22E-02	1.36E-02	1.08E-02

Table A-21. Bedload transport rates for uniform gravel runs. For run number refer to Table A-7.

Appendix 7. Streamwise velocity (ADV) data sets

	Reference [19,20]	AccRate1 [21,22]	AccRate2 [23,24]	AccRate3 [25,26]	AccRate4 [27,28]	AccRate5 [29,30]
Q (l/s)	35.6	40.8	38.8	42.5	45.1	44.9
Depth (mm)	72.9	79.5	76.7	81.15	83.6	83.15
z (mm)			**u (cm/s)**			
7.5	41.06	41.31	39.26	39.20	39.25	39.67
15.5	52.34	53.75	53.08	53.42	54.32	54.09
23.5	58.89	61.55	60.00	61.48	62.03	61.89
28.5	60.54	64.07	62.91	64.32	65.09	65.05
43.5	67.69	70.47	69.00	71.27	71.43	71.67
53.5	70.57	73.46	72.47	74.06	74.33	74.54
61.5	72.04	75.30	74.41	76.06	76.06	76.34
76				78.20	78.44	79.05
u_* (cm/s)	6.39	7.41	7.21	8.15	8.35	8.19
τ (Pa)	4.07	5.47	5.18	6.63	6.96	6.69
B	5.05	4.17	4.15	3.42	3.33	3.46

Table A-22. Streamwise velocity data and parameters. Pilot Runs (each data collected over a 3 min. period and averaged over two repetitions). Numbers between square brackets are the run number (Table A-7).

	AccRate1-R1 [47]			**AccRate1-R2** [48]			**AccRate3-R1** [49]			**AccRate3-R2** [50]			**AccRate5** [51]		
	Q12	**Q12B**	**Q31.5**	**Q12**	**Q12B**	**Q31.5**	**Q12**	**Q12B**	**Q31.5**	**Q12**	**Q12B**	**Q31.5**	**Q12**	**Q12B**	**Q31.5**
Depth h (mm)	32	32	56	32	31	55	32	31	56	32	32	57	30	29	54
Distance from bed (mm)	**Streamwise velocity (cm/s)**														
6	22.47	26.38	33.99	25.53	27.67	41.42	24.10	16.37	38.17	1.71	8.21		10.80	28.61	28.71
7	22.73	23.72	31.13	28.48	31.08	40.58	27.21	28.85	35.34	7.75	8.67	11.98	21.28	31.27	37.47
8	25.68	23.10	34.87	28.25	28.51	46.41	26.85	31.33	42.67	14.36	9.97	26.20	24.46	31.85	40.64
9	29.68	28.05	42.98	30.07	31.86	49.41	28.13	30.86	35.30	27.22	23.16	38.97	27.99	34.23	44.39
11	33.31	31.39	45.45	33.36	34.99	51.77	31.21	29.91	44.73	28.82	28.85	43.12	32.55	33.80	44.45
13	35.85	32.61	46.13	36.55	36.66	54.57	34.27	37.06	50.87	32.95	31.41	45.15	33.48	37.13	47.08
15	38.57	37.00	51.94	37.81	38.34	56.33	34.04	36.46	55.10	37.44	34.97	51.05	36.33	40.19	52.20
17	40.28	38.19	55.09	39.93	38.96	58.55	38.30	40.73	57.18	39.17	34.12	54.68	39.44	40.30	54.18
20	43.19	40.57	58.95	41.00	40.49	60.93	42.06	43.96	61.98	41.15	37.83	59.22	42.06	45.19	58.33
25	45.52	42.90	62.50	43.44	43.78	64.84	45.92	44.27	66.17	45.08	43.63	63.23	42.66	46.91	62.87
35			68.57			71.00			72.06			69.51			68.93
45			74.23			75.45			75.88			74.25			72.89
u_* (cm/s)	6.32	6.46	7.84	4.23	3.43	6.73	6.99	8.73	7.66	7.42	6.90	9.05	8.10	5.04	8.24
τ (kg/m/s2)	3.98	4.16	6.13	1.78	1.17	4.52	4.88	7.60	5.86	5.49	4.75	8.18	6.55	2.53	6.78
z_0 (mm)	1.34	1.60	1.03	0.41	0.18	0.52	1.83	2.65	0.82	2.14	2.07	1.60	2.48	0.62	1.24
z_0Qi/z_0Q12	1.00	1.20	0.77	1.00	0.44	1.27	1.00	1.45	0.45	1.00	0.97	0.75	1.00	0.25	0.50

Table A-23. Streamwise velocity data and resulting parameters. Stage 1 (each data collected over a 2 min. period). Numbers between square brackets are the run number (Table A-7).

	AccRate1-R1 [73]			AccRate3-R1 [74]			AccRate3-R2 [75]			AccRate5-R1 [76]		
	Q12	**Q12B**	**Q29.2**	**Q12**	**Q12B**	**Q29.2**	**Q12**	**Q12B**	**Q29.2**	**Q12**	**Q12B**	**Q29.2**
Depth h (mm)	30	30	50	29	30	51	30	28	49	28	29	51
Distance from bed (mm)	**Streamwise velocity (cm/s)**											
6	32.27	24.64	31.91	27.77	25.26	24.87	19.90	17.60	22.62	12.50	23.60	31.47
7	31.84	24.57	35.90	26.98	30.84	34.75	25.48	21.50	35.54	31.01	29.97	46.17
8	32.75	28.64	44.90	33.18	29.28	38.78	28.69	32.90	40.11	37.70	31.10	48.17
10	37.93	31.55	48.03	36.07	36.90	50.19	33.35	28.01	42.98	37.70	35.19	52.47
12	40.38	38.41	55.19	38.28	36.01	50.00	36.46	35.08	50.04	41.23	36.47	51.96
14	42.47	38.95	56.02	41.55	39.37	54.23	35.32	38.77	55.53	43.32	39.79	56.50
17	45.12	43.26	62.21	45.25	44.82	62.69	41.71	43.72	60.41	46.42	42.01	61.47
22	47.78	45.59	65.93	47.53	47.07	66.96	46.48	44.55	66.24	48.97	43.77	65.87
32			71.01			71.09			71.86			71.09
42			73.56						75.88			76.38
u_* (cm/s)	5.42	8.33	8.70	5.99	6.05	11.62	6.85	9.96	10.51	6.48	5.57	6.73
τ (kg/m/s2)	2.93	6.93	7.55	3.58	3.65	13.47	4.69	9.90	11.02	4.19	3.10	4.52
z_0 (mm)	0.61	2.09	1.03	0.89	0.97	2.11	1.46	2.89	1.74	0.96	0.83	0.45
z_0Qi/z_0Q12	1.00	3.44	1.69	1.00	1.10	2.39	1.00	1.98	1.19	1.00	0.86	0.47

Table A-24. Streamwise velocity data and resulting parameters. Uniform gravel experiments (each data collected over a 2 min. period). Numbers between square brackets are the run number (Table A-7).

Appendix 8. Comparison of bedload equations

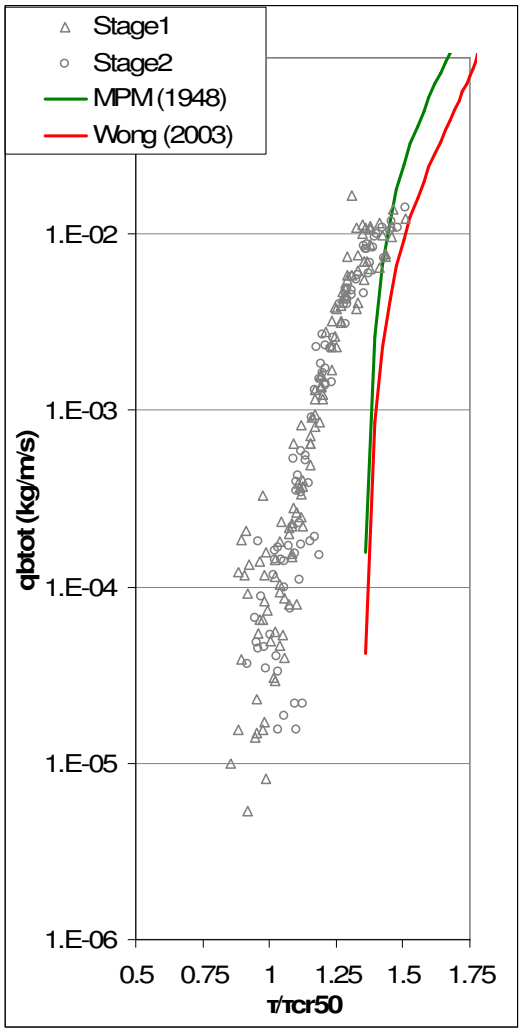

Fig. A- 2. Comparison of results by the original MPM (1948) and Wong (2003) modified equation.

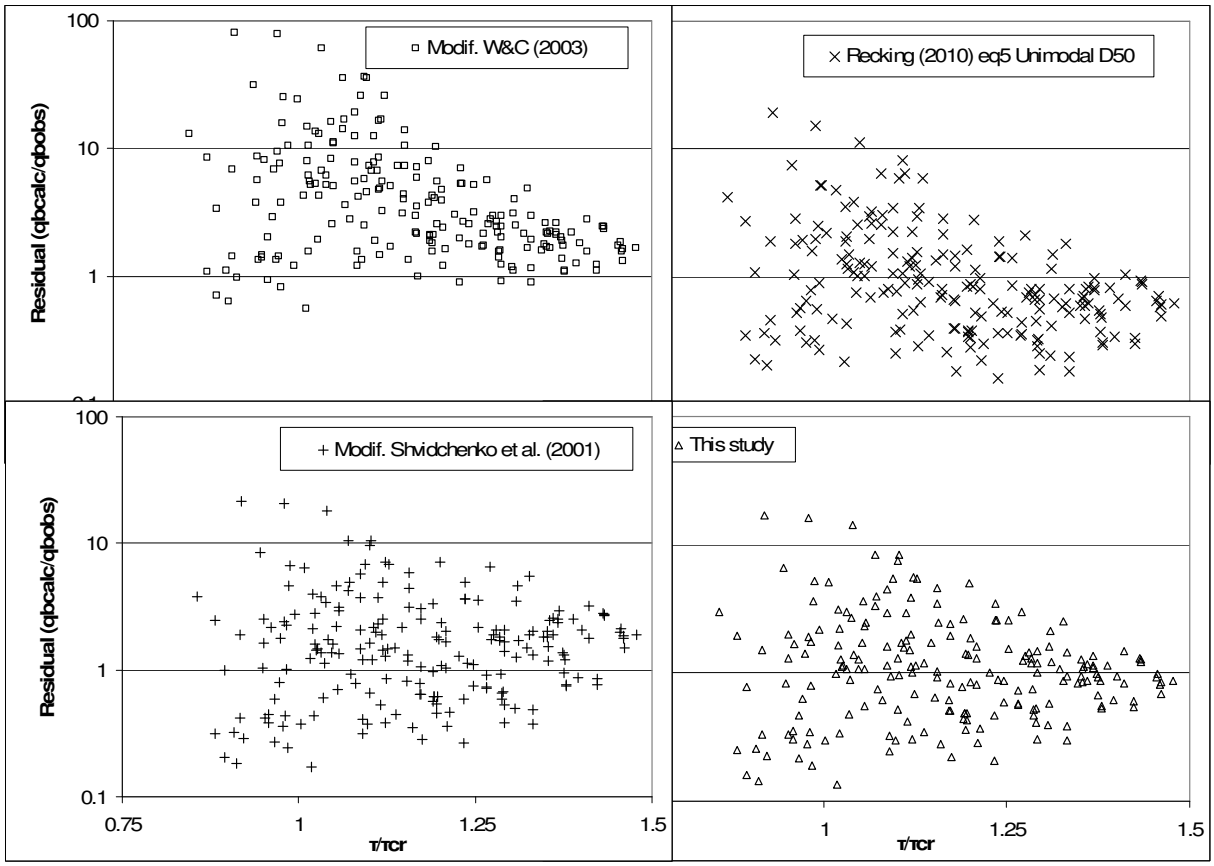

Fig. A- 3. Residuals from bedload equations. Note how errors reduce with stress magnitude for all cases. Recking's (2010) eq. 12 and Wilcock and Crowe (2003) clearly overestimate q_b in larger proportion than Recking's (2010) eq. 5 and equation 5-18 (this study).

Appendix 9. 2009 IAHR Congress paper

Below is a copy of the paper presented at the 33rd IAHR Congress: Water Engineering for a Sustainable Environment held in Vancouver (Canada) between 9th and 14th August 2009 and referenced in this thesis as Piedra *et al*. (2009).

REVIEW OF APPROACHES TO ESTIMATING BED SHEAR STRESS FROM VELOCITY PROFILE MEASUREMENTS

M. M. Piedra[1], H. Haynes[1], T. B. Hoey[2] and A. Ervine[1]

[1]Dept. of Civil Engineering, University of Glasgow, Glasgow, UK, G12 8LT. Tel: +44 (0)141 3304077, Fax: +44 (0) 141 3304557. m.piedra@civil.gla.ac.uk, haynes@civil.gla.ac.uk, ervine@civil.gla.ac.uk

[2]Dept. of Geographical and Earth Sciences, University of Glasgow, Glasgow, UK, G12 8QQ. Tel: +44 (0)141 3304224. trevor.hoey@ges.gla.ac.uk

---

Bed shear velocity is commonly estimated using streamwise velocity profiles and the logarithmic law for the inner layer. However, despite a considerable number of empirical equations being reported in the literature, there is no unified expression of the log-law that is commonly applied to sediment transport studies. Most authors use essentially the same theoretical formulation, but the nomenclature and number of variables and parameters used in the equations are different. Not only does this cause confusion among practitioners and researchers, but it is difficult to compare shear stress values produced by different studies as the equations and assumptions that generate them are inconsistent. The objectives of this paper are therefore: i) to review log-law equations available in literature and compare their parameterisations; ii) to suggest a unified nomenclature for the variables and parameters of the log-law expression; and iii) to compare the main equation types using ADV

measurements taken over a uniform gravel bed and a unimodal gravel bed in laboratory conditions. An additional near-uniform bed was used for validation of the method.

Key words: *shear velocity, shear stress, velocity profiles, logarithmic law.*

1. Introduction

Estimation of bed shear velocities is an essential part of sediment transport studies and flow characterisation. It is generally accepted that the Kármán-Prandtl law of vertical distribution of streamwise velocity, also known as Law of the Wall or log-law, is a good representation of the distribution of time-averaged velocity values for the inner layer of rough turbulent flows; i.e. approximately between the top of the viscous layer and the lowest 20% of the depth. The log-law is therefore commonly used to estimate flow shear velocity (u_*) and shear stress (τ_0), essential parameters for the study of sediment transport. However, there is a considerable variety of expressions used by different authors. Intrinsic in the selection of the specific formulation is the adoption of a number of assumptions related to bed roughness characteristics, position of the origin of distance from the bed, etc. Again, these assumptions vary between authors. This paper aims to summarise the equations used in recent literature and propose a unified formulation and nomenclature for the log-law equation in order to improve understanding and consistency in approach within the hydraulic research community. Flume-based ADV velocity data, for two different grades of gravel bed, were used to analyse the two main log-law expressions. A near uniform bed gravel was used to validate the results.

2. Logarithmic law equations

2.1 Review of available equations

Essentially, all expressions of the logarithmic law cited in the literature have the same formulation. The ratio of time averaged streamwise velocity (u) to a constant velocity scale, called shear velocity (u_*) set equal to the inverse of the von Kármán constant (κ) multiplied by the natural logarithm of vertical distance

from the bed (z) over a length scale parameter representative of the bed or grain roughness (z_0 or k_s). If k_s is used, the equation requires an additional integration constant (B). If z_0 is used, an expression similar to $z_0 = k_s/30$ appears widely used in literature (e.g. Singh *et al*. 2007, Wilcock 1996). Further variations of the same basic equation stem from consideration of the origin of the vertical distance (z). Therefore, velocity profile equations for two-dimensional rough turbulent flow can be classified into two types: Type A (Eq. 1): those that use grain roughness (k_s) plus another parameter (B), and Type B (Eq. 2): those that use bed roughness (z_0) only.

Type A: $$\frac{u(z)}{u_*} = \frac{1}{\kappa}\ln\left(\frac{z}{k_s}\right) + B \qquad \text{(Eq. 1)}$$

Type B: $$\frac{u}{u_*} = \frac{1}{\kappa}\ln\left(\frac{z}{z_0}\right) \qquad \text{(Eq. 2)}$$

The review of related literature shows that there is a wide variety of symbols representing the same variable or parameter, often being a matter of author's choice:

- The vertical coordinate is represented by either *z* (Graf 1998, Wilcock 1996), or *y* (Dey and Raikar 2007).

- The symbol for the time-averaged velocity is consistently *u*; however, some authors use upper case, *U*, (Nezu and Nakagawa 1993, Franca and Czernuszenko 2006) while others use a bar over the symbol, $\overline{u}$, (Song and Chiew 2001, Singh *et al*. 2007, Stone and Hotchkiss 2007) or brackets, $\langle U \rangle$, (Franca and Czernuszenko 2006).

- The shear velocity symbol (u_*) has similar variability to that of time-averaged velocity with respect to font case and position of the asterisk (Maghrebi 2006, Wilcock 1996, Smart 1999, Franca and; Pokrajac *et al*. 2006).

- The symbols used for roughness of the bed and the position of the origin of vertical distance, termed the *zero-plane* (or *virtual bed;* Dey and Raikar 2007) cause even more confusion. The parameter representing the roughness characteristics of the bed can be, depending on the author and whether is referring to bed roughness or grain roughness, y_0, z_0, k_s, ε or k with their actual values depending on the assumptions made by each researcher. If notation differences are only a reflection of the symbol adopted for the vertical coordinate, *y* or *z*, they do not cause significant problems (Maghrebi 2006, Wilcock 1996). Yet, in some cases the same symbol represents different concepts. For example, Graf (1998) uses z_0 to represent the displacement of the zero-plane below that of the roughness crest; whereas, Franca and Czernuszenko (2006) and Pokrajac *et al*. (2006) define z_0 as the distance from the zero-plane at which flow velocity is predicted to be zero (u = 0), which is also termed the bed roughness length.

- The position of the zero-plane also differs depending on the author. Wilcock (1996) and Biron *et al*. (1998) do not consider the displacement of the position of the zero-plane, effectively assuming that the position of the origin of vertical distance coincides with the top of the particles. All other authors cited above include a distance from the top of the roughness elements to the zero-plane; taking the reference level as the crest of the roughness elements seems to be a common assumption. Nevertheless, the symbol representing the zero-plane displacement varies between authors. Song and Chiew (2001) use y_0; Nezu and Nakagawa (1993) and Singh *et al*. (2007) adopt δ; Pokrajac *et al*. (2006) use a lower case d_z whereas Smart (1999) uses an upper case D; Graf (1998) uses z_0; and Stone and Hotchkiss (2007) adopt Δz. All these symbols take different values, related to a proportional value of the Nikuradse equivalent grain roughness ($0.25k_s$ in Song and Chiew 2001 and Dey and Raikar 2007; $0.2k_s$ in Graf 1998) which, in turn, must be estimated from bed size composition. Dey and Raikar (2007), Stone and Hotchkiss (2007) and Song and Chiew (2001) adopted $k_s=D_{50}$; Maghrebi (2006) used $k_s=2D_{50}$; Smart (1999) reported values ranging from $k_s=3\ D_{90}$ to $k_s=10D_{90}$; and Parker (2004) used $k_s=2D_{90}$.

- The integration parameter used by authors that applied Type A equations is also subject to a range of symbols. *B* or *Br* are used by Song and Chiew (2001), Dey and Raikar (2007), Graf (1998), Franca and Czernuszenko (2006) and Stone and Hotchkiss (2007); whereas, Nezu and Nakanagua (1993) use *A* or *Ar* depending on the expression adopted. However, regardless the symbol, parameter values are estimated by the line of best fit to measured data sets. Whilst it is commonly accepted that the value of *B* (*Br* or *Ar*) is close to 8.5 (Graf 1998), a wide range of values have been reported in literature; for example, 4.1-13.5 in Franca and Czernuszenko (2006) and 6.8-9.18 in Dey and Raikar (2007).

In order to establish a common understanding and facilitate further calculations and discussions, the following nomenclature will be used in this review: u = time averaged streamwise velocity (cm/s); u_* = bed shear velocity (cm/s); κ = von Kármán constant; *ln( )* = natural logarithm; z = vertical distance from the bed crests (mm); d = position of the zero-plane below the bed crests; z_0 = bed hydraulic roughness, or distance above the zero-plane, at which u=0 (mm); k_s = grain roughness (mm); D_i = particle size for which i % is smaller (mm); h = flow depth measured from the bed crests (mm); H = flow depth measured from the zero-plane; B = integration constant for Type A expressions.

2.2 Mathematical considerations

Depending on the equation adopted and assumptions made by the users, the number of variables, or unknowns, varies. In all cases, *u(z)* and *z* are known from direct measurements, but the following parameters remain unknown prior to calculations: u_*, κ, d, k_s and B (from Eq. 1) and u_*, κ, d, and z_0 (from Eq.2). Shear velocity u_* and bed roughness length z_0, or integration parameter B are often the sought after parameters. This means adopting values for the von Kármán parameter (κ), the displacement of the origin of *z (d)*, and k_s, prior to calculations.

The von Kármán parameter is widely reported to take the value of 0.4 (Nogueira *et al*. 2008, Smart 1999, Graf 1998). However, κ reduces with bed mobility such that when bed particles are under near-threshold conditions κ=0.35 (Dey and

Raikar 2007) and for strongly mobile gravel bed κ=0.29 (Nikora and Goring 2000). Thus, an appropriate recommendation would be to take κ as 0.40 for stable beds, 0.35 for near-threshold or weakly mobile beds and 0.30 for strongly mobile beds.

In Eq. 1 B can be fixed prior to the calculations and obtain k_s as a result. In this case, the value of B is commonly reported to be around 8.5 for rough turbulent flows (Graf 1998). This assumption is generally important when assessing the value of the bed roughness length (z_0), which is commonly expressed as $z_0=k_s/C$ and therefore establishes a direct relationship with bed grain size (k_s). If the above expression is introduced into Eq.1 then $C=\exp(\kappa B)$; so, if B=8.5 and κ=0.4, then C=30; this value is often used for the estimation of z_0 (Singh *et al.* 2007, Petit 1990, Wilcock 1996). Other expressions of z_0 found in literature are: $z_0 \approx 0.1D_{90}$ (Wilcock 1996) and $z_0 \approx 0.1D_{84}$ (Whiting and Dietrich 1990), which implies $k_s \approx 3D_{90}$ or $k_s \approx 3D_{84}$. These very large values of grain roughness are more a result of the calculations than a reflection of the bed grain size; hence, a more physically-based definition of k_s, easily determined by the user prior to calculations, is proposed. Conceptually, k_s refers to the size of bed grains, which is commonly expressed by a representative particle diameter. Thus, a value of $k_s= D_{90}$ is adopted here, as it is a widely used value representing larger bed grain sizes. As B, z_0 and k_s are inter-related and B and k_s cannot be independently obtained from each other, the authors took the approach of leaving B as a result of the other parameters and obtain z_0 independently.

3. Experimental set up and methodology

Comparison of Eqs. 1 and 2 employed data collected from flume-based experiments using a range of flows and bed materials. A 0.3m x 12m *Armfield* flow-recirculating and tilting flume was set to a slope of 1 in 200. Uniform flow conditions were established for three constant flows: 12.5 l/s, 16.5 l/s and 20.7 l/s, providing water depths between 80mm and 116m, as measured from the bed crests. Two gravel beds were tested: (i) a uniform medium gravel 4.0-5.6mm (D_{50}=4.8mm, D_{90}=5.44mm); and (ii) a unimodal grade 1-16mm (D_{50}=6.9mm, D_{90}=11.1mm). A third data set, previously obtained by the authors over a near

uniform gravel bed 2-8mm (D_{50}=4.8mm, D_{90}=5.6mm) and included in Piedra *et al.* (2008), was also re-analysed.

In all experiments, flows were controlled by an electrical signal inverter that regulated the water pump speed. A *Microelectronics Ltd.* PORTAFLOW™ monitored flow and average velocity in the return pipe with a flow accuracy of 0.01 l/s. A *Nortek* Vectrino 3D side-looking Acoustic Doppler Velocimeter (ADV) measured flow velocity in a 0.16mm^3 sampling volume located in the centre of the flume. Velocity profiles were obtained by recording data at 9 to 11 elevations (depending on flow depth) at a frequency of 25Hz for a 3 minute period; this provided 4500 measurements per sample elevation. Smaller distances between sampling elevations were employed near the bed to increase data coverage within the inner layer of flow. The lowest sampling elevation possible was 6mm above the bed.

Three methods were used to estimate the shear velocity u_* and assess the optimum parameters of the log-law equations: (i) shear stress from Reynolds stress profiles; (ii) estimating shear stress from flow depth and slope; (iii) Clauser method, fitting a straight line to *ln(z+d)-u* data set.

(i) *Nortek* software (ExploreV) was used to obtain Reynolds stresses. The intersection of the straight line fitted to the Reynolds stress data points with $z=z_0$ (elevation for which u=0) provided an estimation of the bed shear stress (τ_0). Using $\tau_0 = \rho \cdot u_*^2$, where ρ= water density, shear velocity from Reynolds stresses can be derived. This is denoted as $u_*(R)$ in the current paper.

(ii) Under uniform flow conditions, bed shear stress can be estimated using: $\tau_0 = \rho g R_h S_0$; where τ_0 = bed shear stress (kg/m/s^2) corrected for wall effects (Cheng and Chua 2005), ρ= water density (kg/m^3), g = gravity acceleration (9.81 m/s^2), R_h = hydraulic radius (m), and S_0 = slope of the energy line (m/m), which is similar to the slope of the water line for uniform flow. The value of u_* determined in this way is denoted as $u_*(S)$ henceforth.

(iii) Shear velocity and log-law equation parameters were obtained for the two analysed equations (Eqs. 1 and 2) using the Clauser method; in the present paper u_* obtained using this methodology is denoted as $u_*(C)$. This was

undertaken after estimating the value of d based on minimising the errors between the data set and the theoretical velocities obtained with a specific set parameters for the corresponding value of d, over the line fitting range. The values of d tested ranged from 0-1k_s at intervals of 0.01k_s, where k_s = D_{90}. The logarithmic profile is commonly applied to the flow depth below 0.2z/h; however, it is often the case that the logarithmic profile stands for a larger proportion of the depth, e.g. 0.4z/h (Franca and Czernuszenko 2006). In the experiments presented here, it was often the case that the straight line applied to $ln(z+d)-u$ fitted well to an even larger proportion of the depth; yet sometimes, the values closest to the bed, typically $z/h \leq 0.1$ deviated from the straight line. This data was used by the authors to extend the fitting line to those data points that followed a straight line; the effect of the depth range over which the fitting line is applied is outside the remit of the present paper, but will be analysed in detail by the authors elsewhere.

4. Results and discussion

Table 1 shows the experimental hydraulic conditions and results for the uniform gravel, the graded gravel and the validation data set obtained with near uniform gravel (Piedra *et al*. 2008). It is noted that the von Kármán constant for the first two data sets is 0.4 as no movement was observed, whereas κ=0.35 for the validation data set, as it was obtained under threshold conditions (Piedra *et al*. 2008).

Values of d/k_s range from 0.0 to 0.15. These values are lower that those often used of $d \approx 0.2k_s$ and generally support adoption of the origin of distance from the bed at the bed grain crests. Values of d/k_s are somewhat larger for the uniform gravel. These results may be explained by the bed composition. The graded gravel contains a variety of grain sizes, where small particles occupy the interstices that larger grains leave, effectively creating a "smooth" surface on the bed, limiting the penetration of the flow below the bed surface. The same effect cannot occur in uniform gravels where the flow is therefore likely to penetrate below the bed crests (d>0). Also, it is noted that experimental beds

were screeded prior to experimentation; this contributes to make $d \approx 0$ and creates a more level bed surface than those found in nature. A similar explanation is afforded for the sensitivity of values of z_0/ks (Table 1) to bed composition, with lower values for the graded bed than for the uniform gravel.

Table 1. Experimental Results

	GRADED GRAVEL			UNIFORM GRAVEL			NEAR UNIFORM GRAVEL				
Q (l/s)	12.5	16.5	20.7	12.5	16.5	20.7	35.6	40.8	38.8	42.5	45.1
h (mm)	81	95	116	80	94	106	73.2	80	77.4	81.7	83.8
U (cm/s)	57.0	60.8	64.8	56.1	61.7	67.4	62.1	64.3	63.7	64.8	65.4
d (mm)	0.0	0.0	0.0	0.0	0.82	0.27	0.0	0.0	0.0	0.0	0.0
d/k_s	0	0	0	0	0.15	0.05	0	0	0	0	0
$u_*(C)$ (cm/s)	5.58	5.75	6.15	5.88	6.42	5.47	5.30	5.68	5.76	6.52	6.79
$u_*(R)$ (cm/s)	4.68	4.96	5.25	4.95	4.75	5.24	5.17	5.35	5.30	5.44	5.27
$u_*(S)$ (cm/s)	5.96	6.39	6.85	5.92	6.38	6.67	5.88	6.14	6.04	6.20	6.27
z_0 (mm)	0.46	0.48	0.58	0.64	0.74	0.35	0.50	0.57	0.63	0.89	0.93
z_0/k_s	0.04	0.04	0.05	0.12	0.14	0.06	0.09	0.10	0.11	0.16	0.17
B	7.98	7.83	7.39	5.34	4.98	6.86	6.92	6.52	6.25	5.25	5.12

Fig. 1-i shows that non-dimensional shear velocity (u_*/U where U=profile depth-averaged velocity) is limited in sensitivity to flow or bed particle size. Fig. 1-ii however does indicate a hierarchy of sensitivity to the method of estimating u_*: $u_*(S) > u_*(C) > u_*(R)$. Values obtained with the slope method are $u_*(S)$~0.1, the Clauser method gives $u_*(C)$~0.09 and the Reynolds stress method suggests $u_*(R)$~0.08. These values are similar to the range 0.06-0.1 by Dey and Raikar (2007) and 0.05-0.1 by Grass and Mansour-Tehrani (1996) for rough flows.

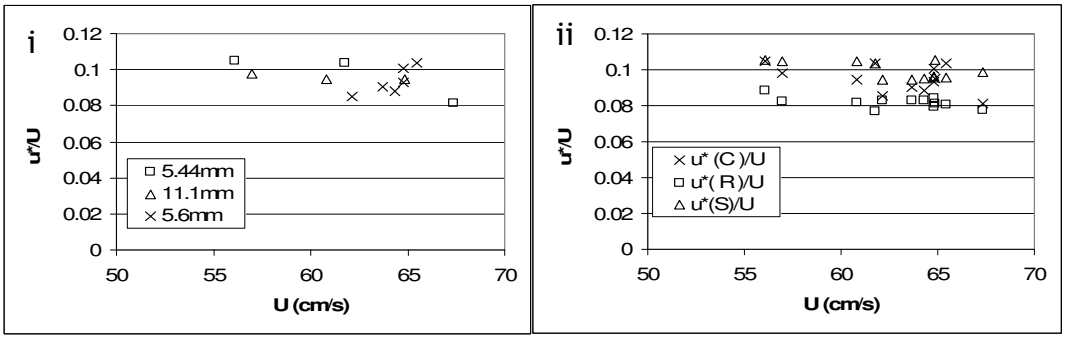

Figure 1. Relationship of non-dimensional shear velocity u_*/U and depth averaged flow velocity U. (i) shows $u_*(C)$ for each bed identified by the D_{50}. (ii) shows u_* obtained from the three alternative methods. Both graphs include validation data from Piedra et al. (2008).

The results for the integration parameter *B* are persistently lower than 8.5, especially for beds of smaller D_{90}. Although *B* does not appear to have a clear relationship with flow (Fig. 2-i), it does show reasonable correspondence with z_0 (Fig. 2-ii), indicating that *B* decreases with hydraulically rougher beds. These results suggest that the value of *B* depends on the bed roughness and previous assumptions of a constant value of *B*=8.5 may not be appropriate. It is also noted that as $ks=D_{90}$ is smaller than those used by other authors (see 2.1) *B* must necessarily be smaller.

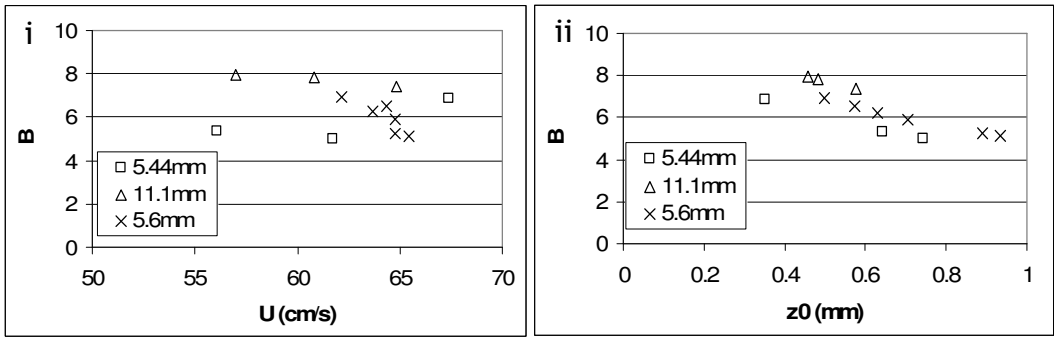

Figure 2. Variation of B with (i) flow magnitude and (ii) bed roughness length.

5. Conclusions

This paper has presented a literature review and experimental data designed to reduce confusion over differences in the equations pertaining to logarithmic velocity profile theory and inconsistency in the associated symbols. The following conclusions are drawn for the experimental data presented in the present paper: (i) a revised symbols list is presented and advocated; (ii) there is a hierarchy of sensitivity to the method of estimating u_* with values for the depth-slope method > Clauser method > Reynolds stress method; (iii) values of *d* are smaller than commonly assumed, often obtaining *d*=0 for the experimental beds tested; (iv) bed roughness length (z_0) appears to adequately reflect the hydraulic roughness of the bed, with uniform beds being rougher than graded beds; and (v) values of *B* obtained are smaller than 8.5, with smaller values for rougher beds.

6. Acknowledgements

The authors acknowledge the financial contribution of Scottish Natural Heritage. This research is part of the main author's doctoral programme, supported by ESPRC.

7. References

Biron, P. M., Lane, S. N., Roy, A. G., Bradbrook, K. F., and Richards, K. (1998). Sensitivity of bed shear stress estimated from vertical velocity profiles: The problem of sampling resolution. *Earth Surface Processes and Landforms*, vol.23, 133-139.

Cheng, N. and Chua, L. H. C. (2005). Comparisons of sidewall correction on bed shear stress in open channel flows. *Journal of Hydraulic Research*, vol. 131, 7, 605-609.

Dey, S. and Raikar, R. V. (2007). Characteristics of loose rough boundary streams at near-threshold. *Journal of Hydraulic Engineering*, vol. 133, No. 3, 288-304.

Franca, M. J. and Czernuszenko, W. (2006). Equivalent velocity profile for turbulent flows over gravel riverbeds. In Ferreira, Alves, Leal and Cardoso (eds.), *Proc. Int. Conf. Fluvial Hydraulics River Flow 2006*, 6-8 September 2006, Lisbon, Portugal. Taylor and Francis Group, London.

Graf, W. H. (1998). *Fluvial hydraulics. Flow and transport processes in channels of simple geometry*. J Wiley & Sons, Chichester, UK.

Grass, A. J. and Mansour-Tehrani, M. (1996). Generalised scaling of coherent bursting structures in the near-wall region of turbulent flow over smooth and rough boundaries. *Coherent Flow Structures in Open Channels*. P. J. Ashworth, S. J. Bennett, J. L. Best and S. L. McLelland (eds.). John Wiley & Sons, UK.

Maghrebi, M. F. (2006). Application of the single point measurement in discharge estimation. *Advances in Water Resources*, 29, 1504-1514, Elsevier.

Nezu, I. and Nakagawa, H. (1993). *Turbulence in open channel flows*. Balkema, Rotterdam, The Netherlands.

Nikora, V., and Goring, D. (2000). Flow turbulence over fixed and weakly mobile gravel beds. *Journal of Hydraulic Engineering*, vol. 126, 9, 679–690.

Piedra, M. Haynes, H. and Hoey, T. B. (2008) Influence of time-varying flows on particle entrainment in gravel bed rivers. *Int. Conf. Fluvial Hydraulics River Flow 2008* , 3-5 2008, Çesme-Izmir Turkey. Kubaba.

Pokrajac, D. Finnigan, J. J. Manes, C. McEwan, I. and Nikora, V. (2006). On the definition of the shear velocity in rough bed open channel flows. In Ferreira, Alves, Leal and Cardoso (eds.), *Proc. Int. Conf. Fluvial Hydraulics River Flow 2006*, 6-8 September 2006, Lisbon, Portugal. Taylor and Francis Group, London.

Singh, K. M., Sandham, N. D., Williams, J. J. R. (2007). Numerical simulation of flow over a rough bed. *Journal of Hydraulic Engineering*, vol. 133, 4, 386-398.

Smart, G. M. (1999). Turbulent velocity profiles and boundary shear in gravel bed rivers. *Journal of Hydraulic Engineering*, vol. 125, 2, 106-116.

Song, T. and Chiew, Y. M. (2001). Turbulence measurement in non-uniform open-channel flow using acoustic Doppler velocimeter (ADV). *Journal of Engineering Mechanics*, vol. 127, 3, 219-232.

Stone, M. C. and Hotchkiss, R. H. (2007). Turbulence descriptions in two cobble-bed river reaches. *Journal of Hydraulic Engineering*, vol. 133, 12, 1367-1378.

Wilcock, P. R. (1996). Estimating local bed shear stress from velocity observations. *Water Resources Research*, vol. 32, 11, 3361-3366.

Whiting, P. J. and Dietrich, W. E. (1990). Boundary shear stress and roughness over mobile alluvial beds. *Journal of Hydraulic Engineering*, vol. 116, 12, 1495-1511.

References

Ackers, P. and White, W. R. (1973). Sediment transport: New approach and analysis. J. Hyd. Div. ASCE 99, HY11, 2041-2060.

Allan, A. F and Frostick, L. E. (1999). Framework dilation, winnowing, and matrix particle size: The behaviour of some sand-gravel mixtures in a laboratory flume. J. of Sedimentary Res., 69, 1, 21-26.

Almedeij, J., Diplas, P. and Al-Ruwaih, F. (2006). Approach to separate sand from gravel for bed-load transport calculations in streams with bimodal sediments. J. Hydraul. Eng., 132, 11, 1176-1185.

Andrews, E. D. (1983). Entrainment of gravel bed from naturally sorted river bed material. Geological Society of America Bulletin, 94, 1225-1231.

Andrews, E. D. and Parker, G. (1987). Formation of a coarse surface layer as the response to gravel mobility. In Thorne, C. R., Bathurst J. C., and Hey, R. D. (eds.). Sediment transport in gravel-bed rivers. John Wiley & Sons.

Ashmore, P. (1988). Bedload transport in braided gravel-bed stream models. Earth Surface Processes and Forms. 13, 677-695.

Ashworth, P. J. and Ferguson, R. I. (1989). Size-selective entrainment of bed load in gravel bed streams. Water Resour. Res., vol. 25, 4, 627-634.

Bagnold, R. A. (1977). Bed Load Transport by Natural Rivers. Water Resour. Res., 13, 2, 303-312.

Bagnold, R. A. (1980). An empirical correlation of bedload transport rates in flumes and natural rivers. Proc. of the Royal Soc. of London, Series A, 372, 453-473.

Barnett, C., J. Hossell, M. Perry, C. Procter and G. Hughes. (2006). A handbook of climate trends across Scotland. SNIFFER project CC03, Scotland & Northern Ireland Forum for Environmental Research, 62pp.

Barry, J. J., Buffington, J. M., Goodwin, P., King, J. G., and Emmett, W. W. (2008). Performance of bed-load transport equations relative to geomorphic significance: predicting effective discharge and its transport rate. J. Hyd. Eng. 13, 5, 601-615.

Batalla, R. (1997). Evaluating bed material transport equations using field measurements in a sandy gravel bed stream, Arbúcies River, NE Spain. Earth Surface Processes and Landforms, 22, 121-130.

Bathurst, J. C. (2007). Effect of coarse surface layer on bed-load transport. J of Hydraul. Eng., 133, 11, 1192-1205.

Bauer, B. O., Sherman, D. J. and Wolcott, J. F.(1992). Sources of Uncertainty in Shear Stress and Roughness Length Estimates Derived from Velocity Profiles. The Professional Geographer, 44, 4, 453-464.

Biron, P. M., Lane, S. N., Roy, A. G., Bradbrook, K. F., and Richards, K. (1998). Sensitivity of bed shear stress estimated from vertical velocity profiles: The problem of sampling resolution. Earth Surface Processes and Landforms, 23, 2, 133-139.

Bluck, B. J. (1987). Bed forms and clast size changes in gravel-bed rivers. In *River channels. Environment and processes*. Edited by K. Richards. The institute of British Geographers. Blackwell, UK, 1987.

Bluck, B. J. (1971). Sedimentation in the meandering River Endrick. Scottish Journal of Geology, 7, 93-138.

Bottacin-Busolin, A., Tait, S., Marion, A., Chegini, A. and Tregnaghi, M. (2008). Probabilistic description of grain resistance from simultaneous flow field and grain motion measurements. Water Resour. Res., 44, W09419, 10.1029/2007WR006224.

Brayshaw, A., Frostick, L. and Reid, I. (1983). The hydrodynamics of particle clusters and sediment entrainment in coarse alluvial channels. Sedimentology, 30, 137-143.

Buffington, J.M. (1999). The legend of A. F. Shields. J. Hydraul. Eng., 125, 4, 376-387.

Buffington, J. M. and Montgomery, D. R. (1997). A systematic analysis of eight decades of incipient motion studies, with special reference to gravel-bedded rivers. Water Res. Res., 33, 8, 1993-2029.

Buffington, J. M. and Montgomery, D. R. (1999a). Effects of hydraulic roughness on surface textures of gravel-bed rivers. Water Resour. Res., 35, 11, 3507-3521.

Buscombe, D., Rubin, D. M., and Warrick, J. A. (2010). A universal approximation of grain size from images of noncohesive sediment. J. Geophys. Res., 115, F02015, doi:10.1029/2009JF001477.

Camenen, B., and Larson, M. (2005). A general formula for non-cohesive bed load sediment transport. Estuarine, Coastal and Shelf Science. 63, 249–260.

Campbell, L., McEwan, I., Nikora, V., Pokrajac, D., Gallagher, M. and Manes, C. (2005). Bed-load effects on hydrodynamics of rough-bed open-channel flows. J. Hydraul. Eng., 131, 7, 576-585.

Carbonneau, P. E., Lane, S. N. and Bergeron, N. E. (2003). Cost-effective non-metric close-range digital photogrametry and its application to a study of coarse gravel river beds. Int. J. Remote Sensing, 24, 14, 2837-2854.

Carbonneau, P. E., Lane, S. N. and Bergeron, N. E. (2004). Catchment-scale mapping of surface grain size in gravel bed rivers using airborne digital imagery. Water Resour. Res., 40, W07202.

Carbonneau, P. E., Bergeron, N. E. and Lane, S. N. (2005). Automated grain size measurements from airborne remote sensing for long profile measurements of fluvial grain sizes. Water Resour. Res., 41, W11426.

Carling, P. (1983). Threshold of coarse sediment transport in broad and narrow natural streams. Earth Surface Processes and Landforms, 8, 1-18.

Carling, P. A. Kelsey, A. and Glaister, M. M. (1992). Effect of bed roughness, particle shape and orientation on initial motion criteria. In Dynamics of Gravel-bed rivers. Billi, P. Hey, R. D. Thorne, C. R and Tacconi, P. (eds.). John Willey & Sons.

Carollo, F. G., Ferro, V. and Termini, D. (2005). Analysing turbulence intensity in gravel bed channels. J. Hydraul. Res., 131, 7, 1050-1061.

Carson, M.A. and Griffiths, G.A. (1985). Tractive stress and the onset of bed particle movement in gravel stream channels: Different equations for different purposes. J. Hydrol., 79, 375-388.

Carson, M.A. and Griffiths, G.A. (1987). Bedload transport in gravel channels. J. Hydrol. (NZ). 26, 1, 1-151.

Chadwick, A., Morfett, J. and Borthwick, M. (2004). Hydraulics in Civil and Environmental Engineering. 4th edition, Spon Press.

Chen, X., and Chiew, Y. M. (2003). Response of velocity and turbulence to sudden change of bed roughness in open-channel flow. J. Hydraul. Eng., 129(1), 35-43.

Church, M. A., McLean, D. G. and Wolcott, J. F. (1987). River bed gravels: sampling and analysis. In Sediment transport in gravel-bed rivers. Eds. C. R. Thorne, J. C. Bathurst and R. D. Hey, pp. 43-88, John Wiley & Sons.

Church, M., Wilcott, J. F. and Fletcher, W. K. (1991). A test of equal mobility in fluvial sediment transport: behaviour of the sand fraction. Water Resour. Res., 27, 11, 2941-2951.

Church, M. and Hassan, M. A. (1992). Size and distance of travel of unconstrained clasts on a streambed. Water Resour. Res., 28, 1, 299-303.

Church, M., Hassan, M. A. and Wolcott, J.F. (1998). Stabilising self-organised structures in gravel-bed stream channels: field and experimental observations. Water Resour. Res. 34, 11, 3169-3179.

Clifford, N. J., Robert, A. and Richards, K. S. (1992). Estimation of flow resistance in gravel-bedded rivers: A physical explanation of the multiplier of roughness length. Earth Surface Processes and Landforms, 17, 2, 111-126.

Cooper, J. R., Aberle , J., Koll , K., McLelland, S. J., Murphy, B. J., Tait, S. J., and Marion, A. (2008). Observation of the near-bed flow field over gravel bed surfaces with different roughness length scales. In Altinakar, Kokpinar, Aydin, Cokgor & Kirkgoz (eds.). Proc. Int. Conf. on River Flow 2008, Turkey, 3-5 September 2008. Kubaba. P. 747-755.

Cui, Y. (2007). The unified gravel-sand (TUGS) model: Simulating sediment transport and gravel/sand grain size distributions in gravel-bedded rivers. Water Resourc. Res., 43, W10436, 1029/2006WR005330.

Cui, Y. and Wilcox, A. (2008) Development and application of numerical models of sediment transport associated with dam removal. Chapter 23 in *Sedimentation Engineering: Theory, Measurements, Modeling, and Practice, ASCE Manual 110.* Garcia, M.H., ed., 995-1020, ASCE, Reston, VA, ISBN 978-0784408149.

Dancey, C. L., Diplas, P., Papanicolau, A. and Bala, M. (2002). Probability of individual grain movement and threshold condition. J. Hydraul. Eng., 128, 12, 1069-1075.

Davoren, A. and Mosley, M. P. (1986). Observations of bedload movement, bar development and sediment supply in the braided Ohau River. Earth Surfaces processes and Landforms, 11, 643-652.

de Linares, M. and Belleudy, P. (2007). Critical shear stress of bimodal sediment in sand-gravel rivers. Journal of Hydraulic Engineering, 133, 5, 555-559.

Dey, S. and Raikar, R. V. (2007). Characteristics of loose rough boundary streams at near-threshold. J. Hyd. Eng., 133, 3, 288-304.

Dittrich, A., Nestmann, F. and Ergenzinger, P. (1996). Ratio of lift shear forces over rough surfaces. In *Coherent Flow Structures in Open Channels*. P. J. Ashworth, S. J. Bennett, J. L. Best and S. L. McLelland (eds.). John Wiley & Sons, UK.

Dixon, M. D. (2003). Effects of flow pattern on riparian seedling recruitment on sandbars in the Wisconsin River, Wisconsin, USA. Wetlands, 23, 1, 125-139.

Drake, T. G., Shreve, R., Dietrich, W. E., Whitings, P. J. and Leopold, L. B. (2008). Bedload transport of fine gravel observed by motion-picture photography. J. Fluid Mech., 192, 193-217.

Einstein, H. A. (1950). The bedload function for sediment transportation in open channel flows. Technical bulletin No. 1026, USDA-Soil Conservation Service, Washington, 71pp.

Einstein, H. A., and R. B. Banks. (1950). Fluid resistance of composite roughness. Trans. AGU, 31, 603–610.

Ferguson, R. I. (1994). Critical discharge for entrainment of poorly sorted gravel. Earth Surface Processes and Landforms, 19, 179-186.

Ferguson, R. I. (1986). River Loads Underestimated by Rating Curves. Water Resour. Res., 22, 1, 74-76.

Ferguson, R. I. (1987). Accuracy and precision of methods for estimating river loads. Earth Surface Processes and Landforms, 12, 95-104.

Ferguson, R., Prestegaard, K., and Ashworth, P. (1989), Influence of sand on hydraulics and gravel transport in a braided gravel bed river. Water Resour. Res., 25, 4, 635-643.

Ferguson, R. I. and Asworth, P. J. (1992). Spatial patterns of bedload transport and channel change in braided and near-braided rivers. In Dynamics of gravel bed rivers. Ed. P. Billy, R.D. Hey, C. R. Thorne and P. Tacconi. John Wiley & Sons.

Forth Fisheries Foundation (2004). River and brook lamprey monitoring of the Endrick Water CSAC/SSSI. Scottish Natural Heritage Commissioned Report No. 057 (ROAME No. F03AC607).

Franca, M. J. and Czernuszenko, W. (2006). “Equivalent velocity profile for turbulent flows over gravel riverbeds”. In Ferreira, Alves, Leal and Cardoso (eds.), Proc. Int. Conf. Fluvial Hydraulics River Flow 2006, Taylor and Francis Group, London, 189-197.

Frey, P. and Church, M. (2009). How river beds move. Science, 325, 1509-1510.

Fripp, J. B. and Diplas, P. (1993). Surface sampling in gravel streams. J.Hydraul. Eng., 119, 4, 473-489.

Garcia, C. M., Cantero, M., Niño, Y. and Garcia, M. (2005). Turbulence Measurements with Acoustic Doppler Velocimeters. J. Hydr. Eng. 131, 1062-1073.

Garde, R. J. and Ranga Raju, K. G. (1977). Mechanics of sediment transportation and alluvial stream problems. Wiley Eastern ltd. New Delhi.

Gilbert, G. K. (1914). The transportation of debris by running water, U.S. Geol. Surv. Prof. Pap., 86, 221 pp.

Gomez, B. (1994). Effects of Particle Shape and Mobility on Stable Armour Development. Water Resour. Res., 30, 7, 2229-2239.

Gomez, B. and Church, M. (1989). An assessment of bedload sediment transport formulae for gravel bed rivers. Water Resourc. Res., 25, 6, 1161-1186.

Goodwin, P. (2004). Analytical solutions for estimating effective discharge. J. Hydraul. Eng. 8, 729-738.

Gordon, E. and Meentemeyer, R. K. (2006). Effects of dam operation and land use on stream channel morphology and riparian vegetation. Geomorphology, 82, 412-429.

Goudie, A. S. (2006). Global warming and fluvial geomorphology. Geomorphology, 79, 384–394.

Graf, W. H. (1998). Fluvial hydraulics. Flow and transport processes in channels of simple geometry. J Wiley & Sons, Chichester, UK.

Graham, D. J, Rice, S. P, and Reid, I. (2005a). A transferable method for the automated grain sizing of river gravels. Water Resour. Res., 41, W07020, doi: 10.1029/2004WR003868.

Graham, D. J., Reid, I. and Rice, S. P. (2005b). Automated Sizing of Coarse-Grained Sediments: Image-Processing Procedures. Mathematical Geology, 37, 1.

Grass, A. J. (1970). Initial instability of fine bed sand. J. Hyd. Div., HY3, 619-632.

Hager, W. H. (2007). Scour in hydraulic engineering. Water Management, ICE Proc., 160, 159-168.

Hassan, M., and Reid, I. (1990). The influence of microform bed roughness elements on flow and sediment transport in gravel bed rivers. Earth Surface Processes and Landforms, 15, 739-750.

Hassan M. A, Church, M. and Schick, A. P. (1991). Distance of movement of coarse particles in gravel bed streams. Water Resour. Res., 27, 4, 503-511.

Hassan, M. A. and Church, M. (2000). Experiments on surface structure and partial sediment transport on a gravel bed. Water Resour. Res., 36, 7, 1885-1895.

Hassan, M. A. and Woodsmith, R. D. (2004). Bed load transport in an obstruction-formed pol in a forest, gravelbed stream. Geomorphology, 58, 2003-221.

Hassan, M. A Egozi, R. and Parker, G. (2006). Experiments on the effect of hydrograph characteristics on vertical grain sorting in gravel bed rivers. Water Resour. Res., 42, W09408, doi: 10.1029/2005WR004707.

Hayakawaa,Y. and Oguchib, T. (2005). valuation of gravel sphericity and roundness based on surface-area measurement with a laser scanner. Computers & Geosciences, 31, 6, 735-741.

Haynes, H and Pender, G. (2007). Stress history effects on graded bed stability. J. of Hydraul. Eng., 133, 4, 343-349.

Haynes H. and Ockelford, A. (2008). A Comparison of time-induced stability differences between a framework-supported and a matrix-supported gravel: sand mixture. Int. Conf. Fluvial Hydraulics River Flow 2008 , 3-5 2008, Çesme-Izmir Turkey. Kubaba.

Hey, R. D and Thorne, C. R. (1983). Accuracy of surface samples from gravel bed material. J. Hydraul. Eng., 109, 6, 842-851.

HM Government UK. (2009). The UK Renewable Energy Strategy.

Hoey, T. B. and Thomas, R. (2006). The impact of a regulated flow regime on stream morphology and habitat. Geophysical Research Abstracts, 8, 04497.

Hoey, T. B. (2004). The size of sedimentary particles. Evans, D. J. A. and Benn, D. I (eds.). A practical guide to the study of glacial sediments. Arnold, UK.

Hoey, T. B. and Sutherland, A. J. (1991). Channel morphology and bedload pulses in braided rivers: a laboratory study. Earth Surface Processes and Landforms, vol. 16, 447-462.

Hollingshead, A. P. (1968). Measurements of bed load discharge of Elbow River. Univ. Alberta M.Sc. thesis (unpubl.).

Kellerhals, R. and Bray, D. I. (1971). Sampling procedures for coarse fluvial sediments. J. Hydraul. Div., HY8, 1165-1179.

King, J. G.; Emmett, W. W.; Whiting, P. J.; Kenworthy, R. P.; Barry, J. J. (2004). Sediment transport data and related information for selected coarse-bed streams and rivers in Idaho. Gen. Tech. Rep. RMRS-GTR-131. Fort Collins, CO: U.S. Department of Agriculture, Forest Service, Rocky Mountain Research Station. 26 p.

Kleinhans, M. G. and van Rijn, L. C. (2002). Stochastic prediction of sediment transport in sand-gravel bed rivers. J. Hydraul. Eng., 128, 4, 412-425.

Knighton, D. (1998). Fluvial forms and processes, a new perspective. Arnold, London, UK, pp. 383.

Kondolf, G., and Wilcock, P. (1996). The flushing flow problem: Defining and evaluating objectives. Water Resour. Res., 32, 8, 2589-2599.

Kramer, H. (1935). Sand mixtures and sand movement in fluvial models. Trans. Am. Soc. Civ. Eng., 100, 798–878.

Krumbein, W. C. (1941). Measurement and geological significance of shape and roundness of sedimentary particles. J. of Sedimentary Petrology, 1, 2, 64-72.

Kuhnle, R. A. (1992). Fractional transport rates of bedload on Goodwin Creek. In Billi, P., Hey, R. D., Thorne, C. R and Tacconi, P. (eds.). Dynamics of gravel bed rivers. John Wiley & Sons, England.

Kuhnle, R. A. (1993). Incipient motion of sand-gravel sediment mixtures. J. of Hydraul. Eng., vol. 119, 12, 1400-1415.

Lamarre, H. and Roy, A. (2005). Reach scale variability of turbulent flow characteristics in a gravel-bed river. Geomorphology, 68, 95–113.

Lane, S. N. Chandler, J. H. and Porfiri, K. (2001). Monitoring river channel and flume surfaces with digital photogrammetry. J. Hydraul. Eng., 127, 10, 871-877.

Larone, J. B. and Carson, M. A. (1976). Interrelationships between bed morphology and bed-material transport for a small, gravel-bed channel. Sedimentology, 23, 67-85.

Lavelle, W. and Mofjeld, H. O. (1987). Do critical stresses for incipient motion and erosion really exist? J. Hydraul. Eng., 113, 3, 370-388.

Lisle, T. E. and Lewis, J. (1992). Effects of sediment transport on survival of salmonid embryos in a natural stream: a simulation approach. Can. J. Fish. Aquat. Sci. 49: 2337-2344.

Lisle, T. E., Nelson, J. M., Pitlick, J., Madej, M. A. and Barkett, B. L. (2000). Variability of bed mobility in natural, gravel-bed channels and adjustments to sediment load at local and reach scales. Water Resour. Res., 36, 12, 3743-3755.

Lisle, T. E., and Church, M. (2002). Sediment transport-storage relations for degrading, gravel bed channels. Water Resour. Res., 38, 11, 1219, doi:10.1029/2001WR001086.

MacLeod, M., Moran, D., Spencer, I. (2006). Counting the cost of water use in hydroelectric generation in Scotland. Energy Policy, 34, 2048-2059.

Marion, A. and Fraccarollo, L. (1997). New conversion model for areal sampling of fluvial sediments. J. Hydraul. Eng., 123, 12, 148-1151.

Marion, A., McEwan, I. K. and Tait, S. J. (1997). On the competitive effects of particle re-arrangement and vertical sorting. Proc. of the Environmental and Coastal Hydraulics: Protecting the Aquatic Habitat Conference. San Francisco, US, August 1997. pp.1493-1498.

Marion, A., Tait, S. J. and McEwan, I. K. (2003). Analysis of small-scale gravel bed topography during armouring. Water Resour. Res., 39, 12, 1334.

Masalo,I., Reig, L. and Oca, J. (2008). Study of fish swimming activity using acoustical Doppler velocimetry (ADV) techniques. Aquacultural Engineering, 38, 1, 43-51.

McEwan, I. and Heald, J. (2001). Discrete particle modelling of entrainment from flat uniformly sized sediment beds. J. Hudraul. Eng., 127, 7, 588-597.

McEwan, I., Sorensen, M., Heald, J., Tait, S., Cunningham, G., Goring, D., and Willetts, B. (2004). Probabilistic modelling of bed-load composition. J. Hydr. Eng. 130, 2, 129-139.

McEwen, L. J. and Lewis, S. G. (1999) Sediment budget of the Endrick catchment. Unpublished Research Report for Scottish Natural Heritage.

McLelland, S. J., Ashworth, P. J., Best, J. L., and Livesey, J. R. (1999). Turbulence and secondary flow over sediment stripes in weakly bimodal bed material. J. Hydraul. Eng., 125, 5, 463-473.

Meyer-Peter, E. and Müller, R. (1948). Formulas for bedload transport. Proceedings of the 2nd Meeting of the International Association for Hydraulic Research, 1948, 3, 39-64.

Miller, M.C., McCave, I. N. and Komar, P. D. (1977). Threshold of sediment motion under unidirectional currents. Sedimentology, 24, 507-527.

Monin, A. S. and Yaglom, A. M. (1971). Statistical Fluid Dynamics: Mechanics of turbulence (vol. 1). The MIT Press (English translation).

Monteith, H. (2001). Entrainment thresholds of naturally-shaped fluvial and marine gravel (granule) sediments: a laboratory study. J. Soc. for Underwater Technology, 25, 1, 15-19.

Monteith, H. and Pender, G. (2005). Flume investigations into the influence of shear stress history on a graded sediment bed. WRR, 41, W12401, doi:10.1029/2005WR004297.

Mori, N., Suzuki, T., and Kakuno, S. (2007). Noise of Acoustic Doppler Velocimeter data in bubbly flows. . Eng. Mech., 133, 1, 122-125.

Mosley, M. P. and Tindale, D. S. (1985). Sediment variability and bed material sampling in gravel-bed rivers. Earth Surface Processes and Landforms, 10, 465-482.

Neill, C. R. and Yalin, M. S. (1969). Quantitative definition of beginning of bed movement. J. Hyd. Div., HY1, 585-588.

Nelson, J. M., Shreve, R. L., McLean, S. R., and Drake, T. G. (1995). Role of near-bed turbulence structure in bed load transport and bed form mechanics. Water Resour. Res., 31, 8, 2071-2086.

Newson, M. and Sear, D. (1998). The role of geomorphology in monitoring and managing river sediment systems. J. CIWEM, 12, 18-24.

Nezu, I. and Nakagawa, H. (1993). Turbulence in open channel flows. Balkema, Rotterdam, The Netherlands.

Nikora, V., McLean, S., Coleman, S., Pokrajac, D., McEwan, I., Campbell, L., Aberle, J., Clunie, D. and Koll, K. (2007). Double-averaging concept for rough-bed open-channel and overland flows: Applications. J. of Hydraulic Engineering, 133(8), 884-895.

Nikuradse, J. (1933). Stromungsgesetz in rauhren rohren, vdi-forschungsheft 361. (English translation: Laws of flow in rough pipes), 1950. Technical report, NACA Technical Memo 1292. National Advisory Commission for Aeronautics, Washinton, DC.

Nystrom, E. A., Rehmann, C. R., and Oberg, K. A. (2007). Evaluation of mean velocity and turbulence measurements with ADCPs. J. Hydraul. Eng., 133, 12, 1310-1318.

Ockelford, A., Haynes, H., Hodge, R., Haynes, R. (2010). Using high resolution laser scanning to indicate mechanisms of stabilisation under varying sub threshold flow exposures. 17th Congress of the Asia and Pacific Division of the International Association of Hydro-Environmental Engineering and Research (IAHR), February 2010, Auckland, New Zealand.

Oertel, H., Prandtl, L., Böhle, M., and Mayes, K. (2004). Prandtl's Essentials of Fluid Mechanics. Springer, 2004. 723 p.

Olafsdottir, A. O. (2006). Determining the effect of flood hydrograph shape on sediment transport. Laboratory experiment. MSc dissertation. University of Glasgow.

Oldmeadow, D. F. and Church, M. (2006). A field experiment on streambed stabilisation by gravel structures. Geomorphology, 78, 335-350, Elsevier.

Paphitis, D. (2001). Sediment movement under unidirectional flows: an assessment of empirical threshold curves. Coastal engineering, 43, 227-245, Elsevier.

Paphitis, D. and Collins, M. B. (2005). Sand grain threshold, in relation to bed Stress history: an experimental study. Sedimentology, 52, 827-838.

Papanicolaou, A. N., Diplas, P., Evaggelopoulos, N. and Fotopoulos, S. (2002). Stochastic incipient motion criterion for spheres under various bed packing conditions. J-Hydraul. Eng., 128, 4, 369-380.

Papanicolaou, A. N., Diplas, P., Dancey, C. L. and Balakrishnan, M. (2001). Surface roughness effects in near-bed turbulence: implications to sediment entrainment. J. of Eng. Mech., 127, 3, 211-218.

Parker, G. (1979). Hydraulic geometry of active gravel rivers. J. Hyd. Eng. 105, 1185-1201.

Parker, G. (1990). Surface-based bedload transport relation for gravel bed rivers. J. Hyd. Res. 28, 4, 417-436.

Parker, G. (2004). Response of the gravel bed of a mountain river to a hydrograph. Proc., 2002 International Conference on Slopeland Disaster Mitigation, Taiwan, 5-6 October 2004.

Parker, G. and Klingemann, P. (1982). On why gravel bed streams are paved. Water Resour. Res., 18, 5, 1409-1423.

Parker, G., Klingeman, P. C. and McLean, D. (1982a). Bedload and size distribution in paved gravel-bed streams. J. Hyd. Div., HY4, 108, 544-571.

Parker, G., Dhamotharan, S., Stefan, H. (1982b). Model experiments on mobile, paved gravel bed streams. Water Resour. Res.,18, 5, 1395-1408.

Parker, G., M.A. Hassan, and P. Wilcock, (2008). Adjustment of the bed surface size distribution of gravel-bed rivers in response to cycled hydrographs. In H. Habersack, H. Piegay and M. Rinaldi, editors, Gravel-Bed Rivers VI: From Process Understanding to River Restoration. Elsevier B.V., 241-289.

Pender,G., Hoey, T. B., Fuller, C. and McEwan, I. (2001). Selective bedload transport during the degradation of a well sorted grade sediment bed. J. Hyd. Res. 39, 3, 1-9.

Pender, G. Shvidchenko, A. B., and Hoey, T. B. (2001). Modelling graded sediments using ISIS sediment. Trans. of the Int. Conf. of River Basin Management, Cardiff, UK, 2001. Edited by R. A. Falconer and W. R. Blain, p.408. WIT Press, UK.

Petit, F. (1990). Evaluation of grain shear stresses required to initiate movement of particle in natural rivers. Earth Surface Processes and Landforms, 15, 2, 135-148.

Petrie, J. and Diplas, P. (2000). Statistical approach to sediment sampling accuracy. Water Resour. Res., 36, 2, 597-605.

Peviani M. & Alterach J. (2005). Sediment transport analysis using the MORIMOR model for the assessment of downstream river effects due to flushing in reservoirs. Trans. of the 3rd Int. Conf. on River Basin Management, Bologna, Italy, 2005. Edited by C.A. Brebbia and J.S. Antunes do Carmo, WIT Press, UK.

Piedra, M. Haynes, H., Hoey, T. B. and Ervine, A. (2009). Review of approaches to estimating bed shear stress from velocity profile measurements. 33rd IAHR Congress Water Engineering for a Sustainable Environment. Vancouver, Canada, 9-14 August 2009.

Pokrajac, D. Finnigan, J. J. Manes, C. McEwan, I. and Nikora, V. (2006). On the definition of the shear velocity in rough bed open channel flows. In Ferreira, Alves, Leal and Cardoso (eds.), Proc. Int. Conf. Fluvial Hydraulics River Flow 2006, Taylor and Francis Group, London, 89-98.

Powell, D. M., Reid, I. and Laronne, J. B. (2001). Evolution of bedload grain size distribution with increasing flow strength and the effect of flow duration on the caliber of bed load sediment yield in ephimeral gravel bed rivers. Water Resour. Res., 37, 5, 1463-1474.

Power, M. E., Dietrich, W. E., and Finlay, J. C. (1996). Dams and downstream aquatic biodiversity: Potential food web consequences of hydrologic and geomorphic change. Journal Environmental Management, 20, 6, 887-895.

Prandtl, L. (1925). ericht über Untersuchungen zur ausgebildeten Turbulenz. Z. Angew. Math, Meth., 5, 136-139.

Recking, A. (2009). Theoretical development of the effects of changing flow hydraulics on incipient bedload motion. Water Resour. Res., 45, W04401, doi: 10.1029/2008WR006826.

Recking, A. (2010). A comparison between flume and field bed load transport data and consequences for surface-based bed load transport prediction. Water Resourc. Res., 46, W03518, doi:10.1029/2009WR008007.

Recking, A., P. Frey, A. Paquier, P. Belleudy, and J. Y. Champagne (2008), Feedback between bed load transport and flow resistance in gravel and cobble bed rivers, Water Resour. Res., 44, W05412, doi:10.1029/2007WR006219.

Reid, I., Brayshaw, A. C. and Frostick, L. E. (1984). An electromagnetic device for automatic detection of bedload motion and its field applications. Sedimentology, 31, 269-276.

Reid, I. Frostick, L. E. and Layman, J. T. (1985). The incidence and nature of bedload transport during flood flows in coarse-grained alluvial channels. Earth Surface Processes and Landforms, 10, 33-44.

Reid, I. and Frostick, L. E. (1986). Dynamics of bedload transport in Turkey Brook, a coarse-grained alluvial channel. Earth Surface Processes and Landforms, 11, 143-155.

Reid, I., and Laronne, J. B. (1995). Bedload sediment transport in an ephemeral stream and the comparison with seasonal and perennial counterparts. Water Resourc. Res. 31, 773-781.

Reid, I., J.C. Bathurst, P.A. Carling, D.E. Walling and B.W. Webb. (1997). Sediment Erosion, Transport and Deposition. In: C.R. Thorne, R.D. Hey, and M.D. Newson (eds.), Applied Fluvial Geomorphology for River Engineering and Management. John Wiley & Sons, England.

Rice, S. and Church, M. (1996). Sampling surficial fluvial gravels: The precision of size distribution percentile estimates. J. of Sedimentary Res., 66, 3, 654-665.

Richards, K. (1982). Rivers : form and process in alluvial channels. London, Methuen. 358 pp.

Richter, B. D., and Richter, H. E. (2000). Prescribing flood regimes to sustain riparian ecosystems along meandering rivers. Conservation Biology, 14, 5, 1467–1478.

Robert, A. (1990). Boundary roughness in coarse-grained channels. Progress in Physical Geography, 14, 1, 42-70.

Robert, A., Roy, A. G and de Serres, B. (1992). Changes in velocity profiles at roughness transitions in coarse grained channels. Sedimentology, 39, 5,725-735.

Rubin, D. M. (2004). A simple autocorrelation algorithm for determining grain size from digital images of sediment. J. Sedimentary Res., 74, 1, 160-165.

Saadi, Y. (2002). The influence of different time varying antecedent flows on the stability of mixed grain size deposits. PhD thesis, Dept. of Civil and Structural Engineering, University of Sheffield.

Sarmiento, O. A. and Falcon, Marco. A. (2006). Critical bed shear stress for unisize sediment. J. Hydraul. Eng., 132, 2, 172-179.

Scottish Environment Protection Agency (SEPA). (2005). The Water Environment (Controlled Activities) (Scotland) Regulations 2005 (CAR). Guidance for applicants on supporting information requirements for hydropower applications.

Scottish Environment Protection Agency (SEPA). (2007). SEPA Position Statement to support the implementation of the Water Environment (Controlled Activities) (Scotland) Regulations 2005: WAT-PS-07-02: Bank Protection. V. 1.0, October 2007.

Shields, A. (1936). Application of similarity principles and turbulence research to bedload movement. (English translation). Hydrodynamics Laboratory, California Institute of Technology, Publication 167, 36pp.

Shvidchenko, A. B. (2000). Incipient motion of streambeds. PhD thesis. University of Glasgow, UK.

Shvidchenko, A. B. and Pender, G. (2000). Flume study of the effect of relative depth on the incipient motion of coarse uniform sediments. Water Resour. Res., 36, 2, 619-628.

Shvidchenko, A. B., Pender, G. and Hoey, T. B. (2001). Critical shear stress for incipient motion of sand/gravel streambeds. Water Resour. Res., 37, 8, 2273-2283.

Sime, L. C. and Ferguson, R. I. (2003). Information on grain sizes in gravel-bed rivers by automated image analysis. J. of Sedimentary Res., 73, 4, 630-636.

Smart, G. M. (1999). Turbulent velocity profiles and boundary shear in gravel bed rivers. J. Hydraul. Eng., 125, 2, 106-116.

Song, T. and Chiew, Y. M. (2001). Turbulence measurement in non-uniform open-channel flow using acoustic Doppler velocimeter (ADV). J. of Eng. Mech., 127, 3, 219-232.

Stone, M. C. and Hotchkiss, R. H. (2007). Turbulence descriptions in two cobble-bed river reaches. J. Hyd. Eng., 133, 12, 1367-1378.

Sutherland, A. J. (1992). Hiding functions to predict self armouring. Proc., Int. Grain Sorting Seminar, Mitt. der Versuchanstaldt für Wasserbau, Hydrologie und Glaziologie (English translation), ETH, Zürich, Switzerland, 117, 273–298.

Sutherland, A. J. (1987). Static armour layers by selective erosion. Sediment transport in gravel-bed rivers. C. Thorne, J. C. Bathurst and R. D. Hey (eds.), John Wiley & Sons ltd.

Tait, S. J., Willetts, B. B. and Maizels, J. K. (1992). Laboratory observations of bed armouring and changes in bedload composition. In Billi, P., Hey, R. D., Thorne, C. R and Tacconi, P. (eds.). Dynamics of gravel bed rivers. John Wiley & Sons, England.

Thompson, S. M. (1985). Transport of gravel by flows up to 500 m3/s, Ohau River, Otago, New Zealand (abstract). Journal of Hydraulic Research, 23, 3, 285-303.

UCDAVIS. (2007). Geology 109L Lab 1A: Sedimentary Particles and Flow Velocity. Lecture notes. In http://www-geology.ucdavis.edu/~GEL109/labs/Particles.pdf (accessed on 16 May 2007).

Unwin, D.J. (1981). Introductory spatial analysis. London. Methuen. 212pp.

Van Rijn, L. C. (2007a). Unified view of sediment transport by currents and waves. I: Initiation of motion, bed roughness, and bedload transport. J. Hyd. Eng. 133, 6, 649-667.

Van Rijn, L. C. (2007b). Unified view of sediment transport by currents and waves. III: Gravel beds. J. Hyd. Eng. 133, 7, 761-775.

Vericat, D., Batalla, R. and Gibbins., C. N. (2008). Sediment entrainment and depletion from patches of fine material in a gravel bed river. Water Resourc. Res., 44, W11415.

Voulgaris, G. and Trowbridge, J. H. (1998). Evaluation of the acoustic Doppler velocimeter (ADV) for turbulence measurements. Journal of Atmospheric and Oceanic Technology, 15, 272-289.

Wahl, T. L. (2000). Analysing ADV data using WinADV. Joint Conference on Water Resources Engineering and Water Resources Planning & Management, 30th July – 2nd August , 2000. Minneapolis, Minnesota, USA.

Wallerstein, N. Thorne, C., Soar, P., Brookes, A., Biedenharn, D., Watson, C., Mooney, D., Little, C., Gibson, S., Green, T., and Coulthard, T. (2006). Accounting for sediment in rivers. Research report (draft). Flood Risk Management Research Consortium (FRMC). June 2006.

Walling, D. E. and Webb, B. W. (1988). The reliability of rating curve estimates of suspended sediment yield: some further comments. Proceedings of the Porto Alegre Symposium on Sediment Budgets, December 1988. IAHS Publ. no. 174.

Wathen, S. J., Ferguson, R. I., Hoey, T. B. and Werritty, A. (1995). Unequal mobility of gravel and sand in weakly bimodal river sediments. Water Resour. Res., 31, 8, 2087-2096.

Werritty, A. with Chatterton, J. (2004). Foresight. Future Flooding Scotland. Office of Science and Technology, Scottish Executive.

Werritty, A. and Hoey, T. (2004). Geomorphological changes and trends in Scotland: river channels and processes. Scottish Natural Heritage Commissioned Report No. 053. (ROAME No. F00AC107B).

White, W. R. and Day, T. J. (1982). Transport of graded gravel bed material. In Gavel-Bed Rivers, Fluvial Processes, Engineering and Management, R. D. Hey, J. C. Bathurst, and C. R. Thorne (eds.), John Wiley & Sons, 181-223.

Whiting, P. J., Dietrich, W. E., Leopold, L. B., Drake, T. G., and Shreve, R. L. (1988). Bedload sheets in heterogeneous sediment. Geology, 16, 105-108.

Wiberg, P. L. and Smith, J. D. (1989). Model for calculating bedload transport of sediment. J. Hyd. Eng. 115, 1, 101-123.

Wilcock, P. R. (1988). Methods for estimating the critical shear stress of individual fractions in mixed-size sediment. Water Res. Res., 24, 7, 1127-1135.

Wilcock, P. (1992). Experimental investigation on the effect of mixture properties on transport dynamics. Billi, P., Hey, R. D., Thorne, C. R and Tacconi, P. (eds.). Dynamics of gravel bed rivers. John Wiley & Sons, England.

Wilcock, P. R. (1993). Critical shear stress of natural sediments. J. of Hydraul. Eng., 119, 4, 491-505.

Wilcock, P. R. (1996). Estimating local bed shear stress from velocity observations. Water Resour. Res., 32, 11, 3361-3366.

Wilcock, P. (1997). The components of fractional transport rate. Water Resour. Res. 33, 1, 247-258.

Wilcock, P. R. and Southard, J. B. (1988). Experimental study of incipient motion in mixed-size sediment. Water Resour. Res., 24, 7, 1137-1151.

Wilcock P. R. and McArdell B. W. (1993). Surface-based fractional transport rates: mobilisation thresholds and partial transport of sand-gravel sediments. Water Resour. Res., 29, 4, 1297-1312.

Wilcock, P., Kondolf, G., Matthews, W., and Barta, A. (1996). Specification of sediment maintenance flows for a large gravel-bed river. Water Resour. Res., 32, 9, 2911-2921.

Wilcock, P. R. and Crowe, J. C. (2003). Surface-based transport model for mixed-size sediment. J. of Hydraul. Eng., 129, 2, 120-128.

Wolman, M. G. (1954). A method of sampling coarse river bed material. Am. Geophys. Union. Trans., 35, 951-956.

Wong, M. (2003). Does the bedload equation of Meyer-Peter & Müller fit its own data? Proc. 30th Congress, Int. Ass. Hyd. Res. Thessaloniki, J.F.K. Competition volume: 73-80.

Wong, M. and Parker, G. (2006). Reanalysis and correction of bedload relation of Meyer-Peter and Müller using their own database. J. Hydraul. Eng., 132, 11, 1159–1168.

Wu, W., Wang, S. and Jia, Y. (2000). Nonuniform sediment transport in alluvial rivers. J. Hyd. Res. 38, 6, 427-434.

Wu, F. C. and Chou Y. J. (2003). Rolling and lifting probabilities for sediment entrainment. J. Hydraul. Eng., 129, 2, 110-119.

Yadav, S. M. and Samtani, B. K. (2008). Bedload transport in Tapi River, India. Global J. of Env. Res. 2, 2, 96-101.

Yalin, M. S. (1963). An expression for bedload transportation. J. Hyd. Div. ASCE, 89, HY3, 221-250.

Yalin, M. S. (1977). Mechanics of sediment transport. 2nd edition. Pergamon Press.

Young, W. J and Warburton, J. (1996). Principles and practice of hydraulic modelling of braided gravel-bed rivers. Journal of Hydrology (NZ), 35, 2, 175-198.

Zhang, X. and McConnachie, G. L. (1994). A reappraisal of the Engelud bed load equation. Hydrological Sciences Journal, 39, 6, 561-567.